Department of Chemical Engineering

Tetrahydrofuran and Natural Gas Hydrates Formation in the Presence of Various Inhibitors

Yenny V Rojas González

This thesis is presented for the Degree of
Doctor of Philosophy
of
Curtin University of Technology

September 2011

DECLARATION

To the best of my knowledge and belief this thesis contains no material previously published by any other person except where due acknowledgment has been made.

This thesis contains no material which has been accepted for the award of any other degree or diploma in any university.

Signature: ……

Date: September 12th, 2011

ABSTRACT

The aim of this thesis is to investigate the formation process of tetrahydrofuran (THF) hydrates and natural gas hydrates, and the effect of kinetic hydrate inhibitors (KHIs) on the formation and growth of these hydrates. Kinetic experiments were conducted in pressure cells in the presence of, or without, KHIs. Interfacial and electrokinetic techniques, including surface tension, Langmuir monolayers and zeta potential, were used to study the adsorption preferences of the inhibitors in two different interfaces, air–liquid and hydrate–liquid. For comparison purposes, selected thermodynamic hydrate inhibitors (THIs) and antiagglomerators (AAs) were investigated in some of the experiments. Sodium chloride was used in experiments where suitable.

Four well known KHI polymers, including a terpolymer of *N*-vinylpyrrolidone, *N*-vinylcaprolactam and dimethylamino-ethylmethacrylate (Gaffix® VC713), poly(*N*-vinylcaprolactam) (Luvicap® EG), and poly(*N*-vinylpyrrolidone) (PVP40, Mn=40k and PVP360, Mn=360k), were selected for the investigation. A copolymer containing both poly(ethylene oxide) and vinylcaprolactam segments (PEO-VCap) that was developed in the Polymer Research lab in Curtin University, was also investigated. Other chemicals, including methanol (MeOH) and monoethylene glycol (MEG) were used as THIs. Sodium dodecyl sulphate (SDS) was used as an AA.

During the THF hydrates kinetic studies, several experimental parameters that are associated with the nucleation and crystal growth process were investigated. The onset of THF hydrates formation, the maximum temperature spike, the magnitude of the temperature rise associated with the hydrate formation, the rate of hydrate formation, and the temperature at the end-point of the hydrate formation, were reported to compare inhibition efficiency. Subcooling was used as the driving force for hydrates formation. The experimental results show that the kinetics of the THF hydrate is affected by the physical chemical environment, which includes the concentration and types of additives used for the inhibition of the hydrates. In comparison to the system containing no inhibitor, there was an increase in

subcooling and a reduced onset temperature of hydrates formation when various inhibitors were used.

Surface tension studies have demonstrated that the adsorption of KHIs molecules at the air–liquid interface is directly related to its effectiveness inhibiting hydrates. The differences in the fundamental properties of the polymer molecules, such as molecular weight and flexibility of the polymer chain, have an impact on the different adsorption behaviours at the air–liquid interface for all of them. The inhibition efficiency of KHIs was enhanced in the presence of NaCl 3.5 wt% for all the inhibitors, and seemed to be associated to maximum packing of polymer molecules in the monolayer and low surface tension values. The zeta potential results, measured at the THF hydrate–liquid interface, have shown some correspondence with the surface tension results at the air liquid–interface. The compound, with a higher adsorption at the air liquid–interface also showed a higher adsorption at the surface of the THF hydrate. It was observed, that the inhibitor showing the higher adsorption on zeta potential measurements was more effective for reducing the onset temperature of hydrates formation.

The kinetic studies have been extended to structure II natural gas hydrates systems, to examine whether the hypothesis proposed for THF hydrates systems were applicable to the gas hydrate systems. Gaffix® VC713, Luvicap® EG, PVP40 and PEO-VCap were used in this investigation. The gas hydrate formation rate was always slower when KHIs were present in the liquid phase. In all cases, the presence of KHI decreases the temperature of the onset hydrate formation. Polymers, such as PVP40 and PEO-VCap, that showed the worse and the best inhibition performances respectively in THF crystals, exhibited the opposite inhibition performance in gas hydrate crystals. This suggests that a different mechanism of KHIs surface adsorption could be operating on different hydrates surfaces.

Overall, the investigation of the kinetics of formation and inhibition on THF hydrates and natural gas hydrates in the presence of KHIs, indicate that the gas hydrate formation rate during gas hydrate formation, is always slower when KHIs are present in the liquid phase. The inhibition mechanism of KHIs in the THF hydrates systems

may differ significantly from that of the gas hydrate systems. Adsorption studies, demonstrate that the adsorption of KHIs are directly related to their effectiveness inhibiting hydrates. Surface tension and zeta potential approaches provide valuable information for understanding hydrates formation and inhibition mechanisms.

ACKNOWLEDGEMENTS

The completion of this research has involved an enormous amount of help from many people. My sincere appreciation goes to the following individuals, whose guidance and support made this work possible:

- To Dr. Mayela Rivero, not only for the opportunity to join CSIRO and Curtin organisations, but also for her friendship and inspiration as an incredibly creative and capable individual.

- A/Professor Xia Lou, my supervisor, for her critical examination and assistance in the course of producing this thesis.

- Professor Ahmed Barifcani for welcoming me to the Clean Gas Technology Australia and for his kind contribution in the use of the Micro-Cell for LNG Production.

- Dr Chi Phan and Dr Bill Richmond for allow me to use their surface tension and Langmuir trough instruments.

- Dr Franca Jones for her valuable discussions in the electrophoresis area, and for allows me to use the zeta potential equipment.

- The technicians Karen Haynes, Ann Carroll, Peter Chapman, Saif Ghadhban, Kristy Blyth, Michael Boddy, and research assistant Tomoko Radomirovic. Their help in laboratories was really appreciated.

- The personnel at the Chemical Engineering Department. Especially to Professor Ming Ang, Jann Bolton, Naomi Mockford and Stephenie Blakiston.

- To my mother, who has always been my true strength and motivation for accomplishment. Thank you for your unending love and support.

- Dad, even when you are with me only in my memory today, I know exactly what your comments would have been after the completion of the thesis.

- My friends in Perth, Venezuela, and beyond. Thank you for been presented all the time encouraging me to continue reaching my goals. Especially to Mauricio, Morella, Carlos, Carolina, Maryorit, Alida, Melissa, Mary Lor, Oliver and Betzabe. Thank you so much for being there when I needed you the most.

- Appreciation is also due to my many friends and colleagues in Curtin University of Technology, for creating a pleasant working atmosphere. Especially Chao, Thu, Deepak, Yuli, Fonny, Monica, and Esther.

- Little baby girl Samantha who arrived at this world filling all the spaces with love and hope.

- The funding organisations, CSIRO and Curtin University of Technology, who believed that this work was important enough to invest time and resources.

This thesis is dedicated to my loved mother

BRIEF BIOGRAPHY OF THE AUTHOR

I am a PhD scholar research in the School of Chemical and Petroleum Engineering at Curtin University, Perth, WA, Australia. I am holding a BSc in Chemical Engineering from University of Los Andes and an MSc in Chemical Engineer (Honourable Mention) from Simon Bolivar University, both in Venezuela. I have a proven track record of creative problem-solving, exceptional background in multidisciplinary research and ability to grasp new scientific and engineering concepts. Previously, I worked for continuous six years as a Research Scientist & Drilling Fluids Engineer at the Technical Support Centre of Petróleos de Venezuela (PDVSA INTEVEP). I was involved in different R&D, technical marketing, and field technical support projects for the Oil and Gas Industry. Recently, I was working in a part-time term position in CSIRO Petroleum Group, Perth, WA, Australia. My technical background includes: drilling and completion fluids, surface and colloid science, gas hydrates and flow assurance, physical chemical formulation and rheological characterization of disperse systems, oil-rock-fluid interactions, and nanotechnology. I have published more than fifteen journal articles, international conference papers and industrial reports, and have two patents of invention in the area of foam technology for underbalanced drilling applications. I have also received a number of awards including: CSIRO Postgraduate Studentship and Curtin International Research Tuition Scholarship, Honourable Mention “Cum Laude” in MSc graduate studies, class ranking 1 out of 41 in MSc graduate studies, and two awards for extraordinary contributions to PDVSA for Low-Density Fluids to Drilling, Workover and Completion Operations, and Well Construction of Low-Pressure Reservoirs.

LIST OF PUBLICATIONS

- Rojas, Y., and X. Lou. 2010. Instrumental Analysis of Gas Hydrates. Asian Pacific Journal of Chemical Engineering 5 (2): 310-323.
- Rojas, Y. V., C. M. Phan, and X. Lou. 2010. Dynamic surface tension studies on poly(*N*-vinylcaprolactam/*N*-vinylpyrrolidone/*N*,*N*-dimethylaminoethyl methacrylate) at the air-liquid interface. Colloids and Surfaces A 355 (1-3): 99-103.
- Rojas, Y. & X. Lou. 2009. Surface behaviour of poly(*N*-vinylcaprolactam) at the air–liquid interface. Chemeca, Burswood Entertainment Complex, Perth, Australia, 28-30 September 2009.
- Rojas, Y. & X. Lou. 2008. Methods and techniques for natural gas hydrates characterisation: A review. Chemeca, Newcastle City Hall, New South Wales, Australia, 28 September to 1 October 2008.

TABLE OF CONTENTS

LIST OF FIGURES

LIST OF TABLES

Chapter 1 INTRODUCTION

1.1 Background

Gas hydrates belong to a general class of inclusion compounds commonly known as clathrates. A clathrate is a compound of molecular cage structure made of host molecules encapsulating guest molecules. It is also considered a chemical substance consisting of a lattice of one type of molecules trapping a second type of molecules (Mahajan et al., 2007).

Natural gas forms such hydrates at low temperatures (<298 K) and elevated pressures (>1.5 MPa), and hydrates are found in the subsurface in permafrost regions, and mostly in oceanic sediments hundreds of meters below the sea floor (Sloan, 1997). These hydrates consist of a host lattice formed by hydrogen bonded water molecules that enclose a large variety of small guest molecules including methane, as shown in Figure 1.1. Therefore, they are also known as clathrate hydrates of natural gases.

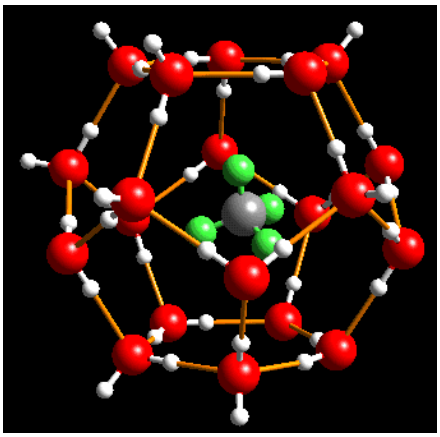

Figure 1.1 The schematic drawing of one type of methane clathrate hydrate (Guan, 2010).

Natural gas hydrates also form in natural gas transmission pipelines due to the favourable operation conditions, i.e. low temperature, high pressure and adequate composition of the gas–water vapour mixture (Hammerschmidt, 1934).

Over a long period following their discovery by Sir Humphry Davy in 1810, interest in clathrate hydrates was purely academic (Chatti et al., 2005). Extensive research on gas hydrates was done some 70 years later when Hammerschmidt indicated that the compounds were responsible for the blockage of flow lines, valves and well heads where the operation conditions are ideal for clathrate hydrates to form (Hammerschmidt, 1934).

Figure 1.2 shows a gas hydrate plug taken from an offshore production line. Gas hydrate plugging can lead to over pressuring and sometimes an eventual shutting down of the operation facilities, causing loss of production and serious safety problems because of possible pressure build-up upon hydrate agglomeration (Mokhatab et al., 2007; Sum et al., 2009). Removal of hydrate plugs from subsea production and transmission systems can be time consuming. In some cases, the loss in drill time has been as long as 70 days (Barker and Gomez, 1989). The economic loss is unquestionably significant.

Figure 1.2 A gas hydrate plug taken from an offshore production line (Alapati and Davis, 2007).

Various strategies have been investigated in order to combat hydrate plugs and to ensure regular flow during oil and gas operations. These include mechanical, thermal, hydraulic and chemical methods (Englezos, 1993; Makogon, 1997; Sloan, 1997; Chatti et al., 2005). More details for each of the four methods will be provided in Chapter 2. The chemical method involves the injection of thermodynamic inhibitors (THIs), such as alcohols, glycols, aqueous electrolytes or a combination of these and others. The injections of these chemicals shift the equilibrium temperature

and pressure conditions and thus prevent gas hydrate crystallisation/formation at the pipeline working conditions. Although the method has proven to be effective in preventing gas hydrate formation, and is currently the most commonly used in the oil and gas industry, the economic drawbacks are significant. Large volumes of the inhibitors are required, generally between 10 and 60% by weight. The cost associated with the operation and recovery of the inhibitors in such volumes is very high. A case study of a small field has demonstrated that the cost associated with the most commonly used thermodynamic inhibitor, methanol is around $5 million per year, which is clearly not a small amount (Koh et al., 2002). The worldwide annual expense for methanol was estimated at US$220 million in 2003 (Sloan, 2003b).

The high demand for more cost-effective and environmentally-friendly inhibitors has led to enormous research activities in the development of various low-dosage gas hydrate inhibitors (LDHIs), including kinetic hydrate inhibitors (KHIs) and anti-agglomerants (AAs), over the past 20 years. LDHIs are often proprietary chemicals that either delay hydrate formation or prevent the agglomeration of hydrate particles in flow lines (Sum et al., 2009). The concentrations of LDHIs used in the operation are in the range of 0.5 to 1% by weight, which is much lower in comparison to the THIs. The research activities of LDHIs have been extensively reviewed by Kelland in a recent report (Kelland, 2006).

Though initially studied as a nuisance to oil and gas exploration, production and transportation, gas hydrates are now regarded as a promising alternative in finding a solution to some important global issues like global carbon cycle, long-term climate change effects, seafloor stability, future energy source, hydrate formation and dissociation properties, physical and chemical properties, and global distribution of hydrate (Mahajan et al., 2007; Ribeiro Jr and Lage, 2008).

It was reported that gas hydrates represent the largest source of hydrocarbons on earth (Englezos, 1993; Sloan, 2003a), and can be utilised as a possible source of energy (Holder et al., 1984; Kvenvolden, 1988; Englezos and Lee, 2005; Dawe and Thomas, 2007; Makogon et al., 2007). A more recent application of gas hydrates has emerged with the growing interest in hydrogen as an energy source, which has prompted the possibility of utilising hydrates as a storage medium for hydrogen

(Florusse et al., 2004; Mao and Mao, 2004; Lee et al., 2005; Strobel et al., 2006; Okuchi et al., 2007). Gas hydrates can also be used as novel technologies in separation processes (Englezos, 1993; Purwanto et al., 2001; Chatti et al., 2005; Max et al., 2006); gas recovery, storage and transportation (Gudmundsson et al., 1998; Sloan, 2000; Thomas and Dawe, 2003; Kerr, 2004; Chatti et al., 2005; Nogami et al., 2008; Sloan and Koh, 2008; Takahashi et al., 2008); carbon dioxide sequestration (Saji et al., 1992; Yamasaki et al., 2000; Lee et al., 2002; Lee et al., 2003; Chatti et al., 2005; Goel, 2006); and in cool storage or air-conditioning applications (Ohmura et al., 2003; Fournaison et al., 2004; Chatti et al., 2005; Xie et al., 2005; Ogawa et al., 2006).

Another issue that has attracted the attention of researchers is related to the role of hydrates in the environment and climate change. It is believed that methane, which is the predominant gas trapped in hydrate deposits, is a major contributor to the greenhouse effect (Hatzikiriakos and Englezos, 1993; Bains et al., 1999; Kvenvolden, 2000; Dickens, 2003). Detailed discussion of the different opportunities presented by gas hydrates has been provided by different authors (Englezos, 1993; Lachet and Béhar, 2000; Sloan, 2003a; Sloan, 2003b; Chatti et al., 2005; Mahajan et al., 2007; Sum et al., 2009).

The positive observations about gas hydrates have motivated increasing research and development activities in the areas of chemical and petroleum engineering, earth and geophysics, chemistry, and environmental sciences. Figure 1.3 reveals the increasing number of publications in the past 10 years (data collected from Engineering Village II data base). An increase of over 350% is shown in the total publications. The increase in characterisation of gas hydrate properties is even higher (data not shown). This further demonstrates the significant importance in gas hydrate studies and management.

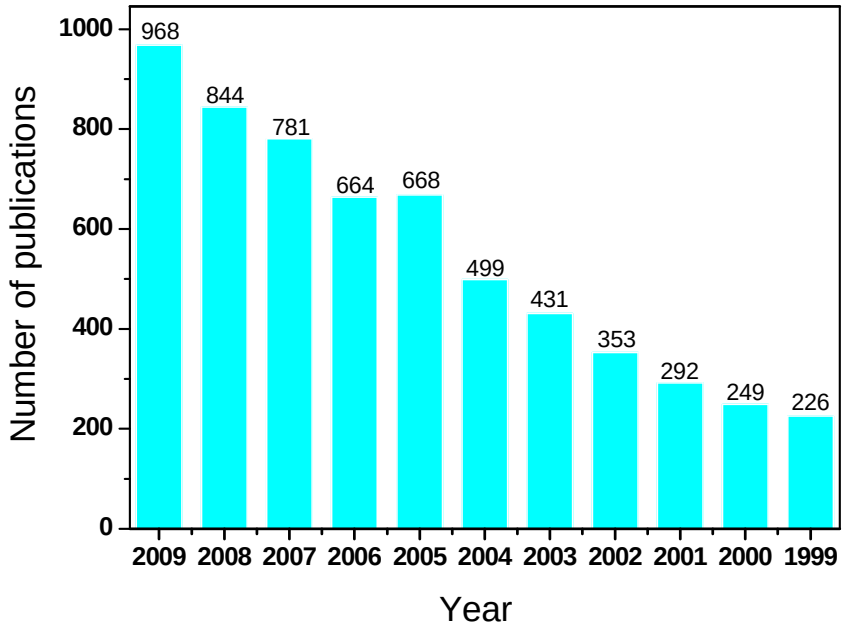

Figure 1.3 Number of publications on gas hydrates between 1999 and 2009 (Engineering Village II data base).

Management of gas hydrates, for both prevention or utilisation, is mostly hindered by technological problems associated with hydrate formation and dissociation including slow formation rates, low conversions and the economics of process scale-up (Ribeiro Jr and Lage, 2008). Efficient management of natural gas hydrates requires insightful understanding of hydrate properties, the mechanisms controlling hydrate formation and dissociation kinetics, and the factors that might affect these properties and processes. Compared to hydrate thermodynamics, hydrate kinetics are still poorly understood (Englezos, 1993; Sloan, 2003a, 2005). An increasing number of studies on hydrate kinetics was observed in the 1980s, most of which was concerned with hydrocarbons and carbon dioxide, obviously driven by gas storage applications (Ribeiro Jr and Lage, 2008).

Traditional studies on both theoretical prediction (molecular thermodynamic simulation) and experimental characterisation of properties, including phase equilibria, structures and occupancy, are generally related to the measurement of parameters, such as pressure, temperature and fluid–phase compositions, and involve mainly macroscopic and mesoscopic instruments, such as high-pressure visual cells,

rheometers, calorimeters, flow loops, flow wheels, and X-ray computerised tomography (Makogon, 1997; Sloan, 1997; Sloan and Koh, 2008). More recent research has shown a shift focus to the obtaining of a more accurate estimation of hydrate properties and more precise information about the characteristics of gas hydrates through the utilisation of more advanced equipment and instrumental technologies (Sloan, 2003a). Many of the recent research activities are focussed on thermal analysis, crystallographic analysis, topographic analysis and, more significantly, spectroscopic analysis at the molecular or atomic level. A number of reviews on hydrate characterisation methods (Malone, 1994; Tulk et al., 2000; Sloan, 2003a; Susilo et al., 2007; Sloan and Koh, 2008; Sum et al., 2009) have become useful references for many studies. More recently, a review covering a large spectrum of instrumental methods that are useful in the characterisation of gas hydrates properties has been reported by Rojas and Lou (2010).

Although the equilibrium thermodynamic and structural properties of gas hydrates have been well characterised, there still remains a need for a fundamental understanding of the mechanisms of gas hydrate formation, decomposition and inhibition. Understanding these mechanisms will be critical to the development of new and improved technologies for controlling gas hydrate formation in subsea pipelines, or for the controlled extraction of methane from methane deposits (Koh et al., 2002).

1.2 Thesis outline and organisation

This study aims to investigate the formation of THF and natural gas hydrates in the presence of, or without, the kinetic inhibitors. Kinetic experiments using pressure cell are carried out in order to characterise the hydrates formation process. Interfacial and electrokinetic techniques, including surface tension, Langmuir monolayers and zeta potential, are used to study the adsorption preferences of the inhibitors in two different interfaces, air–liquid and hydrate–liquid, in order to understand the mechanisms by which KHIs delay the formation and growth of hydrates.

As mentioned in the previous section, KHIs are compounds that delay nucleation and growth of hydrate crystals for a substantial period of time (Kelland et al., 1994). However, the mechanism by which KHIs delay the massive hydrate growth is not well understood. Some studies suggested that the LDHIs affect the water structuring during homogeneous nucleation, thereby preventing the formation of the critical nuclei (Kelland, 2006; Moon et al., 2007). Other researchers have suggested that nucleation and/or crystal growth inhibition is achieved via adsorption on the hydrate surface (Larsen et al., 1998; Hutter et al., 2000). However, nothing has been proven to fully explain all of the phenomena associated with hydrate kinetic inhibition.

Moreover, an understanding of the mechanisms by which KHIs inhibit gas hydrates is of significant importance to the development of new and improved chemical additives for controlling gas hydrate formation in either subsea pipelines or in other industries that require the gas hydrates technologies for other purposes.

Four commercial polymers, which have already been proven for the inhibition of gas hydrate formation and/or growing, including a terpolymer of *N*-vinylpyrrolidone, *N*-vinylcaprolactam and dimethylamino-ethylmethacrylate (Gaffix® VC713), poly(*N*-vinylcaprolactam) (Luvicap® EG), and poly(*N*-vinylpyrrolidone) (PVP40 (Mn=40k) and PVP360 (360k)), are selected for the investigation. A new copolymer containing both poly(ethylene oxide) and vinylcaprolactam segments (PEO-VCap) that was developed in Polymer Research lab in Curtin University will also be investigated as a comparison. Other chemicals, such as sodium chloride (NaCl), methanol (MeOH), monoethylene glycol (MEG), and sodium dodecyl sulphate (SDS), are also investigated in order to compare their inhibition performance with the KHIs.

The kinetics of THF hydrate formation in the presence and absence of hydrate inhibitors will be investigated. The effect of MeOH, MEG, NaCl and SDS on the formation kinetics will also be studied.

The surface and monolayer properties of these compounds at the air–liquid interface will be studied, by evaluation of the surface tension and surface pressure–area

measurements. The effect of polymer concentration, electrolytes and temperature on the adsorption properties of the polymers is presented also.

The adsorption of the KHIs at the THF hydrate–liquid interface will be investigated by electrokinetic phenomena using zeta (ζ)–potential measurements.

Upon completion of these experiments, to obtain a better understanding of the processes occurring during hydrate formation, the focus will be moved to real gas systems. The kinetics of natural gas hydrate formation and effectiveness of hydrate inhibitors will then be further investigated. The results are discussed in terms of the inhibition mechanisms.

The thesis is structured in seven chapters. Firstly, a brief introduction on the gas hydrates is presented in Chapter 1. A general overview of gas hydrates, the proposed theories involved in gas hydrate formation, and the technologies used for gas hydrate mitigation, remediation and prevention will be presented in Chapter 2. The review will be focused on the chemicals and mechanisms used for inhibiting and/or controlling gas hydrate formation, avoiding both nucleation or crystal growth and agglomeration of the hydrate particles. This will be followed by kinetic studies of THF hydrates formation in the presence and absence of hydrate inhibitors in Chapter 3. The surface and monolayer properties of the kinetic inhibitors at the air–liquid interface will be presented in Chapter 4. The electrokinetic phenomena associated with THF hydrate–liquid interface will be discussed in Chapter 5. The kinetics of natural gas hydrates formation in the presence and absence of hydrate inhibitors will be explained in Chapter 6. In Chapter 7, general conclusions are drawn and recommendations for future research will be given.

Chapter 2 LITERATURE REVIEW

2.1 Introduction

This chapter provides a review of the literature on gas hydrates. The first section offers an introduction to the microscopic structures of gas hydrates, physical characteristics and hydrates promoters. This is followed by an overview on the kinetics of hydrate formation and growth, emphasising the fundamental mechanisms of hydrate formation in gas and liquid systems. Methods used for inhibiting and/or controlling gas hydrate formation are discussed next. Then, the present understanding of the mechanisms of hydrates kinetic and anti-agglomerant inhibition is reviewed. Finally, a summary is given of the experimental techniques used to characterise hydrates. This chapter will provide the contextual background so that the following chapters can be better understood.

2.2 Gas hydrates

2.2.1 Crystallographic structures

Clathrate hydrates are nonstoichiometric structures containing various molecules (<10 Å) that are encaged in water cavities (Sloan and Koh, 2008). The three most commonly appearing structures in natural gas hydrates, namely cubic I (sI), cubic II (sII) and hexagonal H (sH), are displayed in Figure 2.1. The main difference between each structure is the size of the water cavities which are the building blocks comprising the hydrates structures and are largely determined by the size of the encaged guest molecules, as can be seen in Table 2.1 (Von Stackelberg, 1949; Ripmeester et al., 1987).

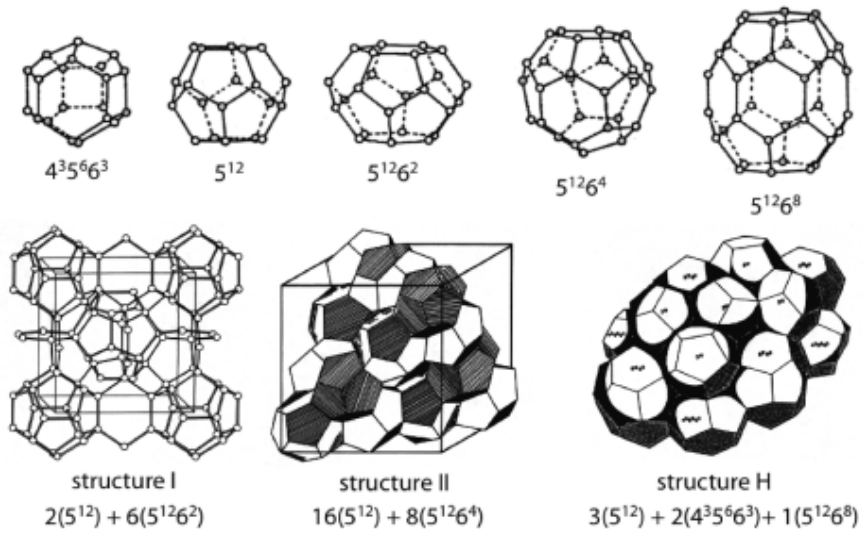

Figure 2.1 Water cavities composing various hydrate crystal structures (Sum et al., 2009).

In general, the structures consist of five polyhedra in which the vertices are the oxygen atoms of the water molecules and the edges represent hydrogen bonds. The five polyhedron, 5^{12}, is the small cavity that forms the fundamental building unit of all hydrate structures. Since the polyhedra share faces in the crystalline structure, only 20 out of the 60 theoretically needed water molecules are required to form this cavity. In a sI hydrate, the cavities 5^{12} are linked together in space through their vertices, whereas in a sII structure, face sharing linking occurs. In each case, the spaces between the 5^{12} cavities form the large cavities $5^{12}6^2$ and $5^{12}6^4$, respectively. In structure H, face sharing takes place only in two dimensions, so that a layer of cavities 5^{12} connects a layer of cavities $5^{12}6^8$ and $4^35^66^3$. Contrary to structures sI and sII, sH requires two different guest molecules for its formation: a small one such as methane and a larger one, typical of a condensate of an oil fraction, with a size larger than 7.4 Å (Ribeiro Jr and Lage, 2008).

Table 2.1 Cavities in gas hydrates (Sloan, 1998).

Structure	sI		sII		sH		
Cavity	Small	Large	Small	Large	Small	Medium	Large
Description	5^{12}	$5^{12}6^2$	5^{12}	$5^{12}6^4$	5^{12}	$4^35^66^3$	$5^{12}6^8$
Number per unit cell	2	6	16	8	3	2	1
Average cavity radius (Å)	3.95	4.33	3.91	4.73	3.91	4.06	5.71

Regardless of the type of crystalline structure, each hydrate cavity contains at most one guest molecule. Molecules smaller than 3.5 Å in diameter are too small to stabilise any cavity, while molecules with a diameter greater than 7.5 Å are too large to enter sI and sII cavities. For pure systems, the size ratio of the guest molecule to cavity is a guide to determining crystal structure. For mixtures, the hydrate structure is usually dictated by the larger guest molecule. Although it is true that general formulas can be written for each hydrate type with all cavities occupied, it is impossible to occupy all cavities, which would correspond to obtaining a perfect crystal. Consequently, all hydrates do contain more water than predicted by the ideal composition (Ribeiro Jr and Lage, 2008). According to Sloan (1998), typical occupancies of large and small cavities are 50% and 95%, respectively. Detailed morphological descriptions of gas hydrates are given elsewhere (Makogon, 1997; Sloan, 1998; Ribeiro Jr and Lage, 2008).

Other hydrate structures including structure T (from trigonal) found in dimethyl ether (DME) hydrate (Udachin et al., 2001) and the high–pressure methane structures MH-II and MH-III (Loveday et al., 2001) have also been reported. These are rarely found in the petroleum industry and are beyond the scope of this study.

2.2.2 Hydrates of gas molecules

Most natural gas molecules, such as methane, ethane, hydrogen sulfide and carbon dioxide, are small (4-5.5 Å) and form structure sI (Sloan, 2003b). Larger molecules (6-7 Å), such as propane, iso-butane form sII hydrates (Sloan, 2003b). Even larger molecules (8-9 Å) such as iso-pentane, 2,2-dimetylbutane, methylcyclohexane and tert-butyl methyl ether, form sH hydrates in the presence of small molecules such as methane (Sloan, 2003b). Interestingly, molecules smaller than 4 Å, including argon, krypton, xenon, oxygen, hydrogen and nitrogen also form sII hydrates (Makogon, 1997; Udachin et al., 2002; Sloan, 2003b; Susilo et al., 2007). Binary, ternary and multi-component gas systems have also been found in gas hydrates, exhibiting transitions between different structures (Sloan, 2003b). Figure 2.2 shows the diameter of typical guest hydrate molecules, the hydrate structures that form with each guest, the cavities occupied by the guests, and the ratio of water molecules to guest molecules in the hydrate structure. Even though different gases can form

hydrates, the focus of this thesis is on natural gas hydrates, including the hydrocarbons and some other organic molecules involved in the oil and gas industry.

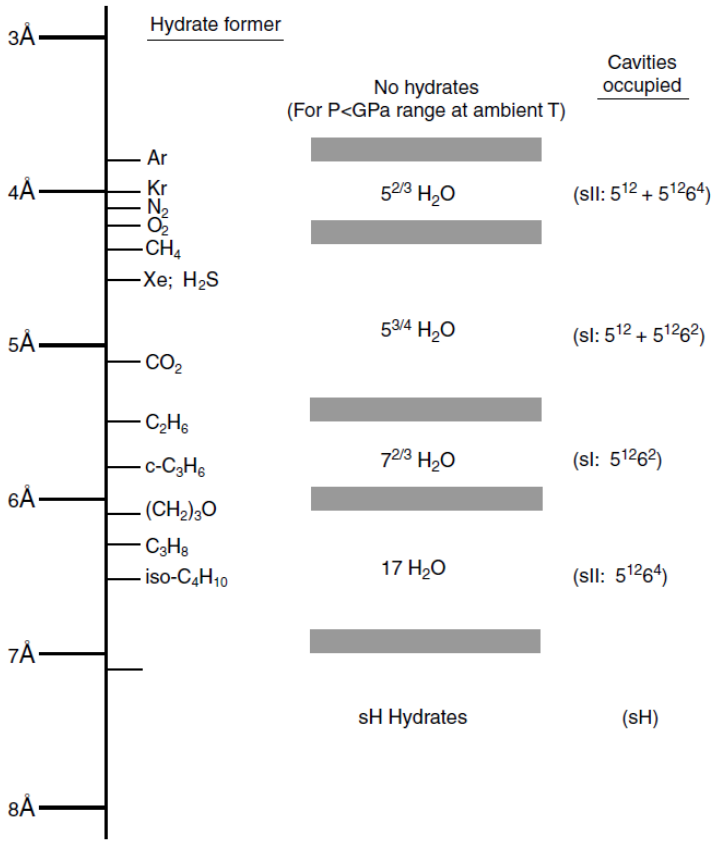

Figure 2.2 Sizes of and cavities occupied by guest molecules in simple hydrates (Sloan and Koh, 2008).

2.2.3 Hydrate of liquid molecules

Substances that are in a the liquid form at room temperature, and form hydrates at low temperature and atmospheric pressure, are of particular interest to many researchers. They form similar types of hydrate structures, as some gas molecules do, and can be used to study the latter without the requirement of high pressures. For example, ethylene oxide forms sI structured hydrates and tetrahydrofuran (THF) forms sII structured hydrates (Koh, 2002) at low temperature and atmospheric pressure. THF hydrate crystals form in the presence of water or sea-water at 277.4 K and at atmospheric pressure at a molar ratio of 1:17 (THF to water). They form sII type structures that are usually found in natural gas hydrates and have been widely

used for screening natural gas hydrate inhibitors (Makogon et al., 1997). Some condensates and oils, such as benzene, cyclopentane, cyclohexane, methylcyclopentane, cycloheptane, methylcyclohexane, and ethylcyclopentane, among others, have also been identified as potential hydrate formers; however, they require the presence of smaller molecules to stabilise the structure (Pickering et al., 2001). Other less commonly investigated liquid hydrates formers include tetrahydropyran (Udachin et al., 2002), chloride fluorocarbon compounds (Owa et al., 1987; Mori and Mori, 1989; Ohmura et al., 1999; Tajima et al., 2007), hydrotrope molecules (Gnanendran and Amin, 2004; Rovetto et al., 2006) and some alcohols (Murthy, 1999; Østergard et al., 2002; Ohmura, Takeya, Uchida, and Ebinuma, 2004; Ohmura, Takeya, Uchida, Ikeda et al., 2004).

2.3 Kinetics of gas hydrates formation

The formation of natural gas hydrates begins with either a heterogeneous or homogeneous nucleation event (Anderson et al., 2005). In a homogeneous nucleation, hydrate formation takes place in a single phase containing no impurities. In a heterogeneous nucleation, hydrate formation takes place in the presence of two or more phases, and/or impurities, which serve as nucleation catalysts. Since gas hydrate initiation usually occurs at the vapour–liquid interface, molecular models of hydrate nucleation have focused on that surface (Sloan and Koh, 2008).

Englezos, (1993) has indicated that two fundamental factors should be considered in hydrate formation, the time required to begin forming hydrate crystals when the conditions of a given hydrate forming mixture are located in the hydrate formation region, and the rate of growth of the hydrate crystals.

Makogon has pointed out that the gas hydrate nucleation and growth processes may be affected by many factors, such as subcooling, pressure, temperature, previous history of water, composition, and state of the gas hydrate forming system (Makogon et al., 2000). The complexity of all these factors has limited the research activities of hydrate formation kinetics and resulted in a paucity of reliable quantitative kinetic

data in the literature. Most of studies are limited to molecular simulations that are short of experimental data to validate (Anderson et al., 2005).

In general, the process considered for hydrates formation and growth is similar to crystallisation, and can be divided into nucleation, kinetic growth, and physical growth processes (breakage and agglomeration of crystals) (Englezos, 1993; Sloan, 1998).

2.3.1 Nucleation

Hydrate nucleation is the process during which small clusters of water and gas (hydrate nuclei) grow and disperse in an attempt to achieve critical size for continued growth. The nucleation step is a microscopic phenomenon involving tens to thousands of molecules and is difficult to observe experimentally. Current hypotheses for hydrate nucleation are based upon the better-known phenomena of water freezing, the dissolution of hydrocarbons in water, and computer simulations of both phenomena (Sloan, 1997).

Three main hypotheses for hydrate nucleation are found in open literature, which are summarised below.

2.3.1.1 Labile cluster hypothesis

Proposed by Sloan et al., (Christiansen and Sloan, 1994; Sloan, 1997), this hypothesis supports homogeneous nucleation, and states that methane molecules in solution are surrounded by a clathrate-like solvation shell with hydrate characteristics but from which water molecules are continually interchanged with the surrounding liquid. Hydrate then forms by agglomeration of these cage-like clusters. In its original form it was thought that the methane solvation shell was distinctly clathrate-like, but as subsequent experimental and theoretical evidence has come to light, this has been modified to consider a propensity for water to become clathrate-like during aggregation (Hawtin et al., 2008). Figure 2.3 depicts the progress of molecular species from water [A] through labile clusters [B] to metastable agglomerates [C] to stable nuclei [D] at the end of the primary nucleation period and the start of growth.

At initial conditions [A], there are no gas molecules dissolved in the water. But as gas molecules dissolve into the water, labile clusters form immediately. Although the water molecules that participate in a labile cluster can exchange with surrounding molecules, the clustering is always present. Agglomerates of labile clusters form [C] as a consequence of hydrophobic bonding. The agglomerates are in quasi equilibrium with each other and the labile clusters until they exceed the critical radius. When an agglomerate exceeds the critical size [D], it is a nucleus for growth of hydrate (Sloan and Koh, 2008).

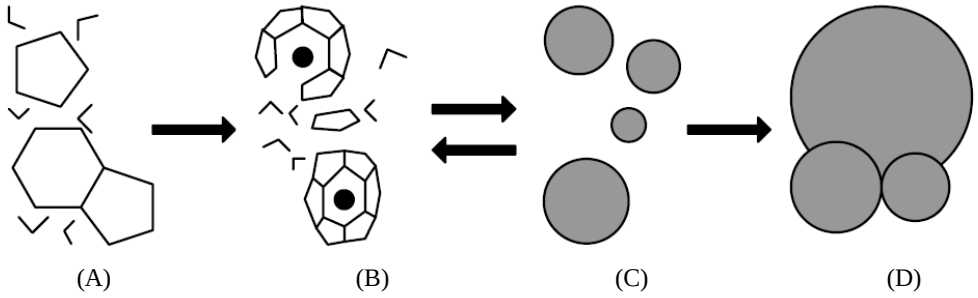

Figure 2.3 Schematic model of labile cluster growth (Sloan and Koh, 2008).

The process of Figure 2.3 can be related to the physical phenomena of an actual pressure–temperature trace at constant volume for hydrate formation and dissociation shown in Figure 2.4, beginning at point 1 with gas and liquid water in a reaction cell. Before point 1, when the system is not pressurised with gas, the water is a hydrogen-bonded network of molecules. At point 1 in Figure 2.4**,** after pressurisation of the system with gas, guest molecules are dissolved in water, and labile clusters have been formed around the apolar guest molecules dissolved in solution. Since the labile clusters are of subcritical size, they must link to other clusters to form aggregates in the metastable period of cooling between point 1 and 2. At point 2**,** the labile clusters have joined to reach the critical size for nucleation. At point 2**,** the primary nucleation is complete and rapid hydrate growth ensues. Rapid hydrate growth is accompanied by a rapid drop in pressure in the constant volume cell due to the encapsulation of gas molecules in the hydrate. In Figure 2.4, the system progresses from point 2 through to the end of the growth period at point 3, where hydrate formation stops. As the system is heated, the temperature rises from point 3 to point A, where the visible hydrate agglomerates decompose into the liquid and vapour

phases, but quasi-crystalline metastable cluster structures remain in the liquid up to a certain degree of superheating. These resilient relics of hydrate structure facilitate rapid growth with subsequent temperature cycles (Christiansen and Sloan, 1994).

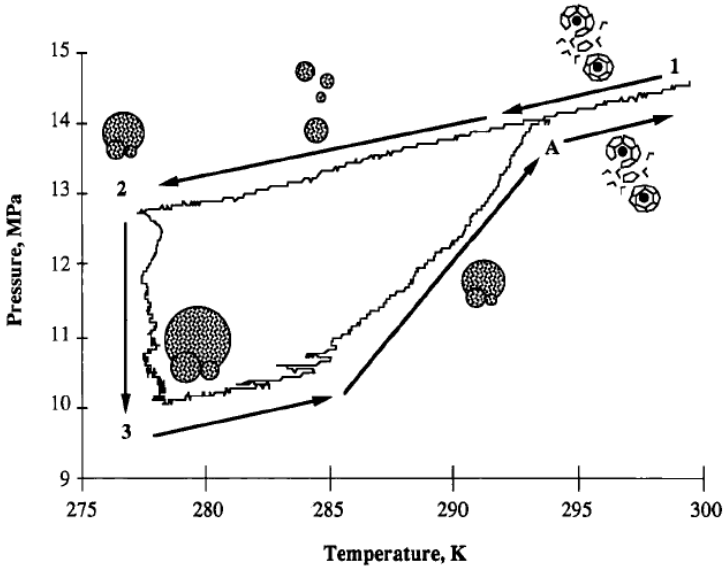

Figure 2.4 Schematic of hydrate formation on an experimental pressure–temperature trace (Christiansen and Sloan, 1994).

2.3.1.2 Nucleation at the interface hypothesis

Supporting heterogeneous nucleation, this conceptual hypothesis was put forward by Kvamme and Long (Long, 1994; Kvamme, 1996). It represents a modification of the labile cluster model, and it is based on the adsorption and clustering on the gas side of the interface (Figure 2.5). It suggests that a gas molecule is transported from bulk to the interface, which is the most favourable site for nucleation. This gas molecule then is adsorbed to the most favourable site at the interface. The water molecule will reorient them around this guest molecule forming first partial and then complete cavities. Labile clusters will agglomerate and grow on the gas side of the interface until the critical size is achieved. The hydrate growth on the gas side of the interface is two times faster than on the waterside, thus hydrate growth on the gas side will dominate (Sloan, 1997).

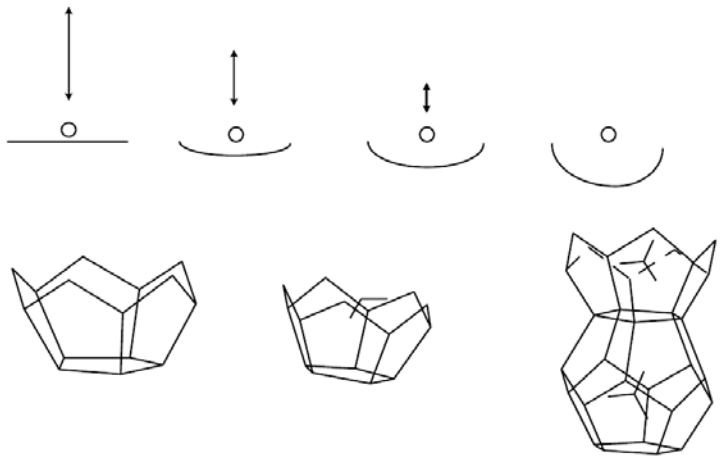

Figure 2.5 Adsorption of gas molecules onto labile hydrate cavities at gas–water interface (Sloan and Koh, 2008).

2.3.1.3 Local structuring hypothesis

An alternative more recent mechanism based on local structuring nucleation (homogeneous nucleation) was suggested by Radhakrishnan and Trout, (2002). It focuses on the local order amongst the guest molecules: random fluctuations (i.e. a thermal fluctuation) eventually lead to a critical number of methane molecules being found in a hydrate-like arrangement that then induces water molecules to adopt a hydrogen bond structure characteristic of hydrates (Hawtin et al., 2008).

At a fundamental level, the difference between this theory and the labile cluster one is whether water-ordering is driven by guest molecules, or guest ordering by water, and the reality is that these are likely to be difficult to separate. At a more practical level, the labile cluster approach relies on particle–cluster aggregation for growth, whereas the local structuring model requires a more collective, longer range motion of the guests (Hawtin et al., 2008). Moon et al., (2003) also proposed a model similar to that of Radhakrishnan and Trout, using MD simulations of methane hydrate nucleation at methane–water interface.

It is plausible that hydrate nucleation proceeds via some combination of these mechanisms. The hydrate nucleation and growth processes may be analogous to the corresponding processes occurring during ice formation. This analogy may be

suggested from the recent MD simulation of ice nucleation and growth resulting in water freezing (Matsumoto et al., 2002). These simulations were run for an extremely long time compared to typical simulations, capturing timescales of up to 500 ns (nanoseconds). Ice nucleation occurs when a sufficient number of relatively long-lived hydrogen bonds develop at the same location to form a compact initial nucleus. The initial nucleus, on reaching a critical size, expands rapidly resulting in the entire system freezing (Sloan and Koh, 2008).

2.3.2 Growth

After nucleation, the second phase of formation involves the growth and coalescence of the crystals to form a solid mass. In this phase, mass and heat transfer become extremely important. The rate of hydrate growth is a combination of two factors kinetics of crystal growth at the hydrate surface, and mass transfer of components to the growing crystal surface. Hydrate growth data and modelling are more tenable than are nucleation phenomena. The state-of-the-art for hydrate growth have been summarised and may be found at the literature (Sloan and Koh, 2008).

2.4 THF hydrates formation

Among numerous compounds known as hydrate formers, THF is unique in that (Iida et al., 2001; Koh et al., 2002):

- It is in the state of a liquid under atmospheric pressure,
- It is unlimitedly soluble in liquid water,
- It forms a sII hydrate, the same hydrate structure formed by natural gas, with a melting point 277.4 K under atmospheric pressure at the molar ratio of THF to water of 1:17 (19.2 wt% of THF),
- If the solution is composed of THF and water at a molar ratio of 1:17, the ratio corresponding to the stoichiometric composition of THF hydrate of sII, any mass transfer process can be eliminated from the process of crystal growth from the

solution, thereby favouring researchers' intention to study hydrate–crystal growth in the most simplified system (Devarakonda et al., 1999),

- It decreases the testing time for hydrate formation compared to the gas–liquid interface due to its miscibility in water that eliminates the problem of interface diffusional resistance during hydrate formation (Rueff and Sloan, 1985; Makogon et al., 1997). Thus, THF hydrate has been employed as a model hydrate for the inhibitor testing (Long et al., 1994; Lederhos et al., 1996), and

- THF hydrate growth can be inhibited by the same KHIs known to be effective against gas hydrates, and it also shows the same memory effect, where recrystallisation occurs rapidly after a brief melting period (Zeng, Wilson et al., 2006). Hydrate reformation in this case is due to heterogeneous, not homogenous nucleation (Zeng et al., 2008).

Owing to its unique nature mentioned above, THF has received the attention of hydrate researchers interested in studying the physical properties (Gough and Davidson, 1971; Ross et al., 1981; Leaist et al., 1982; Ross and Andersson, 1982; Handa et al., 1984; Ashworth et al., 1985; Rueff and Sloan, 1985; White and MacLean, 1985; Tse and White, 1988; Andersson and Suga, 1996). Properties such as density, volume, capacitance, and thermal analysis (heats of formation and dissociation, thermal conductivity, heat capacity and enthalpy of fusion) have been reported for these researchers.

The crystal growth process of THF hydrates has also been a subject of various studies (Pinder, 1965; Scanlon and Fennema, 1971; Makogon et al., 1997; Larsen et al., 1998; Devarakonda et al., 1999; Bollavaram et al., 2000; Hutter et al., 2000; King Jr et al., 2000).

THF forms hydrates in its own right, and as such it affects the thermodynamics of hydrate stability, not just the kinetics. THF is miscible with water, but the H-bond interaction between THF and H_2O is very weak. Therefore, the H-bonding network of water will not be influenced by the addition of THF. This should be related to the promotion of hydrate (Ohtake et al., 2005). With respect to the interaction between

THF and water, recent calculations by Belosludov have indicated that there is considerable polarisation of both the etheric O and water in the host lattice associated when THF is enclosed in a clathrate cage. This does lead to significant perturbations of the water network (General discussion, 2007).

A model reported by Ohtake et al., (2005) shows the formation of THF aqueous THF solutions (Figure 2.6). In this model, THF forms addition-type clusters in aqueous solutions of both, high and low concentrations. It preserves the original hydrogen-bonding network of pure water (including the dodecahedron structure of small hydrate cages) precisely, even in highly concentrated solutions (Figure 2.6 (ii)). As a result, THF can be a guest molecule for hydrate formation (Ohtake et al., 2005).

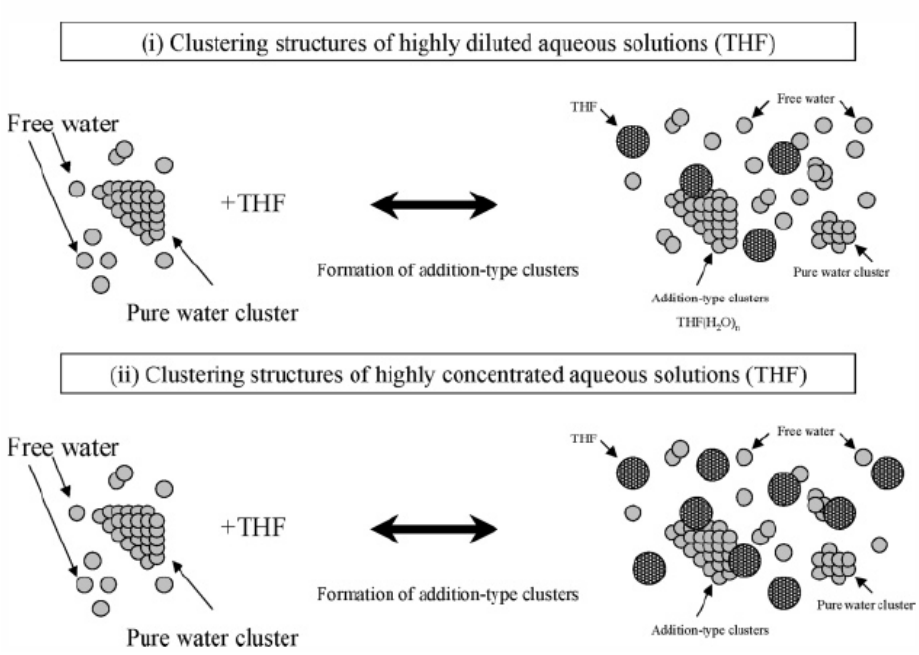

Figure 2.6 Schematic illustrations of clustering structures in aqueous THF solutions (Ohtake et al., 2005).

Another hypothesis for THF hydrate formation was supported by the experimentally observed phenomenon displayed in Figure 2.7. Warm water is loosely hydrogen bonded and the number of these bonds increase as the temperature decreases, forming partial cages. If further cooled without the presence of any foreign atoms or molecules these cages continue to cluster and eventually form ice (Part A, Figure 2.7

b). But guest molecules, like natural gas or THF, enter these cages and form hydrates, which are thermodynamically stable (Part B, Figure 2.7 b). Once crystallisation has begun, THF molecules move into these partial cages stabilising them, thus becoming less available in the bulk. This in turn increases the amount of loose water molecules present in the bulk causing the conductivity to increase. Once these cages are filled, or water is now mostly hydrogen bonded, the conductivity in the bulk starts to drop and finally stabilizes. Conductivity measurements may therefore provide some insight into the THF hydrate formation before and during crystallisation (Devarakonda et al., 1999).

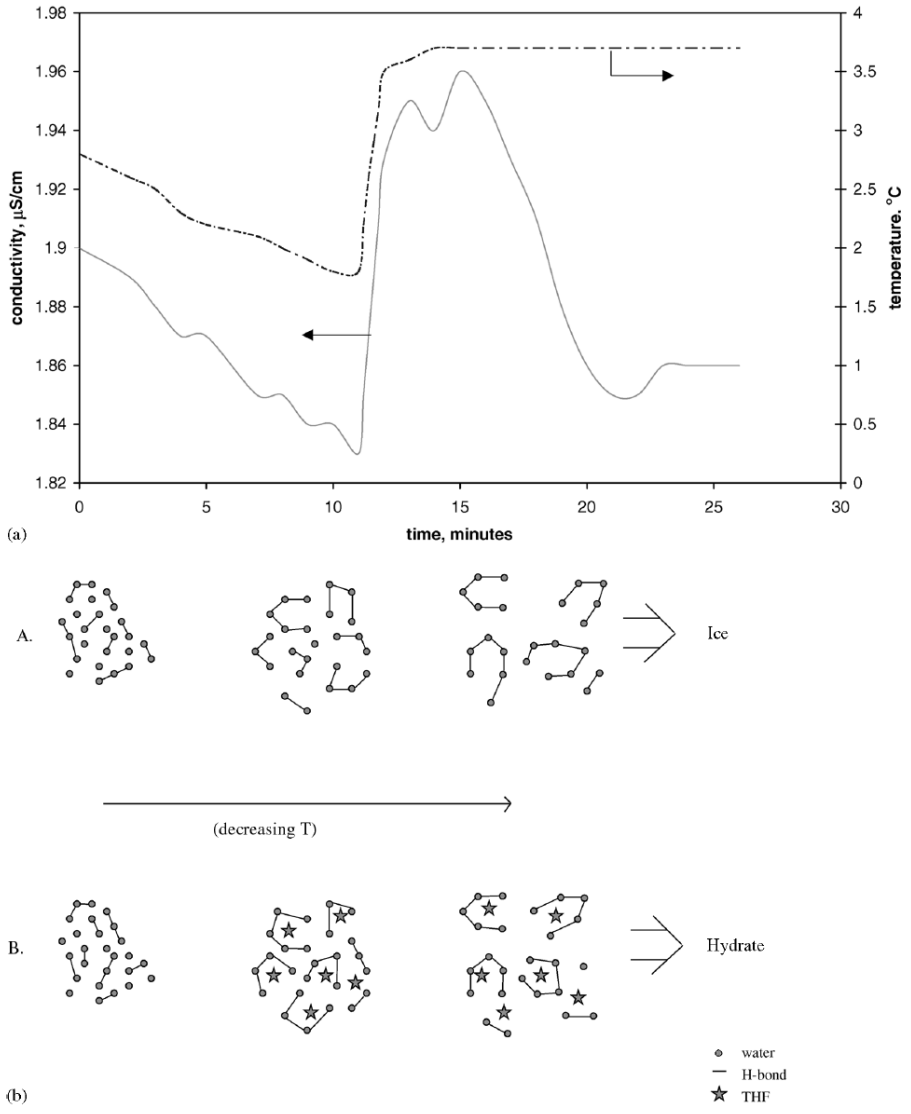

Figure 2.7 (a) Change in conductivity of THF–water solution at fixed hydrate composition with time and temperature; (b) schematic of the proposed hypothesis (Devarakonda et al., 1999).

It should be noted that increasing studies have pointed out that hydrate formation mechanisms for methane hydrate and THF hydrate are very different because THF is miscible with water while the methane is not (Hawtin et al., 2008). This means that methane hydrate formation is predominantly an interfacial phenomenon, whereas THF formation occurs in a bulk aqueous phase. Others reported that the kinetics of formation can be affected by the local inhomogeneities that arise from THF diffusion (Takeya et al., 2007)—an effect that must be greatly enhanced for methane across a methane–water interface (Hawtin et al., 2008).

2.5 Technologies for gas hydrate mitigation, remediation and prevention

Gas hydrates formation requires a source of hydrate forming guest molecules, a supply of water, and a combination of high pressure and/or low temperatures. Several strategies of remediation are based on the modification of one or more of these elements to destabilise the hydrate (Pickering et al., 2001). Four main processes have been investigated in order to combat hydrate plugs and ensure regular flow: chemical, hydraulic, thermal and mechanical processes (Chatti et al., 2005).

The chemical method, which can be used either to prevent or to remove plugs, involves the injection of additives in the pipe that act differently on hydrate agglomeration according to whether the inhibitors are thermodynamic, kinetic or dispersant. The thermodynamic inhibitors, generally methanol (Ng and Robinson, 1985; Bishnoi and Dholabhai, 1999; Jager et al., 2002) or glycols (Elgibaly and Elkamel, 1999; Sun et al., 2001; Mahmoodaghdam and Bishnoi, 2002) and/or aqueous electrolyte solutions (Jager et al., 2002; Englezos and Bishnoi, 1988; Dholabhai et al., 1997), are injected in order to shift the equilibrium temperature, thus enabling gas hydrate crystallization. This method is efficient but limited by the large quantity of additives implemented (60 wt %), which is, moreover, difficult to recover from water, and by the corrosive properties of salts (electrolytes) (Sloan, 1997). A new generation of additives has been developed. These include dispersants such as QAB (quaternary ammonium bromide) that prevent hydrate agglomeration (Koh et al., 2002); and kinetic inhibitors that slow down hydrate crystal growth so

much that it cannot disturb oil transport (Duncum et al., 1993; Sloan, 1995; Lederhos et al., 1996; Karaaslan and Parlaktuna, 2002; Koh et al., 2002). Only small amounts of dispersant and kinetic inhibitors are required to prevent pipeline plugging, making them economically attractive.

The hydraulic removal method is based on the dissociation of the hydrate plug by depressurisation. This method seems promising, given the porous structure of the gas pipeline plugs (Kelkar et al., 1998). However, it is not suitable for liquid hydrocarbons, since depressurisation induces its vaporisation (Chatti et al., 2005). Depressurisation is commonly used for unplanned shutdowns, but it is often impractical for normal operation since the pressures required for transportation of production fluids would usually exceed the hydrate formation pressure at the ambient temperature (Pickering et al., 2001).

The thermal method consists of a local delivery of heat flow towards the plug through the pipe wall in order to raise the system temperature (i.e. insulation, bundles, electric, or hot water heating) above the hydrate formation point. This method is possible for external pipelines but unsuitable for subsea equipment (Sloan, 1997; Kelland, 2000; Chatti et al., 2005).

Finally, a mechanical method, such as pipeline pigging, can be used to prevent hydrate plugs. Pipeline pigs are inserted into the pipe and travel throughout the pipeline, driven by product flow. These projectiles then remove the obstacles or deposits they encounter (Chatti et al., 2005).

Another method to prevent hydrates formation is to remove the supply of water using the separation and dehydration process. This has proven popular for the export of gas, but is impractical for subsea applications. Prevention of formation of hydrates by removing the supply of hydrate forming molecules, perhaps by gas–liquid separation, has also been used for subsea operations. This method could be applied where gas and liquids are separated subsea and transported to the processing facilities in separate pipelines. The gas pipeline still requires hydrate inhibition (through chemical inhibitors), but the liquids line (containing oil and water) is able to operate satisfactorily without forming hydrates due to the absence of water. It is not

known whether such a system has yet been installed and operated in this way (Pickering et al., 2001).

Despite all these methods, which are often very expensive (such as heated pipelines or methanol regeneration facilities), or do not offer a complete solution (i.e. subsea water separation), pipeline blockage by gas hydrates remains a concern in the oil and gas industry, and ongoing research is being conducted in this field (Kelland, 2006). In particular, transmission lines are increasingly being placed in deepwater pipelines. The selection of an optimal method involves taking into account the type of products (gas, liquid hydrocarbon or crude oil) transported and the type of pipeline (external, subsea) used. Sometimes, several strategies are combined to destroy plugs more efficiently; for instance, chemical inhibitors can be used in conjunction with a mechanical removal method (Sloan, 1997; Chatti et al., 2005). Hence, there is a clear need for cheaper technologies such as low dosage chemical technologies (Kelland, 2000).

2.5.1 Chemical inhibition of gas hydrates

The various chemicals available for hydrate prevention fall into three classes: traditional thermodynamic inhibitors, novel kinetic inhibitors and novel anti-agglomerant inhibitors. Table 2.2 presents a summary of applications, and the benefits and limitations of chemical inhibitors. The salient features are summarised below. For a more detailed discussion, Kelland et al., (1995) present a good overview.

Table 2.2 Summary of applications, benefits and limitations of chemical inhibitors (Pickering et al., 2001).

Thermodynamic	Kinetic	Anti-Agglomerant
Applications		
Multiphase Gas & condensate Crude Oil	Multiphase Gas & condensate Crude Oil (limited)	Multiphase Gas & condensate Crude Oil
Benefits		
Robust & effective Well understood Predictable Proven track-record	Lower operational expenditure (OPEX)/capital expenditure (CAPEX) Low volumes (<1 wt %) Environmentally friendly Non-toxic Tested in gas systems	Lower operational expenditure (OPEX)/capital expenditure (CAPEX) Low volumes (<1 wt %) Environmentally friendly Non-toxic Wide range of subcooling
Limitations		
Higher OPEX/CAPEX High volumes (10-60 wt %) Toxic/hazardous Environmentally harmful Volatile-losses to vapour Salting out	Limited subcoolings (<10°C) Time dependency Shutdowns System specific –testing Compatibility Precipitation at higher temperature Limited experience in oil systems No predictable models	Time dependency Shutdowns Restricted to water cuts System specific –testing Compatibility Limited experience No predictable models

2.5.1.1 Thermodynamic hydrate inhibitors (THIs)

These chemicals work by shifting the thermodynamic stability boundary of hydrates (alternating the chemical potential of the aqueous phase) such that the equilibrium dissociation curve is displaced to lower temperatures and higher pressures. Makogon et al., (2000, p.785) reported that, "With an increase in concentration of alcohols in water, a breakdown is observed in the structural organisation of water and in the clathrate-forming aggregates. As a result, the probability of hydrate formation is reduced". This observation suggests that the thermodynamic inhibitors change the structure of water away from that favouring hydrate formation as a part of their effect. A neutron diffraction study of a 1:9 molar ratio methanol–water mixture showed the experimental evidence that water molecules form a disordered hydrogen bonded cage around the methanol molecule.

THIs are added at relatively high concentrations (10-60 wt% in the aqueous phase) and annually, oil and gas companies spend over 500 million U.S. dollars on hydrate prevention via methanol injection, with significant economic costs and potential

environmental effects (Anderson et al., 2005). Examples of THIs include methanol, glycols and electrolytes (Makogon et al., 2000; Pickering et al., 2001).

2.5.1.2 Low dosage inhibitors (LDHIs)

In general, the industry is content with the current technology in dealing with hydrates, i.e. dehydration, heating, and thermodynamic suppression. At the same time, it is widely recognised that the current technology does not always satisfy the economic, operational, and environmental constraints applied in offshore drilling and production operations. Consequently, a new, less conservative, approach has emerged that targets some low concentration inhibitors that can induce one or more of the following effects (Yousif et al., 1994):

- Delay the appearance of the critical nuclei.
- Slow the rate of hydrate formation.
- Prevent the agglomeration process.

In the last 15 years or so, many research efforts have focused on developing what are termed low dosage hydrate inhibitors, or LDHIs, that can kinetically inhibit hydrate formation. LDHIs operate very differently to thermodynamic inhibitors such as methanol. They are often effective at concentrations as low as 0.5 wt% and act by delaying the onset of hydrate formation, whereas thermodynamic inhibitors are effective only at much higher concentrations and act by changing the conditions of hydrate thermodynamic stability (Anderson et al., 2005).

LDHIs are divided into two main product classes: kinetic hydrate inhibitors (KHIs) and anti-agglomerants (AAs) (Kelland et al., 2008).

<u>Kinetic hydrate inhibitors (KHIs)</u>

KHIs are a class of low dosage hydrate inhibitors (LDHIs) that have been in commercial use in the oil and gas industry for about 14 years (Del Villano et al., 2008). This class of chemicals does not alter the thermodynamics of hydrate

formation, but instead modifies the kinetics of hydrate formation. They achieve this both by prevention of nucleation and by hindering crystal growth (Pickering et al., 2001). KHIs delay the nucleation and usually also the crystal growth of gas hydrates. The nucleation delay time (induction time), which is the most critical factor for field operations, is dependent on the subcooling (ΔT) in the system – the higher the subcooling the lower the induction time (Kelland et al., 2008). Their effect is time dependent and ultimately hydrates will form and block the pipeline but only if the transit time through the pipeline is sufficiently long, for example, following a shutdown (Pickering et al., 2001).

KHIs are water-soluble polymers, often with added synergists that improve their performance, which are added at low concentrations (typically less than 1 wt% in the aqueous phase). There are currently only two main classes of polymers used in KHI formulations in oil and gas field operations: homo- and copolymers of vinylcaprolactam, and hyperbranched poly(ester amide)s (Del Villano et al., 2008). Some examples of known and patented inhibitors are poly(*N*-vinylpyrrolidone) (PVP), poly(*N*-vinylcaprolactam) (PVCap), poly(*N*-methyl-*N*-vinylacetamide) (VIMA), poly(*N*-vinylvalerolactam) (PVVam), poly(acryoylpyrrolidine) (PAPYD), poly(acryloylmorpholine) (PAMOR), and poly(vinylmethylacetamide-vinylcaprolactam) (Freer and Sloan Jr, 2000; Pickering et al., 2001).

The activity has been shown to be greatest when the polymers are of low molecular weight (8–16 monomers). LDHIs are generally believed to be active through surface docking—analogous to fish anti-freeze proteins on the surface of ice crystals—but there is no proven mechanism for their activity, and this absence is hindering the rational development of more effective LDHIs (Hawtin and Rodger, 2006).

Natural inhibitors

Antifreeze proteins (AFPs) and antifreeze glycoproteins (AFGPs) have also been shown to be effective LDHIs (Zeng, Moudrakovski et al., 2006; Zeng, Wilson et al., 2006; Zeng et al., 2008). It has been shown that AFPs have higher inhibition activities than the commercial LDHI poly(*N*-vinylpyrrolidone) (PVP) (Zeng, 2007).

Remarkably, active AFPs also demonstrate the novel ability to eliminate the memory effect (that is, faster reformation of hydrate after melting), while PVP did not (Zeng, Moudrakovski et al., 2006; Zeng, Wilson et al., 2006).

These proteins bind to the surface of ice nuclei (Kelland, 2006). They inhibit the formation of ice and recent work has demonstrated that AFPs can also prevent hydrate growth (Zeng et al., 2003). They are naturally synthesised by cold adapted species of fish, plants and insects that live in sub-freezing environments (Al-Adel et al., 2008).

Anti-agglomerant (AAs)

These chemicals do not seek to prevent hydrate formation, but rather to prevent the crystals from agglomerating and forming a blockage. They are surface active chemicals that adhere to hydrate crystals helping to stabilise the crystal in a continuous oil phase. Their main limitation is that they require a continuous oil phase and are therefore only applicable at lower watercuts. AAs are added in low doses (typically less than 1 wt% in the aqueous phase), and examples include alkyl aromatic sulphonates or alkylphenylethoxylates. AAs can also display a kinetic inhibition effect and are sometimes in the class of KHIs (Pickering et al., 2001).

AAs are surfactants that prevent hydrates from accumulating into large masses or depositing in conduits, forming a slurry of fine transportable hydrate particles. The mechanism is dependent on there being a liquid hydrocarbon phase present in which hydrate crystals form the slurry. Therefore, they do not appear to be applicable to water-based drilling fluids (Kelland et al., 2008).

The field implementation of the anti-agglomerant LDHIs demonstrates their ability to provide reliable and cost effective hydrate control solutions for deepwater pipeline operation. The dosage rate of the LDHIs is orders of magnitude lower compared to methanol or glycol, with volume reductions greater than 25 times. This allows for less topsides storage space, easier transportation, and smaller umbilicals. LDHIs can thus provide significant capital expenditure (CAPEX) savings by eliminating bulky

topsides equipment, in addition to potential operational expenditures (OPEX) savings in treatment costs. The use of LDHIs also eliminates the discharge of methanol in overboard water and oil and gas export lines. The proven field success of LDHIs technology will have a major impact on system selection, design, and operation of all new field developments (Mehta et al., 2002).

2.6 Mechanisms of gas hydrates inhibition by LDHIs

There has been much discussion, and disagreement regarding the mechanism by which LDHIs inhibit hydrate formation (Anderson et al., 2005). LDHIs are generally believed to be active through surface docking—analogous to fish anti-freeze proteins on the surface of ice crystals—but there is no proven mechanism for their activity and this absence is hindering the rational development of more effective LDHIs (Hawtin and Rodger, 2006). Furthermore, no proposed mechanism fully explains all of the phenomena associated with hydrate kinetic inhibition, such as increased induction time with sudden growth coupled with the crystal morphology changes observed in inhibited growth conditions (Anderson et al., 2005). Molecular simulation is an increasingly useful tool to probe the still relatively poorly understood microscopic processes by which gas hydrates form or, indeed, are inhibited from forming. The field of hydrate simulation has included several attempts to use molecular simulation to gain an understanding of inhibition mechanisms, with the ultimate aim being to be able to design inhibitors and/or rank their performance without the need for costly laboratory experiments (Hawtin and Rodger, 2006).

2.6.1 Kinetic inhibition mechanism

Several different mechanisms explaining the working of KHIs have been suggested. Most of them relate the action of the KHIs with modification of water structures, increases of the mass transfer resistance, adsorption of the active sites of growing crystals surfaces, and prevention of the hydrate crystal agglomeration (Long, 1994). However, knowledge about their effects on the unavoidable heterogeneous nucleation of gas hydrate is limited (Colle et al., 1999). Following is a discussion of the theoretical approaches suggested by some of the leading hydrate research groups.

A proposed mechanism that has also been observed by molecular dynamics simulations relates the inhibition activities to the effects of the KHIs on the water structures during the homogeneous nucleation preventing the formation of the critical nuclei (Talley and Edwards, 1999; Hawtin and Rodger, 2006; Kelland, 2006; Moon et al., 2007). This suggests the perturbation of the water structure prevents growth of hydrate particles to the critical cluster size or destabilisation of partially formed hydrate clusters. A water-soluble polymer causes water molecules to form cage-like structures around it. Polymers with large hydratation volumes interrupt gas molecules that are clustering in the water. Without clustering, hydrate crystals cannot form (Talley and Edwards, 1999).

Another report suggests that KHI polymers adsorb to the surfaces of "foreign" particles that would otherwise induce hydrate heteronucleation (Zeng et al., 2008). This mechanism is focused on the effect of the LDHI on heterogeneous nucleation and subsequent growth of hydrate crystals. It is well-known that a suitable contaminant or "sympathetic" surface is needed to induce heterogeneous nucleation. Thus, it is reasonable to propose that a good inhibitor of heterogeneous nucleation can adsorb and deactivate the nucleation sites, including impurities such as hydrated oxides of Si or Fe, or even hydrophilic container walls. As a consequence, the probability of subsequent formation of ice/clathrate hydrate is reduced (Zeng, 2007).

A third mechanism involves adsorption of the KHI polymer on the surfaces of growing particles or crystal of hydrate (sub-critical or super-critical size) perturbing their nucleation and/or further growth (Moon et al., 2007; Hutter et al., 2000; Larsen et al., 1998; Lederhos et al., 1996; Carver et al., 1995). For example, hydrophobic hydrocarbyl groups on side-chains of KHI polymers fit as pseudo-guest molecules in incomplete clathrate hydrate cavities (Van der Waals interactions), with extra binding to the surface caused by hydrogen-bonds from nearby amide groups. Binding of several side-chains to the hydrate surface is needed to keep it adsorbed and to provide a barrier for further crystal growth (Del Villano and Kelland, 2009). Among the KHIs tested, PVCap has been recognised as being more effective than PVP (Lederhos et al., 1996). Based on molecular simulations, Makogon and Sloan, (2002) shown that the inhibition mechanism consists of two main components: adsorption of the inhibitor on a hydrate and blockage the diffusion of gas to the hydrate surface.

Inhibitor polymer side groups adsorb to the hydrate crystal surface by hydrogen bonding. By adsorbing onto the hydrate crystal, the polymer forces the crystal to grow around and between the polymer strands, with a small radius of crystal curvature. Inhibitors also sterically block the diffusion of non-polar solutes such as methane from entering and completing a hydrate cavity. A weak interaction between non-polar solute and the hydrophobic part of the inhibitor side groups has been also observed in the model (Makogon and Sloan, 2002).

Based on the local structuring hypothesis summarised briefly in section 2.3.1.3, some researchers from the Massachusetts Institute of Technology (MIT) have proposed that hydrate inhibition occurs via a two-step mechanism (Anderson et al., 2005):

- As potential guest molecules become coordinated by water, form nuclei, and begin to grow, nearby inhibitor molecules disrupt the local organisation of the water and guest molecules, increasing the barrier to nucleation and nuclei propagation (Figure 2.8).

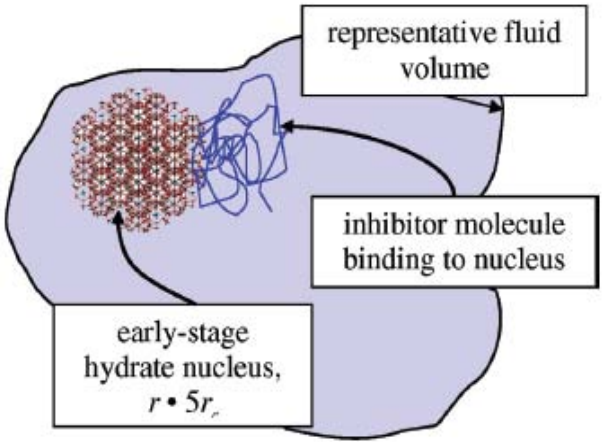

Figure 2.8 Conceptual model for inhibitor binding and crystal growth inhibition. Shown is step one of the two-step mechanism for hydrate inhibition. Inhibitor molecules disrupt the local organisation of water and guest molecules and attach to forming hydrate nuclei, transferring enthalpy locally into the nuclei (Anderson et al., 2005).

- Once nucleation occurs, the inhibitor molecules bind to the surface of the hydrate nanocrystal and retard further growth along the bound growth plane, resulting in a modified planar morphology (Figure 2.9).

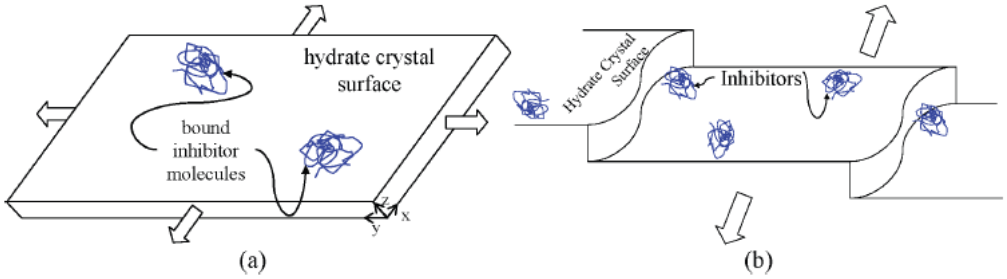

Figure 2.9 Step two of the conceptual model for inhibitor binding and crystal growth inhibition: (a) Once the crystal has nucleated and crystal growth begins, the inhibitor binds to the surface and retards growth in the z-direction by hindering step growth through the process of step-pinning (b) (Anderson et al., 2005).

In the first step, the disruption of newly forming nuclei occurs as proposed by Storr et al., (2004). They found that the hydrophilic group of a new KHIs, tributylammoniumpropylsulfate, enhances the water structure in the mid-long range, but in a way that is incompatible with the hydrate ordering, thus preventing hydrate formation (Storr et al., 2004).

In step two of the mechanism proposed, the hypothesis tested that the degree of inhibition is related to the strength of the binding of the inhibitor to the surface of the hydrate crystal (Anderson et al., 2005). It has based on the experimental observations made by several groups (Makogon et al., 1997; Larsen et al., 1998; Sakaguchi et al., 2003; Storr et al., 2004). These researchers found that addition of PVP and PVCap gave rise to plate-like hydrate crystals. Thus, KHIs adsorbing on the hydrate surface will retard any further growth in that direction and leave only the possibility of growth in other directions. King and co-workers' (King Jr et al., 2000) experiments show that a non-inhibitor, poly(ethylene oxide) (PEO) is not adsorbed on hydrate surface, in contrast to PVP, PVCap and VIMA which do adsorb on the hydrate surface, further supporting the surface binding hypothesis.

Based on these results, it was proposed that the stronger the KHI binds to the hydrate surface, the more disruptive the inhibitor is to the structure of forming hydrate nuclei (Anderson et al., 2005). In addition, two molecular characteristics that lead to strongly binding inhibitors were found (Anderson et al., 2005):

- A charge distribution on the edge of the inhibitor that mimics the charge separation in the water molecules on the surface of the hydrate and,

- An inhibitor size similar to the available space at the hydrate-surface binding site. These two molecular characteristics result in strong hydrogen bonding between the inhibitor molecule and the surface of a forming hydrate crystal, and thus lead to more effective inhibitor molecules.

Using MD, the two-fold mechanism has been tested by four inhibitor molecules (PEO, PVP, PVCap, and VIMA). PVCap and VIMA, the more effective inhibitors, showed strong interactions with the liquid water phase under hydrate-forming conditions, while PVP and PEO appeared relatively neutral to the surrounding water (Anderson et al., 2005).

Using molecular simulations, some researchers at the University of Warwick have studied water–methane–hydrate mixtures focused on PVP, and have suggested that it is the surface energy effect of the PVP oligomers that is responsible for their inhibition effectiveness (Moon et al., 2007). They showed that it destabilised the hydrate without the need for direct contact between the inhibitor and the hydrate, although the PVP was observed to remain within 3-4 water layers of the hydrate surface while the hydrate decomposed. This raises the possibility that inhibition mechanisms other than surface docking may be significant (Hawtin and Rodger, 2006).

They compared the PVP results with those from their earlier study of PDMAEMA, poly(dimethylaminoethylmethacrylate) (Hawtin and Rodger, 2006). This work hypothesised that PVP inhibits hydrate formation by increasing the surface energy of the interfacial region, whereas PDMAEMA inhibits by adsorbing to the surface of hydrate nanocrystal. PVP is present in the interfacial region without binding

irreversibly to the hydrate crystal. The inhibition caused by PVP can be explained as follows (Moon et al., 2007):

- Transient filaments of hydrate water molecules do form from the pyrrolidone groups. Indeed it is possible for several filaments to form from the same oligomer, but in this case they are likely to be incommensurate with each other and so frustrate, rather than reinforce, hydrate formation (Figure 2.10).

- A halo region is created around the hydrate due to initiation of transient filaments around the hydrate cluster that would be disrupted by the incommensurate filaments arising from the PVP. The halo effect caused by the insertion of PVP forms a viable mechanism to explain the kinetic inhibition of hydrate formation.

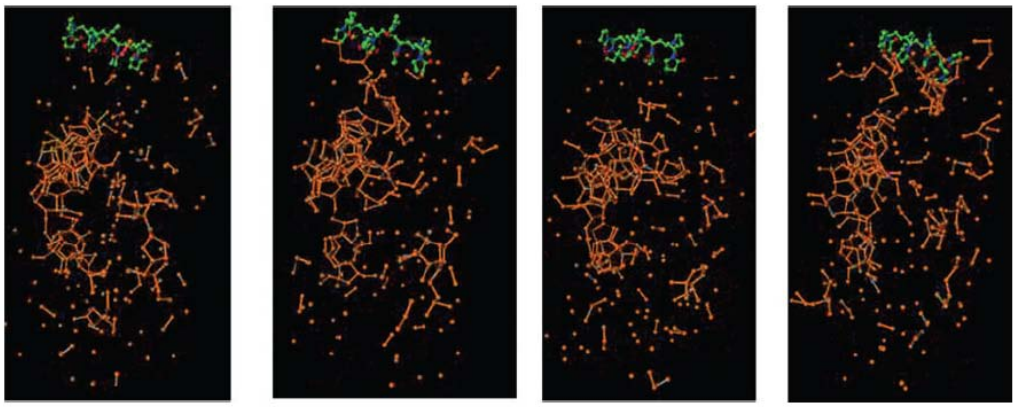

Figure 2.10 Snapshots taken from PVP simulations. The snapshots are presented in chronological order. Hydrate water is depicted in brown, and the PVP carbon, oxygen and nitrogen atoms in green, red and blue, respectively (Moon et al., 2007).

They found that LDHIs (specifically tributylammoniumpropylsulfonate (TBAPS), PVP, PVCap, and poly(dimethylaminoethyl methacrylate) (PDMAEMA)) reduce the degree of the aqueous solvation structure, which would presumably increase the barrier to hydrate nucleation (Anderson et al., 2005).

Kvamme et al., (2005) at the University of Bergen suggested a theory based on interactions between hydrate water and inhibitor. It was proposed that the stronger the interaction between inhibitor–hydrate water, the higher the inhibition efficiency.

Several inhibitors, like PVP, PVCap and Gaffix® VC713 were studied. Based on the analysis, the following conclusions were drawn:

- Both PVP and PVCap have the tendency to position themselves at hydrate – liquid interface and form hydrogen bonds between hydrate water and carbonyl oxygen, thus potentially inhibiting further growth.

- PVCap outperforms PVP as KHI since the potential energy of the inhibitor – hydrate interactions was significantly lower for PVCap then for PVP with both Coulomb and Lennard–Jones contributions (Kvamme et al., 2005) favouring PVCap over PVP.

Later a theoretical hypothesis was put forward suggesting that the PVP reduces the contact area and limit the mass transport between water and hydrate former causing further delays in hydrate formation and growth (Kvamme and Asnes, 2006). In this hypothesis, PVP is assumed to form a separate phase by creating a layer in-between the water and the gas phase. Diffusion of hydrate former through the polymer phase was thus suggested as a limiting factor in the hydrate formation process.

2.6.2 Anti-agglomerant inhibition mechanism

The mechanism of anti-agglomerant LDHI could be different. A hypothetical mechanism for anti-agglomerant hydrate inhibitors could be due to a distorted hydrate lattice formation. Anti-agglomerant inhibitors are hypothesised to promote distorted hydrate crystals leading to reduced crystal size and to form an oleophilic layer that blocks water and disperses crystals in oil (Makogon and Sloan, 2002).

According to Makogon and Sloan, (2002), a tertiary-butyl amine hydrate has a cubic symmetry and a 19Å unit cell, which is larger than a sII unit cell size of 17.3 Å. The distorted hydrate nuclei promote the formation of hydrate, but limit the size of hydrate particles as crystal defects make further growth energetically unfavourable. Simultaneously, the hydrocarbon radicals of anti-agglomerants form an oleophilic barrier on the crystal and block the diffusion of water to the hydrate crystal. If this

hypothesis is correct, one should be able to control the hydrate particle size distribution with the concentration of anti-agglomerant inhibitor. Some substantiation is seen from Monfort et al., (2000). Molecular simulations of this class of chemicals by Storr and Rodger, (2000) showed preferred adsorption locations for quaternary ammonium sulfonate zwitterions and proposed a lock-and key mechanism for these inhibitors (Makogon and Sloan, 2002).

2.7 Experimental measurements on gas hydrates

The growing interests in gas hydrates from various disciplinary fields, which results in the need of management of gas hydrates, for both prevention or utilisation, have demanded extensive studies on gas hydrates properties and characteristics that are associated with their formation, decomposition, and inhibition processes, and the factors that might affect these properties and processes. This in turn requires advanced experimental methods and instrumental techniques for gas hydrate characterisation. The insightful understanding of these properties will help in planning long-term effective and sustainable strategies for the management and application of gas hydrates (Rojas and Lou, 2010).

Traditional studies on both theoretical prediction (molecular thermodynamic simulation) and experimental characterisation of properties, including phase equilibria, structures and occupancy, are generally related to the measurement of parameters, such as pressure, temperature and fluid–phase compositions, and involve mainly macroscopic and mesoscopic instruments such as high-pressure visual cells, rheometers, calorimeters, flow loops, flow wheels, and X-ray computerised tomography (Makogon, 1997; Sloan and Koh, 2008). In recent decades, the development and advancement of more powerful and selective instruments have allowed one to obtain a more accurate estimation of hydrate properties as well as more precise information about the characteristics of gas hydrates (Sloan, 2003a). Many of the recent research activities have shifted to thermal analysis, crystallographic analysis, topographic analysis, and more significantly spectroscopic analysis at the molecular or atomic level.

A review of hydrate characterisation methods has been provided by Malone in the early 1990s (Malone, 1994), which focused mainly on geophysical analysis. Some techniques and selected case studies that are associated with the application of these methods, and the phase equilibria and thermal property measurement have been described by Sloan et al., (Sloan, 1997, 2003a; Sloan and Koh, 2008) and have become useful references for many researchers. Recent studies by Tulk and Susilo and co-workers have, respectively, indicated the importance and dissimilarity of a few spectroscopic methods that are increasingly used in hydrates studies in recent years (Tulk et al., 2000; Susilo et al., 2007). There has not been a handy reference that systematically covers a large spectrum of instrumental methods that are useful in the characterisation of gas hydrates properties.

More recently, the author has co-authored a review on all key instrumental analysis methods that have been employed in the gas hydrate R&D activities in the past 15 years. This review focuses on the gas hydrates property measurements in various phases. Complementary experimental methods which have become increasingly attractive for an ultimate understanding of their formation, dissociation and inhibition, have been provided (Rojas and Lou, 2010). These include thermal analysis, crystallographic analysis, topographic analysis, size and size distribution analysis, spectroscopic analysis, interfacial tension and intermolecular particle force analysis, and methods involving gas hydrates inhibition. A summary of the different methods used for hydrate characterisation is shown in Table 2.3. Some of the basic physical science principles of each method and the gas hydrate properties that each method is capable of detecting, and some modern instrumental analyses that enable direct determination of gas hydrate phases and possible measurement of molecular interactions within the fluid phases, are documented.

Although each of these instrumental techniques provides useful and valuable information about hydrate properties, no single technique can, on its own, reveal the complex gas hydrate systems (Serdyuk et al., 2007). There are challenges ahead. For instance, in situ studies are important for the direct analysis of hydrate systems that require meticulously designed reactors and/or cells that facilitate hydrate formation at high pressure and low temperature (Sloan and Koh, 2008). Some properties and kinetics of gas hydrates are apparatus-dependent (Susilo et al., 2007); accurate

correlation and interpretation of experimental data from different methods require a feasible approach that allows simultaneous measurement on the same hydrate systems using different analytical tools. For the same reason, translation from laboratory to field work, a natural gas pipeline, for example, is also a challenge (Sloan, 1997). Distinguishing hydrates from ice is another challenge for the implementation of most of the aforementioned techniques (Giavarini et al., 2006). Apart from these challenges, extensive data management, excellent computational models, and efficient communication between experimental engineers, scientists, and the molecular simulation engineers are also critical factors (Rojas and Lou, 2010).

In the following chapters, we will investigate the formation and inhibition mechanism of THF hydrates and natural gas hydrates in the presence of, or without, the kinetic inhibitors. Interfacial and electrokinetic techniques will be used together with kinetic experiments for an understanding of the mechanism by which KHIs delay the massive hydrate growth and plugging.

Table 2.3 Instrumental analysis used for gas hydrate characterisation (Rojas and Lou, 2010).

Instrument	Properties of gas hydrates
Thermal	
DSC, MicroDSC, TMDSC	Thermodynamic and equilibrium properties (formation and dissociation enthalpies, thermal conductivity, and heat capacities); solid-liquid phase transitions and compositions under high pressure; slow dynamics; nucleation and melting, lattice destruction and decomposition; kinetics, thermodynamics, polymer-water interactions, mode of action of gas hydrate inhibitors; emulsion stability.
Crystallographic	
XRD	Structure identification; lattice parameters; guest occupancy and composition during formation; decomposition; thermal expansion; growth rate.
PXRD	Size and structure of crystallite; preferential orientation in polycrystalline or powdered solid samples; phase identification; decomposition temperatures; changes in lattice parameters vs. temperature; thermal expansion; phase transitions properties under high pressure.
CT	Formation and dissociation of core samples; location and identification of gas hydrates in sediments; 3-D morphology; pore-space pathways; thermal conductivity, diffusivity and permeability.
Neutron Diffraction	Molecular dynamics; vibrational characteristics; rotational and translational motion; guest/host placement; caging occupancy; hydration structure around guest molecules; kinetics of formation and dissociation and transformation processes.
NPD	Thermodynamic/structural studies; composition and kinetic behaviour; structural changes and transitions during hydrate formation.
INS	Guest/host molecular interactions in the hydrate lattice; thermal conductivity of crystalline clathrates; vibrational dynamics.
SANS	Structure of water molecules around dissolved methane molecules during methane hydrate formation.
Topographic	
OM	Crystal-growth behaviour; equilibrium morphologies; relative growth rates of specific crystallographic planes; equilibrium data; hydrate film thickness and growth rate in a water droplet.
SEM	Growth processes and morphology; phase distribution, crystal contacts and structures; microstructural development in hydrate-bearing sediment assemblages.
Size and size distribution	Hydrate nucleation/formation and growth, hydrates particle formation in water/gas hydrate interface, size and size distribution of hydrate particles, induction time.
Spectroscopic	
NMR/MRI	Structure identification; chemical composition; cage occupancy and water mobility; the magnitude of spin-spin and spin-lattice interactions; relaxation processes and their dependence on temperature and pressure; defects, thermal fluctuations, translation and rotation of molecules in hydrate; enclathrated guest molecules and their concentrations.
Raman	Vibrational energies of the interstitial gas molecules, microstructural features of natural samples, structure and stability, formation and decomposition processes, molecular dynamics, composition and cage occupancies.

Interfacial tension and intermolecular particle forces	Forces between the molecules and interactions between hydrate particles, memory effects and the membrane force working in the hydrate films, effect of the presence of different surfactants and polymers, effect of micelles and critical micellar concentration (CMC) under hydrate-forming conditions.
Minor methods	
IR	Molecular interactions related to the vibrational, rotational, and translational motion of the molecules (Makogon, 1997).
DS	Internal dynamics related to electrical properties of gas/water molecules (Makogon, 1997).
ARS	Measurement of hydrate equilibration temperatures; hysteresis of growth, decomposition and kinetics (Sivaraman, 2003).
EPR	Hydrates formation in water droplets; study of radicals produced in ethane hydrate through irradiation with γ-rays (Kommaredi et al., 1994; Makogon, 1997).
MS	Molecular clustering structure; mass spectra of the clusters of water-methanol and water-propanol solutions (Yamamoto et al., 2000).
LI	Rapid formation and dissociation processes in slow motion (Sivaraman, 2003).
QCM	Screening low dosage hydrate inhibitors (LDHIs); structural changes of macromolecules upon adsorption to the surface; dissociation temperatures (Zeng, 2007).

DSC: differential scanning calorimetry; TMDSC: thermal modulated differential scanning calorimetric; XRD: X-ray diffraction; PXRD: powder X-ray diffraction; CT: X-ray computerised tomography; NPD: neutron powder diffraction; INS: inelastic neutron scattering; SANS: small-angle neutron scattering; OM: optical microscopy; SEM: scanning electron microscopy; NMR: nuclear magnetic resonance; MRI: magnetic resonance imaging; IR: infrared spectroscopy; DS: dielectric spectroscopy; ARS: acoustic resonance spectroscopy; EPR: electron paramagnetic resonance spectroscopy; MS: mass spectrometry; LI: laser imaging; QCM: quartz crystal microbalance.

Chapter 3 KINETICS OF THF HYDRATE FORMATION AND EFFECTIVENESS OF HYDRATE INHIBITORS

3.1 Introduction

In this chapter, the formation kinetics of THF hydrates in the absence and the presence of five kinetic inhibitors are investigated through the measurement of several experimental parameters that are associated with the nucleation and crystal growth process of THF hydrates.

Quantifying and understanding the kinetics of hydrate formation during hydrate nucleation has become an important issue for the gas hydrate research community (Sloan Jr, 1994; Talley et al., 2000). A good knowledge of the kinetics of hydrates formation would provide for the effective control of the hydrate formation rate (Bishnoi and Natarajan, 1996). This would also assist in the design of new inhibitors and the creation of new technologies for effective applications of gas hydrate technologies in other industries (Makogon et al., 2000).

Hydrate formation is viewed as a crystallisation process that includes two stages, i.e., nucleation and growth of hydrate crystals. Hydrate nucleation is an intrinsically stochastic process that involves the formation and growth of gas-water clusters to critical sized, stable hydrate nuclei. The growth process involves the growth of stable hydrate nuclei into solid hydrates (Bishnoi and Natarajan, 1996).

In comparison to hydrate equilibrium thermodynamics, the knowledge on the kinetics of hydrate formation is far from mature due to the complexity of the dynamic process of hydrate formation, and the lack of experimental sets-up to produce consistent and useful data. The latter was due to the difficulty to obtain quantitatively experimental data during the hydrate stability conditions, the event used for the hydrate detection, and the apparatus-dependence of the data (Sloan Jr, 1994; Talley et al., 2000). For the same reasons, the kinetics data on hydrates cannot be clearly interpreted and are not comparable, therefore, cannot be conveniently

translated to gas pipelines conditions (Makogon, 1997; Sloan, 1997; Makogon et al., 2000; Sloan and Koh, 2008).

The first challenge in designing a hydrate kinetics experiment is to establish how hydrates will be detected. The following four events have been used in the experimental design as they are an indicator of the onset of hydrates formation (Talley et al., 2000):

1. A gas volume decrease in excess of vapour–liquid equilibration in a closed, constant-pressure system;
2. A pressure drop in excess of vapour–liquid equilibration in a closed, constant-volume system;
3. An increase in temperature due to the heat of formation of hydrates; and
4. An increased differential pressure drop in a flowing system.

Based on the four events described above, several parameters have been reported to describe hydrate formation and to characterise the effectiveness of hydrate inhibitors in kinetic measurements. These include:

- Induction time at a constant temperature, t_{ind}: Induction time is defined as the elapsed time from the start of the experiments to the onset of hydrate formation (Arjmandi et al., 2005). This is a measure of the ability of a supersaturated system to remain in the state of metastable equilibrium without nucleation (Devarakonda et al., 1999; Kashchiev and Firoozabadi, 2003). The induction time is the most critical factor for field operations (Kashchiev and Firoozabadi, 2003; Del Villano and Kelland, 2009). Long induction time would allow transport of fluids from the production facilities to the processing plants without crystallisation of hydrates in the system (Kashchiev and Firoozabadi, 2003). Induction time has been commonly utilised to infer the molecular mechanisms of the hydrate nucleation process (Vysniauskas and Bishnoi, 1983; Skovborg et al., 1993; Bishnoi et al., 1994; Christiansen and Sloan, 1994; Long et al., 1994; Natarajan et al., 1994; Kelland et al., 1995; Lederhos et al., 1996; Cingotti et al., 2000; Kashchiev and Firoozabadi, 2003). However, the parameter should be used with caution, because, the nucleation process of gas hydrates is random in nature. In other

words, one can get different induction times (nucleation times) for the same conditions of pressure, temperature, and agitation (Lingelem et al., 1994).

- Subcooling: Subcooling is usually considered as the driving force for hydrate formation and a criterion for simulating field conditions (Yousif et al., 1994). It is calculated as the difference between the experimental temperature and the equilibrium temperature at a given pressure at which hydrates form, therefore expressed as $\left| T_{eq}\text{-}T_{exp} \right|$ (Talley et al., 2000; Arjmandi et al., 2005). T_{eq} is defined as the temperature at which a system of fixed composition and pressure is at the hydrate equilibrium (Talley et al., 2000). The maximum subcooling achievable in a system is $\left| T_{eq}\text{-}T_{o} \right|$ in which T_o is the onset temperature of hydrates formation. For most of the experimental works, the onset temperature infers the temperature at which hydrates are first detected due to the macroscopic appearance of the solid phase (Talley et al., 2000; Zhang et al., 2001; Zang et al., 2008). Subcooling at the constant cooling rate appears to be independent of the size and configuration of the reaction vessel, and has been used to investigate the performance of gas hydrates inhibitors. KHIs can be ranked using the achievable subcooling in comparable systems or the values of t_{ind} as a function of subcooling and inhibitor concentration (Talley et al., 2000). Some results from flow loops have indicated that the subcooling data is more reproducible than induction times (Young, 1994). A more recent study has demonstrated that the constant degree of subcooling is an appropriate criterion for up-scaling the tests with pure gas and natural gas (Arjmandi et al., 2005).

- Particle size and morphology: Measurements of hydrate particle size and morphology have also been used to describe hydrate formation and to characterise the effectiveness of hydrate inhibitors in kinetic measurements (morphology refers to the size, shape, and state of agglomeration of the hydrate crystals) (Young, 1994). Since particle size is often difficult to measure directly, many researchers photograph hydrate crystals, for the comparison of both particle size and morphology (Young, 1994). The first work to recognise the importance of the growth of gas hydrate particles in a crystallisation process was that of Englezos et al., (1987a, b). They studied the formation kinetics of hydrates of methane, ethane and their mixtures. However, they could not measure particle size distribution in

their experiments. Nerheim et al., (1992) used a laser light scattering technique to measure the size of nuclei in a static system during the nucleation period. They reported that the critical nuclei sizes were in the range 5-30 nm. In another study, Monfort and Nzihou, (1993) measured the particle size distribution using laser light scattering during cyclopropane hydrate formation. The measured crystals of cyclopropane hydrate were found in the range 5.6 to 564 μm. The study also demonstrated that the size of crystals rapidly increases due to hydrates growth and agglomeration. Monfort et al., (2000) further reported the growth rates calculated using the same experimental method. The calculated maximum growth rates for ethane and propane were 0.35 and 0.045 μm/s, respectively. Makogon, (1997) reported the morphology of methane, ethane and propane hydrates during growth at both static and stirred conditions. He characterised the morphology by defining three types of crystals (massive, gelly and whiskery crystals). Makogon et al., (1999) observed that high porosity gel-like hydrate structures and microcrystals covered with a layer of water form in stirred conditions. Herri et al., (1996) developed an experimental technique (Herri et al., 1999) to use turbidimetry measurements to characterise kinetic inhibitors during the crystallisation of methane hydrate. Their technique allowed them to study the effect of additives on the induction delay and effect of additives on the quantity of hydrates formed. However, their apparatus was only able to measure particle diameters down to 10 μm (Herri et al., 1996). Devarakonda et al., (1999) used an in situ particle size analyser to observe the transient particle size distribution during THF hydrate formation. However, they made no attempt to quantify the intrinsic kinetics of hydrate formation. More recently, Clarke et al., (2005) measured in situ particle size distribution of CO_2 hydrates with a focused beam reflectance method (FBRM) probe.

- The temperature spike at the hydrates formation onset or onset temperature: Hydrate formation is an exothermic reaction. The spike is a good indication of the onset of hydrate formation, and can be conveniently detected using different instruments (Yousif et al., 1994; Devarakonda et al., 1999). The spike is dependent on the reactor volume and the mixing rate (Young, 1994). It is a qualitative tool to detect the onset of hydrate formation. It also has been used to yield quantitative information about the amount of hydrate formation (Yousif et

al., 1994). The spike in the frequency count of the scattered laser light at 90° angle has also been used as an indication of the appearance of the first nuclei of hydrate (Yousif et al., 1994).

- Other parameters: Viscosity as well as conductivity changes have been used to investigate the kinetics of hydrates formation (Devarakonda et al., 1999). Volume or total fraction of hydrate crystallised during a determined time has also been reported together with pressure–temperature hydrate behaviour to quantify the amount of solid hydrates generally formed in a stirred cell (Makogon et al., 2000; Makogon and Holditch, 2001). The volume of hydrate crystallised based on the estimate of moles of gas consumed over a determined time, which is the experimentally accessible quantity (Kashchiev and Firoozabadi, 2003).

Among the above mentioned parameters, onset temperature and induction time are the two parameters most commonly used to describe the hydrate nucleation. Subcooling is also used to investigate the hydrate nucleation and the performance of gas hydrates inhibitors, since it is usually used as the driving force for hydrate formation. The crystal size and morphology are useful for the investigation of hydrates growth rate, and also have potential for comparing results obtained under different experimental conditions. Other parameters might be used for both.

In this chapter, the onset temperature has been chosen as the parameter to detect the onset of THF hydrates formation. It is indicated by an increase in the temperature due to the exothermic crystallisation reaction. Other parameters such as the maximum temperature spike, and the magnitude of the temperature rise associated with the hydrate formation, have also been determined. The time required for the hydrate formation and growth, and the temperature at the end-point of the hydrate formation were also measured.

Five polymer kinetic inhibitors including Gaffix® VC713, Luvicap® EG, PVP40 and PVP360 and a copolymer of poly(ethylene oxide) and vinylcaprolactam (PEO-VCap) were used for this study. MeOH and MEG were also investigated as a comparison to the KHIs. The anti-agglomerant inhibitor SDS has also been evaluated as a

comparison to the KHIs. Sodium chloride (NaCl) was used to mimic seawater in some cases. By comparing the onset temperatures and the rest of the parameters associated to the THF hydrates formation, and growth from different systems, we expect to investigate the effect of various gas hydrates inhibitors on the THF hydrates formation and growth process.

A 0.5 L agitated crystalliser was used in these experiments. A thermocouple was used to register the temperature as a function of the time during the whole course of the experiments. A stereomicroscope was used to monitor the crystal growing during crystallisation. Optical micrographs were taken on the top of the reaction vessel during the crystal growing process.

3.2 Materials and methods

3.2.1 Materials

Gaffix® VC713, Luvicap® EG, PVP40 and PVP360 were purchased from the suppliers without further purification. PEO-VCap was synthesised in Polymer Research lab of Curtin University. More information of these polymers can be found in Table 3.1 and Figure 3.1 respectively.

Table 3.1 Description of the polymers used as KHIs.

Commercial name	Description	MW (g/mol)	Supplier
Gaffix® VC713	Terpolymer of *N*-vinylpyrrolidone, *N*-vinylcaprolactam and dimethylamino-ethylmethacrylate in ethanol in ethanol (37 wt%)[1].	83,000	International Speciality Products (ISP)
Luvicap® EG	Solution of poly(*N*-vinylcaprolactam) in ethyleneglycol (40 wt%).	2,000[3] (Polydispersion ratio 2.5)	BASF Germany
PVP40	Poly(*N*-vinylpyrrolidone).	40,000	Sigma Aldrich
PVP360		360,000	
PEO-VCap	Copolymer of poly(ethylene oxide) and vinylcaprolactam	27,212	Made in house

[1] (Lederhos et al., 1996), [2] (Sloan and Koh, 2008), [3] Average nominal MW.

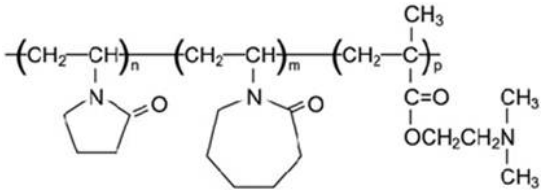

(a) Gaffix® VC713

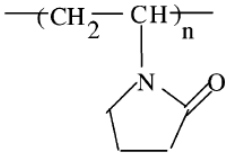

(b) Poly(*N*-vinylpyrrolidone) (PVP)

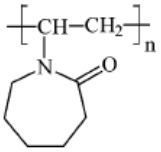

(c) Luvicap® EG

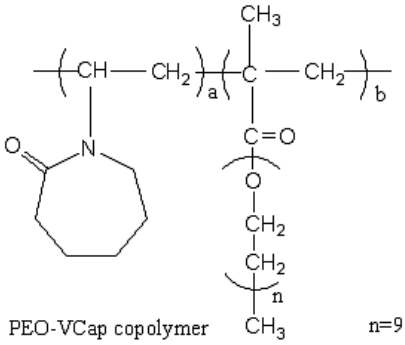

(d) Poly(PEO-*co*-VCap)

Figure 3.1 Structure of the polymer inhibitors.

Sodium chloride, analytical grade, was purchased from BDH Laboratory Supplies England. Methanol was supplied by Labserv, Biolab Aust. Ltd., analytical grade. Ethylene glycol ≥ 99%, reagent plus® was supplied by Sigma Aldrich. Sodium dodecyl sulphate, supplied by BDH Laboratory Supplies England, especially pure was used as anti-agglomerant hydrate inhibitor. Tetrahydrofuran (THF) (ChromAR® 99.8% Mallinckrodt Chemicals) has been used in all the experiments as a hydrate former.

All testing solutions were freshly prepared prior to the measurement. The samples were weighed using an analytical balance of precision ±0.01 mg. The water used in the experiments was purified by a Millipore Milli-Q system, and it is referred to as pure water. The inhibitor was first dissolved in pure water (or NaCl 3.5 wt%, which was made by adding 3.5 g NaCl into 96.5 mL of pure water, following by continuous

stirring at 200 RPM for 1 hour) and was stirred at 100 RPM for 1 hour. After that, the THF was added to the chemical solution in the stoichiometric concentration of 19.2 wt%. The solutions were further stirred at 100 RPM for about 20 minutes. All the solutions were prepared in the same way. Chemical composition of these solutions can be found in Table 3.2. The weight percentage is calculated based on the total mass of the solution.

Table 3.2 Chemical composition of all formula used for the THF hydrates kinetics experiments.

Inhibitor	**System evaluated**	**Composition (wt%)**			
		THF	H_2O	Inhibitor	NaCl
None		19.2	80.80	-	-
Thermodynamic	NaCl	19.2	77.30	-	3.5
	MeOH	19.2	80.70	0.10	-
		19.2	78.80	2.00	-
	MEG	19.2	80.70	0.10	-
		19.2	78.80	2.00	-
Kinetic	Gaffix® VC713	19.2	80.70	0.10	-
	Luvicap® EG	19.2	80.70	0.10	-
	PEO-VCap	19.2	80.70	0.10	-
	PVP40	19.2	80.70	0.10	-
	PVP360	19.2	80.70	0.10	-
Kinetic + thermodynamic	Gaffix® VC713	19.2	77.20	0.10	3.5
		19.2	77.05	0.25	3.5
	Luvicap® EG	19.2	77.20	0.10	3.5
		19.2	77.05	0.25	3.5
	PEO-VCap	19.2	77.20	0.10	3.5
		19.2	77.05	0.25	3.5
	PVP40	19.2	77.20	0.10	3.5
		19.2	77.05	0.25	3.5
	PVP360	19.2	77.20	0.10	3.5
		19.2	77.05	0.25	3.5
Anti-agglomerant	SDS	19.2	80.70	0.10	-

3.2.2 Experimental procedure

The experiments were conducted in a crystalliser consisting of a jacketed glass vessel with an internal diameter of 53.80 mm and a height of 98.14 mm (Figure 3.2 (a)). The glass vessel was connected to a refrigerated water bath circulator for temperature control. Figure 3.2 (b) and (c) show the photos of the experimental set-up.

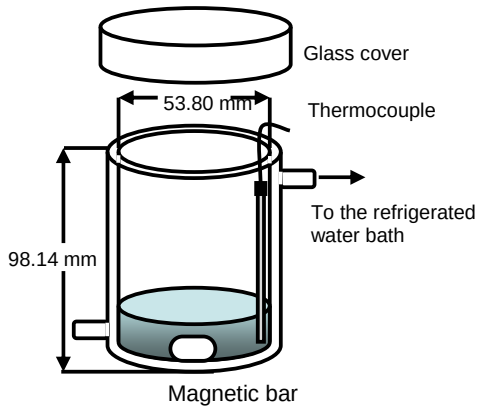

(a) Details of the crystalliser

(b) Front view of the experimental equipment

(c) Details of the stereomicroscope

Figure 3.2 Pictures showing the experimental equipment used.

In brief, 20 mL of experimental solution with a fixed composition was fed into the vessel. Then the vessel was covered to prevent THF from volatilising and was cooled from room temperature to the onset temperature. A thermocouple was used to

measure the temperature of the bulk solution contained in the crystalliser. The temperature changes were produced at a cooling rate of approximately 0.9 to 1.7 K/min. The temperature was maintained at a uniform level by using a magnetic stir plate with stir bar (6.00 mm diameter and 24.62 mm length) at a speed of 150 RPM. The change of temperature was recorded against time until the vessel was full of crystals/hydrates. The morphology of the crystals was photographed at various time intervals using a video digital photography system QImaging Go-3. The latter was connected to the stereomicroscope Olympus SZ61 taking the photos of the top of the vessel. The terminal was connected to a computer to export images. Each solution was monitored from the onset of THF hydrates formation during mixing until the end of the crystallisation process. The onset of THF hydrates formation was evidenced by a sudden increase in the temperature of the mixture, due to the enthalpy change of hydrate crystallisation. At the end of the crystallisation process, the vessel was full of crystals/hydrates. For all experiments, the stirring stopped immediately once the onset points of crystallisation were detected.

3.3 Results and discussion

3.3.1 Uninhibited THF hydrate nucleation and growth

The plots of the solution temperature changes and associated times are shown in Figure 3.3 for the THF 19.2 wt% hydrate. At the beginning of the experiment, the initial temperature is T_i. The solution is then cooled down and the temperature decreases monotonically with time. A sudden rise of temperature indicates the onset of hydrates formation. We define T_o, as the temperature at which the increase of temperature starts to be observed. At this temperature the macroscopic appearance of the solid phase first takes place. Once it reaches T_p, peak temperature, the nucleation period has already finished and the crystals start to grow. The magnitude of the temperature rise, ΔT_r, is the maximum temperature increase at the onset point, and represents qualitative information about the amount of hydrate formed. The temperature starts falling after it reaches T_p and gradually becomes constant. T_e is the temperature at the end-point of hydrate growth, which is determined by the visual observation that the testing mixture has been converted to the solid phase to the extent that the motion of the magnetic stirrer has stopped. At this point, the crystalliser is fully blocked with hydrate crystals. Δt_1 is the time difference between

T_i and T_o and indicates the time required to reach the nucleation period, since the system has been cooling down from room temperature. Δt_2 is the time difference between T_p and T_o , the time taken from nuclei growth to reach the critical size. Δt_3 is the time difference between T_e and T_o, which represents the crystal growing period.

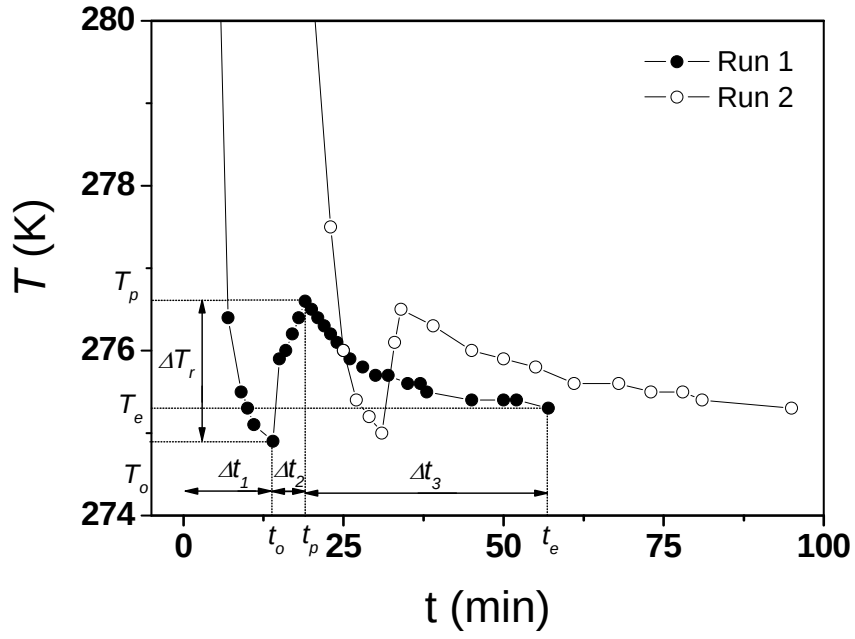

Figure 3.3 Typical exothermal spike recorded during the onset hydrate formation measurement for the THF 19.2 wt% hydrate.
Cooling rates for Runs 1 and 2 were 1.7 K/min and 1.0 K/min, respectively.

There is a time difference between the two plots displayed in Figure 3.3. This is due to the effect of the two different cooling rates used during the experiments. The reason why the cooling rate was different for some of the experiments was due to the refrigerated bath used, which did not allow for fully programmable control of the cooling rate; thus the cooling rate was controlled manually. Run 1, T_o 275.1 K, T_p 276.8 K, ΔT_r 1.7 K, T_e 275.5 K, Δt_1 14 min, Δt_2 5 min and Δt_3 is 38 min approximately.

For Run 2, T_o 275.2 K, T_p 276.7 K, ΔT_r 1.5 K, T_e 275.5 K, Δt_1 31 min, Δt_2 3 min and Δt_3 is 61 min approximately. Although the time differences Δt_1, Δt_2 and Δt_3 were affected by the cooling rate, the values of T_o, T_p, ΔT_r and T_e were not significantly

affected since they are only affected by the inhibitors used and the volume of hydrates formed.

It was also observed that the appearance of the first solid phase does not occur exactly at the equilibrium temperature of the THF–water system (277.4 K according to the THF hydrate–water phase diagram) (Jones et al., 2008). A subcooling of 2.3 K (T_{eq}-T_o) (compared to the average onset temperature of 275.1 K) was necessary to start the nucleation process. This is in agreement with some researchers who have considered that it is difficult for the THF nucleation process to happen, because the crystal nucleation in the liquid phase interior needs a great deal of energy to overcome the surface barrier (Cha et al., 1988; Wilson et al., 2005; Zang et al., 2008).

The progress of the THF hydrate growing process is photographed and shown in Figure 3.4. The photographs were taken on the top of the reaction crystalliser at various time intervals. The recorded time in this figure was counted from the moment when the increase in the temperature was first observed (T_o). Therefore, the real time at which the photo was taken should be the time denoted in each photograph plus $\Delta t_{1,}$ which is 14 min for the first plot in Figure 3.3. At this time, the first macroscopic appearance of crystals was detected. At about 19 min (corresponding to 5 min in Figure 3.4) the hydrate underwent growth for several minutes. A more rapid growth was observed after a further 5 minutes, and the crystals growth process continued from small crystal grains into a critical dimension. The sample was totally converted to the solid phase and the entire crystal-growing period finished (Δt_3). For Run 1, ΔT_3 is approximately 38 minutes.

We can see from Figure 3.4 that once THF hydrate crystals are detected, they start to grow and agglomerate together. It becomes difficult to distinguish the shape and size of each crystal. It was also observed that for all the runs using this system, the crystals started to form at the borders of the crystalliser and glass walls of the container. Some clearer images are displayed in Figure 3.5, taken from Run 2. Observation of hydrates formation at the surface of the liquid phase or near the wall of sample tubes have been reported by other researchers (Zhang et al., 2001; Wilson et al., 2005). This is probably due to the fact that the solid surface of the glass wall is

the coolest area in the vessel, and therefore provides favourable conditions for the transient clusters to deposit, grow and agglomerate (Zhang et al., 2001).

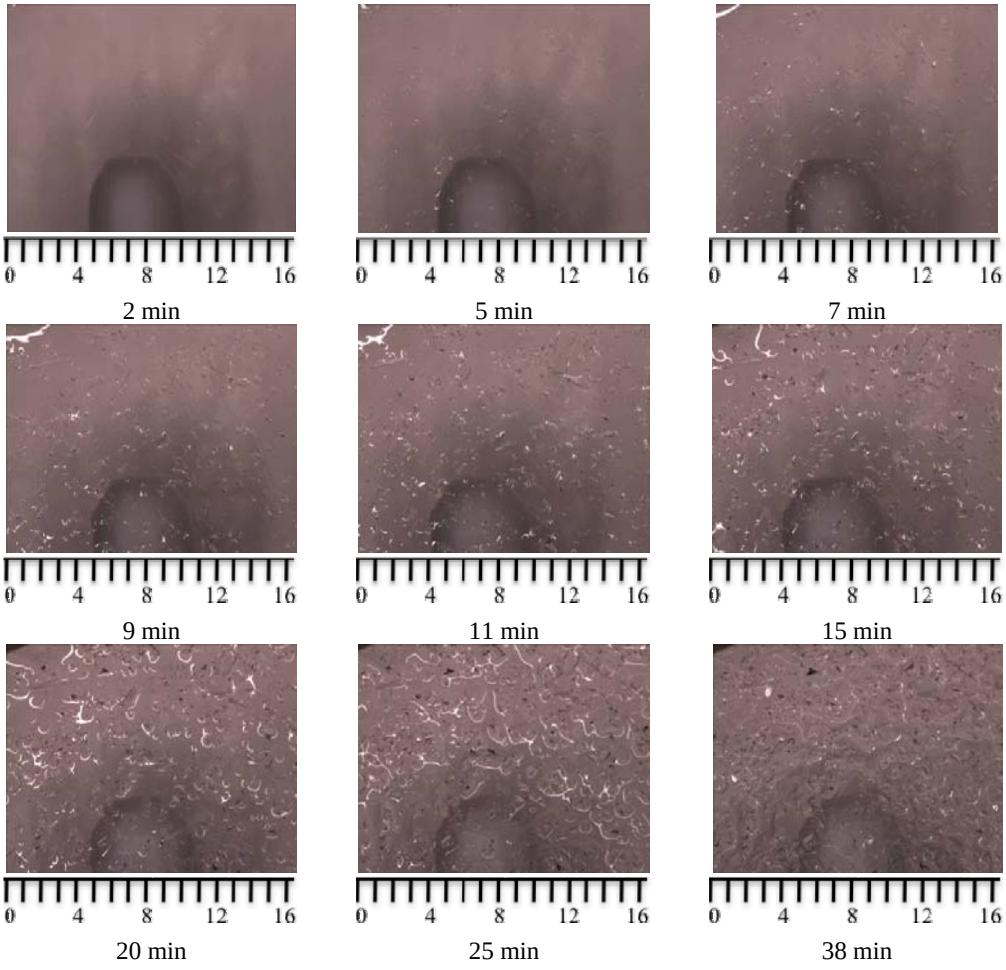

Figure 3.4 Sequence of growth and morphology of a stoichiometic THF 19.2 wt% hydrates. Images are taken from the top of the solution for Run 1. Scale is expressed in millimetres.

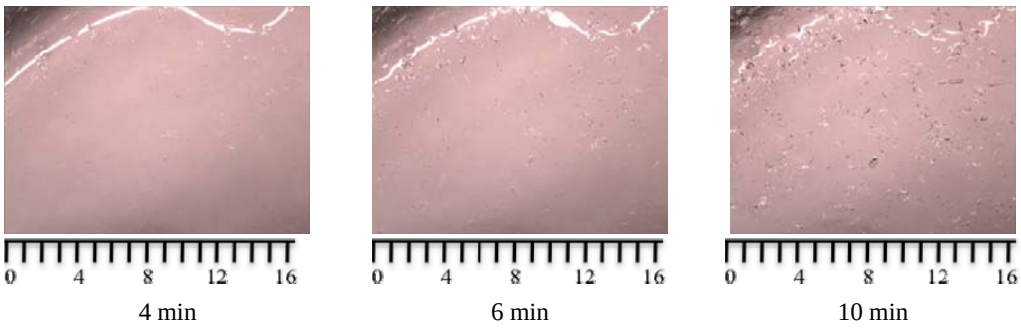

Figure 3.5 Growth and morphology of a stoichiometic THF 19.2 wt% hydrates. Images are taken from the top of the solution for Run 2. Scale is expressed in millimetres.

Table 3.3 Relevant parameters measured during the hydrates formation and growing in the absence and the presence of thermodynamic, kinetic and anti-agglomerant inhibitors.

System	T_i (K)	CR (K/min)	T_o (K)	$\overline{T}_o$ (K)	σT_o (K)	T_p (K)	$\overline{T}_p$ (K)	σT_p (K)	ΔT_r (K)	$\Delta \overline{T}_r$ (K)	$\sigma \Delta T_r$ (K)	T_e (K)	$\overline{T}_e$ (K)	σT_e (K)	Δt_1 (min)	Δt_2 (min)	Δt_3 (min)
THF 19.2 wt%	298.7	1.7	275.1	275.1	0.2	276.8	277.0	0.4	1.7	1.9	0.6	275.5	275.7	0.4	14	5	38
Pure water	301.4	1.0	275.2			276.7			1.5			275.5			31	3	61
	299.5	1.5	274.9			277.4			2.6			276.2			64	1	45
THF 19.2 wt%	298.5	1.2	271.6	271.6	0.1	274.8	274.2	0.8	3.2	2.7	0.8	271.7	271.8	0.1	37	6	45
NaCl 3.5 wt%	298.7	1.3	271.5			273.6			2.1			271.8			23	5	24
MeOH 0.1 wt%	298.8	1.1	268.9	269.0	1.9	275.2	275.5	0.3	6.3	6.5	1.8	269.3	269.3	2.2	32	1	13
THF 19.2 wt%	295.9	1.2	270.9			275.7			4.8			271.5			27	1	10
Pure water	297.4	1.1	267.2			275.5			8.3			267.1			36	1	20
MeOH 2.0 wt%	296.2	0.9	265.5	265.4	1.5	274.8	274.7	1.1	9.3	9.3	2.6	265.5	266.2	0.8	39	1	12
THF 19.2 wt%	295.4	1.1	263.8			275.7			11.9			266.1			38	1	5
Pure water	295.5	1.1	266.8			273.5			6.7			267.0			31	1	11
MEG 0.1 wt%	296.1	1.2	265.3	265.9	1.6	276.2	276.2	0.1	10.9	10.3	1.5	265.7	266.3	0.9	41	0	10
THF 19.2 wt%	295.7	1.1	264.8			276.1			11.3			265.8			40	0	8
Pure water	298.1	1.1	267.7			276.3			8.6			267.3			36	0	13
MEG 2.0 wt%	298.1	1.2	266.9	266.3	1.6	275.7	275.2	0.8	8.8	8.9	2.2	266.9	266.8	0.9	30	1	12
THF 19.2 wt%	297.6	1.2	266.7			275.2			8.5			267.1			31	1	13
Pure water	296.0	0.9	264.0			275.7			11.7			265.5			46	1	10
	296.7	1.2	267.7			274.1			6.4			267.5			28	1	13
Gaffix® VC713	298.4	1.2	269.3	269.4	0.1	275.6	275.9	0.3	6.3	6.5	0.2	270.2	270.2	0.3	33	2	19
0.1wt%	298.6	1.3	269.5			276.2			6.7			270.0			30	0	25
THF 19.2 wt%	300.7	1.0	269.5			275.9			6.4			270.5			63	1	14
Pure water																	
Gaffix® VC713 0.1	298.6	1.2	263.4	265.0	1.8	271.3	271.4	0.5	7.9	6.4	1.9	265.0	265.9	1.0	57	1	9
wt%	298.0	1.2	263.7			271.0			7.3			265.4			54	1	6
THF 19.2 wt%	298.6	1.2	267.1			271.3			4.2			266.8			32	0	13
NaCl 3.5 wt%	298.4	1.2	264.1			272.2			8.1			265.0			47	1	14
	298.0	1.2	266.8			271.3			4.5			267.1			34	0	9

System	T_i (K)	CR (K/min)	T_o (K)	$\bar{T}_o$ (K)	σT_o (K)	T_p (K)	$\bar{T}_p$ (K)	σT_p (K)	ΔT_r (K)	$\Delta \bar{T}_r$ (K)	$\sigma \Delta T_r$ (K)	T_e (K)	$\bar{T}_e$ (K)	σT_e (K)	Δt_1 (min)	Δt_2 (min)	Δt_3 (min)
Gaffix® VC713	301.5	0.9	263.1	263.1	0.1	271.4	271.4	0.1	8.3	8.3	0.0	265.8	265.6	0.4	47	1	4
0.25 wt%	296.9	1.1	263.0			271.3			8.3			265.3			38	1	4
THF 19.2 wt%																	
NaCl 3.5 wt%																	
Luvicap® EG 0.1	298.7	1.3	271.5	271.6	0.2	275.7	276.0	0.5	4.2	4.4	0.6	272.2	272.6	0.7	26	1	21
wt% THF 19.2 wt%	298.4	0.9	271.4			276.5			5.1			273.4			31	4	23
Pure water	299.9	1.4	271.8			275.7			3.9			272.2			25	2	19
Luvicap® EG 0.1	298.2	0.9	264.7	265.7	1.6	271.4	272.2	1.1	6.7	6.5	2.3	265.4	268.1	2.1	46	1	11
wt% THF 19.2 wt%	297.4	1.2	264.1			273.3			9.2			269.8			68	4	5
NaCl 3.5 wt%	298.4	1.2	264.9			273.4			8.5			270.3			87	1	3
	298.4	1.2	267.7			273.1			5.4			270.9			28	1	4
	298.4	0.9	266.5			270.5			4.0			266.5			40	1	18
	297.9	1.1	268.0			271.4			3.4			268.2			28	2	12
	297.8	1.2	266.0			271.4			5.4			266.5			34	1	9
	297.4	1.2	264.0			273.0			9.0			266.9			41	1	5
Luvicap® EG 0.25	300.2	0.9	262.5	262.5	0.0	271.0	272.1	1.5	8.5	9.6	1.5	264.5	268.4	0.4	51	1	4
wt% THF 19.2 wt%	298.3	1.1	262.5			273.1			10.6			265.1			43	0	5
NaCl 3.5 wt%																	
PVP40 0.1 wt%	298.0	1.3	271.3	273.3	1.7	276.7	276.4	0.4	5.4	3.1	1.8	271.8	273.3	1.4	63	3	26
THF 19.2 wt%	298.0	1.4	271.6			275.6			4.0			271.8			98	3	56
Pure water	298.3	1.0	274.6			276.0			1.4			274.6			52	2	116
	294.5	1.1	274.2			276.6			2.4			274.7			100	1	47
	299.2	1.3	276.0			276.1			0.1			274.8			35	2	60
	293.8	0.8	273.9			276.6			2.7			274.2			117	5	48
	296.8	0.9	272.6			276.6			4.0			272.8			92	1	64
	297.2	1.0	272.0			276.7			4.7			271.9			84	1	47
PVP40 0.1 wt%	298.1	1.3	265.3	265.7	1.5	271.1	271.5	1.2	5.8	5.8	2.2	264.8	266.2	0.8	41	1	22
THF 19.2 wt%	299.3	0.9	263.9			271.1			7.2			266.0			57	2	7
NaCl 3.5 wt%	297.7	1.3	264.9			273.6			8.7			266.7			50	1	11
	298.1	1.2	267.7			271.0			3.3			266.8			29	1	46
	298.1	1.2	266.9			270.8			3.9			266.6			36	1	31

System	T_i (K)	CR (K/min)	T_o (K)	$\overline{T}_o$ (K)	σT_o (K)	T_p (K)	$\overline{T}_p$ (K)	σT_p (K)	ΔT_r (K)	$\Delta \overline{T}_r$ (K)	$\sigma \Delta T_r$ (K)	T_e (K)	$\overline{T}_e$ (K)	σT_e (K)	Δt_1 (min)	Δt_2 (min)	Δt_3 (min)
PVP40 0.25 wt%	298.0	1.1	263.3	263.5	1.2	272.0	272.7	0.6	8.7	9.3	1.3	269.5	267.8	1.6	41	1	6
THF 19.2 wt%	296.0	1.1	262.4			273.2			10.8			266.3			42	0	10
NaCl 3.5 wt%	298.5	1.1	264.7			273.0			8.3			267.6			40	1	6
PVP360 0.1 wt%	297.6	1.3	269.5	269.4	0.2	275.9	276.0	0.6	6.4	6.5	0.4	270.0	270.1	0.4	25	1	26
THF 19.2 wt%	298.3	1.3	269.6			276.6			7.0			270.5			28	4	30
Pure water	297.7	1.0	269.2			275.4			6.2			269.8			95	0	18
PVP360 0.1 wt%	298.5	1.2	264.4	264.0	0.4	270.8	271.3	0.4	6.4	7.3	0.8	265.2	265.1	0.2	44	0	15
THF 19.2 wt%	298.2	1.3	263.9			271.5			7.6			265.1			42	1	14
NaCl 3.5 wt%	298.4	1.2	263.6			271.5			7.9			264.9			39	1	15
PVP360 0.25 wt%	294.9	0.9	262.2	262.7	0.7	271.0	271.2	0.3	8.8	8.5	0.4	266.0	266.0	0.0	43	1	3
THF 19.2 wt%	295.0	1.1	263.2			271.4			8.2			266.0			37	1	3
NaCl 3.5 wt%																	
PEO-VCap 0.1 wt%	297.7	1.1	263.7	263.5	1.2	275.9	275.6	0.3	12.2	12.1	1.1	264.3	264.0	1.2	40	0	7
THF 19.2 wt%	297.7	1.2	264.6			275.6			11.0			265.0			37	0	7
Pure water	294.4	0.8	262.2			275.3			13.1			262.6			46	1	7
PEO-VCap 0.1 wt%	296.9	0.8	261.1	261.0	0.2	271.6	272.1	0.7	10.5	11.2	0.9	262.7	263.0	0.4	49	1	6
THF 19.2 wt%	297.7	1.1	260.8			272.6			11.8			263.3			45	1	4
NaCl 3.5 wt%																	
PEO-VCap 0.25	297.8	1.1	266.3	264.7	2.3	270.9	271.9	1.3	4.6	7.2	3.7	266.1	265.8	0.5	32	1	6
wt%	297.9	1.2	263.0			272.8			9.8			265.4			38	1	3
THF 19.2 wt%																	
NaCl 3.5 wt%																	
SDS 0.1 wt%	298.6	1.2	268.3	268.6	0.3	276.2	276.1	0.7	7.9	7.5	0.7	268.4	268.9	0.6	44	1	25
THF 19.2 wt%	299.7	1.0	268.6			275.3			6.7			268.9			40	1	19
Pure water	298.6	1.2	268.8			276.7			7.9			269.5			46	0	16

$\overline{T}$ represents the average value of the temperature, σ represents the standard deviation, and CR represents is the cooling rate.

3.3.2 Inhibited THF hydrate nucleation and growth

3.3.2.1 Thermodynamic hydrate inhibitors

Figures 3.6 to 3.10 shows the plots of temperature change with time for all the runs conducted using NaCl 3.5 wt%, MeOH and MEG at varying concentrations. These figures show the onset temperature used for detection of the onset of hydrate formation.

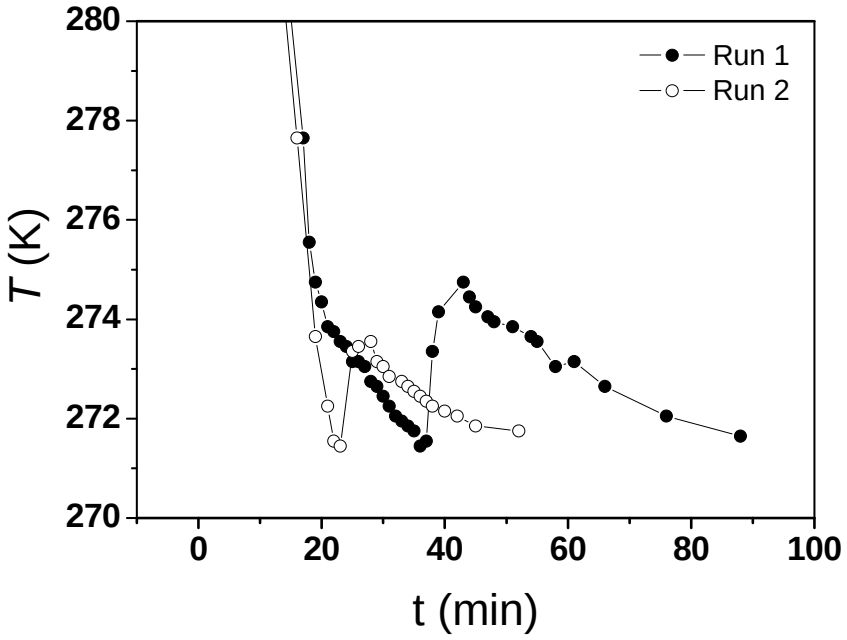

Figure 3.6 Temperature change in THF 19.2 wt% – 3.5 wt% of NaCl system. Cooling rates for Runs 1 and 2 were 1.2 K/min and 1.3 K/min, respectively.

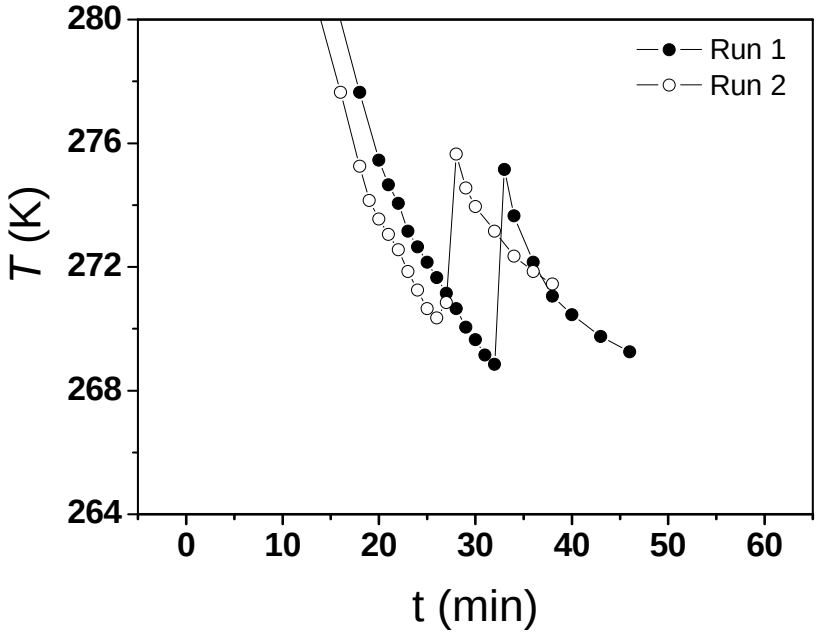

Figure 3.7 Temperature change in THF 19.2 wt% – 0.1 wt% of MeOH. Cooling rates for Runs 1 and 2 were 1.1 K/min and 1.2 K/min, respectively.

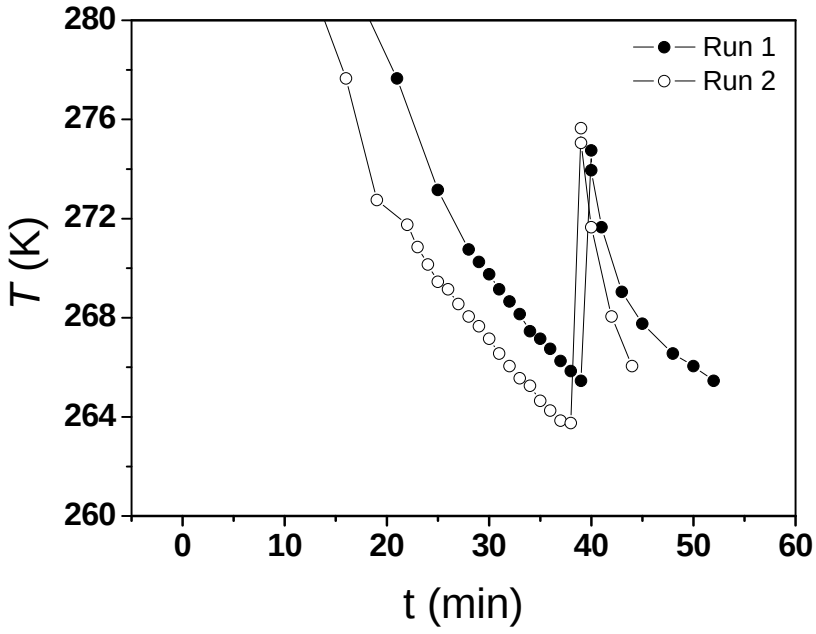

Figure 3.8 Temperature change in THF 19.2 wt% – 2 wt% of MeOH. Cooling rates for Runs 1 and 2 were 0.9 K/min and 1.1 K/min, respectively.

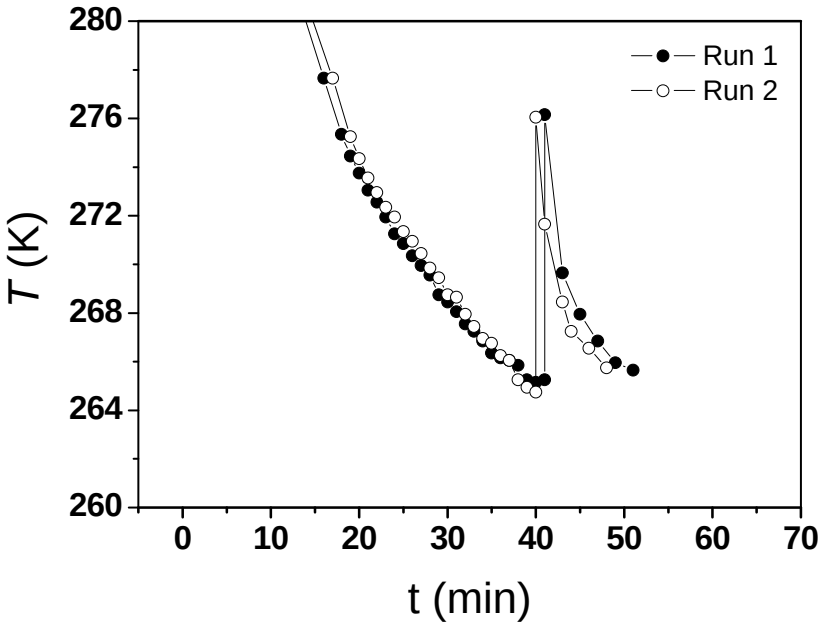

Figure 3.9 Temperature change in THF 19.2 wt% – 0.1 wt% of MEG. Cooling rates for Runs 1 and 2 were 1.2 K/min and 1.1 K/min, respectively.

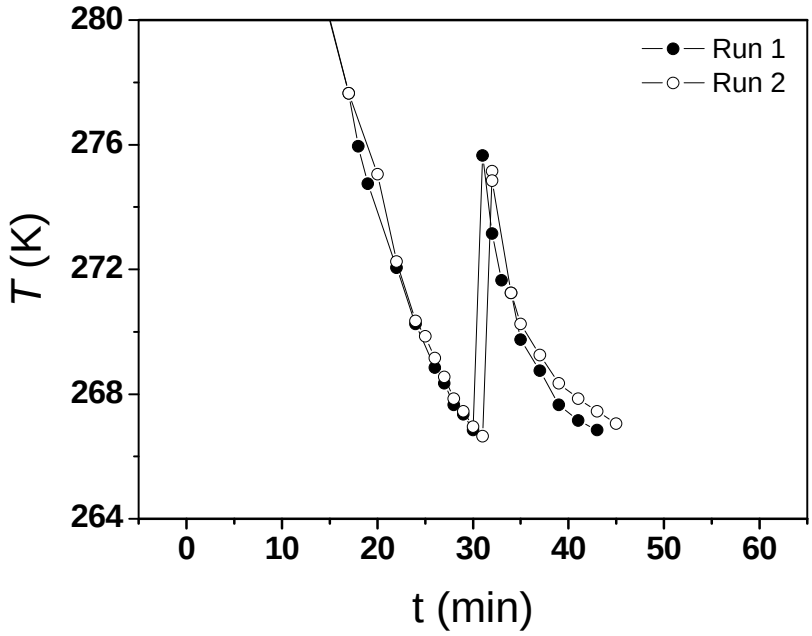

Figure 3.10 Temperature change in THF 19.2 wt% – 2 wt% of MEG. Cooling rates for Runs 1 and 2 were 1.2 K/min.

It is shown in Figure 3.6 two plots of the THF hydrate system containing NaCl 3.5 wt% (they correspond with Runs 1 and 2 at a cooling rate of 1.2 K/min and 1.3 K/min, respectively). The experiments started from T_i (298.5 K and 298.7 K for Run 1 and 2, respectively). Then, the solutions were cooled down until the onset point of hydrates formation, indicated by an increase in temperature. After having reached the maximum temperature, T_p, the temperature started dropping until reaching T_e, indicating the end of the growing period. At this point, the cell was fully blocked with hydrate crystals. The measured values of all parameters are reported in Table 3.3. For Run 1, T_o is 271.6 K, T_p 274.8 K, ΔT_r 3.2 K, T_e 271.7 K, Δt_1 37 min, Δt_2 6 min and Δt_3 is 45 min approximately. For Run 2, T_o 271.5 K, T_p 273.6 K, ΔT_r 2.1 K, T_e 271.8 K, Δt_1 23 min, Δt_2 5 min and Δt_3 is 24 min approximately. A difference of about 1.1 K in ΔT_r was observed between these two runs. This represents a small difference in the amount of crystals formed. Among the three time differences, Δt_1 is different which is probably due to the different cooling rate. Δt_2 are quite close to each other indicating a similar time required from nuclei growth to reach the critical size. However, a significant difference was observed in Δt_3. This could be due to heat transfer effects, which limit the growing of the crystals. Even when the degree of subcooling was the same for both runs, it was observed that the amount of crystals formed in each run was different (inferred from ΔT_r values). In Run 1, the temperature spike reaches 3.2 K compared to 2.1 K reached for Run 2. The higher temperature registered for Run 1 could induce a decrease in the hydrate growth rate of the hydrate crystals.

Similar trends in the temperature–time plot have been found for both methanol and glycol (Figures 3.7 to 3.10). Table 3.3 summarises all the results for these inhibitors in terms of the parameters T_i, T_o, T_p, ΔT_r, T_e, Δt_1, Δt_2 and Δt_3. Table 3.4 presents extracted data from Table 3.3 for direct comparison among the THIs inhibitors.

Table 3.4 Parameters observed during THF hydrates formation in the presence of different THIs.

Inhibitor	Hydrates Systems	Characteristics							
		t_o (min)	T_o (K)	T_{or} (K)	T_p (K)	T_{pr} (K)	ΔT_r (K)	ΔT_{rr} (K)	t_e (min)
None		14-64	275.1	-	277.0	-	1.9	-	38-61
THIs	NaCl	23-37	271.6	3.5	274.2	2.8	2.7	0.8	24-45
	MeOH 0.1 wt%	27-36	269.0	6.1	275.5	1.5	6.5	4.6	10-20
	MeOH 2.0 wt%	31-39	265.4	9.7	274.7	2.3	9.3	7.4	5-12
	MEG 0.1 wt%	36-41	265.9	9.2	276.2	0.8	10.3	8.4	8-13
	MEG 2.0 wt%	28-46	266.3	8.8	275.2	1.8	8.9	7.0	10-13

t_o is the time at which T start increasing; T_o is the T at which temperature start increasing; ; T_{or} is the reduction in T_o due to the presence of the inhibitor; T_p is the T at which the nucleation period has already finished and the crystals start to grow; T_{pr} is the reduction in T_p due to the presence of the inhibitor; ΔT_r is the magnitude of the temperature rise; ΔT_{rr} is the reduction in ΔT_r due to the presence of the inhibitor; t_e is the completion time, the time required to the blocking of the cell.

In comparison to the uninhibited system, a decrease in both T_o and T_p has been observed for all systems containing inhibitors. The presence of NaCl 3.5 wt% lower the T_o and T_p in around 3.5 K and 2.8 K respectively, compared to the uninhibited system. For MeOH, the reductions in T_o were 6.1 K for 0.1 wt% of MeOH and 9.7 K for 2.0 wt% of MeOH, respectively. For T_p the temperature was reduced in 1.5 K for 0.1 wt% of MeOH and 2.3 K for 2.0 wt% of MeOH, respectively. For MEG, the reductions in T_o corresponded to 9.2 K for 0.1 wt% of MEG and 8.8 K for 2.0 wt% of MEG, respectively. For T_p, the reductions were 0.8 K for 0.1 wt% of MEG and 1.8 K for 2.0 wt% of MEG, respectively. These reductions in T_o and T_p indicate that additional subcooling is required for the hydrates to form when THIs are present in the system. MeOH and MEG have shown a higher ability to suppress the hydrate formation temperature (a higher subcooling is required) than NaCl. When the concentration of MeOH and MEG is increased, a higher degree of suppression becomes apparent (Table 3.4).

It is known that alcohols such as MeOH and MEG, and electrolytes such as NaCl, lower the chemical potential of water and hydrogen bond energy (Makogon et al., 2000). Such inhibitors shift the thermodynamic stability boundary of hydrates to lower temperature by aggregating with water molecules, and preventing their arrangement into a hydrate lattice (Makogon et al., 2000). In the case of salt, it ionises in water and aggregates water molecules in solvation shells around ions. The presence of solvated ions near a hydrate crystal causes a hindrance for the water and guest molecules adsorbing on a hydrate surface (Makogon et al., 2000). Alcohol

when dissolved in aqueous solutions normally form a hydrogen bond with the water molecules, hence making it difficult for the water molecules to participate in the hydrate structure (Yousif et al., 1994). This was why the values of T_o and T_p were reduced when alcohols and NaCl were used in the THF hydrate system.

On the contrary, to the behaviour observed for T_o and T_p, when the ΔT_r values are compared, it can be observed that the THIs are increasing the magnitude of the temperature rise, compared with the system containing no inhibitor; this qualitatively infers that the amount of the crystals formed immediately after the onset point, are higher compared to the uninhibited system. Figure 3.11 compares the average values of T_o, T_p and ΔT_r for all the thermodynamic inhibitors and the system containing no inhibitor.

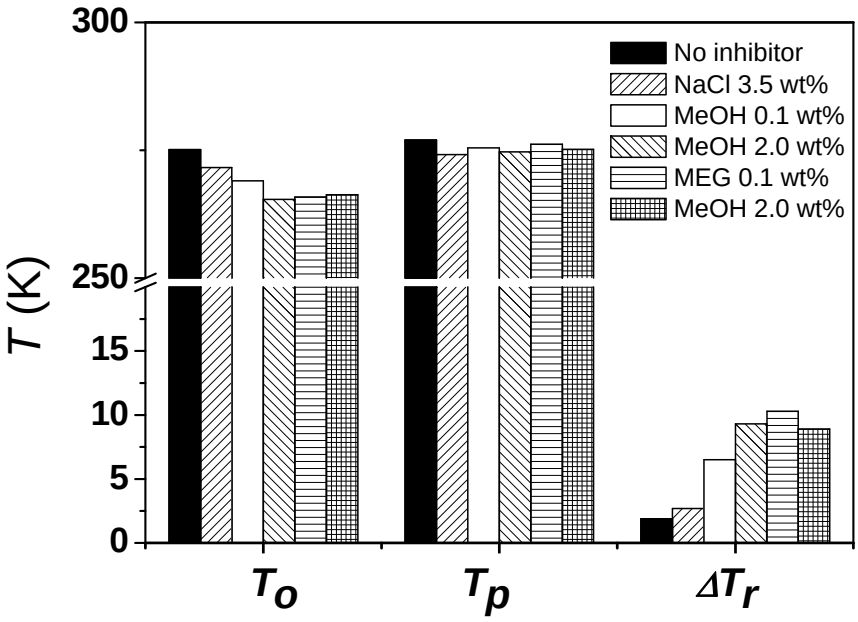

Figure 3.11 Average T_o and T_p and ΔT_r values for all the thermodynamic inhibitors.

For T_o, MeOH 2.0 wt% < MEG 0.1 wt% < MEG 2.0 wt% < MeOH 0.1 wt% < NaCl 3.5 wt% < no inhibitor. For ΔT_r, the trend was: no inhibitor < NaCl 3.5 wt% < MeOH 0.1 wt% < MEG 2.0 wt% < MeOH 2.0 wt% < MEG 0.1 wt%. These results indicated that MeOH 2 wt% and MEG 0.1 wt% are more effective preventing the hydrates formation, but also increasing the amount of crystals formed.

Figure 3.12 shows the amounts of crystals formed in THF systems that contain

various THIs. It can be seen that although MeOH & MEG have lead to more supercooling (Figure 3.11), they have also accelerated the growth of the crystals, when compared to the uninhibited system. The Δt_2 and Δt_3 values obtained for MeOH and MEG are quite similar and are usually shorter than the ones obtained for the pure THF–water system. The fast growth of the crystals observed in the systems containing MeOH & MEG can be explained as a consequence of the lowered temperature (more subcooling). Another possibility was reported by (Yousif et al., 1994) who stated that when alcohols are used at low concentrations, the alcohol molecules can hydrogen bond and form clumps of tightly packed water molecules, which act as nucleation sites. A more recent study by Bobev and Tait (2004) has indicated that under certain concentrations, methanol can act as both a thermodynamic inhibitor of hydrate formation, and a kinetic promoter for the formation of gas hydrates. Bobev and Tait explain these rapid rates of formation when methanol is present in the system as hydrogen bonding effects, which presumably constrain a particular orientation of the methanol molecule within the hydrate cage. These interactions within the cages will be much stronger than the typical van der Waals bonding in simple hydrates and may contribute to the spectacular magnitude of the promoting effect (Bobev and Tait, 2004).

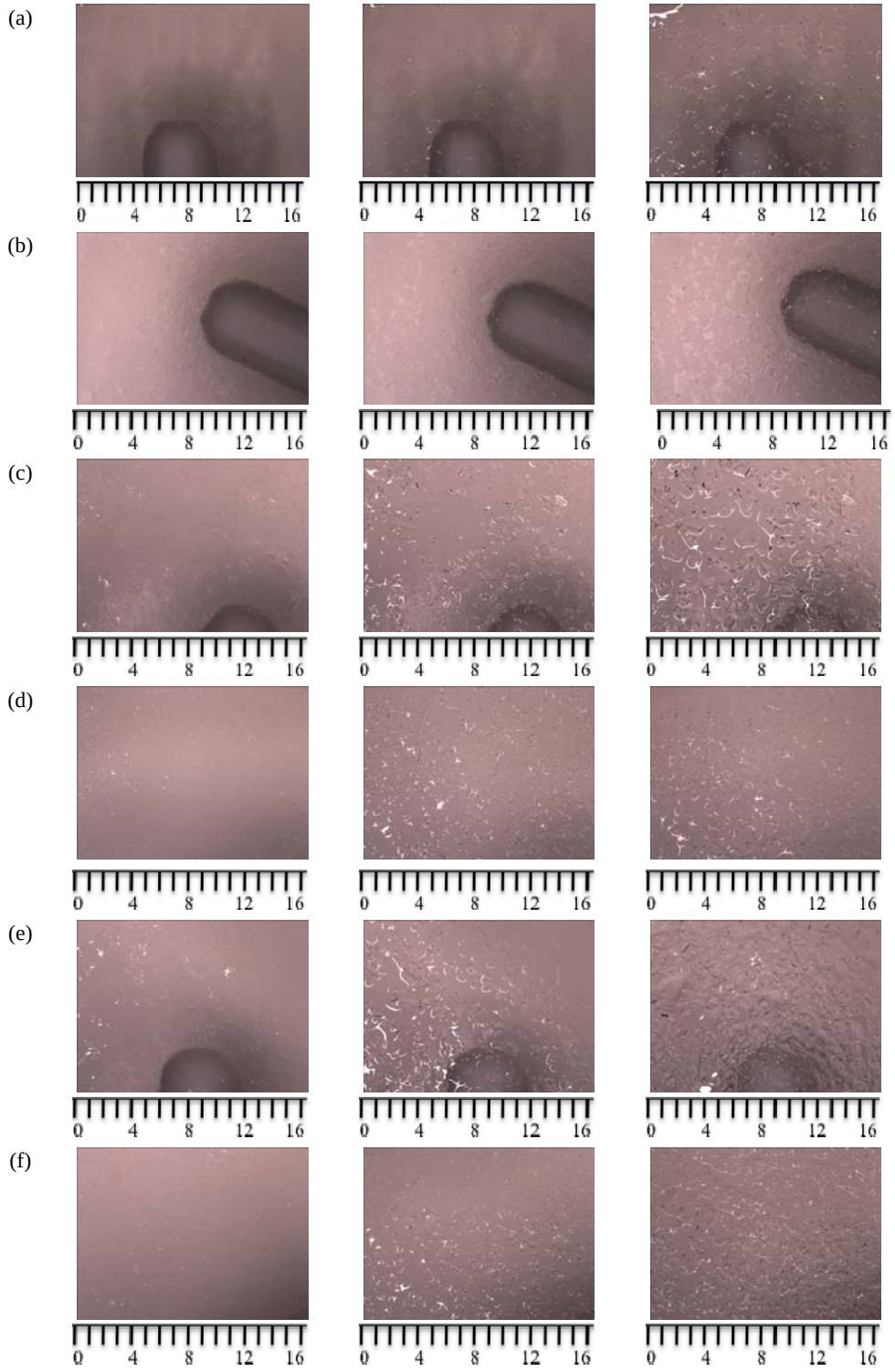

Figure 3.12 Sequence of growth and morphology of THF hydrates. (a) No inhibitor, (b) NaCl 3.5 wt%, (c) MeOH 0.1 wt%, (d) MeOH 2 wt%, (e) MEG 0.1 wt%, (f) MEG 2 wt%. Scale is expressed in millimetres.

3.3.2.2 Kinetic hydrate inhibitors

Figures 3.13 to 3.17 present the plots *T* vs. *t* showing a clear onset temperature induced by the hydrate formation in the presence of the KHIs.

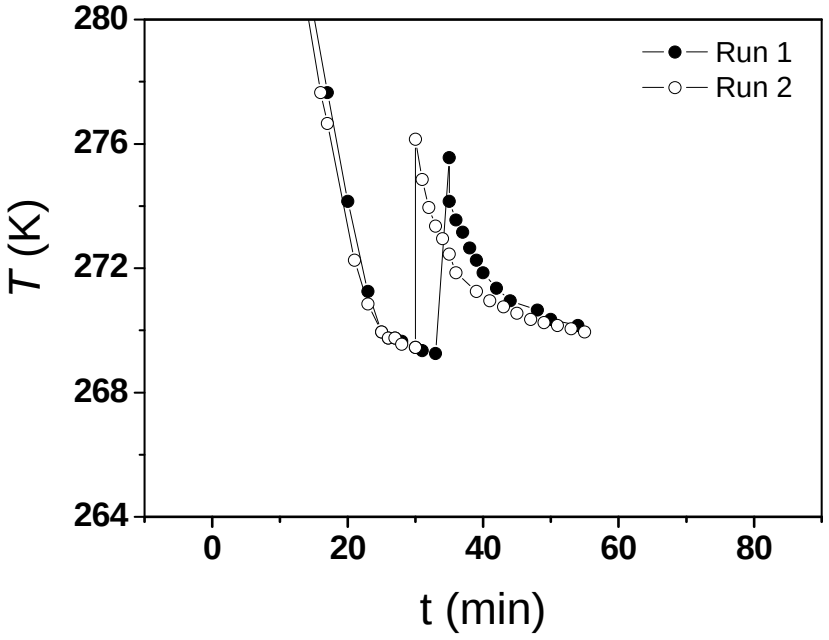

Figure 3.13 Temperature change in THF 19.2 wt% – 0.1 wt% of Gaffix® VC713. Cooling rates for Runs 1 and 2 were 1.2 K/min and 1.3 K/min respectively.

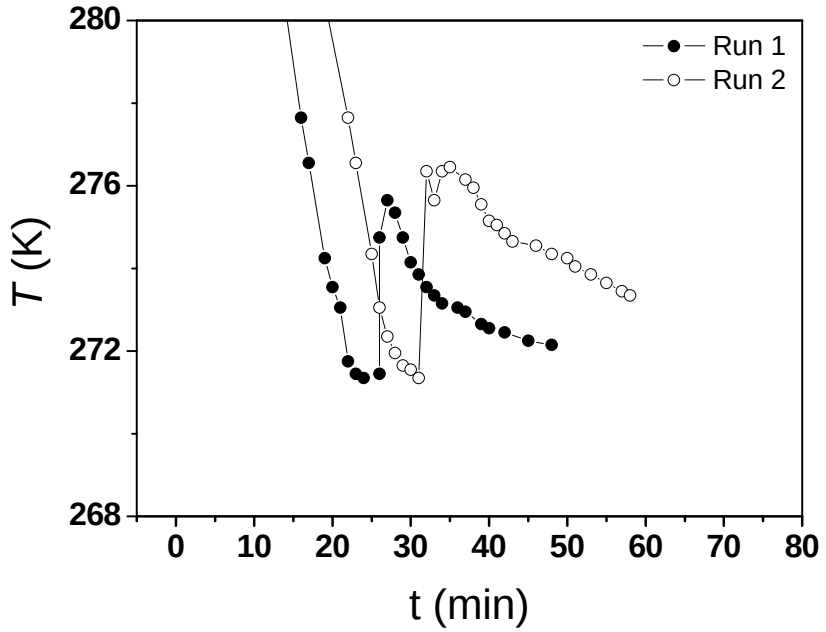

Figure 3.14 Temperature change in THF 19.2 wt% – 0.1 wt% of Luvicap® EG. Cooling rates for Runs 1 and 2 were 1.3 K/min and 0.9 K/min, respectively.

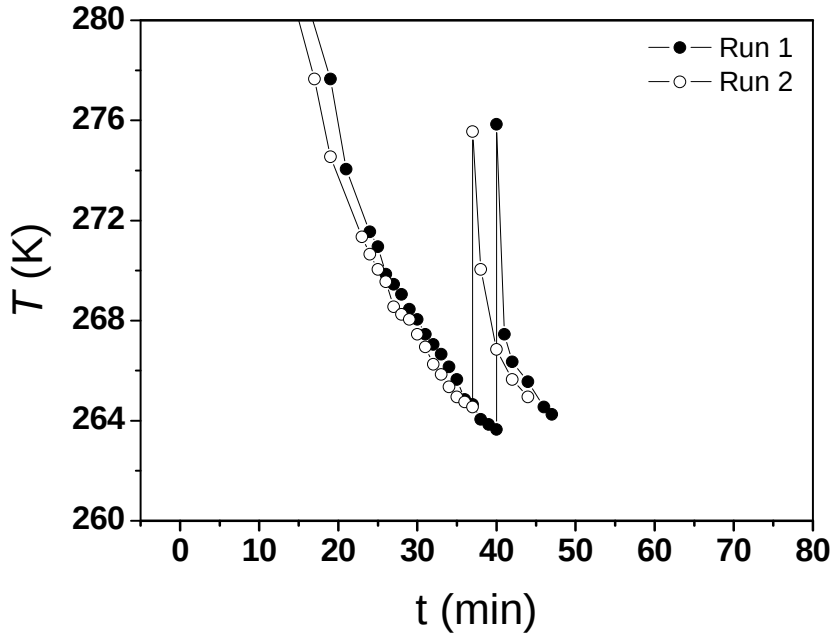

Figure 3.15 Temperature change in THF 19.2 wt% – 0.1 wt% of PEO-VCap. Cooling rates for Runs 1 and 2 were 1.1 K/min and 1.2 K/min, respectively.

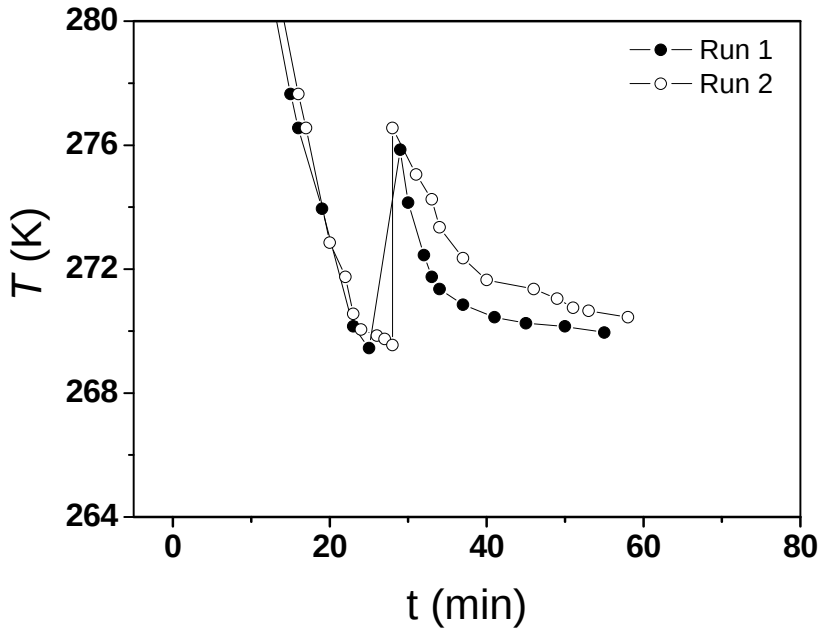

Figure 3.16 Temperature change in THF 19.2 wt% – 0.1 wt% of PVP360. Cooling rates for Runs 1 and 2 were 1.3 K/min.

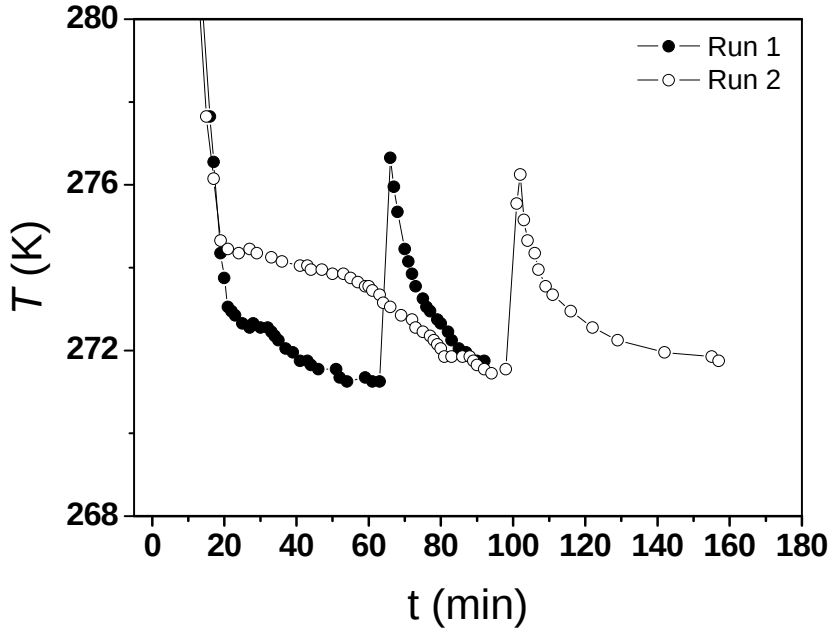

Figure 3.17 Temperature change in THF 19.2 wt% – 0.1 wt% of PVP40. Cooling rates for Runs 1 and 2 were 1.3 K/min and 1.4 K/min until 277.65 K, and 0.07 K/min and 0.05 K/min since 277.65 K respectively.

Shown in Figure 3.13 are the two *T*–*t* plots of the THF hydrate systems containing Gaffix® VC713 0.1 wt% (they correspond with Runs 1 and 2). The trend of the temperature change is the same for both of them. Run 1, T_o 269.3 K, T_p 275.6 K, ΔT_r 6.3 K, T_e 270.2 K, Δt_1 33 min, Δt_2 2 min and Δt_3 is 19 min approximately. For Run 2, T_o is 269.5 K, T_p 276.2 K, ΔT_r 6.7 K, T_e 270.0 K, Δt_1 30 min, Δt_2 0 min and Δt_3 is 25 min approximately. The results for the two runs are quite similar. The average T_o and T_p for these runs are around 269.4 K and 275.9 K respectively. The average T_e, is 270.1 K.

Compared to the system containing no inhibitor, Gaffix® VC713 0.1 wt% has reduced T_o and T_p for 10.1 K and 1.1 K, respectively (Table 3.5). The average ΔT_r value was about 6.5 K for this system, which is 4.6 K greater than that of the uninhibited solution. It suggests that the inhibition efficiency of Gaffix® VC713 0.1 wt% is manifesting in a lower reduction of T_o and T_p (lower subcooling needed before hydrate formation). The temperature reduction is due to hydrogen bonding (hydrophilic interactions) between water and the polar groups in Gaffix® VC713 and also from hydrophobic interactions between the nonpolar groups and water. The magnitude of the temperature spike obtained for Gaffix® VC713 0.1 wt% suggests a higher amount of crystals formed than in the system containing no inhibitor, probably due to the higher degree of subcooling.

A similar behaviour temperature–time plot has been found for other KHIs, excepting for PVP40 as seen in Figures 3.14 to 3.17. However, the reduction in T_o and T_p is dependent on the KHIs used. The values of T_o, T_p, ΔT_r, T_e, Δt_1, Δt_2 and Δt_3 of these systems are summarised in Table 3.3. Table 3.5 presents extracted data from Table 3.3 for a direct comparison among the KHIs inhibitors.

Table 3.5 Parameters observed during THF hydrates formation in the presence of different KHIs at a concentration of 0.1 wt%.

Inhibitor	Hydrates Systems	Characteristics							
		t_o (min)	T_o (K)	T_{or} (K)	T_p (K)	T_{pr} (K)	ΔT_r (K)	ΔT_{rr} (K)	t_e (min)
None		14-64	275.1	-	277.0	-	1.9	-	38-61
KHIs	Gaffix® VC713	30-63	269.4	5.7	275.9	1.1	6.5	4.6	14-25
	Luvicap® EG	25-31	271.6	3.5	276.0	1.0	4.4	2.5	19-23
	PEO-VCap	37-46	263.5	13.9	275.6	1.4	12.1	10.2	7
	PVP40	35-117	273.3	1.8	276.4	0.6	3.1	1.2	26-116
	PVP360	25-95	269.4	5.8	276.0	1.0	6.5	4.6	18-30

t_o is the time at which T start increasing; T_o is the T at which temperature start increasing; ; T_{or} is the reduction in T_o due to the presence of the inhibitor; T_p is the T at which the nucleation period has already finished and the crystals start to grow; T_{pr} is the reduction in T_p due to the presence of the inhibitor; ΔT_r is the magnitude of the temperature rise; ΔT_{rr} is the reduction in ΔT_r due to the presence of the inhibitor; t_e is the completion time, the time required to the blocking of the cell.

For PVP40 (Figure 3.17), the temperature–time plot indicated that the different cooling rates were used for this polymer. At the beginning of the experiment until 277.65 K the system was cooled at cooling rates of 1.3 K/min and 1.4 K/min for Runs 1 and 2 respectively. Because of the difficulty detecting the presence of crystals with this system, the cooling rate was reduced to 0.07 K/min and 0.05 K/min since 277.65 K for Runs 1 and 2 respectively, until the onset was reached. Therefore, the curves in Figure 3.17 are slightly different from those in other figures. PVP40 0.1 wt% reduced T_o and T_p for 1.8 K and 0.6 K, respectively. The average ΔT_r value for these runs was 4.7 K, which is 2.8 K greater than that of the uninhibited solution.

Simultaneous measurements of T_o and T_p during THF hydrate formation presented in Figures 3.13 to 3.17 and Table 3.5 revealed that for a concentration of 0.1 wt% of polymers in pure water PEO-VCap exhibits the lowest values of T_o 263.5 K and T_p 275.6 K. It represents a reduction of 11.6 K and 1.4 K in T_o and T_p respectively compared to the uninhibited system. From the lowest to the highest value of T_o PEO-VCap (263.5 K) was followed by Gaffix® VC713 and PVP360 which shows the same average temperature (269.4 K), Luvicap® EG (271.6 K) and PVP40 (273.3 K). The same trend was observed for T_p from the lowest to the highest value. PEO-VCap (275.6 K) was followed by Gaffix® VC713 (275.9 K), PVP360 and Luvicap® EG, which showed the same temperature (276.0 K), and PVP40 (276.4 K). This trend indicates distinct inhibition activities of the KHIs, which is probably due to different,

specific adsorptions of the polymers on the hydrates crystals. Figure 3.18 shows a clearer comparison between T_o and T_p average values for these inhibitors. Average ΔT_r values are also included in Figure 3.18 for comparison.

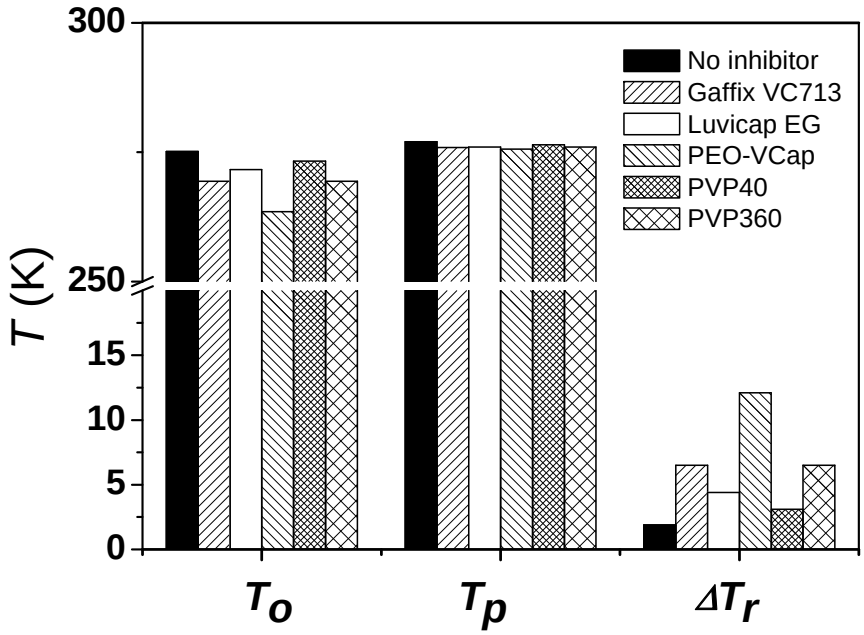

Figure 3.18 Average T_o, T_p and ΔT_r values for all the kinetic inhibitors.

A reduction in the onset temperature has been observed for all the polymers compared to the uninhibited THF system (Figure 3.18). These results are in agreement with observations suggested by Kashchiev and Firoozabadi (2002), who pointed out that the effect of the nucleation–inhibiting additives manifests itself lowering the threshold temperature.

The average ΔT_r values shown in Figure 3.18 indicate that PEO-VCap is the inhibitor producing higher amount of crystals after the hydrates formation. It is followed by Gaffix® VC713 and PVP360 which shows the same average temperature (6.5 K), Luvicap® EG (4.4 K) and PVP40 (3.1 K). It means that the KHIs that showed the lowest T_o and T_p (lower subcooling) are also producing more crystals after the onset of hydrates formation.

Figure 3.19 compares the progress of the THF hydrate formation in the presence of

the five different KHIs at the same concentration of 0.1 wt%. The results for Gaffix® VC713 (Figure 3.19 (b)), were observed as being the opposite to those obtained for ΔT_r. This suggested a higher amount of crystals formed than in the system containing no inhibitor. The photographs indicated that there was no significant presence of crystals at 5 min compared to the uninhibited solution. However, it was also noticed that the morphology of the crystals formed was different compared to the uninhibited solution. This could explain the increase in the magnitude of the temperature spike obtained for Gaffix® VC713 0.1 wt%.

The same behaviour was observed for Luvicap® EG, PVP40 and PVP360 for the same period of time (Figures 3.19 (c), (e) and (f), respectively). In the case of PVP40, it did not show significant growing of the crystals after 10 min. This might due to the specific adsorption of the polymer molecules on the hydrates surface, which block the active growth centres on the surface or steric hindrance.

At 9 min, the most crystal growth was observed in the system containing PEO-VCap. This is followed by Luvicap® EG, Gaffix® VC713, PVP360 and PVP40. The hydrate growth rate was higher when PEO-VCap and Luvicap® EG were added into the uninhibited system. This behaviour is expected if it is noticed that the subcooling applied for these inhibitors to reach the hydrates formation was also higher than the applied to the uninhibited system. From the lowest to the highest T_o values, PEO-VCap showed the lowest temperature (263.5 K), followed by Gaffix® VC713 and PVP360 (269.4 K), Luvicap® EG (271.6 K) and PVP40 (273.3 K).

It is interesting to note that Gaffix® VC713 and PVP360, which having different chemical structures (Figure 3.1), showed the same T_o and a quite similar surface nucleation and crystal growth controlling ability in THF hydrates (observed in Table 3.3 and Figure 3.19).

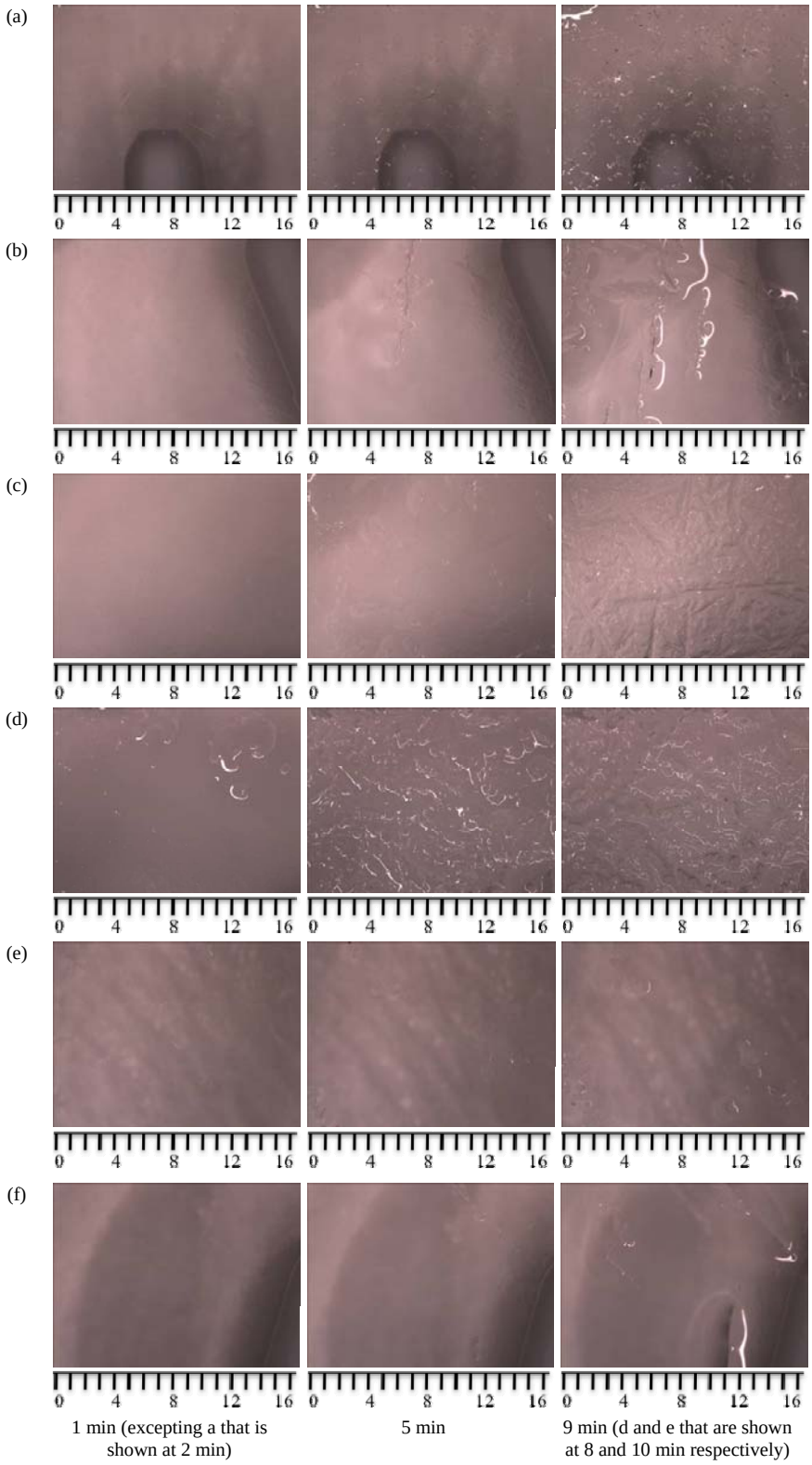

Figure 3.19 Sequence of growth and morphology of THF hydrates in the presence of 0.1 wt% KHIs. (a) no inhibitor, (b) Gaffix® VC713, (c) Luvicap® EG, (d) PEO-VCap, (e) PVP40, (f) PVP360. Scale is expressed in millimetres.

It has been proved that KHIs prevent growth in crystal size and retard formation of large hydrate agglomerates and solid plugs (Makogon et al., 2000). However, the values of Δt_3 presented in Table 3.3 are between 7 min (for PEO-VCap) and 116 min (for PVP40) for these inhibitors, and are sometimes smaller and sometimes greater than that in the uninhibited system. This is again due to the greater subcooling required for the hydrates to form when KHIs were present, and the different subcooling required for each inhibitor to induce the hydrates formation.

It was also observed in Table 3.3 that polymers such as PVP40 showed very different values of Δt_3 (between 26 min and 116 min), even when T_o and T_p have quite similar values. It suggested that once the crystals formed, the number of adsorbing polymeric sites of PVP sometimes is not high enough to inhibit the further growth of the hydrate crystals. The same observation has been done by Pic et al., (2000). Zeng et al., (2008) have indicated that the lower inhibition activity of PVP is because the polymer forms a non rigid layer with more trapped solution. Based on simulations, Moon et al., (2007) have suggested that surface adsorption cannot be responsible for the activity of PVP because PVP remained at least 5-10 Å away from the surface of any hydrate clusters–crystals, and the water structure consistent with the hydrate phase is actually suppressed in the vicinity of the PVP.

If T_o and T_p obtained using KHIs, are compared with those ones obtained using THIs, a higher reduction of the T_o and T_p is generally found for THIs (Table 3.3). This is due to the different mechanisms used for the chemicals to inhibit the hydrate formation. THIs are shifting the thermodynamic stability boundary of hydrates to lower temperatures, and is the reason for a higher reduction of the T_o and T_p. For KHIs, the effect of the inhibiting additives is also manifested lowering the onset temperature of hydrates formation. However, they have showed limited subcooling compared to THIs.

3.3.2.3 Kinetic inhibitors in NaCl 3.5 wt%

To further investigate the nature of the inhibition of KHIs, different concentrations of KHIs were investigated in blends with seawater (NaCl 3.5 wt%). Figures 3.20 to 3.29 present the plots of T vs. t showing the onset temperature of hydrates formation.

Table 3.3 summarises all the results for these inhibitors.

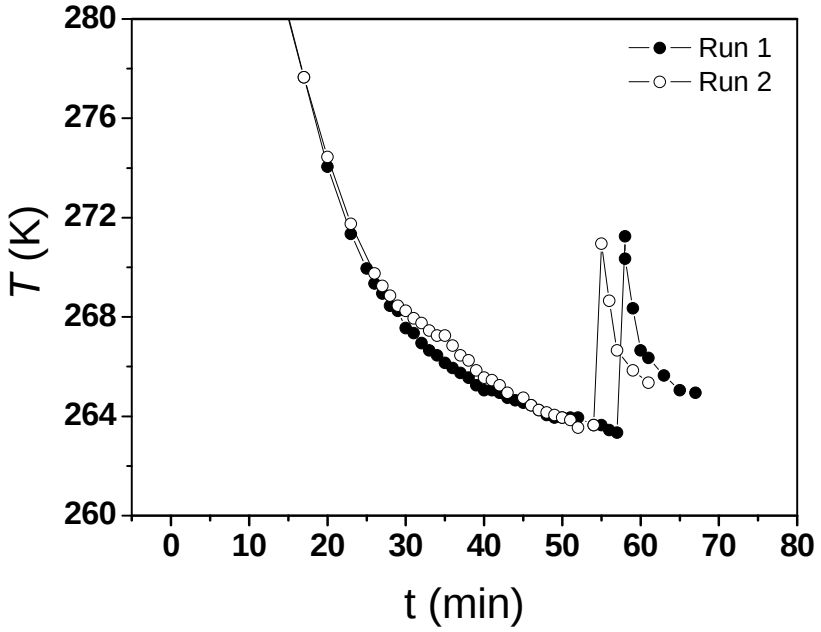

Figure 3.20 Temperature change in THF 19.2 wt% – 0.1 wt% of Gaffix® VC713 and 3.5 wt% NaCl. Cooling rates for Runs 1 and 2 were 1.2 K/min.

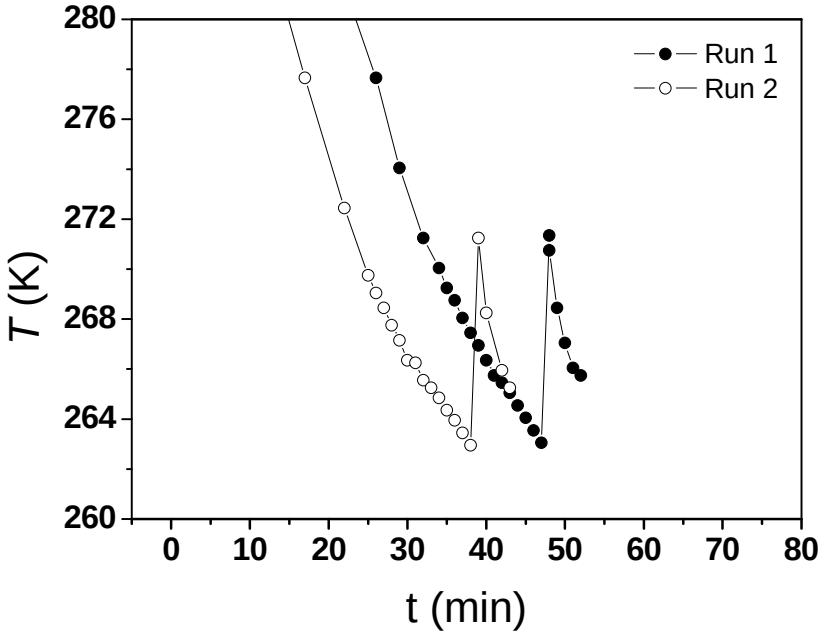

Figure 3.21 Temperature change in THF 19.2 wt% – 0.25 wt% of Gaffix® VC713 and 3.5 wt% NaCl. Cooling rates for Runs 1 and 2 were 0.9 K/min and 1.1 K/min, respectively.

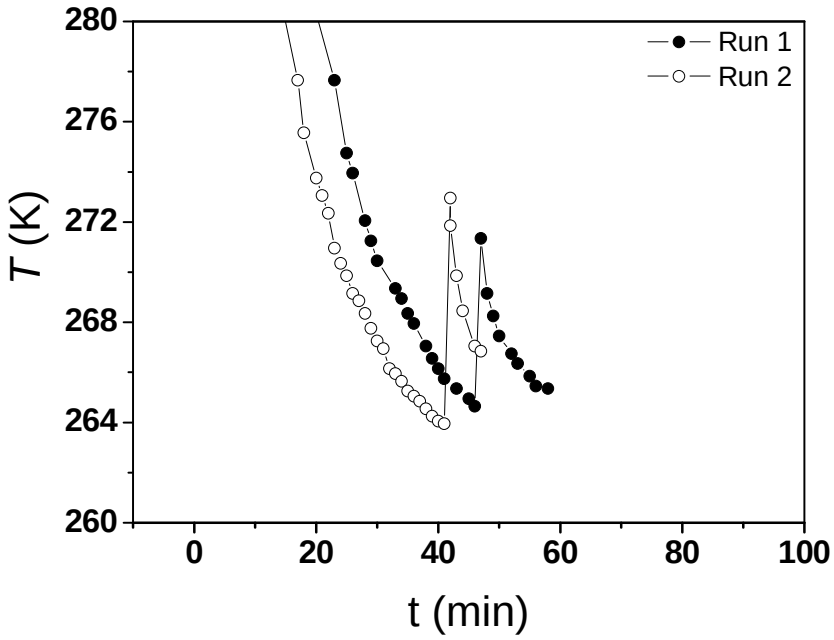

Figure 3.22 Temperature change in THF 19.2 wt% – 0.1 wt% of Luvicap® EG and 3.5 wt% NaCl. Cooling rates for Runs 1 and 2 were 0.9 K/min and 1.2 K/min, respectively.

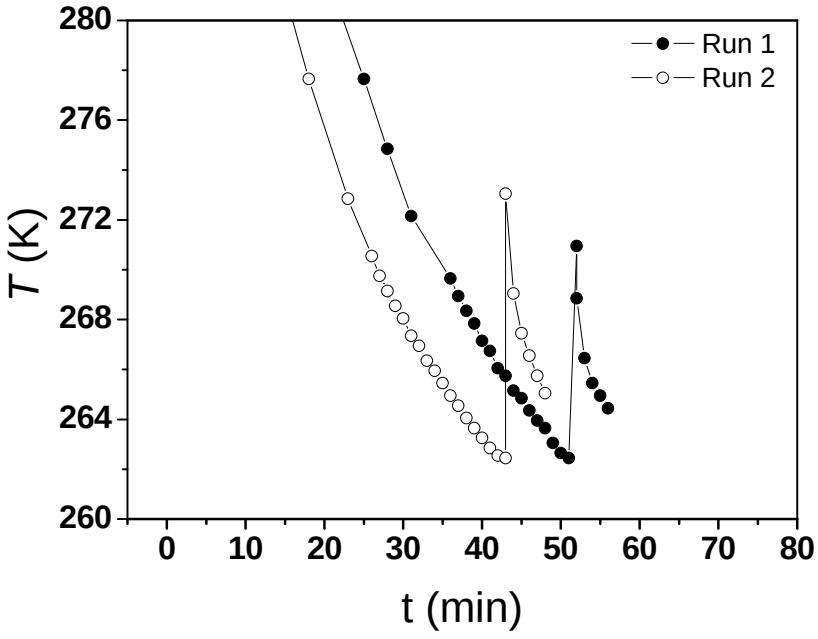

Figure 3.23 Temperature change in THF 19.2 wt% – 0.25 wt% of Luvicap® EG and 3.5 wt% NaCl. Cooling rates for Runs 1 and 2 were 0.9 K/min and 1.1 K/min, respectively.

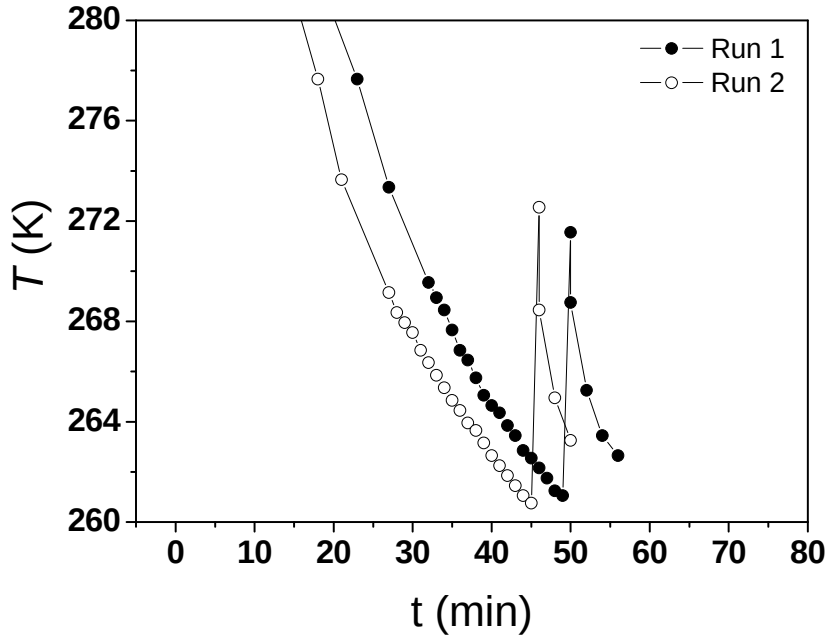

Figure 3.24 Temperature change in THF 19.2 wt% – 0.1 wt% of PEO-VCap and 3.5 wt% NaCl. Cooling rates for Runs 1 and 2 were 0.8 K/min and 1.1 K/min, respectively.

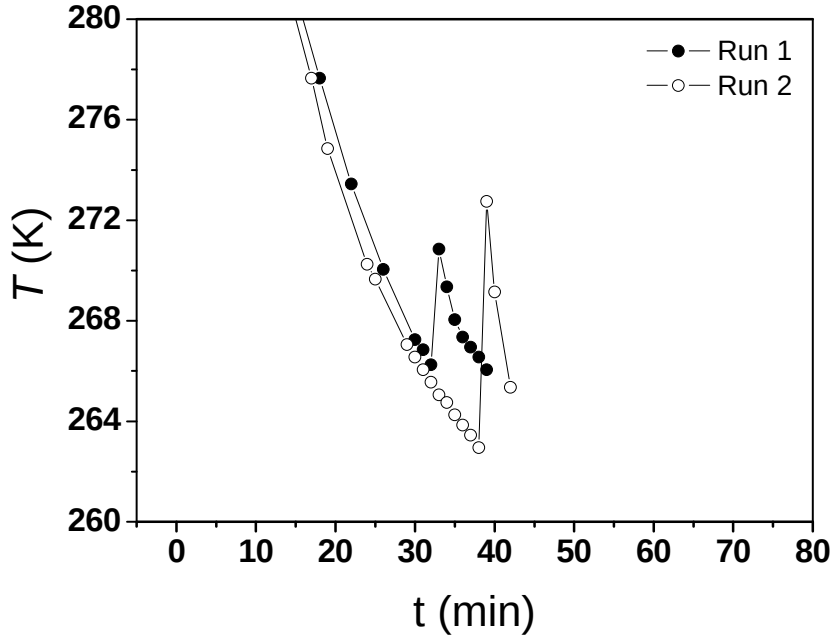

Figure 3.25 Temperature change in THF 19.2 wt% – 0.25 wt% of PEO-VCap and 3.5 wt% NaCl. Cooling rates for Runs 1 and 2 were 1.1 K/min and 1.2 K/min, respectively.

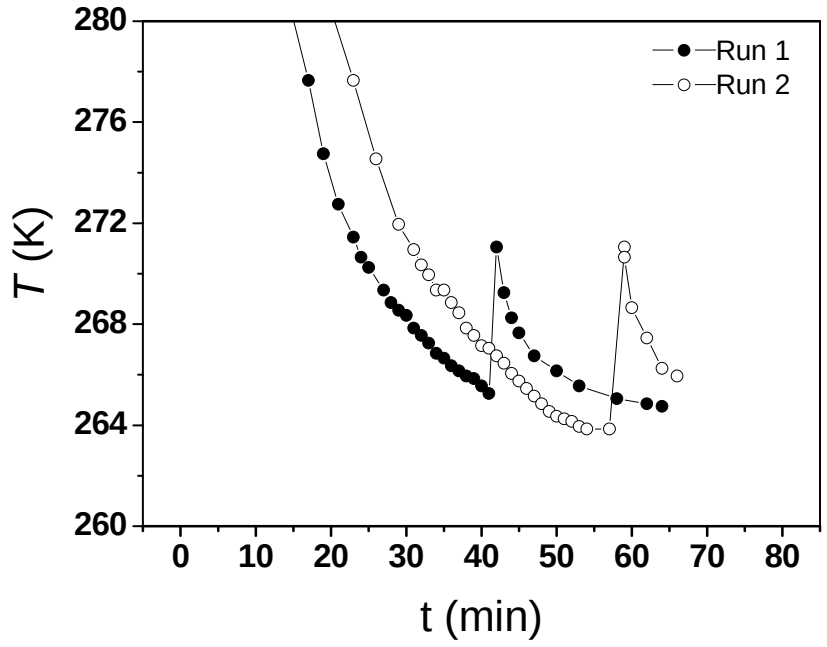

Figure 3.26 Temperature change in THF 19.2 wt% – 0.1 wt% of PVP40 and 3.5 wt% NaCl. Cooling rates for Runs 1 and 2 were 1.3 K/min and 0.9 K/min, respectively.

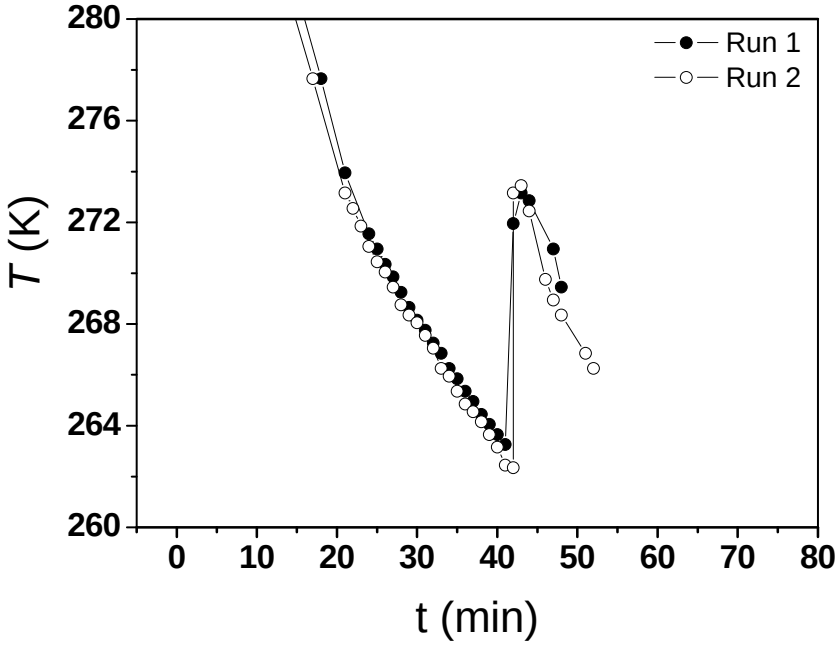

Figure 3.27 Temperature change in THF 19.2 wt% – 0.25 wt% of PVP40 and 3.5 wt% NaCl. Cooling rates for Runs 1 and 2 were 1.1 K/min.

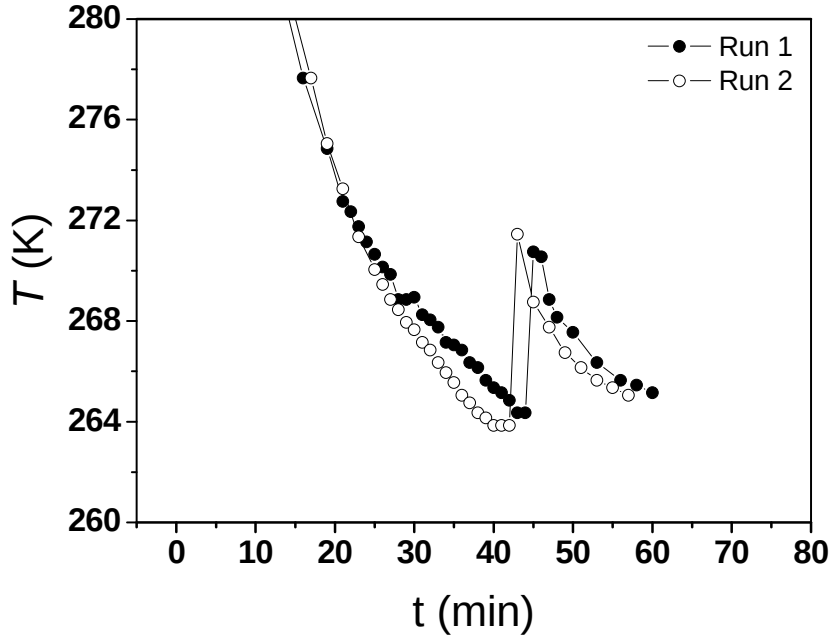

Figure 3.28 Temperature change in THF 19.2 wt% – 0.1 wt% of PVP360 and 3.5 wt% NaCl. Cooling rates for Runs 1 and 2 were 1.2 K/min and 1.3 K/min, respectively.

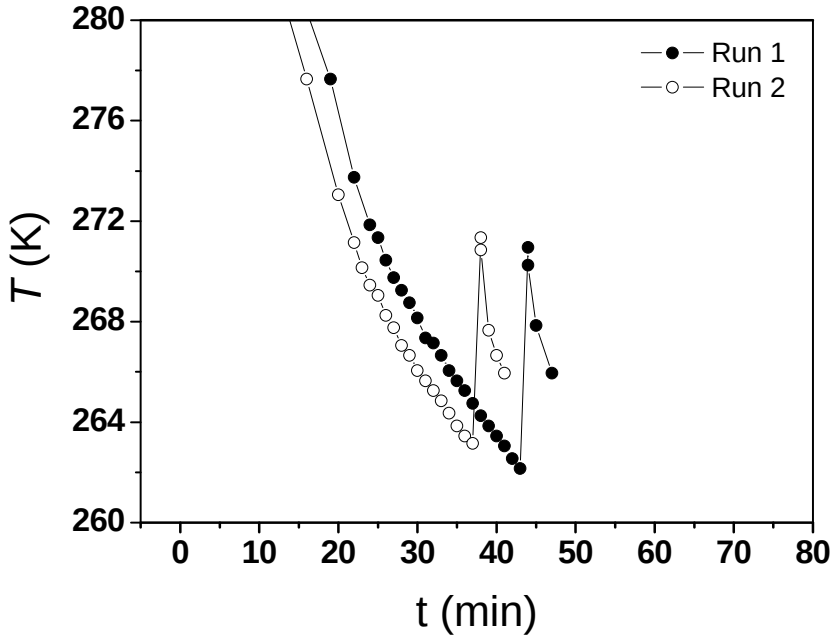

Figure 3.29 Temperature change in THF 19.2 wt% – 0.25 wt% of PVP360 and 3.5 wt% NaCl. Cooling rates for Runs 1 and 2 were 0.9 K/min and 1.1 K/min, respectively.

Figure 3.20 shows two plots of the THF hydrate system containing Gaffix® VC713 0.1 wt% in seawater (they correspond with Runs 1 and 2). A similar trend is observed for both of them. For Run 1 T_o 263.4 K, T_p 271.3 K, ΔT_r 7.9 K, T_e 265.0 K, Δt_1 57 min, Δt_2 1 min and Δt_3 is 9 min approximately. Run 2, T_o 263.7 K, T_p 271.0 K, ΔT_r 7.3 K, T_e 265.4 K, Δt_1 54 min, Δt_2 1 min and Δt_3 is 6 min approximately. The onset of hydrates formation was observed at different times, depending on the cooling rate used, when the T_o and T_p reaches around 263.6 K and 271.2 K respectively. It was indicated by a sudden rise in temperature. After this, the temperature decreases again and gradually becomes constant, until the cell is totally plugged with hydrates. Compared to the system containing the same concentration of KHIs in pure water, the addition of NaCl has produced further decreases in T_o and T_p, as can be observed in Table 3.6.

Table 3.6 Parameters observed during THF hydrates formation in the presence of different KHIs and NaCl 3.5 wt%.

Inhibitor	**Hydrates Systems**	**Characteristics**							
		t_o **(min)**	T_o **(K)**	T_{or} **(K)**	T_p **(K)**	T_{pr} **(K)**	ΔT_r **(K)**	ΔT_{rr} **(K)**	t_e **(min)**
None		14-64	275.1	-	277.0	-	1.9	-	38-61
KHIs	Gaffix® VC713 0.1 wt%	30-63	269.4	5.7	275.9	1.1	6.5	4.6	14-25
	Luvicap® EG 0.1 wt%	25-31	271.6	3.5	276.0	1.0	4.4	2.5	19-23
	PEO-VCap 0.1 wt%	37-46	263.5	13.9	275.6	1.4	12.1	10.2	7
	PVP40 0.1 wt%	35-117	273.3	1.8	276.4	0.6	3.1	1.2	26-116
	PVP360 0.1 wt%	25-95	269.4	5.8	276.0	1.0	6.5	4.6	18-30
KHI + NaCl	Gaffix® VC713 0.10 wt%	32-57	265.0	10.1	271.4	5.6	6.4	4.5	6-14
	Gaffix® VC713 0.25wt%	38-47	263.1	12.0	271.4	5.6	8.3	6.4	4
	Luvicap® EG 0.10 wt%	28-87	265.7	9.4	272.2	4.8	6.5	4.6	3-18
	Luvicap® EG 0.25 wt%	43-51	262.5	12.6	272.1	4.9	9.6	7.7	4-5
	PEO-VCap 0.10 wt%	45-49	261.0	14.1	272.1	4.9	11.2	9.3	4-6
	PEO-VCap 0.25 wt%	32-38	264.7	10.4	271.9	5.1	7.2	5.3	3-6
	PVP40 0.10 wt%	29-57	265.7	9.4	271.5	5.5	5.8	3.9	7-46
	PVP40 0.25 wt%	40-42	263.5	11.6	272.7	4.3	9.3	7.4	6-10
	PVP360 0.10 wt%	39-44	264.0	11.1	271.3	5.7	7.3	5.4	14-15
	PVP360 0.25 wt%	37-43	262.7	12.4	271.2	5.8	8.5	6.6	3

t_o is the time at which T start increasing; T_o is the T at which temperature start increasing; ; T_{or} is the reduction in T_o due to the presence of the inhibitor; T_p is the T at which the nucleation period has already finished and the crystals start to grow; T_{pr} is the reduction in T_p due to the presence of the inhibitor; ΔT_r is the magnitude of the temperature rise; ΔT_{rr} is the reduction in ΔT_r due to the presence of the inhibitor; t_e is the completion time, the time required to the blocking of the cell.

For Gaffix® VC713 the addition of salt produced reductions in T_o and T_p of 4.4 K and 4.5 K respectively, whereas compared to the solution containing no salt, and ΔT_r there was no significant change. Luvicap® EG showed decreases of T_o 5.9 K and T_p 3.8 K, and increases of ΔT_r 2.1 K. For PEO-VCap, the reductions in T_o and T_p were 2.5 K and 3.5 K, respectively, and ΔT_r decreases 0.9 K. The low molecular weight of PVP (PVP40) showed a further decrease in T_o and the presence of salt, than did the high molecular weight PVP (PVP360); thus revealing 7.7 K compared to 5.4 K, respectively. For T_o, the decreases corresponded to 4.9 K and 4.7 K, respectively for PVP40 and PVP360. ΔT_r increases 2.7 K vs. 0.8 K for PVP40 and PVP360, respectively. It is not clear why the salt is affecting T_o, T_p, ΔT_r of KHIs. It could be due to a synergy effect. However, it seems more likely that the addition of salt could change the polymer conformations in solution and thus increase the ability of the inhibitors to adsorb to the hydrate surface (Sloan et al., 1998).

Further decreases in T_o and T_p are also noticed at the same salt concentration of 3.5 wt%, when the concentration of the KHIs was increased from 0.1 wt% to 0.25 wt%, as can be seen in Table 3.6. Compared to the solution containing 0.10 wt% of Gaffix® VC713, when the polymer concentration was increased to 0.25 wt% T_o reduced 1.9 K, T_p was unchangeable, and ΔT_r increased 1.9 K. Luvicap® EG 0.25 wt% reduced T_o 3.2 K, T_p was unchangeable, and ΔT_r increased 3.1 K, compared to solution containing 0.10 wt% of the polymer. For PEO-VCap, the increase in the polymer concentration reduced T_o 0.2 K, increased T_p 1.2 K, and also reduced ΔT_r 4 K. Concentrations of 0.25 wt% of PVP40 and PVP360 produced further reductions in T_o 2.2 K vs. 1.3 K, T_p 1.2 K vs. 0.1 K, and increases in ΔT_r 3.5 K vs. 1.2 K, respectively, compared to the lower concentration. It means that the subcooling ability of KHIs is significantly affected for the polymer concentration used.

It has been reported that the performance of some KHIs improve with the presence of electrolytes (Long et al., 1994; Lederhos et al., 1996). KHIs are currently applied in the industry together with THIs, in wells and in pipelines (Makogon et al., 2000). More recently, the effect of NaCl concentrations on the performance of Luvicap® EG and Gaffix® VC713 was tested on THF hydrates using a ball-stop time (Ding et al.,

2010). The authors demonstrated that the performance of the KHIs is affected significantly by the concentration of the inhibitors and salt strength.

Figure 3.30 compares the values of T_o, T_p and ΔT_r for all the kinetic inhibitors and the system containing no inhibitor. It can be seen in Figure 3.30 that for a concentration of 0.1 wt% of polymer in NaCl 3.5 wt%, PEO-VCap exhibits the lowest T_o (261 K), followed by PVP360 (264 K), Gaffix® VC713 (265 K), PVP40 and Luvicap® EG; these last two exhibit the same T_o (265.7 K). For T_p the trend observed from the lowest to the highest value was PVP360 (271.3 K) < Gaffix® VC713 (271.4 K) < PVP40 (271.5 K) < PEO-VCap (272.1 K) < Luvicap® EG (272.2 K). The trend observed in ΔT_r was PVP40 (5.8 K) < Gaffix® VC713 (6.4 K) < Luvicap® EG (6.5 K) < PVP360 (7.3) < PEO-VCap (11.2 K).

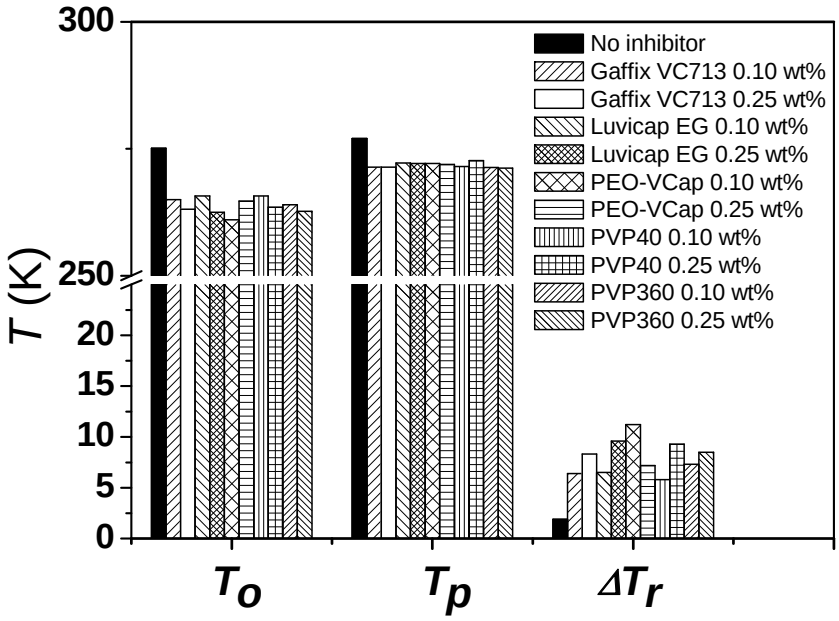

Figure 3.30 Average T_o, T_p and ΔT_r values for all the kinetic inhibitors in NaCl 3.5 wt%.

For a concentration of 0.25 wt% of polymer in NaCl 3.5 wt% the trend from the lowest to the highest T_o and T_p temperatures was the next. For T_o, Luvicap® EG (262.5 K), PVP360 (262.7 K), Gaffix® VC713 (263.1 K), PVP40 (263.5 K), and PEO-VCap (264.7 K). For T_p, PVP360 (271.2 K), Gaffix® VC713 (271.4 K), PEO-

VCap (271.9 K), Luvicap® EG (272.1 K) and PVP40 (272.7 K). For ΔT_r, PEO-VCap (7.2 K), Gaffix® VC713 (8.3 K), PVP360 (8.5 K), PVP40 (9.3 K) and Luvicap® EG (9.6 K).

These results indicated that for a concentration of 0.1 wt% of polymer in NaCl 3.5 wt%, PEO-VCap is more effective preventing the hydrates formation, but also increasing the amount of crystals formed (lower subcooling). However, when polymer the concentration is increased to 0.25 wt%, the PEO-VCap is the less effective inhibitor preventing the hydrates formation. This indicates that the performance of this inhibitor is affected by the concentration.

Figures 3.31 and 3.32 show the sequence of growth and morphology of a stoichiometic THF 19.2 wt% hydrate in the presence of 0.10 wt% and 0.25 wt% kinetic inhibitors and 3.5 wt% NaCl respectively.

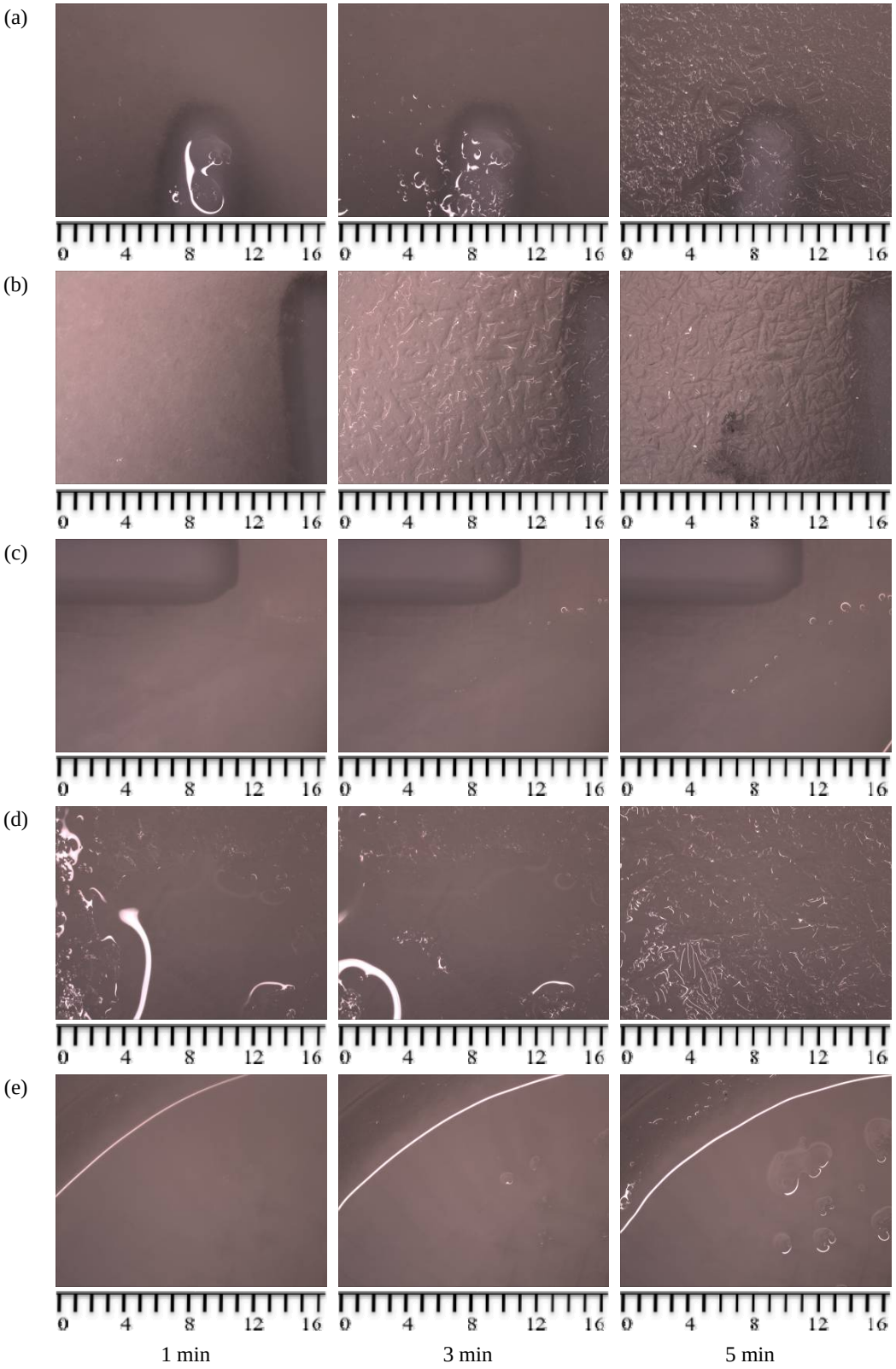

Figure 3.31 Sequence of growth and morphology of THF hydrates in the presence of 0.1 wt% KHIs and 3.5 wt% NaCl. (a) Gaffix® VC713, (b) Luvicap® EG, (c) PVP40, (d) PEO-VCap, (e) PVP360. Scale is expressed in millimetres.

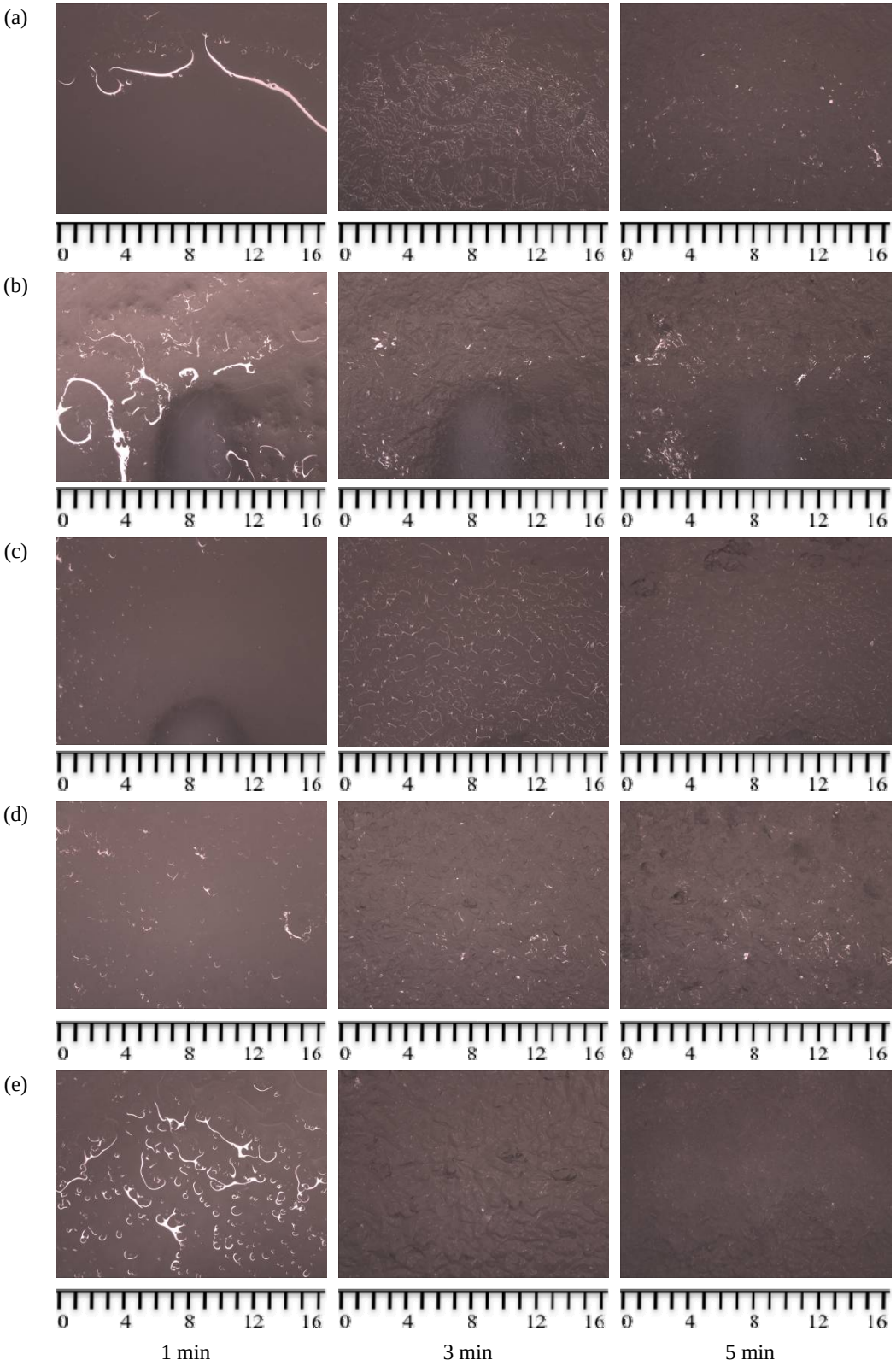

Figure 3.32 Sequence of growth and morphology of THF hydrates in the presence of 0.25 wt% KHIs and 3.5 wt% NaCl. (a) Gaffix® VC713, (b) Luvicap® EG, (c) PVP40, (d) PEO-VCap, (e) PVP360. Scale is expressed in millimetres.

Compared at the same period of crystals growth, and for both concentrations studied, PVP40 showed the best control rate of hydrate formation after hydrates nucleation. Similar to the behaviour of KHIs in pure water, Δt_2 and Δt_3 values presented in Table 3.3 showed no correspondence compared to the uninhibited system. However, these time differences were lower for the KHIs containing NaCl 3.5 wt% than for those ones prepared in pure water. It proves that for lower T_o and T_p (higher subcooling) a higher hydrate growth rate is observed.

3.3.2.4 Anti-agglomerant hydrate inhibitor

Figure 3.33 shows the typical curve temperature vs. time obtained for SDS 0.1 wt% in the presence of THF 19.2 wt%, and used for the detection of the onset of hydrate formation. It behaves similar to previous systems.

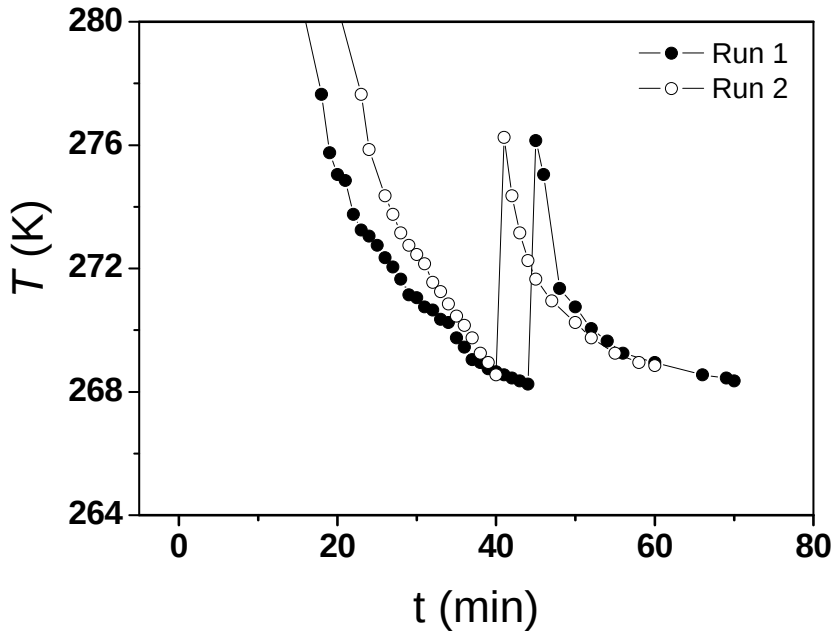

Figure 3.33 Onset temperature change in THF 19.2 wt% –SDS 0.1 wt%.
Cooling rates for Runs 1 and 2 and were 1.2 K/min and 1.0 K/min, respectively.

For the two plots displayed in Figure 3.33 Run 1, T_o 268.3 K, T_p 276.2 K, ΔT_r 7.9 K, T_e 268.4 K, Δt_1 44 min, Δt_2 1 min and ΔT_3 is 25 min approximately. For Run 2, T_o 268.6 K, T_p 275.3 K, ΔT_r 6.7 K, T_e 268.9 K, Δt_1 40 min, Δt_2 1 min and Δt_3 is 19 min approximately. The time differences Δt_1, Δt_2 and Δt_3 were slightly affected by the

cooling rate; however, the values of T_o, T_p, ΔT_r and T_e were not significantly different. Table 3.3 summarises all the key parameters measured for these system, as well the average values and standard deviations estimated for all the experimental runs. Table 3.7 presents extracted data from Table 3.3 for direct comparison among the anti-agglomerant activity compared to the uninhibited system.

Table 3.7 Parameters observed during THF hydrates formation in the presence of AAs.

Inhibitor	Hydrates Systems	Characteristics							
		t_o (min)	T_o (K)	T_{or} (K)	T_p (K)	T_{pr} (K)	ΔT_r (K)	ΔT_{rr} (K)	t_e (min)
None		14-64	275.1	-	277.0	-	1.9	-	38-61
AAs	SDS 0.1 wt%	40-46	268.6	6.5	276.1	0.9	7.5	5.6	16-25

t_o is the time at which T start increasing; T_o is the T at which temperature start increasing; ; T_{or} is the reduction in T_o due to the presence of the inhibitor; T_p is the T at which the nucleation period has already finished and the crystals start to grow; T_{pr} is the reduction in T_p due to the presence of the inhibitor; ΔT_r is the magnitude of the temperature rise; ΔT_{rr} is the reduction in ΔT_r due to the presence of the inhibitor; t_e is the completion time, the time required to the blocking of the cell.

According to the results observed in Table 3.7, for the experimental conditions evaluated in this work, the presence of 0.1 wt% SDS produced a decrease of around 6.5 K in T_o and around 0.9 K in T_p respectively, compared to THF 19.2 wt% in pure water. This reduction in both temperatures could be explained because SDS acts also as an electrolyte, and decreases the water activity. ΔT_r increases in 5.6 K compared to the system containing no inhibitor.

Figure 3.34 shows the evolution of the crystals growth in the absence and the presence of SDS as a function of time. An increase in the hydrate crystals growth can be observed in the presence of SDS compared to the uninhibited system for the same period of time reported. This observation is in agreement with several studies that have indicated that surfactants when added in low concentrations to water can accelerate hydrate growth (Yousif et al., 1994; Karaaslan and Parlaktuna, 2000; Zhong and Rogers, 2000; Daimaru et al., 2007). SDS increases the hydrate nucleation rate by reducing the interfacial tension between hydrate and liquid, and also accelerates hydrate growth rate by increasing the total surface area of hydrate particles and the air–liquid interfacial area (Zhang et al., 2007).

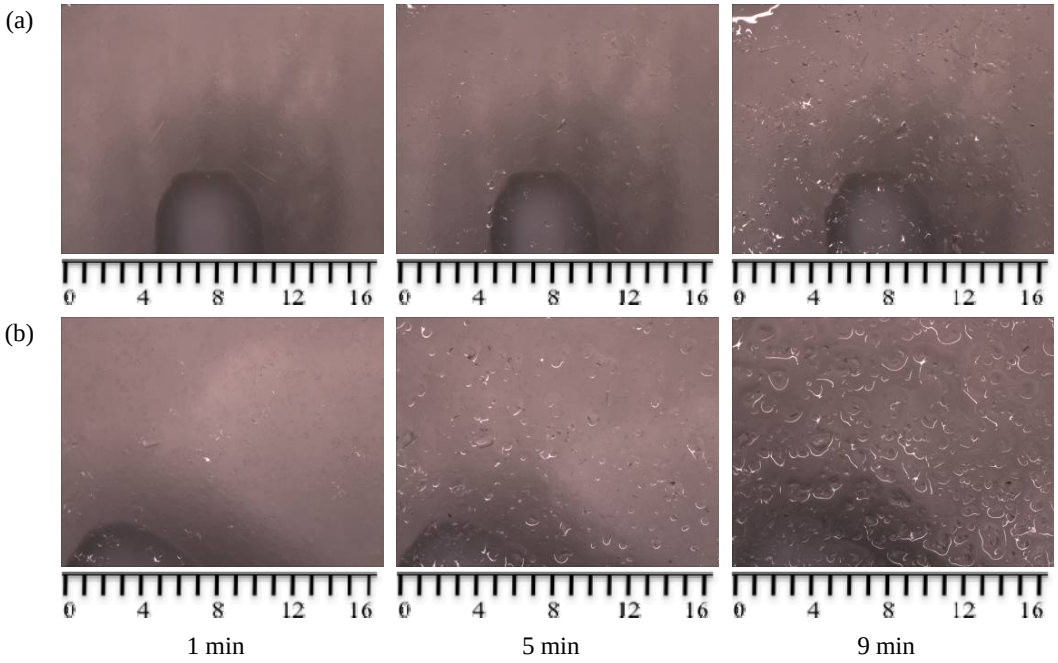

Figure 3.34 Sequence of growth and morphology of a stoichiometic THF 19.2 wt% hydrate in the absence (a) and the presence (b) of anti-agglomerant inhibitor SDS 0.1 wt%. Scale is expressed in millimetres.

In addition, the crystals growth occurred firstly along the borders of the glass vessel (as a ring) and at the surface. Similar observations have been reported by Gayet et al., (2005).

3.4 Conclusions

The kinetic of THF hydrates formation and the performance of three THIs, five KHIs, some mixtures of thermodynamic and kinetic inhibitors and one AAs on THF hydrates have been evaluated using the onset temperature of hydrates formation for the detection of the onset hydrate formation. The maximum temperature spike, the magnitude of the temperature rise with the hydrate formation, the rate of hydrate formation, and temperature at the end-point of the hydrate formation were used to compare the inhibition efficiency.

A summary of the key parameters is provided in Table 3.8. The following conclusions are made based on these data.

Table 3.8 Summary of the key parameters for all the inhibitors.

Inhibitor	Hydrates Systems	Characteristics							
		t_o (min)	T_o (K)	T_{or} (K)	T_p (K)	T_{pr} (K)	ΔT_r (K)	ΔT_{rr} (K)	t_e (min)
None		14-64	275.1	-	277.0	-	1.9	-	38-61
THIs	NaCl	23-37	271.6	3.5	274.2	2.8	2.7	0.8	24-45
	MeOH 0.1 wt%	27-36	269.0	6.1	275.5	1.5	6.5	4.6	10-20
	MeOH 2.0 wt%	31-39	265.4	9.7	274.7	2.3	9.3	7.4	5-12
	MEG 0.1 wt%	36-41	265.9	9.2	276.2	0.8	10.3	8.4	8-13
	MEG 2.0 wt%	28-46	266.3	8.8	275.2	1.8	8.9	7.0	10-13
KHIs	Gaffix® VC713 0.1 wt%	30-63	269.4	5.7	275.9	1.1	6.5	4.6	14-25
	Luvicap® EG 0.1 wt%	25-31	271.6	3.5	276.0	1.0	4.4	2.5	19-23
	PEO-VCap 0.1 wt%	37-46	263.5	13.9	275.6	1.4	12.1	10.2	7
	PVP40 0.1 wt%	35-117	273.3	1.8	276.4	0.6	3.1	1.2	26-116
	PVP360 0.1 wt%	25-95	269.4	5.8	276.0	1.0	6.5	4.6	18-30
KHI + NaCl	Gaffix® VC713 0.10 wt%	32-57	265.0	10.1	271.4	5.6	6.4	4.5	6-14
	Gaffix® VC713 0.25wt%	38-47	263.1	12.0	271.4	5.6	8.3	6.4	4
	Luvicap® EG 0.10 wt%	28-87	265.7	9.4	272.2	4.8	6.5	4.6	3-18
	Luvicap® EG 0.25 wt%	43-51	262.5	12.6	272.1	4.9	9.6	7.7	4-5
	PEO-VCap 0.10 wt%	45-49	261.0	14.1	272.1	4.9	11.2	9.3	4-6
	PEO-VCap 0.25 wt%	32-38	264.7	10.4	271.9	5.1	7.2	5.3	3-6
	PVP40 0.10 wt%	29-57	265.7	9.4	271.5	5.5	5.8	3.9	7-46
	PVP40 0.25 wt%	40-42	263.5	11.6	272.7	4.3	9.3	7.4	6-10
	PVP360 0.10 wt%	39-44	264.0	11.1	271.3	5.7	7.3	5.4	14-15
	PVP360 0.25 wt%	37-43	262.7	12.4	271.2	5.8	8.5	6.6	3
AAs	SDS 0.1 wt%	40-46	268.6	6.5	276.1	0.9	7.5	5.6	16-25

t_o is the time at which T start increasing; T_o is the T at which temperature start increasing; ; T_{or} is the reduction in T_o due to the presence of the inhibitor; T_p is the T at which the nucleation period has already finished and the crystals start to grow; T_{pr} is the reduction in T_p due to the presence of the inhibitor; ΔT_r is the magnitude of the temperature rise; ΔT_{rr} is the reduction in ΔT_r due to the presence of the inhibitor; t_e is the completion time, the time required to the blocking of the cell.

1. The kinetics of the THF hydrate is affected by the physical chemical environment, which includes the concentration and types of additives used for the inhibition of the hydrate. An increase in subcooling and a reduced onset temperature of hydrates formation, were observed when various inhibitors were used, compared to the system containing no inhibitor.

2. The presence of THIs reduces the T_o and T_p values due to the shifting of the thermodynamic stability boundary of hydrates to lower temperature. These reductions in T_o and T_p indicate that additional subcooling is required for the hydrates to form when THIs are present in the system. MeOH and MEG have shown a higher ability to suppress the hydrate formation temperature (a higher subcooling is required) than NaCl. When the concentration of MeOH and MEG is increased, a higher degree of suppression becomes apparent. However, when the onset temperature is reached, THIs increase the growth of hydrate crystals.

3. The presence of KHIs is reflected in a reduction of T_o and T_p values (lower degree of subcooling needed before hydrate formation). For a concentration of 0.1 wt% of polymer in pure water, PEO-VCap exhibits the lowest values of T_o and T_p. From the lowest to the highest value of T_o PEO-VCap was followed by Gaffix® VC713 and PVP360 which showed the same temperature, Luvicap® EG and PVP40. For T_p, the trend observed from the lowest to the highest value was PEO-VCap, followed by Gaffix® VC713, PVP360 and Luvicap® EG, which showed the same temperature, and PVP40. However, ΔT_r obtained for KHIs suggests a higher amount of crystals formed than in the system containing no inhibitor, probably due to the higher degree of subcooling.

4. If T_o and T_p obtained using KHIs are compared with those ones obtained using THIs, a higher reduction of the T_o and T_p is generally found for THIs. This is due to the different mechanisms used for the chemicals to inhibit the hydrate formation. At the investigated concentration range, 0.1-2.0 wt%, MeOH and MEG, were more effective than the KHIs in preventing the formation of THF hydrates, even at such low concentrations. KHIs have showed limited subcooling compared to THIs.

5. Different performances of KHIs have been observed in a system THF–water and THF—NaCl. The performance of some KHIs is improved with the presence of NaCl. For a concentration of 0.1 wt% of polymer in NaCl 3.5 wt% PEO-VCap exhibits the lowest T_o, followed by PVP360, Gaffix® VC713, PVP40 and

Luvicap® EG; these last two exhibiting the same T_o. For the same concentration, the trend observed for T_p from the lowest to the highest value was PVP360 < Gaffix® VC713 < PVP40 < PEO-VCap < Luvicap® EG. For a concentration of 0.25 wt% of polymer in NaCl 3.5 wt% the trend from the lowest to the highest temperatures was the next. For T_o, Gaffix® VC713, PVP40, Luvicap® EG, PVP360 and PEO-VCap. For T_p, PVP360, Gaffix® VC713, PEO-VCap, Luvicap® EG and PVP40.

6. NaCl alone was not very effective in preventing the formation of hydrates in a concentration of 3.5wt%. However, the inhibition efficiency of most KHIs used in this study was enhanced with the presence of NaCl 3.5 wt%, showing a strong synergy effect.

7. The presence of 0.1 wt% SDS decreases the temperature required to form the hydrate, compared to THF 19.2 wt% in pure water, but enhances the rate of hydrate formation.

8. THIs and AA have been evaluated in this chapter to provide a comparison with the behaviour of KHIs preventing the hydrates formation and growing. According to the results, THIs seem more effective preventing the formation of hydrates than KHIs, even at such low concentrations. However, the growing of the crystals is accelerated with the presence of both THIs and AAs. So far, THIs and AAs have been more widely applied by the industry than KHIs because of the ability to handle high subcoolings, whist, the kinetic inhibition technology provides an attractive cost-saving alternative to THIs; and improves the safety of operation and their environmental impact.

More investigations are necessary to answer the following questions: why the different KHIs are producing distinct onset of hydrates formation, why the presence of electrolytes is improving the inhibition efficiency of most KHIs, which is the mechanism by which KHIs are delaying the growth of hydrate crystals, whether the KHIs inhibition efficiency is the same in both THF and gas hydrates systems. The

following chapters will investigate these problems in order to provide further understanding about the kinetic inhibition mechanism of hydrates.

Chapter 4 INTERFACIAL AND MONOLAYER PROPERTIES OF THE KINETIC INHIBITORS AT THE AIR–LIQUID INTERFACE

4.1 Introduction

It was demonstrated in the previous chapter that the kinetic of THF hydrates formation is affected by the concentration and types of additives used for the inhibition of the THF hydrate. In comparison to the system containing no inhibitor, when various inhibitors were used, it was observed that there was an increase in subcooling and a reduced onset temperature of hydrates formation. The inhibition efficiency of most KHIs used in this study was enhanced with the presence of NaCl 3.5 wt%. We believe that the inhibiting efficiency of KHIs is relevant to the adsorption of KHIs molecules on the hydrate crystal surface, as this leads to a lowering of interfacial tension. Therefore, the adsorbed KHIs molecules sterically block gas molecules from entering and completing hydrate cavities, forcing the crystals to grow around and between the polymer strands (Peng, Sun, Liu, Liu et al., 2009). Since it is not possible to directly measure surface tensions involving a solid phase (Spelt et al., 1986), the measurement of the surface tension is often carried out in the absence of hydrates, but in conditions near to those ones where hydrates formation would normally occur (Peng, Sun, Liu, and Chen, 2009). In this chapter, we will investigate the adsorption of KHIs at the air–liquid interface, in order to establish a quantitative understanding about the adsorption characteristics of the inhibitors onto interfaces. We understand that the interfacial behaviour of the KHIs at the air–liquid interface might be totally different to the behaviour at the solid–liquid interfaces. However, a quantitative description of the KHI adsorption properties, such as the adsorption constant and the saturated surface excess at the air–liquid interface, and the diffusion coefficient in the liquid, will provide some useful information for understanding KHI behaviour in a more complex hydrate system that contains not only solid and liquid, but also gaseous phases.

Most of the KHI polymers we have investigated are water-soluble polymers containing both hydrophilic and hydrophobic components in their macromolecules. It

confers to KHI polymers interesting adsorption behaviour, and, surface–active properties. The interfacial adsorption of amphiphilic polymers is a critical process for the application of a wide range of technologies, due to its significant importance in stabilising and controlling colloidal systems. The properties of polymers near an interface are distinctively different from its bulk properties (Fleer et al., 1993). The quantitative description of these macromolecules in solution, and at interfaces, have been studied extensively in the last few decades, yet any clear understanding remains unsatisfactory due to experimental and theoretical difficulties (Gilányi et al., 2006).

Recent years have seen an increase in research activities on amphiphilic polymers, that are used to slowing down the process of natural hydrate formation during oil and gas industry operations (Kelland, 2006). Some studies have suggested the surface adsorption of the polymer onto growing crystals, and correlated this adsorption with the effectiveness of the inhibitor (Hutter et al., 2000; King Jr et al., 2000). This further demonstrates that the quantitative description of the adsorption characteristics of KHIs, as denoted by interfacial tension measurements, is important for providing a deeper insight into the mechanism of hydrate inhibition.

This chapter aims to investigate the surface activity of Gaffix® VC713 in the form of both, solutions and spread layers of polymer at the air–liquid interface. The polymer is known as one of the most efficient kinetic inhibitors of natural gas hydrates. It contains a hydrophobic polymer back bone, and a mixture of three types of hydrophilic pendent groups which include, a five and a seven member lactam ring and a branched amide group. The description of this polymer is shown in Table 3.1, and its chemical structure is shown in Figure 3.1 (a).

It is generally accepted that in a gas hydrate formation process, the hydrophilic pendant groups of the polymer bind onto the surface of hydrate particles in the early stage of nucleation and growth; therefore, preventing the particle from reaching the critical size (the size at which hydrate particle growth becomes thermodynamically favourable), or slowing down the growth of particles that have reached the critical size (Kelland et al., 1995). This property is particularly important when the hydrate formation time is required to be longer than the gas residence time in the pipeline (Kelland, 2006). A proposed hypothesis, based on inhibitor performance experiments

and modelling, suggests that the inhibition mechanism of such kinetic inhibitors involves the adsorption of polymers on the growing particles or crystals of hydrate perturbing their further growth (Carver et al., 1995; Lederhos et al., 1996).

Consequently, an understanding of the interfacial properties is important for the development of effective gas hydrate inhibitors (Rojas and Lou, 2009, 2010). In fact, interfacial phenomena analysis has been employed to study gas hydrates formation systems in the presence of surfactants (Sun et al., 2004; Luo et al., 2006; Zhang et al., 2007; Okutani et al., 2008). Some studies have focused on the interactions between hydrate particles in the presence of anti-agglomerants and/or hydrate promoters (Taylor et al., 2007; Anklam et al., 2008; Nicholas et al., 2009). The first study analyses theoretically the mechanisms of hydrate agglomeration, and the effects of surface-active additives on antiagglomeration (Anklam et al., 2008). In the second and third studies, adhesion forces between THF hydrate particles in *n*-decane (Taylor et al., 2007), and cyclopentane hydrates and carbon steel (Nicholas et al., 2009) are measured using micromechanical and force balance techniques, respectively. The investigation of interfacial tension at the gas–liquid interface is capable of providing information, which is helpful in revealing the mechanism of hydrate formation and inhibition. A recent study by Peng et al., (2009) has shown that the presence of a kinetic inhibitor in the hydrate formation region, lowers the interfacial tension between methane and aqueous solutions of different contents of Gaffix® VC713, promotes nucleation, but reduces the growth rate of hydrates at the methane–Gaffix® VC713 interface. The authors calculated the surface adsorption free energies of methane, in order to investigate the effect of this kinetic inhibitor on the nucleation of hydrates. Results show that the presence of the inhibitor lowers the interfacial tension, increases the concentration of methane on the surface of the aqueous phase, and thus promotes the nucleation of hydrates at the gas–liquid interface. Additionally, the lateral growth rate of hydrate film on the surface of a methane bubble, suspended in the aqueous phase, was measured at different pressures to investigate the effect of Gaffix® VC713 on the growth of hydrates. The results reveal that the lateral growth rate of hydrate film from aqueous Gaffix® VC713 solution is much lower than that from pure water, demonstrating that Gaffix® VC713 significantly inhibits hydrate growth (Peng, Sun, Liu, Liu et al., 2009).

On the other hand, it is well known that water-soluble proteins and soluble polymers with hydrophilic groups, are able to form stable “insoluble” monolayers at the air–water interface (Langmuir and Schaefer, 1939; Trurnit, 1960; Zatz and Knowles, 1971; Kuzmenka and Granick, 1988; MacRitchie, 1991; Gargalló et al., 2005), either by spreading the polymer on the interface (Langmuir monolayers), or by adsorption of the polymer from the bulk (Gibbs monolayers) (Díez-Pascual et al., 2007). The formation of “insoluble” monolayers of water-soluble proteins, by direct spreading of aqueous solutions at the air–water interface has been used to estimate the molecular weights of proteins (Lou et al., 2000). If the molecular weight of a soluble polymer is known, the low-pressure region of the isotherm of the spread polymer can be used to estimate the spreading efficiency, and hence infer the packing density in the monolayer (Lou et al., 2000). Accordingly, we can use this principle to semi-quantify the surface area occupied by these polymers at the air–liquid interface.

To semi-quantify the surface area occupied by these polymers at the air–liquid interface, one needs to measure the surface pressure as a function of the area of subphase available to each molecule that forms the monolayer. This can be carried out at a constant temperature using a Langmuir trough. The ultimate parameter resulting from this measurement is known as a surface pressure–area isotherm. Usually an isotherm is recorded by compressing the film (reducing the area with the barriers) at a constant rate while continuously monitoring the surface pressure, which is the difference between the surface tension in absence of a monolayer and the surface tension with the monolayer present (*KSV minitrough operation manual. Revision 1.1*).

Overall, the work reported in this chapter includes the following two parts.

1. We investigate the processes governing the adsorption, and the rate of the transport of Gaffix® VC713 from the bulk into the air–liquid interface. A sodium chloride solution (3.5 wt% which is 0.6 mol/L) was used as a solvent. The experimental data was collected using a pendant bubble method at both an ambient temperature, and a temperature that is close to that of hydrates formation. The surface tension data was then analysed based on equilibrium and dynamic adsorption models, using different theoretical and computational methods. The

influence of polymer concentration and temperature on the adsorption of the polymer is discussed. The adsorption isotherms of Luvicap® EG, two PVPs (including PVP40 and PVP360), a copolymer that contains both poly(ethylene oxide) and vinylcaprolactam segments (PEO-VCap), and a new PVCap that was synthesised in house, are also presented in this chapter for comparison. The effect of sodium chloride and tetrahydrofuran on the adsorption behaviour of the polymers is also discussed.

2. We also investigate the spread monolayer behaviour of Gaffix® VC713, Luvicap® EG and PVP360 at the air–liquid interface using a Langmuir trough by measuring the surface pressure–area isotherms using a Langmuir balance. This is to supplement the surface tension studies.

4.2 Materials and methods

4.2.1 Materials

Six polymeric KHIs have been used for the surface tension measurements. Five of them, Gaffix® VC713, Luvicap® EG, PVP40, PVP360 and PEO-VCap have been evaluated in the previous chapter. A brief description of each one is presented in Table 3.1. PVCap made in house also has been evaluated in this chapter. Gaffix® VC713, Luvicap® EG and PVP40 were also used for the measurement of the surface pressure–area isotherms.

The water used in the experiments was purified by a Millipore Milli-Q system, and it is referred to as pure water. Sodium chloride (AnalaR, BDH) solution (3.5 wt% which is 0.6 mol/L) was made using pure water for all measurements. Tetrahydrofuran (THF) (ChromAR® 99.8% Mallinckrodt Chemicals) was used as received. The chloroform (Sigma Aldrich) was a spectroscopic grade.

4.2.2 Surface tension (γ) measurements

Surface tension was measured by the pendant bubble method using a commercial Profile Analysis Tensiometer PAT-1 (SINTERFACE Technologies, Germany). Figure 4.1 (a) and (b) shows a photograph and a sketch of this instrument. The main

principle of this method is to determine the surface tension of a liquid from the shape of the bubble (Figure 4.1 (c)) (Miller et al., 1994).

(a)

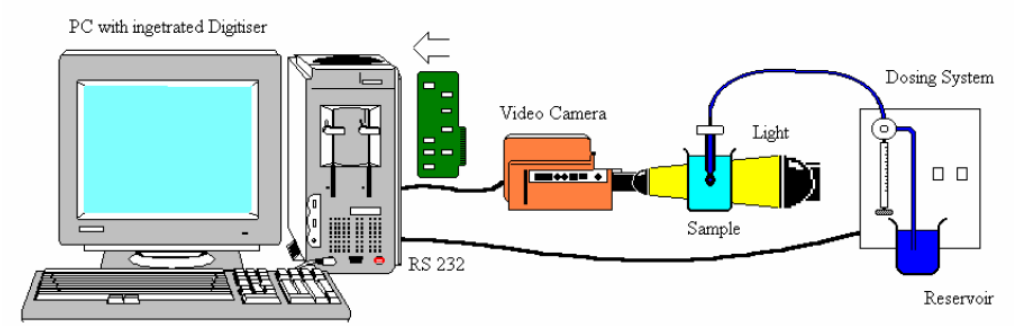

(b)

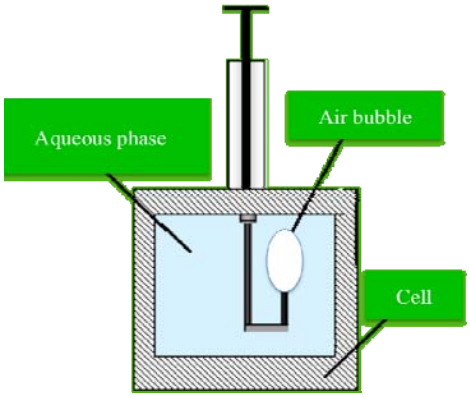

(c)

Figure 4.1 Profile Analysis Tensiometer PAT-1 (*Profile analysis tensiometer PAT1 operation manual*, 2005).

The transient surface tension was determined by fitting the Laplace equation to the coordinates of the bubble shape, using the surface tension as a fitting parameter. The

instrument allows continuous measurement, up to five per second, of the surface tension as a function of time with an accuracy of ±0.1 mN/m. Because achieving equilibrium in polymer solutions can take a long time, and may never be reached, the surface tension was considered at its equilibrium when it became a pseudo plateau, after approximately 1 hour, unless otherwise indicated. The glass cell containing the solution was sealed to prevent evaporation. Prior measuring each of the polymer solutions, calibration of the instrument using deionised water was carried out to ensure no contamination was present in the system. Temperature was kept constant at 293 or 278 K ± 0.2 K respectively by circulating thermostated fluid from an external bath. The measured polymer concentrations ranged from 0.01 to 1.00 wt%. The samples were prepared by weighing using an analytical balance of precision ±0.01 mg.

4.2.3 Surface pressure area (*Π-A*) measurements

Surface pressure–area (*Π–A*) isotherms of spread monolayers of the polymers at the air–water interface, were measured using a Teflon Langmuir surface balance KSV Minitrough LB System. Figure 4.2 provides a drawing of the experimental equipment. The entire system was covered with a box of poly(methyl methacrylate) in order to prevent environmental pollution. Solutions of monolayer polymer were prepared in a concentration of 0.1 wt% of polymers in chloroform. The polymer monolayers were deposited on a fresh aqueous subphase contained in a Teflon trough. Placing the polymer monolayer on the subphase was undertaken with care, by expressing aliquots from a Hamilton microsyringe down a glass rod dipping into the water (Trurnit, 1960). The aqueous subphases were made of pure water or a sodium chloride solution (3.5 wt%). This technique has been found useful for spreading of “insoluble” monolayers of water-soluble polymers and proteins (Langmuir and Schaefer, 1939; Trurnit, 1960; MacRitchie, 1991).

The Langmuir trough and the barriers were cleaned first with a soft brush covered in ethanol, and then rinsed with pure water. The barriers were placed on top of the trough with special care to avoid touching them directly with the fingers. An aspirator tip was used to remove the water in excess from the trough. The trough was

then filled with the subphase, by pouring the subphase gently on to the trough so that the level of the water rose distinctly (at least 3mm) above the level of the trough. Using the KSV Minitrough software, the aspirator was turned on and the barriers were brought together. Contaminants on the surface of the water were picked up by the barrier. The aspirator was run along both barriers several times, when they were fully closed, several times to remove contaminants. Sufficient water was removed to lower the water surface until it was level with the trough. The Wilhelmy plate was cleaned using pure water, and then placed over a flame for a few seconds, to remove residues on the plate's surface. Once it was cool, the plate was dipped into the water in the trough and then hung from the balance hook. The plate was arranged so that about two thirds of it was covered and was perpendicular to the barriers. The barriers were opened and zeroed with pure subphase and then closed. It is to be noted that pure water does not cause the surface pressure to change, so any change in surface pressure is caused by contaminants. If the surface pressure does not exceed 0.2 mN/m the water can be considered sufficiently clean. About 30 μl of the monolayer polymer solution contained in a Hamilton microsyringe was injected to produce the monolayer, by expressing aliquots of the solution down a glass rod dipping into the subphase. The surface pressure was measured during the formation of the monolayer with a platinum Wilhelmy plate to a sensitivity of 0.01 mN/m. The surface pressure changes did not exceed 0.5 mN/m during the monolayer injection. Before beginning the compression, 30 min were allowed for the solvent to evaporate. The data was obtained at a constant compression rate of 5 mm/min. The surface pressure and the mean molecular area were continuously monitored during compression. Water, as the subphase, was purified by a Millipore Milli-Q system and had a resistivity greater than 18.0 MΩ.cm. The temperature was kept constant at 298 and 278 ± 0.5 K by circulating thermostated water from an external bath.

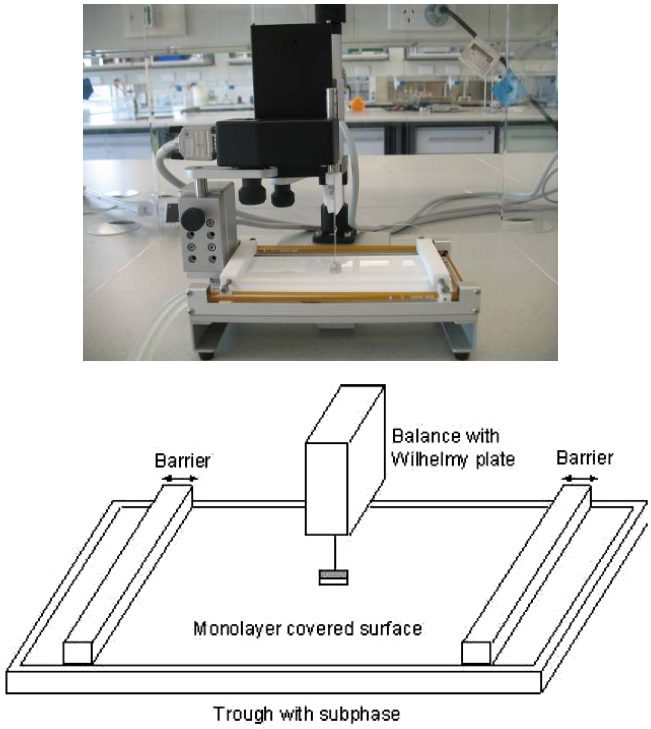

Figure 4.2 KSV MiniMicro LB System (*KSV minitrough operation manual. Revision 1.1*).

4.3 Quantifying polymer adsorption properties

4.3.1 Equilibrium surface tension

Equilibrium surface tension is often used to describe the adsorption behaviour and the molecule arrangement at the air–liquid interface (degree of packing and/or the orientation of the surface-active substances at the surface). The dependence of the equilibrium surface tension on polymer concentration and surface excess concentration of polymer adsorbed at the interface, Γ, can be calculated by the Gibbs adsorption equation, assuming monodispersed polymers:

$$\Gamma = -\frac{1}{RT}\left(\frac{d\gamma}{d\ln(c_b)}\right) \tag{4-1}$$

where γ is the superficial tension; c_b is the bulk polymer concentration, R is the gas constant, T is the absolute temperature; Γ is the equilibrium surface excess (Lankveld and Lyklema, 1972).

The molecular adsorption of polymers on the fluid surface can also be computed using Langmuir adsorption isotherm (Rosen, 1989):

$$\Gamma = \Gamma_m \frac{c_b}{(c_b + a_L)} \tag{4-2}$$

Where a_L is the adsorption constant and Γ_m is saturated surface excess. The analogous surface equation of state for the Langmuir isotherm is the Szyszkowski (Eastoe and Dalton, 2000) obtained by combination of Eqs. (4-1) and (4-2):

$$\gamma_0 - \gamma = -RT\Gamma_m \ln\left(1 + \frac{c_b}{a_L}\right) \tag{4-3}$$

where γ_0 is the surface tension in the absence of polymer.

Both a_L and Γ_m are related to the standard free energy of adsorption ΔG^0_{ads} and to the areas covered by the polymer at the interface (chemical structure) respectively and can be estimated by fitting the experimental data to Eq. (4-3).

4.3.2 Dynamic surface tension

To further understand the surface activity of the investigated polymer, the adsorption dynamics of the inhibitors at the air–sodium chloride solution interface was analysed. Two different computational methods were applied: a diffusion-controlled model and asymptotic approximation.

In general, the dynamic adsorption of a polymer at the air–liquid interface can be described in terms of the surface tension using a generalised adsorption isotherm:

$$\gamma_0 - \gamma(t) = -RT\Gamma_m \ln\left(1 - \frac{\Gamma(t)}{\Gamma_m}\right) \tag{4-4}$$

Where $\gamma(t)$ is the (dynamic) surface tension in the presence of a polymer, $\Gamma(t)$ is the dynamic adsorption density (the dynamic surface concentration).

The dynamic adsorption density can also be described by the celebrated Ward and Tordai equation (Ward and Tordai, 1946):

$$\Gamma(t) = 2c_b\sqrt{Dt/\pi} + 2\sqrt{D/\pi}\int_0^t c_s(t)d\left(\sqrt{t-\tau}\right) \tag{4-5}$$

Where D is the polymer diffusion coefficient, c_s is the polymer concentration at the subsurface layer, t is the reference time, and τ is the integration variable.

Since c_s is not known in advance, a second equation is required in the determination of the dynamic adsorption density. The second equation can be either an adsorption isotherm, or a kinetic equation depending on the rate of the adsorption/desorption step (Chang and Franses, 1995).

For the investigated polymer systems, an instantaneous adsorption/desorption step is assumed, i.e. the overall adsorption dynamic is controlled by polymer diffusion only. Consequently, the subsurface concentration can be related to the surface excess by the adsorption isotherm, i.e. Eq. (4-2), and given as:

$$c_s(t) = a_L\frac{\Gamma(t)}{\Gamma_m - \Gamma(t)} \tag{4-6}$$

Eqs. (4-5) and (4-6) can be solved numerically for $\Gamma(t)$, which then yield the dynamic surface tension from Eq. (4-4).

The above numerical model is only effective for rapid changes in dynamic surface tension. On the other hand, the dynamic surface tension of polymers usually displays a long and gradual reduction after the initial rapid reduction. Consequently, an asymptotic solution to the Ward and Tordai equation was also employed. The asymptotic solution to the Ward and Tordai equation is well known for the

description of dynamic surface tension when $\gamma(t)$ is close to the equilibrium value γ (Fainerman et al., 1994). As $t \to \infty$ the subsurface concentration will get closer to the bulk concentration, and c_s can be factored outside the 2nd integral in Eq. (4-5). Hence:

$$\Delta c_{t\to\infty} = c_b - c_s = \Gamma\sqrt{\frac{\pi}{4}Dt} \tag{4-7}$$

Combining Eq. (4-7) with Eq. (4-1) and taking limit as $\Delta c \to 0$, the long time approximation can be written in the following form:

$$\left(\frac{d\gamma}{dt^{-1/2}}\right)_{t\to\infty} = \frac{RT\Gamma_m^2}{c_b}\sqrt{\frac{\pi}{4D}} \tag{4-8}$$

4.4 Results and discussion

4.4.1 Surface tension measurement

Figures 4.3 and 4.4 show the time dependence of surface tension of Gaffix® VC713 at the air–sodium chloride solution interface at 293 and 278 K, respectively. For all solutions investigated, a rapid reduction of the surface tension was observed in the first 10 min, followed by a gradual reduction as the time was increased. This means the polymers adsorb faster towards the interface at the beginning, and after 10 min the adsorption is reduced. This is probably due to the progressive ordering of polymer molecules within the surface layer. For the period considered for the experiment (1 h), Figures 4.3 and 4.4 reveal that the pseudo plateau observed at long periods of time might represent mesoequilibrium as the surface tension still continues decreasing very slowly.

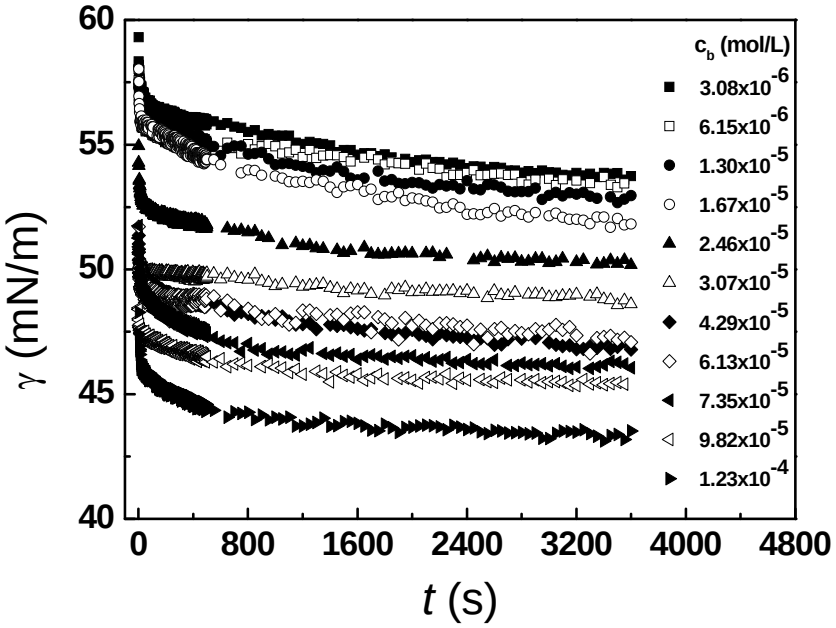

Figure 4.3 Time dependence of the surface tension at various Gaffix® VC713 concentrations – 293 K.

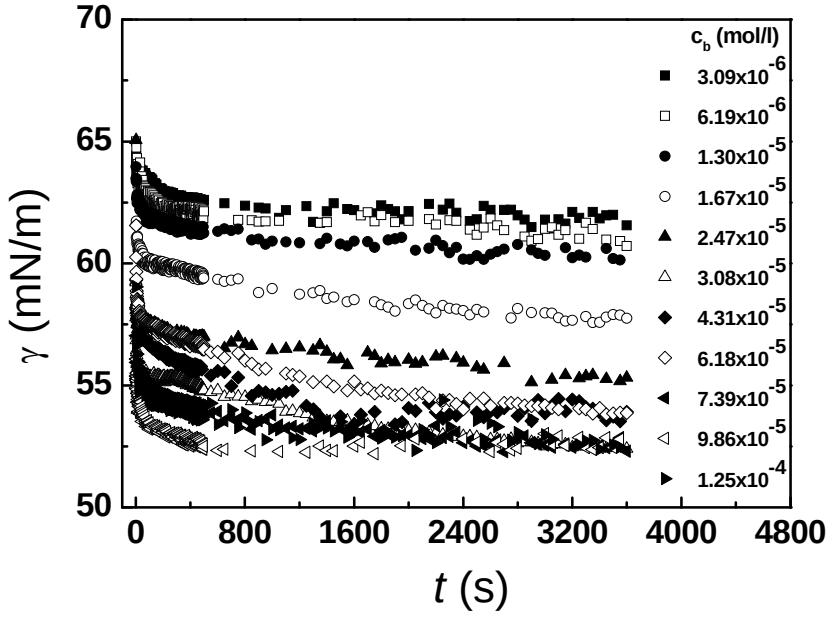

Figure 4.4 Time dependence of the surface tension at various Gaffix® VC713 concentrations – 278 K.

The general behaviour of these polymers is similar to surfactant systems, although it takes a much longer time to reach equilibrium due to continuous conformation

rearrangements that occur for extraordinary long time periods before equilibrium adsorbance. The adsorption of polymers is typically slower than surfactants because of their high molecular weight and consequent slow rate of diffusion in the solvent (Duro et al., 1999).

Similar to short-molecule surfactants, the experimental data of Gaffix® VC713 did not show a plateau induction region, at $t \rightarrow 0$ where $\gamma(t) \approx \gamma_0$, as seen in similar polymers and proteins elsewhere (Nahringbauer, 1995; Miller, Fainerman, Wtistneck et al., 1998; Miller, Fainerman, Wustneck et al., 1998; Gilcreest and Gilcreest, 2006; Phan et al., 2006). The exact reason for this induction period is not clear in similar polymer systems. However, it can be associated to an energy barrier to adsorption subsequent to the formation of surface (Nahringbauer, 1995). The absence of this region in our system can be explained as the consequence of the polymer ordering effects. Only in the beginning of the adsorption process, can the polymer chains be adsorbed randomly. Later the adsorbed chains interact which each other and form ordered domains. This domain forming process may or may not cause the induction period.

It is clear from Figures 4.3 and 4.4 that an increase in the polymer concentration, independent of the temperature evaluated, leads to a decrease in surface tension. It reveals the presence of polymer chains at the interface. The slower reduction of surface tension at a higher concentration zone is a result of further adsorption of macromolecules from the aqueous solution that contains greater amounts of polymers. The surface activity of the polymer increased with the increase in temperature. For instance, at polymer concentrations of 1.30×10^{-5} mol/L, the surface tension increased from 52.85 at 293 K (Fig. 4.3) to 60.14 mN/m at 278 K (Figure 4.4). Concentration and temperature dependence are further analysed in Section 4.4.2.

4.4.2 Equilibrium surface tension

Although no equilibrium was observed, the surface tension reduction was extremely slow after 1 hour. Consequently, Eq. (4-3) was fitted using the surface tension data at 1 h (Figure 4.5), with the fitted values of parameters tabulated in Table 4.2.

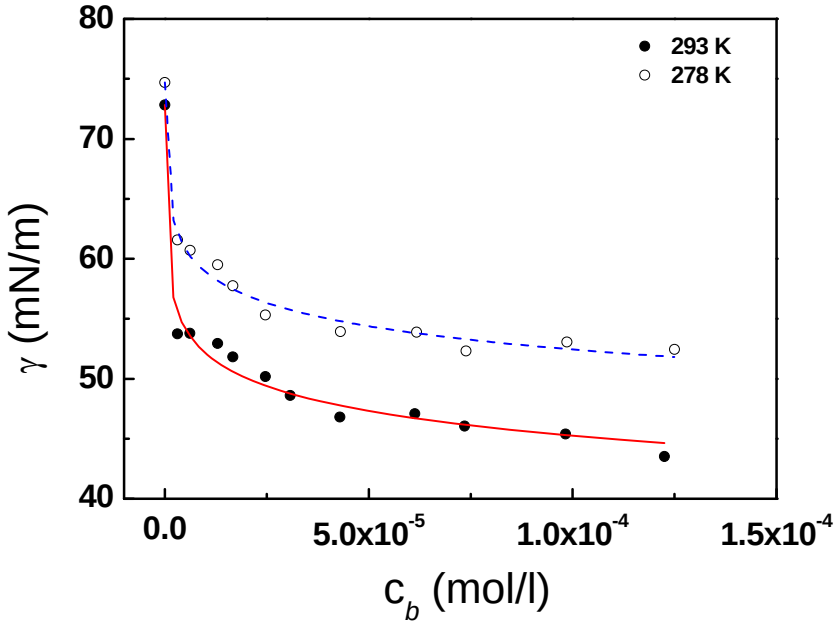

Figure 4.5 Gaffix® VC713 concentration dependence of equilibrium surface tension. Lines represent Eq. (4-3).

Figure 4.5 indicates a strong activity of Gaffix® VC713 at the air–liquid interface. For instance, 3.08×10^{-6} mol/L polymer reduced the surface tension from 72.83 to 53.74 mN/m at 293 K and from 74.70 to 61.56 mN/m at 278 K. The rapid reduction in surface tension continued with increasing polymer concentrations until reaching a pseudo plateau region from which (3.07×10^{-5} mol/L) the reduction in the surface tension became less significant. The initial rapid decrease of the surface tension reveals the presence of polymer chains at the interface. Once the pseudo plateau is reached, the aqueous phase is saturated of polymer molecules and the tension remains almost unchangeable.

In comparison with solvent, the influence of temperature was more profound for polymer solutions. For all polymer concentrations, the differences of 1 h surface tension between 293 K to 278 K were larger than the differences in solvent surface tension (72.83 mN/m at 293 K and 74.70 mN/m at 278 K, for sodium chloride respectively).

The adsorption parameters shown in Table 4.1 also indicated the influence of the temperature. The effect of the temperature was observed as being mostly related to

the Langmuir adsorption constant, a_L, which varies from 9.65×10^{-9} mol/L at 293 K to 3.56×10^{-8} mol/L at 278 K, whereas surface excess at saturation, Γ_m, varied insignificantly with temperature (1.22×10^{-6} mol/m^2 and 1.21×10^{-6} mol/m^2 for 293 and 278 K, respectively). As to be expected, a_L decreases with increasing temperature.

Table 4.1 Computed polymer adsorption parameters for Gaffix® VC713.

Equilibrium model				Dynamic models			
T (K)	a_L (mol/L)	Γ_m (mol/m^2)	c_b (10^{-5} mol/L)	*Diffusion-controlled model*			*Asymptotic*
				a_L (mol/L)	Γ_m (mol/m^2)	D (m^2/s)	D_s (m^2/s)
293	9.65×10^{-9}	1.22×10^{-6}	0.31				1.11×10^{-10}
			0.62	-	-	-	4.32×10^{-11}
			1.30	-	-	-	1.03×10^{-11}
			1.67	-	-	-	6.36×10^{-12}
			2.46	-	-	-	4.88×10^{-12}
			4.29	4.55×10^{-8}	1.30×10^{-6}	2.20×10^{-8}	1.94×10^{-12}
			6.13	-	-	-	1.09×10^{-12}
			7.35	1.11×10^{-7}	1.39×10^{-6}	8.00×10^{-10}	1.09×10^{-12}
			9.82	4.55×10^{-8}	1.40×10^{-6}	1.11×10^{-10}	8.83×10^{-13}
			12.3	3.57×10^{-8}	1.38×10^{-6}	1.00×10^{-10}	4.42×10^{-13}
278	3.56×10^{-8}	1.21×10^{-6}	0.31	-	-	-	1.42×10^{-9}
			0.62	-	-	-	2.46×10^{-10}
			1.30	-	-	-	3.85×10^{-11}
			1.67	-	-	-	1.05×10^{-11}
			2.47	-	-	-	5.48×10^{-12}
			3.08	-	-	-	1.98×10^{-12}
			4.31	1.84×10^{-7}	1.34×10^{-6}	1.85×10^{-9}	9.61×10^{-13}
			6.18	5.00×10^{-8}	1.00×10^{-6}	1.02×10^{-10}	3.73×10^{-13}
			7.39	1.63×10^{-7}	1.34×10^{-6}	2.56×10^{-10}	7.59×10^{-13}
			9.86	1.62×10^{-7}	1.34×10^{-6}	7.31×10^{-10}	4.24×10^{-12}
			12.5	5.56×10^{-7}	1.54×10^{-6}	8.80×10^{-11}	4.94×10^{-13}

4.4.3 Modelling of the dynamic surface tension

The adsorption dynamics was modelled for selected concentrations, 6.18×10^{-5} and 1.23×10^{-4} mol/L, which are indicated in Figure 4.6, using Eqs. (4-5), (4-6) and (4-4). The model was only fitted against experimental data for the first 200 seconds, where rapid reduction occurred (Figure 4.6; this was because the computational calculations, required for the longer time periods, were themselves time consuming, and the parameters were not changed significantly.

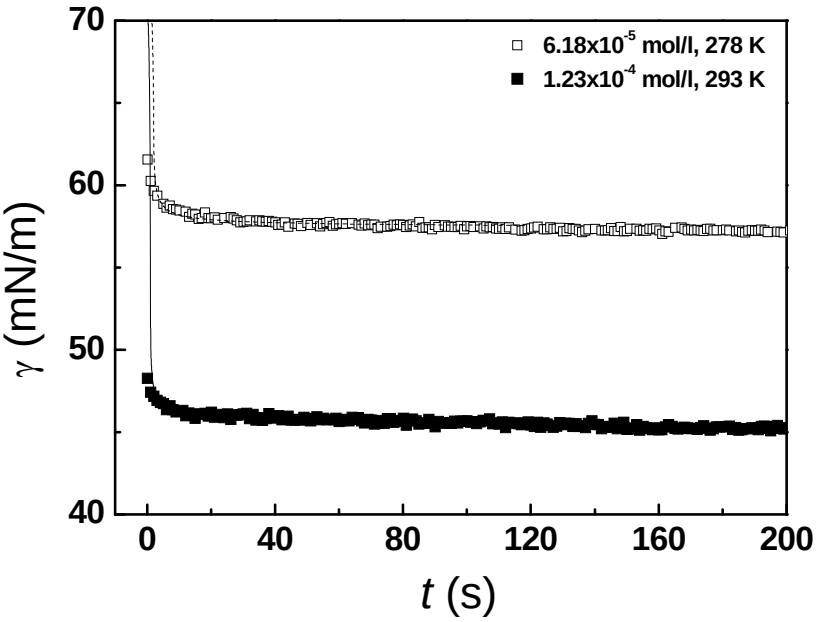

Figure 4.6 Experimental data fitting of Gaffix® VC713 at the air–sodium chloride solution interface based on Eqs. (4-5), (4-6) and (4-4).

A summary of the fitted parameters using the diffusion-controlled model at 293 K and 278 K is shown in Table 4.1. The computed surface excess at saturation at both temperatures is close to that estimated at 1 h from Eq. (4.3) for most of the polymer concentrations. The values of Γ_m at 293 K were around 1.30×10^{-6} mol/m^2 and 1.40×10^{-6} mol/m^2 compared to 1.22×10^{-6} mol/m^2 obtained at 1 h. For 278 K, Γ_m was around 1.00×10^{-6} mol/m^2 and 1.54×10^{-6} mol/m^2 compared to 1.21×10^{-6} mol/m^2 obtained at 1 h.

However, the a_L values differ from the equilibrium values in approximately one order of magnitude. At 293 K, a_L values were around 1.11×10^{-7} mol/L to 4.55×10^{-8} mol/L, and at 278 K they were about 1.62×10^{-7} mol/L to 5.00×10^{-8} mol/L (compared to 9.65×10^{-9} mol/L and 3.56×10^{-8} mol/L obtained at 1 h for 293 K and 278 K, respectively). One reason for the difference is that the equilibrium model was applied to 1 hour surface tension instead of the true equilibrium values. The result suggests some modelling limitations when applying to macromolecule systems.

The estimated diffusion coefficients within the first 200 seconds decreased with increasing the polymer concentration at both temperatures. These results indicate that the diffusion of Gaffix® VC713 molecules from solution to the interface is slower at higher polymer concentration. This is probably due to the high average molecular weight (83,000 g/mol) of Gaffix® VC713, which consequently affects the slow rate of diffusion of this polymer in the solvent. Furthermore, possible interactions between and within polymer chains and the spatial effect of the macromolecules, which are more critical at higher polymer concentrations could be severely restricting the motion of the polymer molecules to the air–liquid interface. Finally, an increase in the viscosity of the solution as the polymer concentration increases, could also be affecting the diffusive transport rate of the polymer as the medium in which diffuses become more viscous.

Beyond 400 seconds, $\gamma(t)$ were approximated by an asymptotic solution (Figures 4.7 and 4.8), i.e. Eq. (4-8). From Table 4.1, it can be seen that the asymptotic diffusion coefficients, D_s, are much smaller than the corresponding coefficient from Eq. (4-5), D. The difference indicates a change in the dominating mechanism, from diffusion to interfacial reorganisation (unfolding of the polymer coil, rearrangements of the adsorbed molecules, etc.). Moreover, D_s clearly decreased with increasing the polymer concentration, and increasing temperature as shown in Figure 4.9, which indicates that the kinetics of polymer rearrangement on the interface is strongly dependent on adsorbed polymer concentrations and temperature.

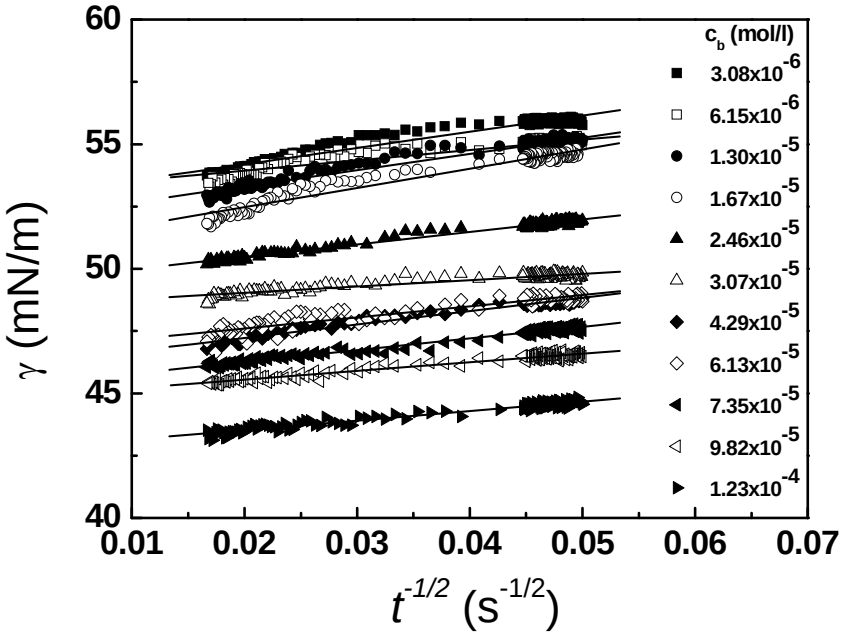

Figure 4.7 Experimental and fitted value of surface tension at various Gaffix® VC713 concentrations (293 K).

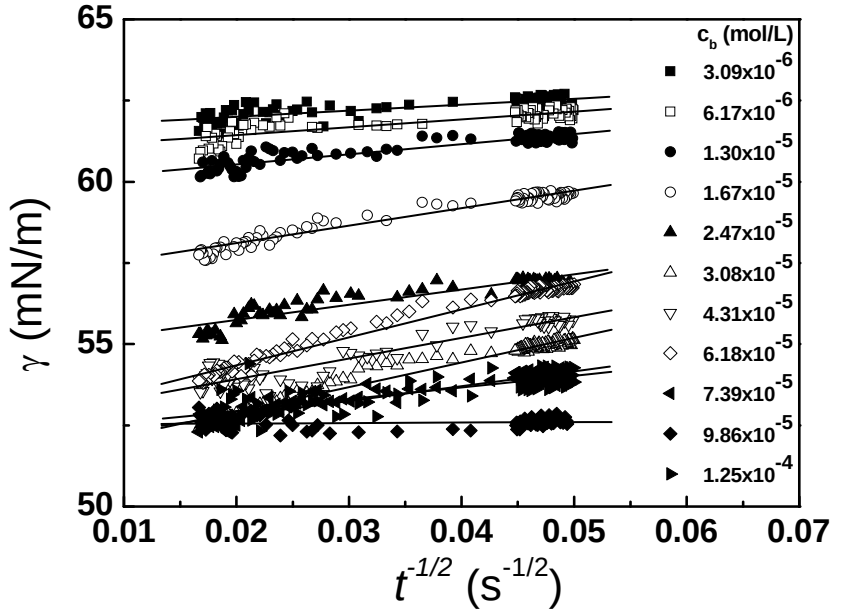

Figure 4.8 Experimental and fitted value of surface tension at various Gaffix® VC713 concentrations (278 K).

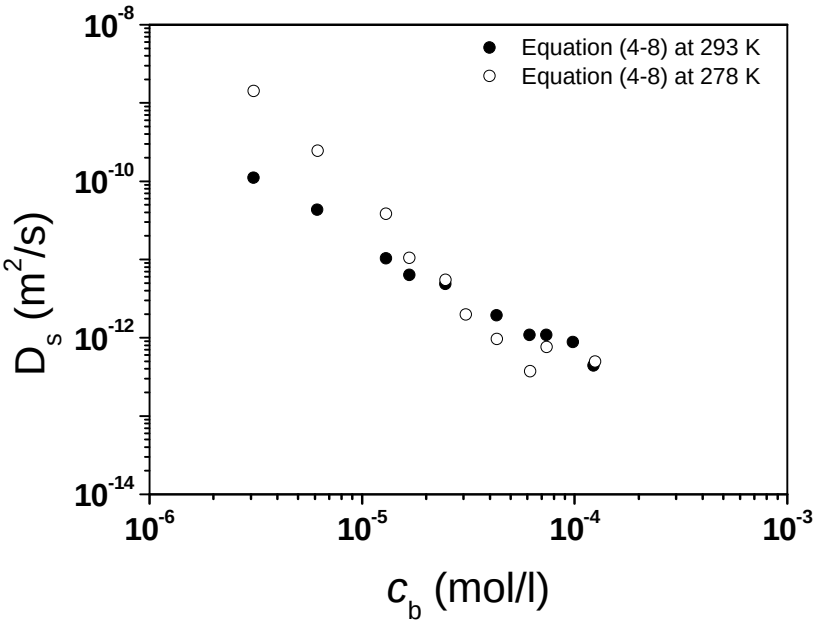

Figure 4.9 Diffusion coefficients of Gaffix® VC713 in sodium chloride solution.

4.4.4 Adsorption isotherms

Similar surface tension measurement has applied to the rest of KHIs. The measurement was carried in NaCl 3.5 wt% so as to correlate the results to the observations in Chapter 3. Figure 4.10 shows the surface tension of NaCl 3.5 wt% containing various KHIs of varying concentration at 278 K, all taken 30 minutes after formation of the interface. The bulk polymer concentration, c_b is expressed this time in weight percentage for an easier comparison among all the polymers.

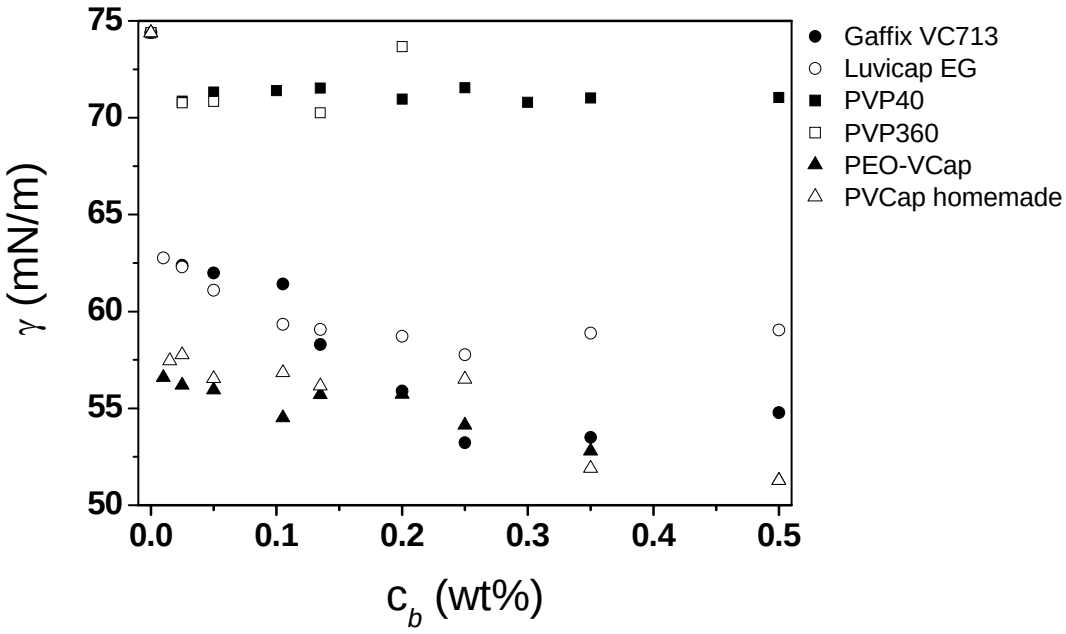

Figure 4.10 Surface tension of different KHIs at the air–sodium chloride solution interface at 278 K. All tensions are reported at 30 min

For Gaffix® VC713 the surface tension decreased rapidly at low polymer concentrations, revealing the adsorption of the polymer molecules at the air–liquid interface. Above 0.25 wt% of polymer, the surface tension did not change significantly, due to the saturation of the air–liquid interface. Similarly, strong adsorption behaviour was observed for Luvicap® EG.

For PEO-VCap and PVCap further reductions of the surface tension were observed in Figure 4.10 compared to Gaffix® VC713 and Luvicap® EG. However, contrary to Gaffix® VC713 and Luvicap® EG, the surface tension was still reducing at concentrations of 0.5 wt% of the polymer. This could be due to the presence of polydispersity, which creates a competitive adsorption, producing the continuous displacement of the smaller molecules by the slower larger ones. Therefore, the surface tension will exhibit reductions as a function of the polymer concentration.

It is interesting to see, from Figure 4.10, that the surface tension reduced from 74.70 mN/m (for NaCl 3.5%) to about 71 mN/m when different concentrations of PVP40 and PVP360 were used in the system, indicating no significant surface activities of

these two polymers at the air–liquid interface. Neither the polymers concentration effect nor the molecular weight dependence, was observed from the surface tension measurements. In the PVP–water solution, a strong hydrogen-bonding interaction exists between the electronegative oxygen atom in the carbonyl group and the surrounding water molecules (Huang and Wanga, 1996). These interactions can also result in intra- and inter-chain associations, and may lead to the formation of polymer aggregates in the bulk solution (Huang and Wanga, 1996). Therefore, the explanation as to why PVPs do not show surface activity could be attributed to PVP being mostly bound to water molecules in the interior of the polymer solution, and therefore, there is negligible adsorption of the PVP molecules at the air–liquid interface. This indicates that adsorption layers of PVP are not formed at the interface for the period of time and concentrations evaluated in this study.

We also see from Figure 4.10, that when the polymer concentration is below 0.25 wt%, the surface tension follows a trend with the order of PEO-VCap, ~ PVCap < Luvicap® EG ~ Gaffix® VC713 << PVP40 ~ PVP360. When the polymer concentration becomes greater than 0.25wt%, the trend is altered as Gaffix® VC713 < Luvicap® EG < PEO-VCap ~PVCap << PVP40, PVP360. At 0.2 wt%, Gaffix® VC713 ~ PVCap < Luvicap® EG ~ PEO-VCap << PVP40, PVP360. This means that depending on the concentration evaluated, some of the inhibitors are more effective than others at reducing surface tension. A recent study has investigated the concentration effect and electrolyte dependence of some of these inhibitors on the inhibition efficiency of THF hydrates (Ding et al., 2010). The authors demonstrated that the performance of KHIs is affected significantly by the concentration of the inhibitors and electrolyte strength, and reported a specific critical concentration for each inhibitor in different environments (Ding et al., 2010).

Polymer molecules adsorbed at the air–water interface appear as trains, loops, and tails. Trains are sequences of polymer segments in actual contact with the surface; whereas loops and tails are sequences of polymer segments in the solution. Loops have both ends connected to trains, whereas a tail is at one or both ends of the polymer chain (Nahringbauer, 1995). According to Lankveld and Lyklema (1972), the time dependence of the reduction in surface tension by a polymer molecule must

involve an increase in the number of adsorbed segments per unit area with time. This means that the surface properties of a polymer solution depend on the length and distribution of trains, loops, and tails. A change in the conformation of the adsorbed macromolecules can cause a drastic effect, both on the fraction of the segments directly in contact with the surface, i.e., on the surface tension, and on the thickness of the adsorbed polymer layer (Nahringbauer, 1995). This different surface activity observed for the KHIs can be attributed to differences in the fundamental properties of the polymer molecules, including the flexibility of the polymer chain, which leads to different conformations of the adsorbed macromolecules and interactions between and within the polymer chain, and molecular weight.

Particularly for Gaffix® VC713, the nature and conformation of the side groups and the specific interactions between these side groups and the solvent, seem to play an important role in the preferential adsorption behaviour of this polymer. The presence of three different monomer units results in a more irregular chain structure, than the rest of the polymers whose structure consists of generally only one basic monomeric unit (excepting PEO-VCap, which has 2 monomeric units). This allows Gaffix® VC713 a higher flexibility in the polymer chain. Furthermore, the steric factor induced by the size of the hydrophilic pendant groups (7-membered lactam ring) of Gaffix® VC713, enable them to adopt a fairly extended conformation in liquid water, as opposed to a tight coil. Consequently this also allows the polymer a high degree of versatility in adopting various conformations, in comparison to the other polymers, and also enhances the level of interaction between the terpolymer and the water solution (Koh et al., 2002). For this polymer, the charge groups could also be contributing substantially to the chain's stiffness, and the chain's conformational degrees of freedom when coupled with the electrostatic ones (Netz and Andelman, 2003).

Some authors (Kashchiev, Firoozabadi and Anklam) have proposed that the inhibiting efficiency of KHIs is higher when they adsorb strongly at the solution–gas interface or onto the surfaces of nucleation–active microparticles and solid substrates present in the solution. They propose a model where the adsorption of inhibitor

molecules leads to a lowering of interfacial tension or edge energy on the crystal surface (Kashchiev and Firoozabadi, 2002) (Anklam and Firoozabadi, 2005).

If the adsorption behaviour of these polymers is compared to its effectiveness inhibiting THF hydrates showed in the previous chapter (compared in the presence of 3.5 wt% of NaCl), for a polymer concentration of 0.1 wt%, the trend observed in terms of T_o was PEO-VCap < PVP360 < Gaffix® VC713 < Luvicap® EG ~ PVP40. For a concentration of 0.25 wt% of polymer, the trend observed in T_o was Gaffix® VC713 < PVP40 < Luvicap® EG < PVP360 < PEO-VCap. This means that the polymers with the highest inhibition efficiency observed in terms of T_o were the ones that produced lower surface tension values in Figure 4.10 (excepting for PVP40 and PVP360 which did not show any significant reduction of the surface tension). In this case, PEO-VCap for 0.1 wt% of polymer concentration, and Luvicap® EG ~ Gaffix® VC713 for 0.25 wt% of polymer.

4.4.5 Surface–pressure area isotherms

The surface pressure–area (*Π*–*A*) isotherms for Gaffix® VC713 on pure water, and 3.5 wt% aqueous NaCl solution subphase at 293 and 278 K is shown in Figure 4.11. At large values of surface area (low surface pressures), the Gaffix® VC713 molecules are far enough away from each other that they do not significantly interact. Compression results in a relatively small increase in surface pressure for the polymer molecules. Polymer segments are diluted in the surface, and a reduction of available surface area forces water molecules into the subphase. As the surface area is further reduced, intermolecular distances decreases bringing the polymer segments into contact with one another; the resultant compression causes the surface pressure to rise more steeply. Finally, at higher concentrations (small areas per polymer molecules) a maximum surface pressure value is observed for this polymer, which depends markedly on temperature and subphase evaluated. No gradual transformation to change the polymer conformations to a new one occupying a smaller surface area or phase change of the monolayer was observed, as illustrated in Figure 4.11 (no plateau region is observed at small areas per polymer molecules).

A similar behaviour of the surface pressure–area (*Π*–*A*) isotherms is observed for

Luvicap® EG and PVP40, which is shown in Figures 4.12 and 4.13, respectively. The mean molecular area (Mma) can be linear extrapolated through the measurement points in the liquid condensed state at Π=0 for every curve in these figures. The data are tabulated in Table 4.2.

In comparison of the Mma values, one can find that Gaffix® VC713 molecules are closely packed when NaCl 3.5 wt% is used as a subphase at low temperature (1450 $Å^2$/molecule). This is because under these conditions, the conformation of the polymer molecules allows the polymer to occupy a minimum fraction of the surface coverage. The high Mma values obtained for the Gaffix® VC713 (Table 4.2) indicates that probable cooperative attachment of segments could be adsorbing. For Luvicap® EG, the minimum Mma was reached for both pure water at 293 K, and NaCl 3.5 wt% at 293 K (29 $Å^2$/molecule, respectively). This means that the polymer molecules of Luvicap® EG are occupying less surface area when NaCl 3.5 wt% is used as a subphase, independent of the temperature evaluated. PVP40 revealed maximum packing when NaCl 3.5 wt% was used as subphase at 293 K (700 $Å^2$/molecule).

The maximum surface pressure also can be extracted from Figure 4.11. For Gaffix® VC713, the increases with the presence of salt at 293 K (14.51 for NaCl 3.5 wt% vs. 11.75 mN/m for pure water), and with increasing temperature for the same concentration of NaCl (14.51mN/m at 293 K vs. 11.54 mN/m at 278 K). This means that the adsorption of the polymer segments at the interface is favoured by the presence of salt at high temperature. In the case of Luvicap® EG (Figure 4.12), the maximum surface pressure increases with the presence of the salt at 293 K (10.24 for NaCl 3.5 wt% vs. 8.18 mN/m for pure water), and with increasing temperature for the same concentration of NaCl (10.24 for at 293 K vs. 8.54 mN/m at 278 K). Similar to Gaffix® VC713, the adsorption of the polymer segments at the interface is favoured with the presence of salt at high temperature. For PVP40 (Figure 4.13) the maximum surface pressure increases with the presence of the salt at 293 K (3.34 for NaCl 3.5 wt% vs. 3.14 mN/m for pure water), and with decreasing temperature for the same concentration of NaCl (3.34 for at 293 K vs. 3.54 mN/m at 278 K). The data is tabulated in Table 4.2.

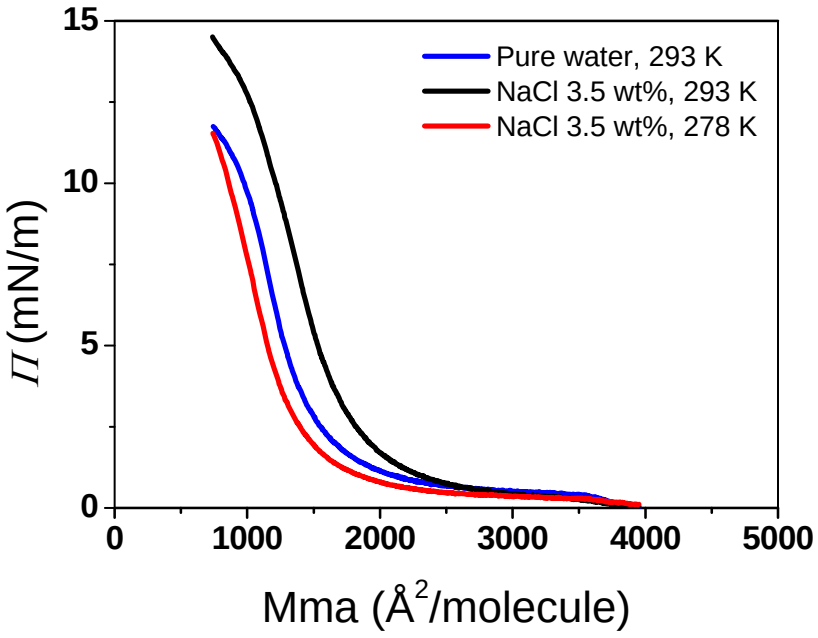

Figure 4.11 Surface pressure–area (*Π*–*A*) isotherms for Gaffix® VC713.

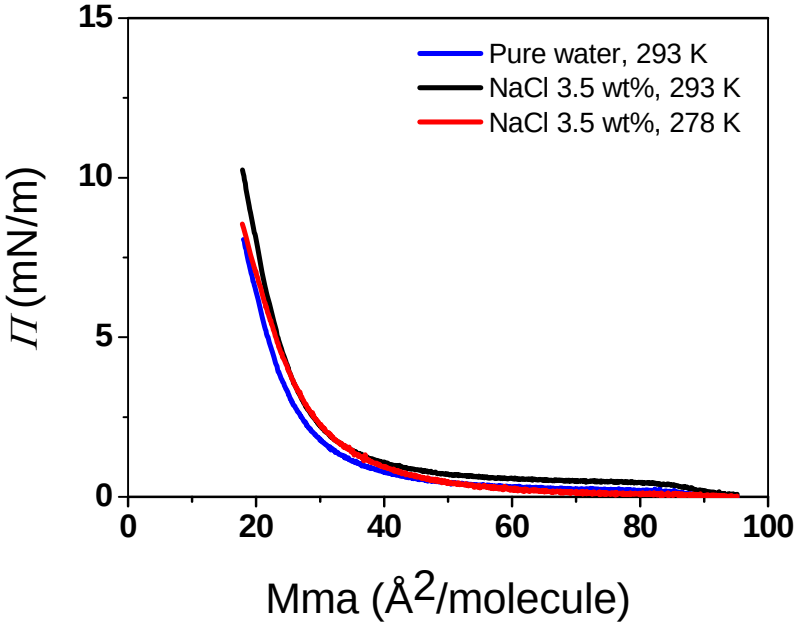

Figure 4.12 Surface pressure–area (*Π*–*A*) isotherms for Luvicap® EG.

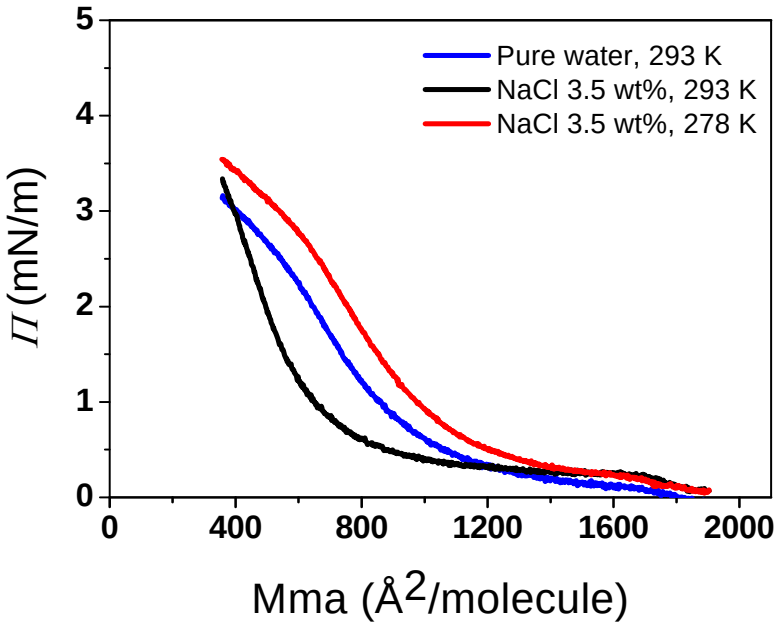

Figure 4.13 Surface pressure–area (*Π*–*A*) isotherms for PVP40.

Table 4.2 Summary of key parameters of various systems containing 0.1 wt% of KHIs in different subphases at different temperatures.

	Gaffix® VC713	**Luvicap® EG**	**PVP40**
Mma			
Pure water (Å^2/molecule) at 293 K	1570	29	1050
NaCl 3.5 wt% (Å^2/molecule) at 293 K	1860	29	700
NaCl 3.5 wt% (Å^2/molecule) at 278 K	1450	32	1160
Π_{max}			
Pure water (mN/m) at 293 K	11.75	8.18	3.14
NaCl 3.5 wt% (mN/m)) at 293 K	14.51	10.24	3.34
NaCl 3.5 wt% (mN/m)) at 278 K	11.54	8.54	3.54
γ (mN/m) at 60 min			
NaCl 3.5 wt% (mN/m) at 293 K	52.95	52.58	-
NaCl 3.5 wt% (mN/m) at 278 K	59.50	58.84	71.40
T_o			
Pure water (K) at 278 K	269.4	271.6	273.3
NaCl 3.5 wt% (K) at 278 K	265.0	265.7	265.7

In order to correlate the mean molecular area and maximum surface pressure data presented in Table 4.2 to the interfacial activities and inhibition behaviour of these polymers, surface tension and onset temperatures of THF hydrates systems containing the KHIs are also included Table 4.2. It can be seen from these data that the inhibition efficiency is associated to the maximum packing of polymer molecules in the monolayer and low values of surface tension.

4.5 Conclusions

This chapter has investigated the adsorption of the KHIs at the air–liquid interface by surface tension measurements. It was demonstrated that excepting for PVP40 and PVP360 that do not show a significant reduction in the surface tension (from 74.70 mN/m (for NaCl 3.5%) to about 71 mN/m), all of the KHIs evaluated reduced the surface tension at the air–sodium chloride solution interface. The presence of highly hydrophilic amide group molecules in these polymers could be facilitating the adsorption of the inhibitor molecules at the surface. The differences in the fundamental properties of the polymer molecules, such as molecular weight and flexibility of the polymer chain have produced different adsorption behaviour at the air–liquid interface for all of them.

For the same polymers concentrations, the polymers with the highest inhibition efficiency (PEO-VCap for 0.1 wt% of polymer concentration, and Luvicap® EG ~ Gaffix® VC713 for 0.25 wt% of polymer) were also the ones that produced lower surface tension values. These findings suggest a relation of the surface tension of the aqueous KHI polymer solutions and the inhibition efficiency of the KHIs on hydrate formation/growth. The lower surface tension values indicate a higher adsorption of KHIs molecules on the surfaces of growing particles or crystal of hydrate perturbing their nucleation and/or further growth. The trend observed in inhibition efficiency for the rest of the KHIs could not be easily correlated to the same trend observed in surface tension measurements for the same polymer concentrations.

The phase behaviour of the monolayer is mainly determined by the physical and chemical properties of the polymer, the subphase temperature and the subphase composition.

Better inhibition efficiency of KHIs is achieved in the presence of NaCl 3.5 wt% for all inhibitors, and seems to be associated to the maximum packing of polymer molecules.

A more detailed study of the dynamic and equilibrium surface tension measurements of Gaffix® VC713 has shown strong surface activities of the polymer at the air–

sodium chloride solution interface at low concentrations (less than 0.2×10^{-3} mol/L). The dynamic surface tension was monitored for 1 hour without observing equilibrium. A rapid reduction within the first 10 min was observed and followed by a long and gradual reduction, in which the surface tension reduction was proportional to $t^{-1/2}$. The rapid reduction is dominated by diffusion, whereas the gradual reduction is a slow reorganisation of polymers at the interface. More importantly, the kinetics of this interfacial reorganisation is both concentration and temperature dependent. The higher computed asymptotic diffusion coefficient values at lower temperature (278 K) for low concentration ranges are a strong reflection of Gaffix® VC713 being an effective low dose gas hydrate inhibitor.

Chapter 5 ELECTROKINETIC PHENOMENA ASSOCIATED WITH THF HYDRATE–LIQUID INTERFACE

5.1 Introduction

The previous chapter has established some quantitative understanding about the adsorption characteristics of KHIs at the air–liquid interface by interfacial tension measurements; it demonstrated that the adsorption of some KHIs at the air–liquid interface reduces the surface tension. The differences in the fundamental properties of the polymer molecules, such as molecular weight and flexibility of the polymer chain have lead to different adsorption behaviour at the air–liquid interface. The presence of highly hydrophilic amide groups in these polymers could be facilitating the adsorption of the inhibitor molecules at the surface. It was established that there was a relationship between the inhibition efficiency and the surface tension. Because the interfacial behaviour of the KHIs at the air–liquid interface might perform differently in solid–liquid interfaces, in this chapter we will further study the adsorption of Gaffix® VC713, Luvicap® EG, PVP40 and PVP360 on THF hydrates. The investigation aims to quantitatively analyse the behaviour of these polymeric inhibitors, directly at the hydrate–liquid interface through zeta (ζ)–potential measurements, and to compare these behaviours to those at the air–liquid interface.

ζ–potential is a physical property that has been routinely used to characterise adsorption properties of solid material in liquid systems. It is a function of the surface charge that develops when any material is placed in a liquid. It is also a useful index of the magnitude of the electrostatic repulsive interaction between particles (Weiner et al., 1993). ζ–potential can provide valuable information about the accumulation of a polymer at the hydrate–water interface. In principle, when a solid surface is in contact with an aqueous solution, the formation of an interfacial charge causes a rearrangement of the local free ions in the solution to produce a thin region of nonzero net charge density near the interface. The arrangement of the charges at the solid–liquid interface and the balancing counterions in the liquid is usually referred to as the electrical double layer (EDL). There is a thin layer of counterions immediately next to the charged solid surface, called the compact layer

or Stern layer. The counterions in the compact layer are immobile due to the strong electrostatic attraction. Counterions outside the compact layer are mobile. This part of the EDL is called the diffuse layer. The ζ–potential (Figure 5.1) is the electrostatic potential at the boundary (the surface of hydrodynamic shear or slipping plane) dividing the compact layer and the diffuse layer (Sze et al., 2003).

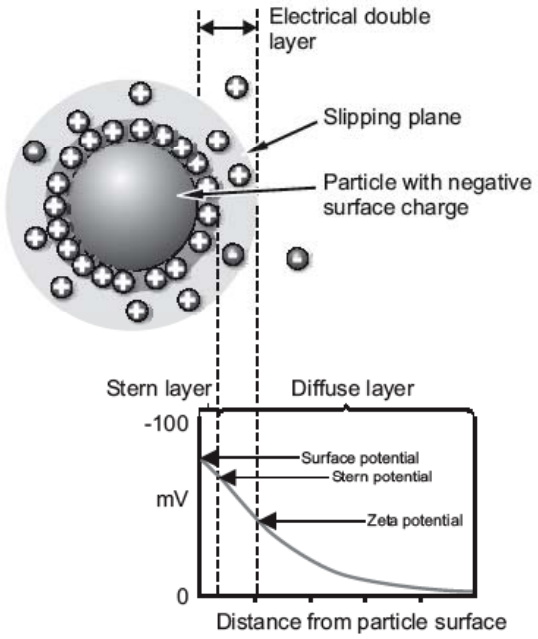

Figure 5.1 Electrical double layer and potentials (*Zetasizer nano series user manual. MAN 0317 issue 2.1* 2004).

The importance of the ζ–potential to so many applications in science and engineering has lead to the development of a number of techniques for measuring this quantity; it is based on one of three electrokinetic effects: electroosmosis, the streaming potential, and electrophoresis (Sze et al., 2003). Electroosmosis is the motion of a liquid through an immobilized set of particles, a porous plug, a capillary, or a membrane, in response to an applied electric field. The streaming potential is the potential difference at zero electric current, caused by the flow of liquid under a pressure gradient through a capillary, plug, diaphragm, or membrane. Electrophoresis is the movement of charged colloidal particles or polyelectrolytes, immersed in a liquid, under the influence of an external electric field (Delgado et al., 2005).

In the electrophoresis method, the ζ–potential is determined by measuring the particles mobility, U_E, defined as the ratio of the electrophoretic velocity of the particle to the applied electric field strength (*Zetasizer nano series user manual. MAN 0317 issue 2.1* 2004). The mobility is then related to the ζ–potential at the interface using the Smoluchowski equation (Sze et al., 2003).

$$U_E = \frac{2\varepsilon\zeta f(ka)}{3\eta} \tag{5-1}$$

where ε is the dielectric constant, ζ is the zeta potential, η is the viscosity of the suspending medium and *f(Ka)* is the Henry's function approximation which corresponds to a value of 1.5 for aqueous systems (*Zetasizer nano series user manual. MAN 0317 issue 2.1* 2004).

The equipment used in this study is a Malvern Zetasizer Nano ZS. The essence of a classical electrophoresis system is a cell with electrodes at either end to which a potential is applied (Figure 5.2). Particles move towards the electrode of the opposite charge, their velocity is measured and expressed in unit field strength as their mobility (*Zetasizer nano series user manual. MAN 0317 issue 2.1* 2004).

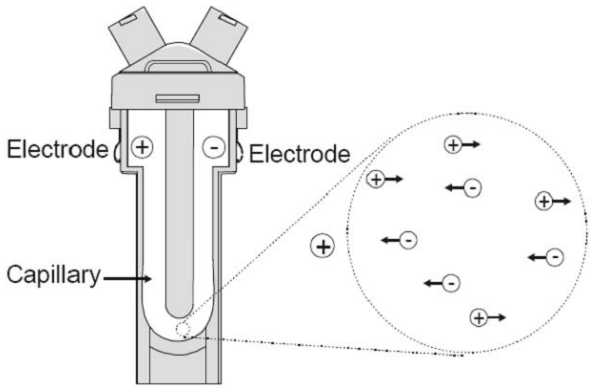

Figure 5.2 An illustration of the movement of charged particles in an electric field (*Zetasizer nano series user manual. MAN 0317 issue 2.1* 2004).

The instrument uses a Laser Doppler Velocimetry (LDV) technique to measure this particle velocity. The receiving optics is focussed so as to relay the scattering of particles in the cell. The light scattered at an angle of 17° is combined with the

reference beam. This produces a fluctuating intensity signal, where the rate of fluctuation is proportional to the speed of the particles. A digital signal processor is used to extract the characteristic frequencies in the scattered light (Figure 5.3) (*Zetasizer nano series user manual. MAN 0317 issue 2.1* 2004).

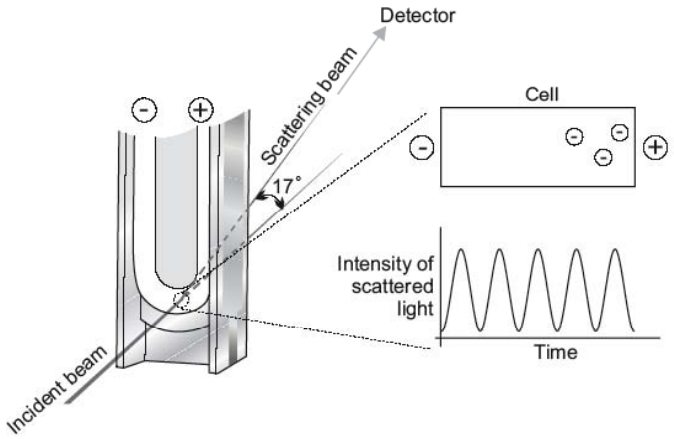

Figure 5.3 Working principle of the Laser Doppler Velocimetry (LDV) (*Zetasizer nano series user manual. MAN 0317 issue 2.1* 2004).

Once the velocity of the particle and the electrical field applied are identified, the ζ–potential is determined using two known constants of the samples – viscosity and dielectric constant, using Eq. (5.1). Zetasizer Nano ZS also uses the Phase Analysis Light Scattering (PALS) to improve the accuracy of the measurement of low particle mobility (*Zetasizer nano series user manual. MAN 0317 issue 2.1* 2004).

ζ–potential measurement has not been extensively used in hydrates systems because of experimental difficulties in keeping stable hydrates–water systems at a suitably low temperature (Drzymala et al., 1999), and also controlling the size of the hydrates particles to ensure that the size will be in the required range of ζ–potential measurements. Recent progress in the design of instruments for electrophoretic mobility determination has provided for, more sensitive techniques, to detect particle mobility and particle size, and the ability to control the temperature of the sample. Therefore removing most of the experimental obstacles of performing reliable and accurate measurements.

Drzymala et al., (1999) first reported the ζ–potential of an ice–water system. More recently, Zhang et al., (2008) measured the ζ–potential of several gas hydrate systems. Their studies were focused on the adsorption of sodium dodecyl sulphate (SDS) at the THF hydrate–liquid interface, the adsorption of SDS and its derivatives on cyclopentane hydrates or on tetrabutylammonium bromide hydrates (Lo, Zhang, Somasundaran et al., 2008; Lo et al., 2010), and the adsorption study of PVP and PVCap, on cyclopentane hydrates (Lo, Zhang, Couzis et al., 2008; Zhang et al., 2009).

We will adapt the methods that have been used by these two groups for the studies on the adsorption of selected KHIs on THF hydrates.

5.2 Materials and methods

5.2.1 Materials

The chemicals used in this study include THF, Gaffix® VC713, Luvicap® EG, PVP40 and PVP360. Information relating to these chemicals can be found in Chapter 3. About twenty THF hydrate–water systems were prepared for the ζ–potential measurement. These systems contain different inhibitors of varying concentrations.

The samples were prepared by weighing using an analytical balance of precision ±0.01 mg. The water used in the experiments was purified by a Millipore Milli-Q system, and it is referred to as pure water. The polymer was first dissolved in pure water and it was stirred at 100 RPM for 1 hour. After that, the THF was added to the chemical solution in the stoichiometric concentration of 19.2 wt%. The solutions continued to be stirred at 100 RPM for about 20 minutes. All the solutions were prepared in the same way. The chemical composition of each solution is tabulated in Table 5.1.

Table 5.1 Chemical composition of all formula used for ζ–potential measurements.

Experiment	System evaluated	Composition (wt%)		
		THF	H_2O	Polymer
THF effect	THF in pure water	10.0	90.00	-
		19.2	80.80	-
KHIs effect	THF Gaffix® VC713 in pure water	19.2	80.79	0.01
		19.2	80.75	0.05
		19.2	80.70	0.10
		19.2	80.55	0.25
		19.2	80.45	0.35
		19.2	80.30	0.50
	THF Luvicap® EG in pure water	19.2	80.75	0.05
		19.2	80.70	0.10
		19.2	80.55	0.25
		19.2	80.30	0.50
	THF PVP40 in pure water	19.2	80.70	0.10
		19.2	80.55	0.25
		19.2	80.30	0.50
	THF PVP360 in pure water	19.2	80.70	0.10
		19.2	80.55	0.25
		19.2	80.30	0.50

5.2.2 Zeta (ζ)–potential measurements

ζ–potential measurements were carried out using a method reported by Zhang et al., (2008) in which a stable THF hydrate suspension was developed and maintained at the 276.4 K temperature. In brief, a solution (100 mL) was prepared according to the chemical composition in Table 5.1. 25 mL of the solution was then put into a glass container and sealed to prevent THF evaporation. The solution was then placed in a freezer at a temperature of around 269 K for 1 night, to allow for the formation of THF hydrates. At this temperature both THF hydrates and ice are formed. The THF hydrates and ice mixtures were then removed from the freezer and placed in an ultrasonic bath, at room temperature (for about 1-3 min) to allow most crystals to melt, and to remove any bubbles from the suspension by ultrasonication. The reason why hydrates are put into an ultrasound bath to allow melting, is because the high mass fraction of solid THF hydrates (high particle size) when removed from the freezer cannot be injected directly on to the capillary cell. Otherwise, it would be not possible to makes ζ–potential measurement. Furthermore, during the hydrates melting, a lot of bubbles are produced which would interfere with the ζ–potential measurement, and therefore should be removed by ultrasonification. A 1-mL aliquot of the hydrates suspension was transferred to a folded capillary zeta cell (DTS1060 from Malvern Instruments) (Figure 5.4 (a)).

(a) Folded capillary zeta cell, DTS1060

(b) Zetasizer Nano ZS (Malvern Instruments)

Figure 5.4 The capillary cell and the Zetasizer used for the ζ–potential measurements.

The cell was then inserted into a Zetasizer Nano ZS (Malvern Instruments), shown in Figure 5.4 (b). The cell area is completely self-enclosed and controls the sample temperature over the range 275 K to 363 K. The temperature of the cell was kept at 276.4 K for 30 min to equilibrate the sample before the measurement commences, by programming the Zetasizer Nano ZS software; this is just below the equilibrium temperature of 277.4 K at the atmospheric pressure for THF hydrates at the stoichiometric molar ratio with water (1:17). Five consecutive measurements of ζ–potential were carried out after the cell was maintained at 276.4 K for 30 min (equilibration time) to allow the hydrate formation to occur inside the cuvette cell (during this time the hydrates crystals form but it is not enough time to grow and totally block the cell). It is known that the mean size of THF hydrate particles increases as more hydrates form (Devarakonda et al., 1999). The in-situ formation of THF hydrates into the cell is utilised to ensure that the size of some of the THF hydrate particles fall in the range of ζ–potential measurements (between 3 and 6 μm). 30 readings were taken for each measurement, at 10 seconds apart from one another. The reported value of the ζ–potential was an average of five measurements (Drzymala et al., 1999; Zhang et al., 2008). Statistical formulas were used to determine mean and standard deviation of the experimental data.

5.3 Results and discussion

5.3.1 Reliability analysis of the results

According to the Zetasizer Nano Series User Manual, the detection of a phase change is more sensitive to changes in mobility, than the traditional detection of a frequency shift in the scattered light (*Zetasizer nano series user manual. MAN 0317 issue 2.1* 2004). Phase Analysis Light Scattering is used as a parameter to check if the ζ–potential results meet quality criteria including the phase data, distribution data, presence of bubbles, appropriate concentration of the sample, and intensity of the signal. Figure 5.5 (a) shows a phase plot obtained from the Zetasizer Nano ZS showing a good phase behaviour for sample containing Gaffix® VC713 0.10% THF 19.2% in pure water. If any of the above mentioned criteria were to go wrong, the phase might become noisy as shown in Figure 5.5 (b) for the same sample; thus the reading of the ζ–potential might not be reliable. Therefore Phase Analysis Light Scattering has been used in our study to ensure a reliable measurement of the ζ–potential value.

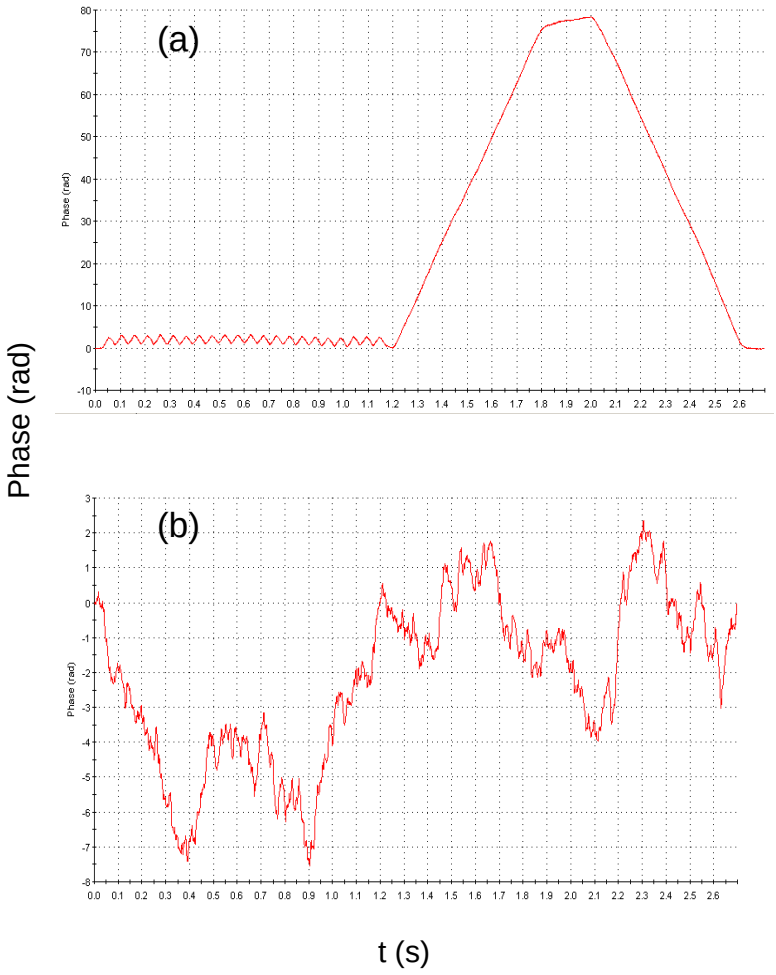

Figure 5.5 Typical phase plot obtained from the Zetasizer Nano ZS showing (a) good phase behaviour and (b) bad phase behaviour. Sample used in this measurement contain 0.10% Gaffix® VC713 and 19.2 % THF in pure water.

5.3.2 The effect of THF concentration

The effect of THF concentration on the measured ζ–potential values was investigated using THF hydrates prepared in pure water at two concentrations, 10 and 19.2 wt%. The mean ζ–potential value was 5.07 ± 2.58 mV for the 10 wt% THF system and 5.34 ± 0.76 mV for the 19.2 wt% THF system. The positive charge of the ζ–potential values indicate that a positive charge exits at the boundary, dividing the compact layer and the diffuse layer of the THF hydrate–water interface. This charge comes from preferential adsorption of positively charged species on the hydrate surface, and shows no difference in the double electrical layer between the two hydrates systems.

These values demonstrated that the mass fraction of solid 19.2 wt% THF hydrates formed during the 30 min is not too high to make a valid ζ–potential measurement. Therefore 19.2 wt% THF was chosen to make other measuring formulas. This also ensures the ζ–potential values can be related to other experimental results.

The small positive value of ζ–potential on the surface of THF hydrate–liquid interface could be due to the preference adsorption of OH^-, H^+, and all possible ionisation and dissociation groups of THF in water, as well water dipoles. The structure of the electrical double layer depends on many factors, including the nature of the surface, its charge (often determined by pH), and the nature of the solvent (Delgado et al., 2005). The measured pH value for THF 19.2 wt% is 3.29 (Table 5.2) indicating that $[H^+]$ is greater than $[OH^-]$ in the THF hydrate suspension, the surface charge should then be positive. Zhang et al., (2008) have reported a negative value of -100 ± 10 mV for the ζ–potential of THF hydrate–liquid interface. They explained that the samples having been exposed to the atmosphere during preparation and measurements became saturated with carbon dioxide. Zhang et al., (2008) also reported that the anions that can exist in open THF + water systems are hydroxide (OH^-), bicarbonate (HCO^{3-}), and carbonate (CO_3^{2-}) in fresh deionised water. However, Drzymala et al., (1999) have demonstrated that there is no preferential adsorption of OH^- over H^+ at the ice–water interface and the surface charge is dependent on pH. Therefore, ice particles below pH 7 are positive, unless other anions other than OH^- adsorbs at ice–water interface. Ice and hydrates surfaces are similar because the molecular arrangement of the hydrogen bonds are not too different from each other (Suga et al., 1992). Lo et al., (2008) have reported a possible explanation for anion adsorption at ice–water, is that pendant hydrogens on the crystals surface form hydrogen bonds between the anions, and this could be the same for anion adsorption at the hydrate–liquid interface.

Table 5.2 Measured pH values of different solutions.

System	pH
THF 19.2 wt%	3.29 @ 26.1 °C
Gaffix® VC713 0.1 wt% THF 19.2 wt%	4.07 @ 26.4 °C
Luvicap® EG 0.1 wt% THF 19.2 wt%	3.33 @ 23.2 °C
PVP360 0.1 wt% THF 19.2 wt%	2.99 @ 25.4 °C
PVP40 0.1 wt% THF 19.2 wt%	2.88 @ 26.4 °C

5.3.3 The effect of KHIs

Table 5.3 presents the mean ζ–potential and standard deviation values obtained for THF 19.2 wt% in the presence of different inhibitors of varying concentration. At the same concentration, the mean ζ–potential of Gaffix® VC713 is > Luvicap® EG > PVP40 ~ PVP360, indicating a more positively charged double electrical layer of the hydrates surface of Gaffix® VC713 than that of Luvicap® EG, PVP40 and PVP360. This can be due to the number of monomer units bounding to the surface and the conformation of the adsorbed polymers, which is thought to be reflective of its charge density. In the case of Gaffix® VC713, which contains a high charge density consisting of the monomers pyrrolidone, caprolactam and dimethylaminoethylmethacrylate (Figure 5.6 (a)), a more positive and expanded adsorbed layer is expected than that for the other polymers that only contain monomers pyrrolidone and caprolactam. This layer reduces the diffusion of hydrate formers from the bulk phase to the hydrate surface. High-charge density polymers are believed to be relatively stiff due to intrachain repulsion, and to adsorb flat configurations characterised by many train segments—consecutive repeat units in contact with surface sites. Conversely, lower-charge density polymers tend to adsorb as layers, characterised by a higher proportion of loop and tail segments extending away from the surface into solution (Tartakovsky et al., 2003). The pH values of the polymer solutions (Table 5.2), which are often used to infer about the charge of the surface (usually lower pH values indicates a more positive charged double electrical layer), show that the pH of Gaffix® VC713 is > Luvicap® EG > PVP360 > PVP40. This means that even when the charge of the surface in the presence of all the inhibitors is positive, a more positive charged double electrical layer was expected for Gaffix® VC713 (lower pH value), because of the high charge density of the polymer. The strength of the hydrogen bonding interactions between oxygen of the cyclic amide groups in Gaffix® VC713 and pendant hydrogens on the hydrate surface, and hydrophobic interactions between the Gaffix® VC713 molecules and the hydrate surface, are also expected to contribute with the more positively charged double electrical layer of the hydrates surface of this polymer.

Table 5.3 Mean ζ–potential and standard deviation values obtained for THF 19.2 wt% in the presence and the absence of inhibitors at 276.4 K and 30 min.

System	Mean ζ–potential, mV	Standard deviation, mV
Gaffix® VC713 0.01%	7.68	0.00
Gaffix® VC713 0.05%	17.20	2.41
Gaffix® VC713 0.10%	24.10	2.14
Gaffix® VC713 0.25%	17.80	0.74
Gaffix® VC713 0.35%	14.60	0.47
Gaffix® VC713 0.50%	19.40	0.89
Luvicap® EG 0.05%	11.70	1.39
Luvicap® EG 0.10%	22.90	2.28
Luvicap® EG 0.25%	4.80	0.82
Luvicap® EG 0.50%	1.31	0.26
PVP40 0.10%	5.13	0.04
PVP40 0.25%	1.98	0.10
PVP40 0.25%	1.93	0.75
PVP40 0.50%	1.69	0.36
PVP360 0.10%	-0.14	0.59
PVP360 0.25%	0.61	1.29
PVP360 0.50%	0.84	2.99

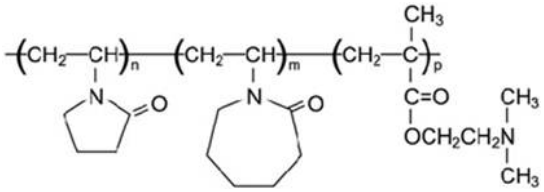

(a) Gaffix® VC713 (n=20, m=75, p=5) (Peng, Sun, Liu, Liu et al., 2009).

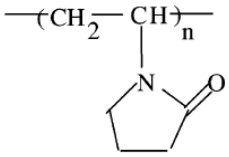

(b) Poly(*N*-vinylpyrrolidone)

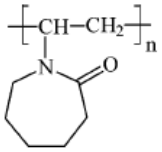

(c) Luvicap® EG

Figure 5.6 Structure of the polymer inhibitors indicating the different pendent groups.

When the concentration of each polymer was changed, the measured ζ–potential value also changed (Figures 5.7 to 5.9). For Gaffix® VC713, the ζ–potential value increased from 7.68 mV to 24.10 mV when its concentration was increased from 0.01wt% to 0.10 wt%. A decrease in ζ–potential value was observed when its concentration became greater than 0.10 wt%, but remained above 15 mV. This decrease is probably due to the saturation of polymer in the surrounding interfacial region and the bulk solution, and also steric effects that could be affecting the ions

mobility, hence the ζ–potential. As mentioned above, the increase in the ζ–potential is due to adsorption of amides groups at the hydrate–liquid interface, which brings more positive charge to the hydrate particles (Zhang et al., 2009). Peng et al., (2009) have pointed out that the high density hydrophilic amide groups in Gaffix® VC713 molecules may form hydrogen bonds with water molecules both in liquid and in hydrate phases, which facilitate the adsorption of Gaffix® VC713 molecules on the hydrate crystal surface The above behaviour looks like a typical Langmuir-like adsorption in which the amount of polymer adsorbed increases with the bulk concentration, until complete monolayer coverage. Differently charged hydrate particles and not fully equilibrium conditions at the hydrate–water interface may have been responsible for the dissemination of the data in Figure 5.7.

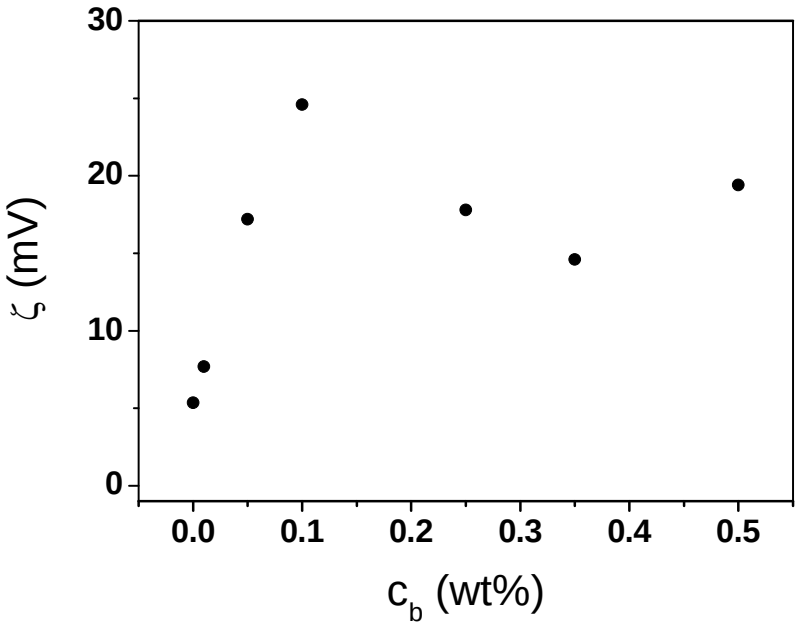

Figure 5.7 ζ–potential of THF hydrate slurries at various concentrations of Gaffix® VC713.

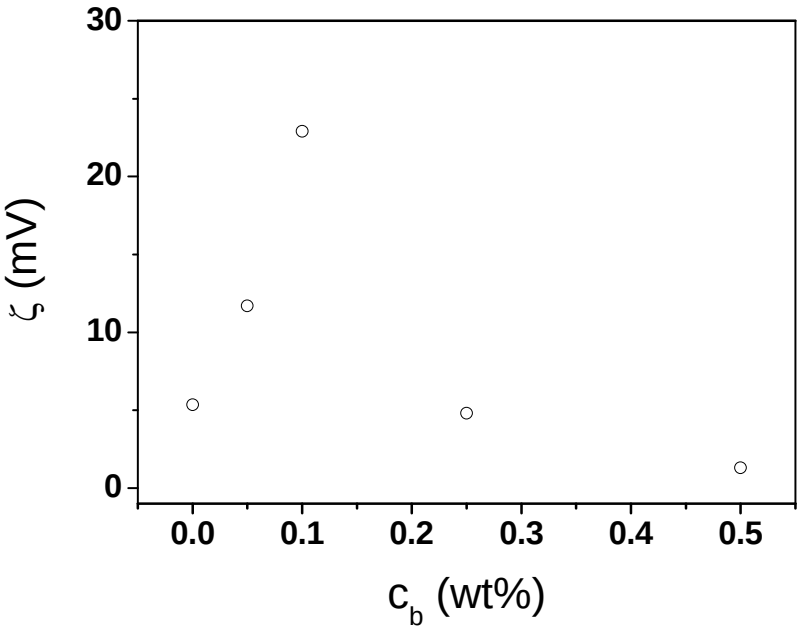

Figure 5.8 ζ–potential of THF hydrate slurries at various concentrations of Luvicap® EG.

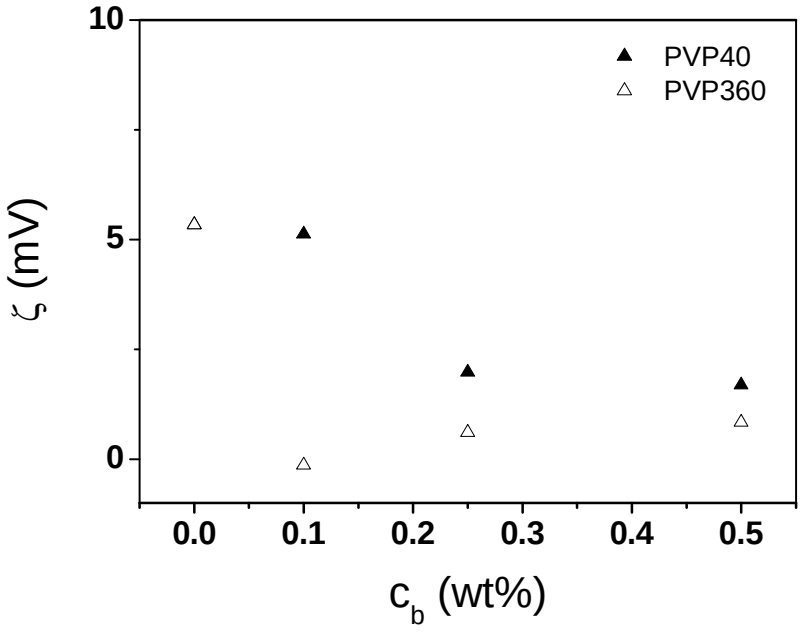

Figure 5.9 ζ–potential of THF hydrate slurries at various KHIs concentrations.

A similar trend was observed in Luvicap® EG systems. However the decrease of ζ–potential after reaching the peak value at 0.1 wt% was more rapid than that was observed in Gaffix® VC713. It is not clear from ζ–potential measurements what is

the reason for this decrease, observed after the saturation of polymer in the surrounding interfacial region. However, steric effects could be affecting the ions mobility at high polymer concentration.

For PVP40 and PVP360 THF systems, there was no initial increase in ζ–potential. This is probably due to the chains of the PVP polymers adsorbing to the surface of several particles at the same time, binding them together in spite of the electrostatic forces that would normally make them repel each other.

These results are in agreement with recent observations of the adsorption of PVCap and PVP on cyclopentane hydrates reported by Zhang et al., (2009). Even though they have observed negative charge for the cyclopentane hydrate without any inhibitor, these hydrates exhibit the same trend in the surface charge of becoming less negative as the inhibitors concentration increases, indicating that the inhibitors compete with anions for the adsorption sites (Zhang et al., 2009).

The ζ–potential can be used to qualitatively analyse the density of polymers adsorbed on the hydrates particles. We can postulate that the increase in the ζ–potential is due to the adsorption of the cyclic amides groups of the polymers at the hydrate–liquid interface, which brings more positive charge to the hydrate particles. These hydrophilic groups may form hydrogen bonds with water molecules, both in liquid and in hydrate phases, which facilitate the adsorption of polymer molecules on the hydrate crystal surface. It explains that Gaffix® VC713, which contains a high density of hydrophilic amide groups, exhibited the higher value of ζ–potential.

It should be noted that an attempt to measure the particles size and particles size distribution of the crystals before to run the ζ–potential measurement was not successful, due to the condensation of liquid in the walls of the cell due to the long measurement time.

Figure 5.10 compares the ζ–potential values for all the inhibitors at the same concentrations of 0.10, 0.25 and 0.50 wt%.

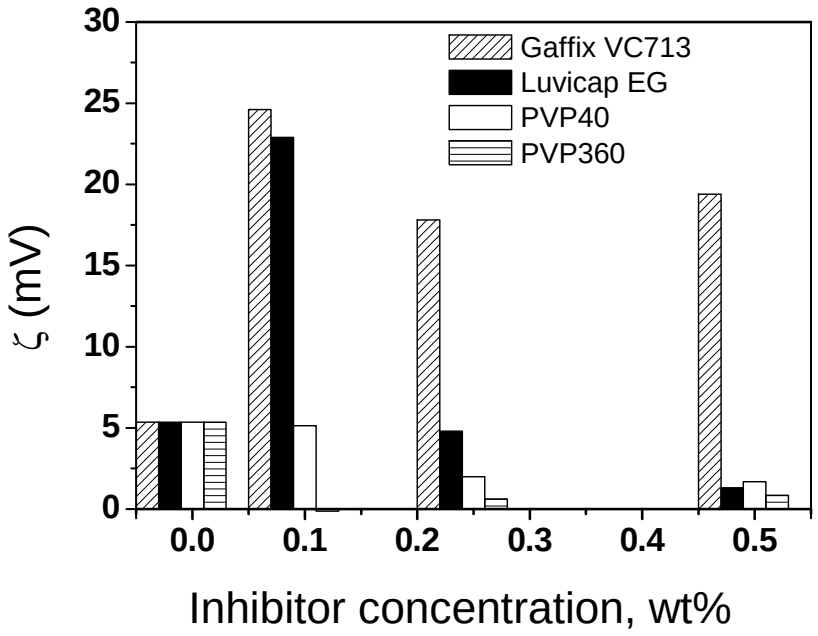

Figure 5.10 ζ–potential comparison for all the inhibitors at different concentrations.

It can be observed from Figure 5.10 that the hydrate surfaces for all the polymers have low ζ–potential values. A lower ζ–potential value means that the attraction forces are stronger to the repulsion ones and the particles will agglomerate. Based on this, the results might indicate that the suspensions containing Gaffix® VC713 or Luvicap® EG will resist more aggregation than these ones that contain PVP40 and PVP360.

As we know, the affinity of polymers to the hydrate surface is not simply proportional to the free energy of binding of corresponding monomers, but affected by both the number of monomer units bound to the surface, and the configuration of adsorbed polymers (Zhang et al., 2009). The multilayer adsorption of Gaffix® VC713 and Luvicap® EG with a large molecule size makes these polymers more effective than PVP40 and PVP360 in terms of reducing the tendency of particle agglomeration or decelerating the diffusion of guest molecules, water molecules, or both from the bulk phase to the hydrate–water interface (Zhang et al., 2009).

The ζ–potential for these inhibitors can be related to the onset temperature of THF hydrates formation, T_o, in the presence of KHIs, which is presented in Table 3.3 in

Chapter 3. For the same interface (THF–water) and polymer concentration (0.1 wt%) it is observed that the inhibitor showing the higher adsorption from ζ–potential measurements is the most effective reducing T_o. The polymers evaluated showed the same trend from the lowest to the highest T_o Gaffix® VC713, Luvicap® EG, PVP360 and PVP40, which is also the same trend observed in ζ–potential from the highest to the lowest adsorption value.

The ζ–potential results can also be related to the surface tension measurements obtained for the same KHIs, presented in Chapter 4 (Figure 4.10). It can be observed that Gaffix® VC713 exhibit the lowest surface tension at the air–liquid interface, follow by Luvicap® EG, PVP40 and PVP360, these last two showing a similar surface tension. A similar adsorption behaviour is observed in the ζ–potential KHIs curves, from the highest to the lowest value, Gaffix® VC713 > Luvicap® EG > PVP40 > PVP360. Although the quantitative adsorption of the KHIs has been evaluated in different interfaces (air–liquid (NaCl 3.5 wt%) and THF–hydrate interfaces), some correspondence is shown in our studies.

It should be noted that ideally a hydrate system made in THF-NaCl should be used for the measurement; however, the presence of NaCl causes rapid corrosion of the measuring cells, leading to unreliable results and the damage of cells. Therefore, only pure water was used as solvent in this study.

5.4 Conclusions

In this chapter, we have qualitatively analysed the adsorption of four KHIs on the THF hydrate–liquid interface. In the absence of KHIs, the charge density of the THF hydrate surface is slightly positive.

The adsorption of Gaffix® VC713 and Luvicap® EG increase the positive charge density of THF hydrates particles until a concentration of 0.1 wt%, due to the adsorption of cyclic amides groups at the hydrate–liquid interface. Further increases in polymer concentration decrease the ζ–potential values. The adsorption of Gaffix®

VC713 and Luvicap® EG display a Langmuir-like adsorption isotherm. PVP40 and PVP360 reduce the positive charge density of THF hydrates particles.

The ζ–potential results have shown some correspondence with the surface tension results at the air liquid–interface. The compound with higher adsorption to the surface, also show higher adsorption at the THF hydrate.

It was also observed that the inhibitor showing the higher adsorption on ζ–potential measurements is the most effective for reducing the onset temperature of hydrates formation. It demonstrated that the adsorption of the inhibitor is directly related to its effectiveness inhibiting hydrates. The polymers evaluated showed the same trend from the lowest to the highest onset temperature, Gaffix® VC713, Luvicap® EG, and PVP40, which is also the same trend observed in ζ–potential measurements from the highest to the lowest adsorption value.

Chapter 6 KINETICS OF GAS HYDRATE FORMATION AND EFFECTIVENESS OF HYDRATE INHIBITORS

6.1 Introduction

The kinetics of THF hydrate formation and the effectiveness of hydrate inhibitors were evaluated in the previous chapters. The purpose of this chapter is to, measure the onset of hydrate formation and growth kinetics of natural gas systems in the presence of KHIs, to compare the effectiveness of various hydrate inhibitors in gas hydrates systems, and to examine whether the hypothesis proposed for THF hydrates systems are applicable to the gas hydrate systems.

The importance of investigating hydrate formation kinetics has been explained in the previous chapters. Until now, the study has focused on the use of THF hydrates as a substitute for natural gas hydrates. The advantages of using the THF hydrate system for such studies has been emphasised in Chapter 2. THF hydrates has been used as a model compound to investigate natural gas hydrate formation, and for screening potential gas hydrate inhibitors in kinetic measurements (Christiansen and Sloan, 1994; Kelland et al., 1995; Lederhos et al., 1996; Devarakonda et al., 1999; King Jr et al., 2000; Iida et al., 2001; Zeng et al., 2003; Carstensen et al., 2004; Wilson et al., 2005). However, the transferability of THF hydrate properties to gas hydrate properties is yet to be demonstrated due to the many differences between the two systems (Lee et al., 2007).

THF is a cyclic ether which forms hydrates readily at conditions close to room temperature (277.4 K) and atmospheric pressure (1 bar) at a molar ratio of 1:17 (THF to water). THF is miscible with water, a characteristic which eliminates the problem of interface diffusion resistance during hydrate formation (Rueff and Sloan, 1985). In contrast to natural gas hydrates former, the presence of an oxygen atom in the heterocycle of THF molecule allowing the compound to form hydrogen bonds with water molecules. For this reason, hydrates of nonclathrate-forming gas nature can also be formed in the THF–water system (Manakov et al., 2003).

On the contrary, the water solubility of methane is very limited. Also, methane is a nonpolar molecule, i.e., the dipole moment is zero. However, the dipole moment of THF is as high as that of water (Table 6.1). THF molecule is ~1.5 times larger than the methane molecule. Yet the permittivity of THF is very low in relative to water, and approaches a value comparable to that for nonpolar fluids such as methane (Lee et al., 2007). Table 6.1 shows a compilation of different properties of THF, methane and water ice.

Table 6.1 Properties of Methane and THF, their hydrates, and water ice (Lee et al., 2007).

Property	Methane	Tetrahydrofuran (THF)	Water Ice
Properties of Guest Molecule			
Molecular formula	CH_4	C_4H_8O	H_2O
Molecular size, Å	4.36	6.3	~1.8
Dipole moment, D	0	1.63	1.85
Molecular polarisability, $Å^3$	2.6	7.9	1.5
Permittivity	1.7	7.5	80
Density, kg/m^3 at 293.5 K	N/A	888	1000
Viscosity, cP at 298.5 K	N/A	0.46	0.89
Surface tension, N/m at 293.5 K	0.00676 at 140 K	0.028	0.0728
Solubility in water at 293.5 K	$0.04x10^{-3}$ (mole fraction of gas)*	Miscible	N/A
General Characteristics			
Hydrate structure	I	II	N/A
Hydrate cavity diameter, Å	7.9, 8.66	7.82, 9.46	N/A
Ideal hydrate stoichiometric ratio	$CH_4.6H_2O$	$C_4H_8O.17H_2O$	N/A
Thermal Properties of the Frozen State			
Heat capacity, kJ/(kg K), at 270 K	2.07	2.07	2.10
Heat of dissociation, kJ/kg, at 273 K	338.7	262.9	333.5
Thermal conductivity, W/(m K)	0.5 at 270 K	0.5 at 270 K	2.2 at 263 K
Thermal diffusivity, m^2/s	$3x10^{-7}$ at 270 K	$2.8x10^{-7}$ at 270 K	$8.43x10^{-7}$ at 273 K
Thermal linear expansivity, K^{-1}, at 200 K	$77x10^{-6}$	$52x10^{-6}$	$56x10^{-6}$
Mechanical Properties of the Frozen State			
Density, kg/m^3 at 273 K	910	910	917
Interfacial tension, J/m^2	0.017, 0.032	0.016, 0.031	0.029, 0.032
Adiabatic bulk compressibility, Pa at 273 K	$\sim 14x10^{-11}$	$\sim 14x10^{-11}$	$12x10^{-11}$
Isothermal Young's modulus, Pa at 268 K	$\sim 8.4x10^9$	$\sim 8.2x10^9$	$9.5x10^9$
Shear wave speed V_s, m/s	1950	1890	1950, ~1990
Compressional wave speed V_p, m/s	3370, ~3800	3670	3890, ~3910
Strength, MPa	2 to 10**	0.9 to 44***	0.6 to 1
Electrical Properties of the Frozen State			
Electrical conductivity, S m^{-1}	~0.01	0.01	0.01
Dielectric constant at 273 K	~2.5	4.3	2.8

* Measured at 0.1 MPa and 278.15 K; ** At 50 MPa confining pressure and 270 K for methane hydrate and the same confining pressure and 260 K for ice; *** Measured with no confinement and at 276 K.

In terms of hydrate properties, THF hydrate forms as sII, with THF filling only large cavities. In contrast, methane hydrate most commonly occurs as sI, with methane filling both large and small cavities (Lee et al., 2007). sII methane hydrates has been found in natural gas systems in the presence of propane (Sloan, 1997). Tetrahydrofuran is not a constituent of natural gas or of natural gas hydrates. However, all the water (hydrogen) bonds in the THF hydrate structure are identical with those in normal sII natural gas hydrates. Since the hydrogen bonds of the hydrate lattice are the primary targets to be affected by any inhibitors, THF hydrate experiments have been used to extrapolate normal natural gas hydrates (Rueff and Sloan, 1985).

The comparison of the mechanical and electrical properties, and some thermal properties (i.e., heat capacity, thermal conductivity) of the two hydrates, reveals gross similarities (Table 6.1). The heat capacity of methane and THF hydrates is 2.07 kJ/(kg K), and the thermal conductivity is 0.5 W/(m K) at 270 K, respectively. On the other hand, there are apparent differences in thermal expansivity ($77x10^{-6}$/K for methane hydrates and $52x10^{-6}$/K for THF hydrates), the heat of dissociation (338.7 kJ/kg for methane hydrates and 262.9 kJ/kg for THF hydrates), and the degree to which equilibrium temperature depends on pressure for the two hydrates (adiabatic bulk compressibility and isothermal Young's modulus in Table 6.1).

With these in mind, we dedicate this chapter to the exploration of natural gas hydrates morphology, and the formation of kinetics using similar inhibitors that have been employed in the previous three chapters. This investigation was carried out using a high-pressure sapphire cell over a pressure range of 20 to 80 bars at the onset temperature of hydrates formation. We hope to find out whether, and how much of the knowledge obtained from THF hydrate inhibition studies, are applicable to natural gas hydrates, and if the inhibition mechanisms are different for THF hydrate and gas hydrates.

6.2 Materials and methods

6.2.1 Materials

Natural gas was supplied by Alinta, Australia. The gas composition (Table 6.2) was analysed by Amdel Bureau Veritas (Perth Australia) using gas chromatography. Other properties presented in Table 6.3 were also provided by Amdel Bureau Veritas.

Table 6.2 Natural gas composition.

Component	Composition (mole %)
Nitrogen	2.40 ± 0.08
Methane	87.3 ± 0.3
Carbon dioxide	2.30 ± 0.10
Ethane	6.02 ± 0.18
Propane	1.51 ± 0.05
iso-butane	0.14 ± 0.01
n-butane	0.21 ± 0.01
neo-pentane	<0.01
iso-pentane	0.04 ± 0.01
n-pentane	0.04 ± 0.01
Hexanes	0.02 ± 0.01
Heptanes	0.01 ± 0.01
Octanes	<0.01
Nonanes	<0.01
Water	-

Table 6.3 Properties of the natural gas.

Property*	Value
Compressibility	0.9975
Real specific gravity	0.6390
Real density, kg/m^3	0.7830
Real gross calorific value, MJ/m^3	39.000
Real gross calorific value, MJ/kg	49.900
Real nett calorific value, MJ/m^3	35.200
Real nett calorific value, MJ/kg	45.000
Average molecular weight	18.500
Wobbe index, MJ/m^3	48.800

* Calculated values ISO 6976. Metric standard conditions- dry, 15 °C, 101.325 kPa

The water used in the experiments was purified by a Millipore Milli-Q system, and it is referred to as pure water. KHIs including Gaffix® VC713, Luvicap® EG, PEO-VCap and PVP40 were used for this investigation. Details of these materials can be found in Table 3.1 of Section 3.2.1. Table 6.4 presents a list of all formulas used for

the kinetic experiments detailing inhibitors, systems evaluated and chemical composition. The concentrations are based on the total mass of the solution.

Table 6.4 List of all liquid formula used for the kinetic experiments.

System	Pressure evaluated (bars)	Composition (wt%)	
		H_2O	Inhibitor
Pure water	20.8	100	-
	59.3	100	-
	62.0	100	-
	80.4	100	-
Gaffix® VC713	59.3	99.90	0.10
Gaffix® VC713	59.4	99.75	0.25
PEO-VCap	59.3	99.90	0.10
Luvicap® EG	59.2	99.90	0.10
PVP40	59.1	99.90	0.10

6.2.2 Experimental apparatus

The apparatus used in this study is a Micro-Cell for Liquefied Natural Gas (LNG) Production, designed by ST Sanchez Technologies (France) and owned by Clean Gas Technology Australia. The schematic diagram of the apparatus is given in Figure 6.1 (no more details of the design can be disclosed due to confidentiality requirements). A cylindrical high-pressure sapphire cell with an effective internal volume of 60 mL is contained inside a temperature controlled air bath, and is capable of maintaining temperatures from 113.15 K to 373.15 K with 0.1 K of accuracy. The temperature of the air bath, and the rate of cooling/heating was set by purpose designed computer software. Pressure maintenance at the required level during the experiment was achieved by using a computer controlled positive displacement pump with 500 mL volume capacity. In addition to visual observations of phase changes through the bulk solution, the cell was equipped with a fibre optic system to detect the solid crystallisation process, as well as condensation.

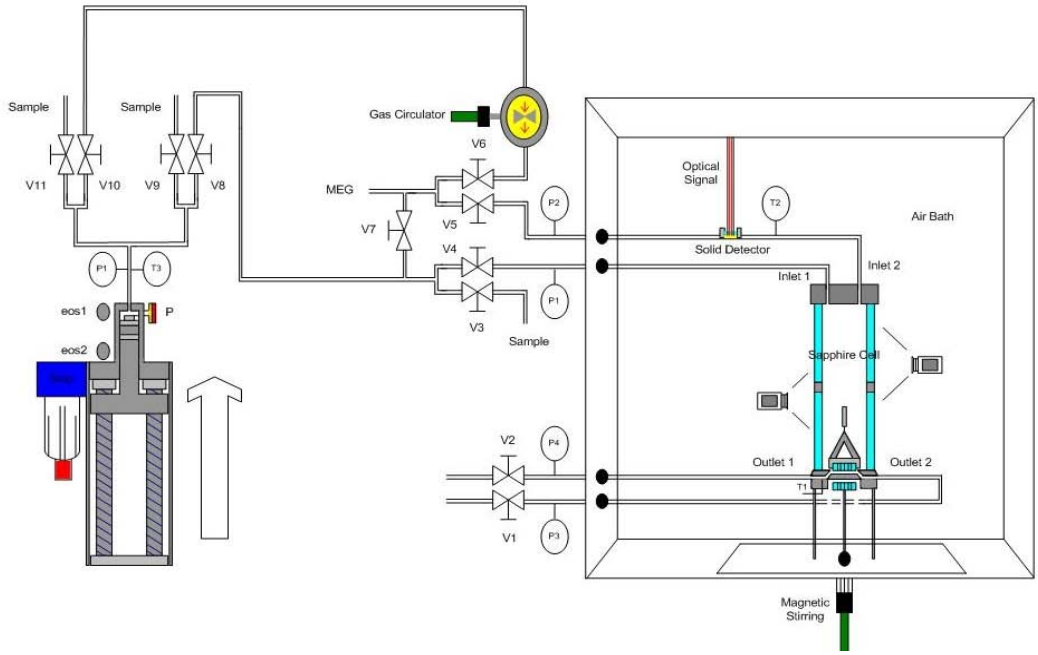

Figure 6.1 Schematic diagram of the hydrate testing cell (provided by Clean Gas Technology Australia). P: pressure, T: temperature, V: valve.

6.2.3 Experimental procedure

First, the high-pressure cell was washed using pure water and methanol; then it was rinsed several times with pure water, and then thoroughly dried with pressured air. After the cell was thoroughly cleaned, it was evacuated for around 5-10 minutes using a vacuum pump. A vacuum pressure of approximately -2.2 bars was used to ensure the absence of air. 5 mL aqueous phase (pure water or the desired polymer solution, usually in a concentration of 0.1 wt %) was injected into the cell using a needle. Experiments using salts were not conducted because of corrosion problems in the cell.

After vacuuming all the gas injection lines for around 5-10 minutes, the cell was loaded with natural gas to the desired pressure using the cylinder pressure, a pressure gas booster and finally by using a computer controlled positive displacement pump. The solution in the cell was stirred/agitated using a magnetic stirrer between 96 and 120 RPM.

The positive displacement pump was charged with enough gas prior to the start of the experiment, so as to retain its pressure in the cell throughout the entire process. The experiment was carried out under constant pressure, for which the hydrate former gas consumed in the hydrate formation process is continually supplemented externally. Pressure gauges and a computer controlled positive displacement pump were used for digital measurement and control of the pressure. Meanwhile, the data acquisition programs were activated. Once the pressure was stabilised and a set point of temperature 303 K was achieved (this allows same initial temperature for all solutions), the cell was cooled to 283 K using a chiller at a cooling rate of around 0.3 K/min. The temperature was further reduced using a much slower cooling rate (0.03-0.05 K/min) until it reached the onset temperature of hydrates formation at the desired pressure. At this point, the cooling procedure was stopped and the temperature kept constant at T_e. Temperature–pressure readings for the cell were recorded continuously throughout the process in order to detect the onset of hydrate formation.

The onset of hydrate formation was determined by visual observation of the video camera images by the appearance of hydrate crystals in the cell. After the onset of hydrate formation was detected, system temperature was maintained at a constant level by controlling the temperature set point on the software. Temperatures at the bottom (T_b) of the cell and pressure inside the cell were recorded as a function of the time. The cell was visualised and monitored using a high-resolution video camera. This allowed recording of nucleation and crystal growth in the cell. The experiments were run until the hydrates blocked the cell (t_e). In case the cell was not plugged by hydrates, the experiment was kept running for the maximum period of about 8 hours (since the beginning of the experiment). All the measurements were completed within 8 hours due to the Clean Gas Technology Australia requirements.

6.3 Results and discussion

6.3.1 Pressure–temperature phase equilibria diagram

The theoretical pressure–temperature phase diagram (Figure 6.2) was computed using two commercial model prediction software programs Multiflash™ and

CSMGem (developed by Infochem Computer Services Ltd., and the Center for Hydrate Research Colorado School of Mines, respectively). The phase diagram was used to determine the thermodynamic conditions at which hydrates form from a mixture of pure water and natural gas. The softwares used, represent non-ideal hydrate solid solution models for multi-phase equilibria at any given temperature and pressure using an algorithm based on Gibbs energy minimisation by Gupta and Bishnoi. For the theoretical hydrate prediction calculations, free water was added to the hydrocarbon gas mixture to make a concentration of 10% of the original gas mixture. This is a requirement to run the softwares. Structure II gas hydrates were used for the modelling. Table 6.5 shows the adjusted natural gas composition used to perform the phase equilibria calculations.

Table 6.5 Theoretical adjusted natural gas composition used for the modelling of the phase-equilibria calculations.

Component	**Original composition (provided by Amdel Bureau Veritas) (mole %)**	**Theoretical adjusted composition* (mole %)**
Nitrogen	2.40 ± 0.08	2.16
Methane	87.3 ± 0.3	78.58
Carbon dioxide	2.30 ± 0.10	2.07
Ethane	6.02 ± 0.18	5.42
Propane	1.51 ± 0.05	1.36
iso-butane	0.14 ± 0.01	0.13
n-butane	0.21 ± 0.01	0.19
neo-pentane	<0.01	-
iso-pentane	0.04 ± 0.01	0.04
n-pentane	0.04 ± 0.01	0.04
Hexanes	0.02 ± 0.01	0.02
Heptanes	0.01 ± 0.01	0.01
Octanes	<0.01	-
Nonanes	<0.01	-
Water	-	10.00

*The adjusted gas composition includes water in a concentration of 10% of the original gas mixture.

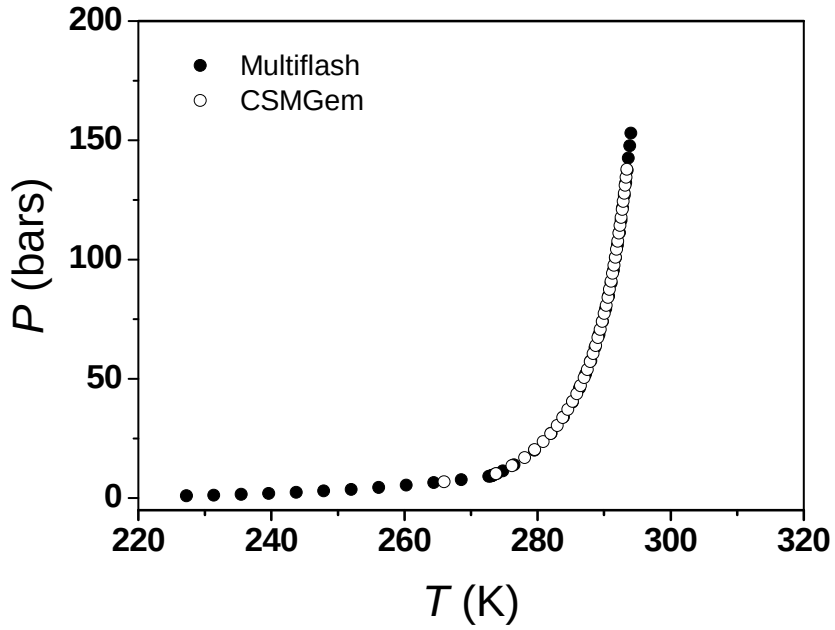

Figure 6.2 Hydrate phase diagram showing the equilibrium curve for natural gas.

It is clear that the results obtained from Multiflash™ and CSMGem are similar (Figure 6.2). Equilibrium temperature at various pressures was determined from this curve for all experiments involving gas hydrates in pure water. For the following experiments using gas hydrates in pure water, four pressures were selected, 20.8, 59.3, 62.0 and 80.4 bars.

The pressure and temperature conditions indicated by both curves in Figure 6.2 mark the limits to hydrates formation. At higher temperatures or lower pressures of both curves, hydrates cannot form; the system will contain only aqueous and hydrocarbon fluid phases, while hydrate formation can occur to the left of the curves.

6.3.2 Nucleation and growth of gas hydrates in pure water

The constant pressure method was used in this study. Four different pressures were used (20.8, 59.3, 62.0 and 80.4 bars) in order to evaluate the kinetics of gas hydrates in pure water. The temperature and pressure change during the hydrate formation process was recorded and shown in Figures 6.3-6.6.

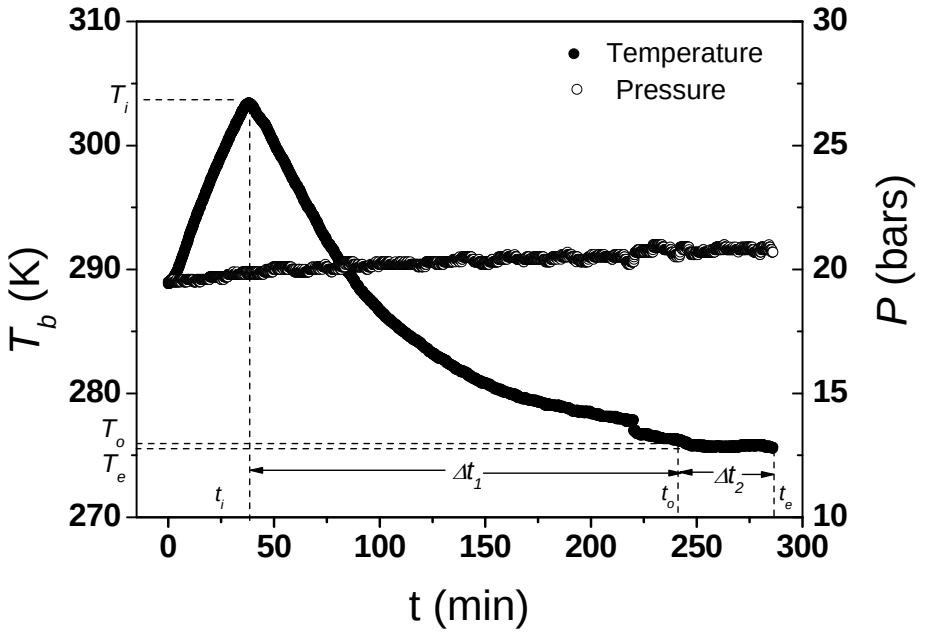

Figure 6.3 Temperature–pressure changes with the time for pure water at 20.8 bars. Initial and final cooling rates are 0.30 K/min and 0.03 K/min, respectively. Onset of hydrate formation occurs at 243.8 min (276.05 K).

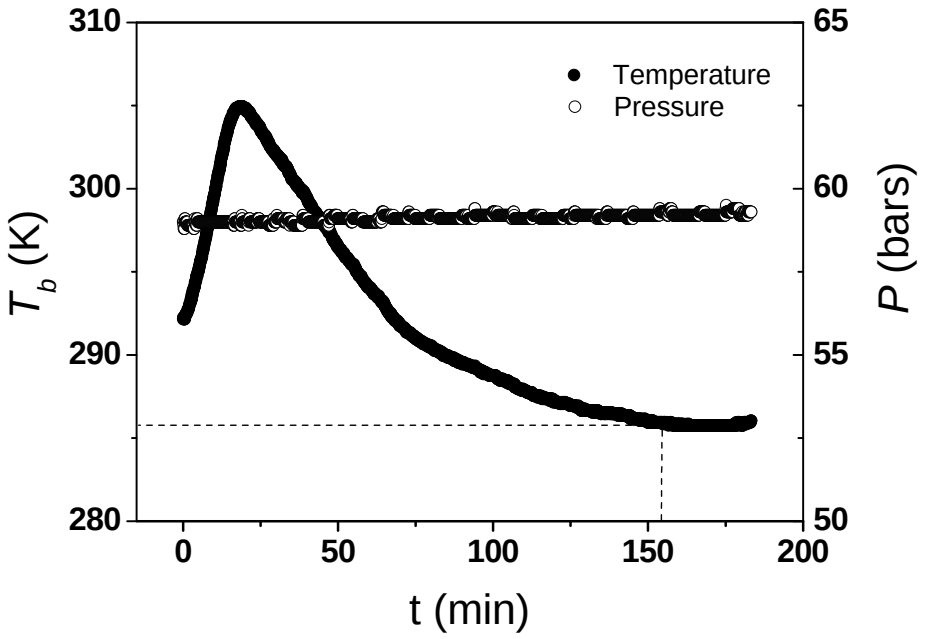

Figure 6.4 Temperature–pressure changes with time for pure water at 59.3 bars. Initial and final cooling rates 0.26 K/min and 0.04 K/min, respectively. Onset of hydrate formation occurs at 155.8 min (285.85 K).

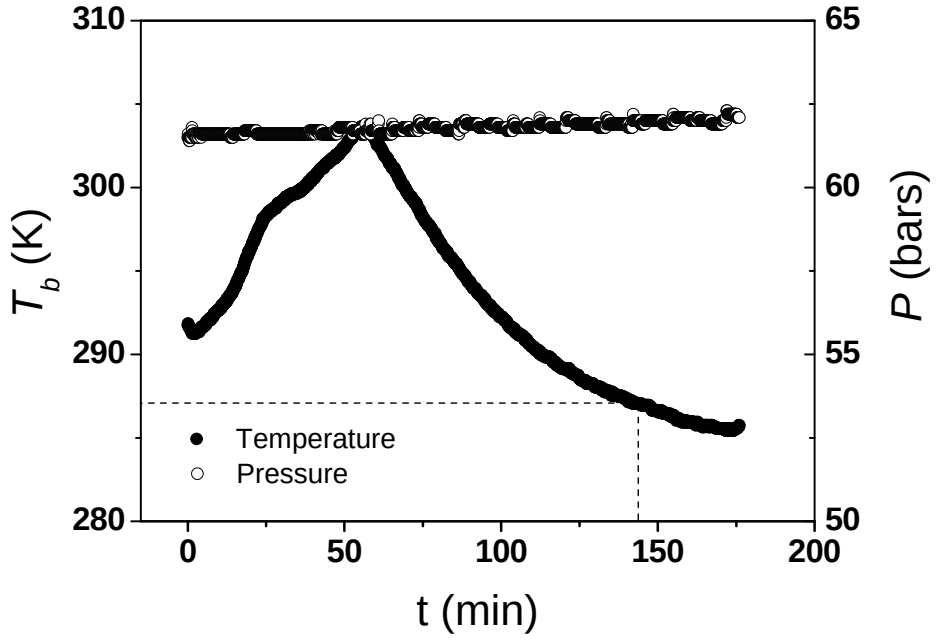

Figure 6.5 Temperature–pressure changes with time for pure water at 62.0 bars. Initial and final cooling rates 0.26 K/min and 0.07 K/min, respectively. Onset of hydrate formation occurs at 146 min (286.95 K).

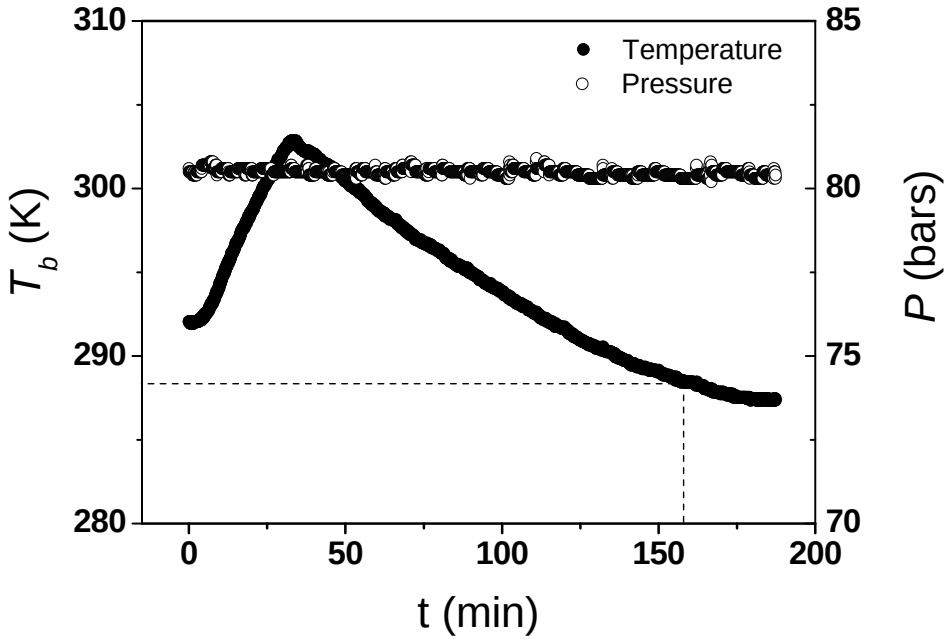

Figure 6.6 Temperature–pressure changes with time for pure water at 80.4 bars. Initial and final cooling rates 0.05 K/min. Onset of hydrate formation occurs at 162.5 min (288.25 K).

It should be noted that both T_b and P were recorded from the beginning of the experiments until the reactor was fully blocked by formed hydrates. No significant changes in the pressure were observed during this process; the experiments were conducted under constant pressure, and the gas consumed in the hydrate formation process was continually supplemented externally. Furthermore, no changes in temperature were observed at the onset of hydrate formation. Therefore, the detection of hydrates formation was determined visually, by the video camera, by the appearance of hydrate crystals in the cell.

The pattern of temperature change is similar to all of the experiments. An increase in the initial temperature T_i of about 303.45 K, was purposely set to make sure all experiments start from the same temperature. The time to reach T_i, was recorded as t_i (Figure 6.3). After having reached T_i, a rapid reduction in temperature was initiated which became slower towards t_e, the end of the process. This is particularly apparent at 20.8 bars (Figure 6.3). To explain the variations in temperature change, the visual observation records corresponding to these curves are displayed in Figure 6.7 (a)-(d). Figure 6.7 shows the visual observation of the crystal growth as a function of the time for pure water at different pressures. The time denoted below to each of the images is not the real time of the process. The first image (denoted as 0 min) was taken at the onset time at which hydrates crystals were first observed in the system, presented as t_o (corresponding to the onset temperature T_o) in Figure 6.3 and summarised in Table 6.6. Visual observation was maintained until the reaction vessel was fully plugged by crystals. The temperature and the times at which the vessel was blocked are represented as T_e, t_e in Figure 6.3.

For the experiment being carried out at 20.8 bars, the first crystals were observed at the gas–liquid interface (highlighted area of Figure 6.7 (a)). The real time corresponding to this observation is 243.8 min (Table 6.6). No significant amount of crystals was observed on the wall of the vessel. The crystals appear like a film along the interface. A similar observation has been reported by Yousif as due to a higher supersaturation of gas molecules near the interface than the liquid water phase (Yousif, 1997). After 3 min, the bulk solution turned hazy, indicating the formation of nuclei of gas hydrates in the bulk. The breaking down of the crystals that had already formed at the bottom of the film was constantly observed. This was due to

the mechanical force caused by the agitation. The observation is in agreement with Yousif's report (Yousif, 1997). The nuclei continued to grow until the cell was totally blocked with hydrates. The time was recorded as t_e= 286 min (Table 6.6).

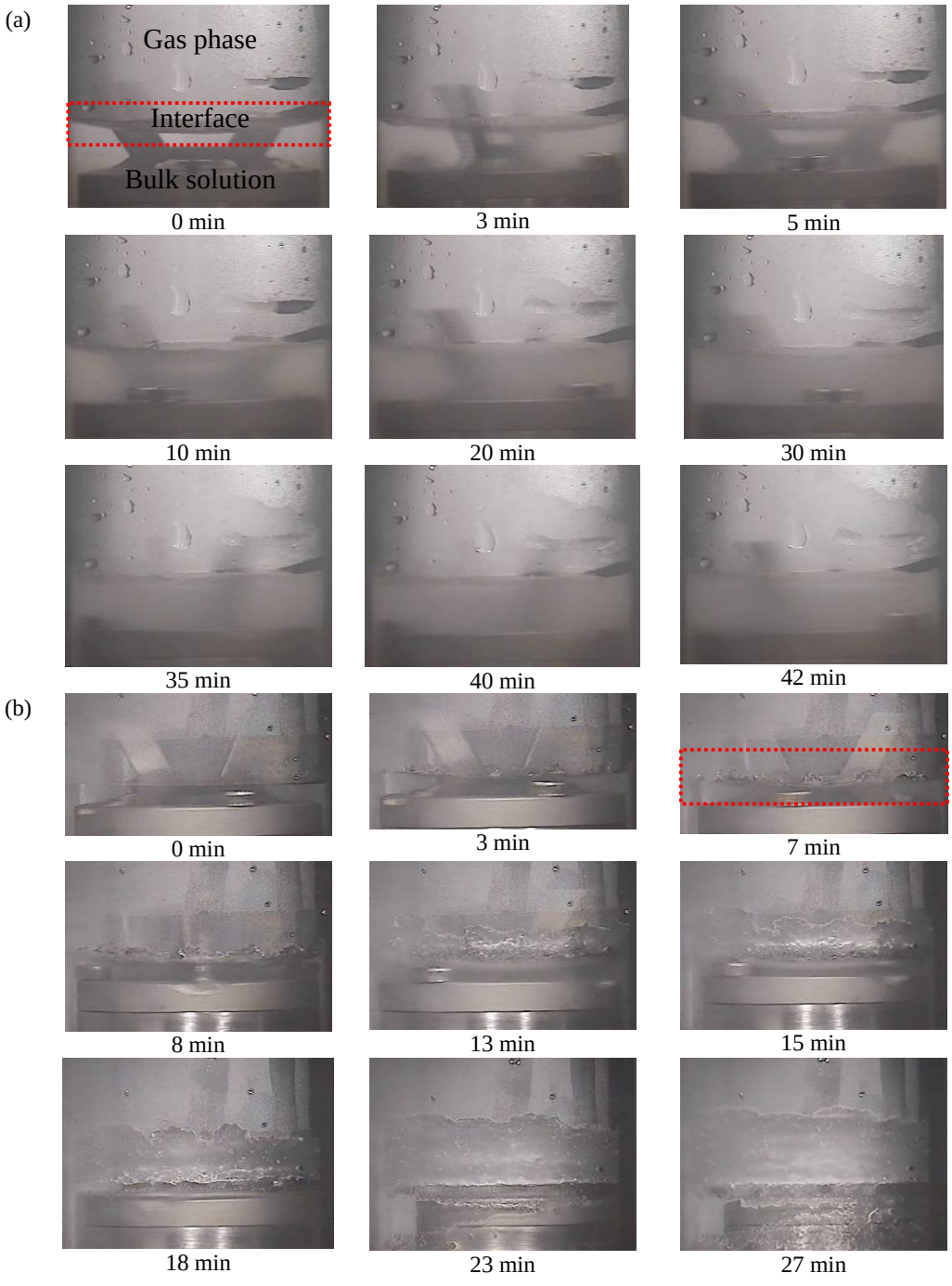

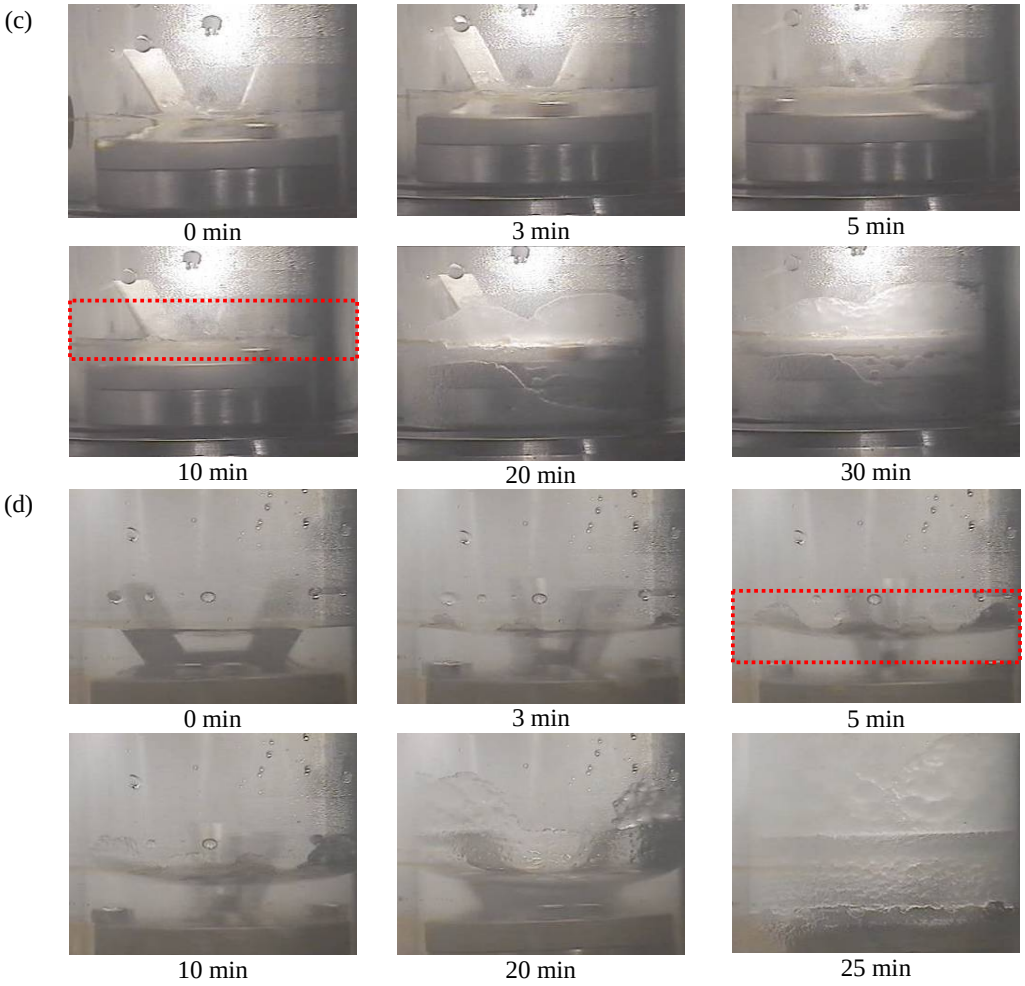

Figure 6.7 Gas hydrates crystal growth observed for pure water at various pressures (a) 20.8 bars, (b) 59.3 bars, (c) 62 bars, (d) 80.4 bars.

The crystal formation and growth process is well reflected in the temperature change shown in Figures 6.3-6.7. Taking Figure 6.3 as an example, starting from the set point of T_i=303.45 K, t_i=38.1 min, the temperature decreased rapidly at the beginning due to cooling. However, when the hydrates began to form at t_o, the decrease in temperature was compensated by the heat generated by the hydrate's formation. Further compensation, from t_o to t_e was induced by the more rapid growth of the crystals; therefore a generally constant temperature was observed. It should be noted that cooling was stopped at t_o.

A similar behaviour was observed for the rest of the experiments conducted at higher pressures, where crystal growth also started at the gas–liquid interface. However, the

growth of crystals at the wall of the cell above gas–liquid interface was more apparent at higher pressure (highlighted area of Figure 6.7 (b), (c), (d)). Several factors could be contributed to the formation of the crystals observed on the wall of the vessel: 1) a higher supersaturation of gas molecules on the wall, since there were less water molecules, 2) more effective cooling are less affected by the heat generated from the crystal formation, 3) roughness/imperfection of the vessel can act as nuclei which is very common for crystallisation process, 4) the bouncing of the gas molecules off the interface due to their kinetic energy, which is elevated at higher pressure, and thus makes them readily available for adsorption on the surface of the growing crystals. Consequently, most of the growth takes place on the gas side of the interface (Yousif, 1997).

An increase in the rate of hydrate formation with the increasing pressure was also observed in Figure 6.7 when the images were compared for the same period of time. Higher pressure is associated to the less time required for a total blocking of the cell with hydrates. This is also due to a higher supersaturation of gas at high pressure. A faster diffusion of gas molecules at higher pressure is another reason for such observations.

In order to make a comparison between the results of the four experiments, the above mentioned key parameters including, the initial conditions of the experiment (T_i, t_i), the onset point of hydrates formation with the temperature measured at the bottom of the cell (in the bulk solution) (T_o, t_o) and the top of the cell (in the gas phase) (T_t, t_o), and the conditions at which the cell is plugged with crystals (T_e, t_e), are presented in Table 6.6. The time required for the first appearance of the crystals since the cooling was started, Δt_1, and the time required for the plugging of the vessel, Δt_2, were also summarised in Table 6.6.

Table 6.6 Parameters observed during gas hydrates formation of natural gas and pure water hydrates systems.

P (bars)	T_i (K)	t_i (min)	T_t (K)	T_o (K)	t_o (min)	T_e (K)	t_e (min)	Δt_1 (min)	Δt_2 (min)
20.8	303.45	38.1	275.70	276.05	243.8	275.65	286.0	205.7	42.2
59.3	304.95	19.3	285.80	285.85	155.8	286.05	183.1	136.5	27.3
62.0	303.65	55.3	286.27	286.95	146.0	285.75	176.0	90.7	30.0
80.4	302.85	34.3	287.81	288.25	162.5	287.35	187.3	128.2	24.8

It is indicated in Table 6.6, that both the time required for the formation of the hydrates since the system starts to cooling down, Δt_1, and the time required for the growing of the crystals until the total plugging of the cell, Δt_2, appears to be shorter when the pressure increases. It should be noted that the cooling rate for the fourth experiment at 80.4 bars is much slower than the other three. This could affect the times required for the formation and growth of the hydrate crystals in this experiment.

It is also shown in Table 6.6, that a higher onset of the hydrates formation temperature requires less subcooling when the pressure is increased. It is observed that from 20.8 bars to 62 bars the change in onset temperature was around 10.9 K. However, no significant differences in the onset temperature were observed from 62 bars and 80.4 bars, showing a slight change of around 1.3 K. This behaviour compares well with the model predictions observed from the theoretical phase equilibria diagram for water and natural gas (Figure 6.8); this indicates that the hydrates formation requires lower temperatures at lower pressures. The experimental points are quite close to the theoretical curve, displaced a little bit at the left. The differences from the theoretical curve is the subcooling required when forming the hydrates; this is commonly observed in experimental work (Arjmandi et al., 2005).

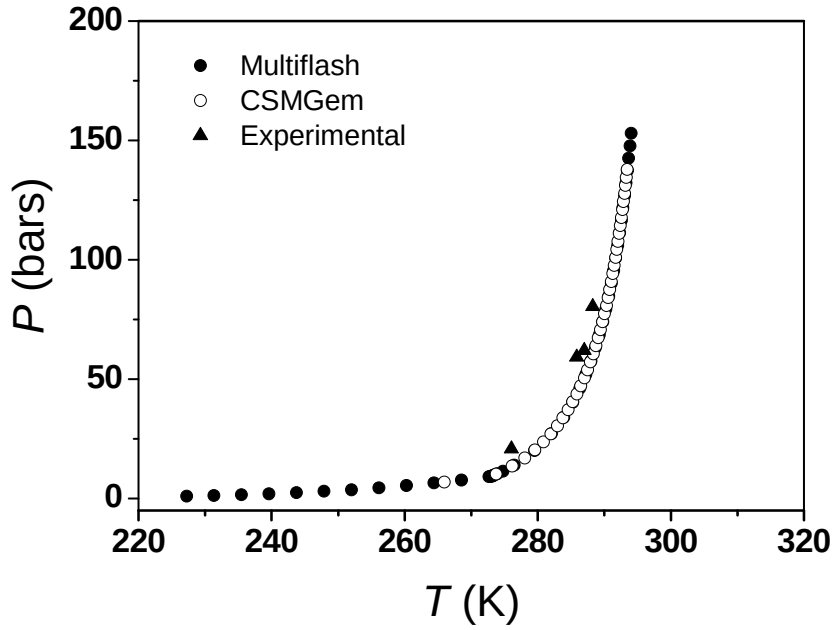

Figure 6.8 Comparison between the theoretical and the experimental hydrate phase diagram for water and natural gas.

We have reported in chapter 3, that the THF hydrates also form first at the walls of the reaction vessel, and/or the air–liquid interface. However, there was no haziness of the solutions noticed in the THF hydrates forming process. This is probably due to the greater miscibility of THF with water.

For the THF hydrates, once the temperature reached the onset point, both hydrate nucleation and crystal growth occurred in about 43 to 64 min. For natural gas, the crystal growing process took almost the same period of time at 20.8 bars (42 min), it was quicker with the increasing pressure in the system (around 25 min for 80.4 bars). However, it is important to note that different conditions were used to conduct the experiments in gas and THF systems. In the case of THF, the experiment was conducted in a dynamic condition until the detection of hydrates formation. The stirring was stopped immediately after the first crystals were observed. Further growing of the crystals was recorded in static conditions. For gas systems, the experiment was conducted in dynamic conditions from the beginning to the end. Also the reaction volume of the cells was slightly different (around 55 mL for the THF cell, and about 60 mL for the natural gas cell).

6.3.3 Nucleation and growth of gas hydrates in pure water containing KHIs

A similar plot of temperature–pressure as a function of the time was observed when KHIs were used in the system. In Figure 6.9, the plot of the gas hydrate system containing 0.1 wt% PEO-VCap is shown. As the figure reveals, the temperature dropped several degrees in the first 60 min, due to a forced cooling from the set point 303.25 K, to 287.25 K. After that, the temperature reduction became slower because a lower cooling rate 0.08 K/min was applied. The onset of hydrates formation was observed at about 178.8 min when the temperature reached 280.85 K. Similar to the systems containing no inhibitors the onset of hydrate formation was determined by visual observation, given that there was no detected increase of temperature or drop of pressure. The experiment was stopped at about 370 min (191.2 min after the detection of the hydrates formation) when the cell was totally blocked by the presence of hydrates.

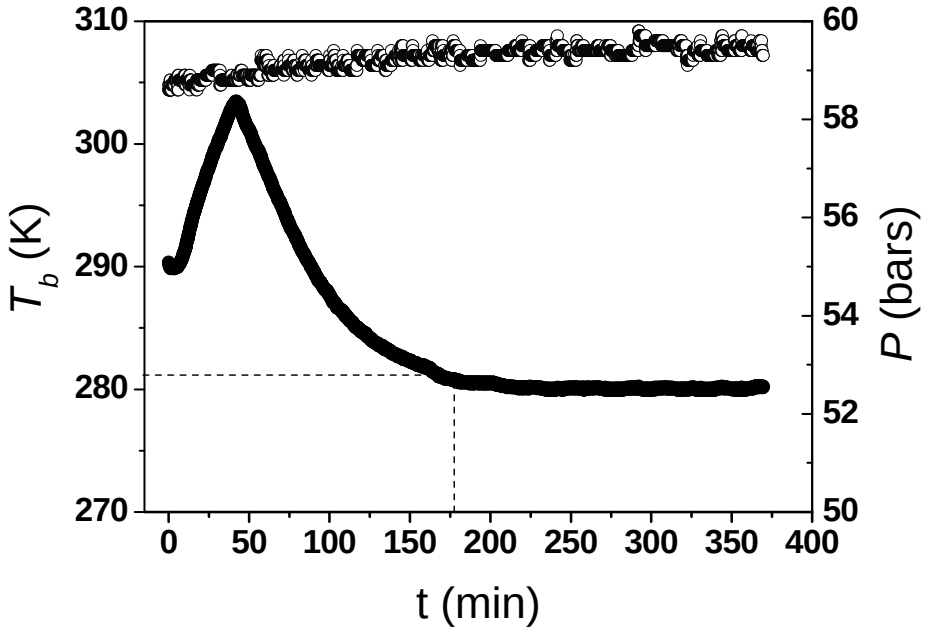

Figure 6.9 Temperature–pressure changes with time for a system containing PEO-VCap. Initial and final cooling rates 0.29 K/min and 0.08 K/min, respectively. Onset of hydrate formation occurs at 178.8 min (280.85 K).

Figure 6.10 shows the evolution of crystal growth with the time for PEO-VCap at 0.1 wt%.

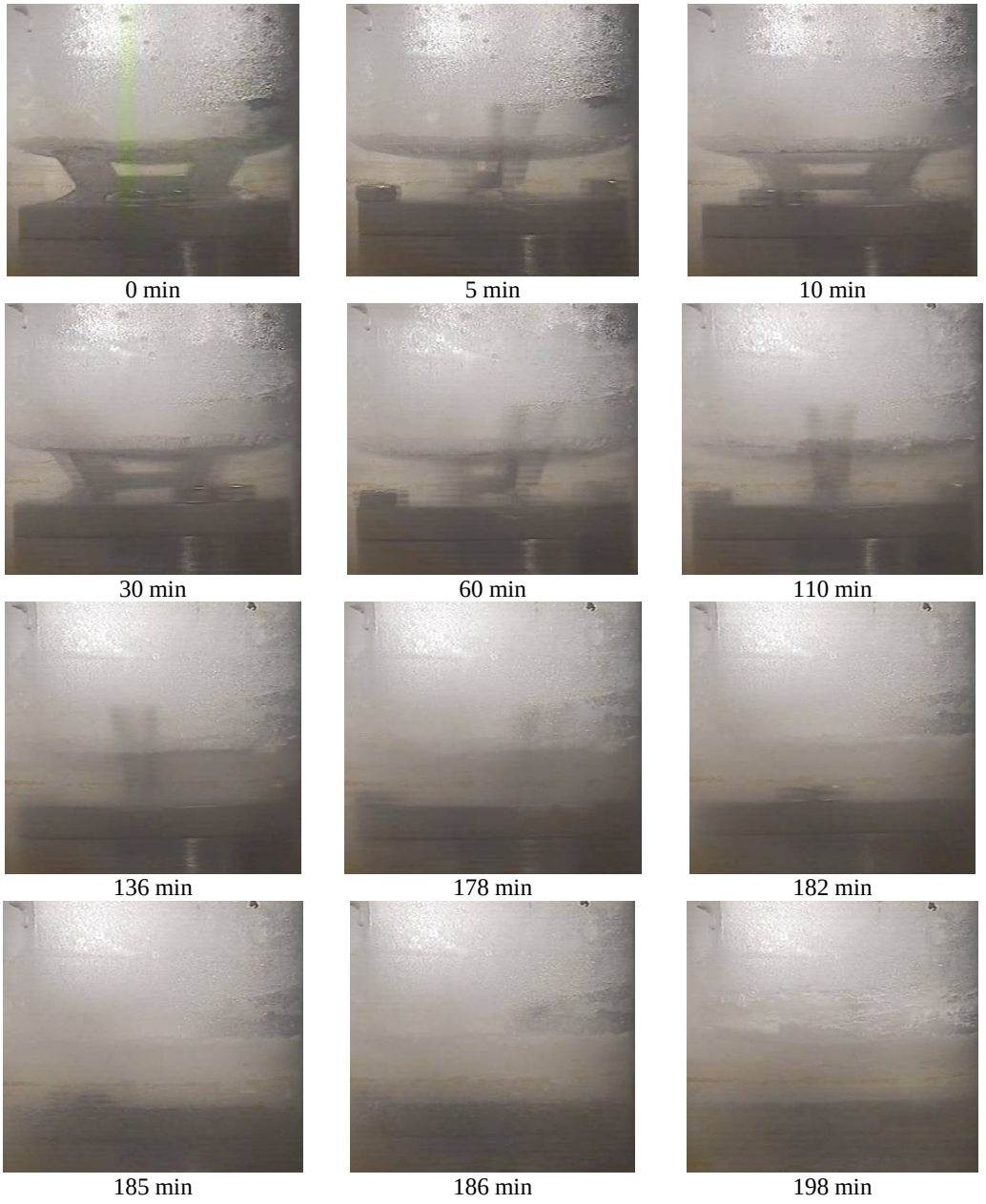

Figure 6.10 Gas hydrates crystals observed for PEO-VCap at a concentration of 0.1 wt%.

The crystals were first observed as a film at the gas–liquid interface at 0 min (it represents 178.8 min in the *T-t* curve in Figure 6.9). After 5 min, crystal growth also started to occur at the wall above the gas–liquid interface. Slow hydrate growth continued at the gas–liquid interface and the solution turned hazy at about 136 min. At 178 min (almost 3 h after the appearance of the first crystals at the interface), the thickness of the hydrate film at the gas–liquid interface increased quickly over time,

as well as acceleration in crystal growth. Catastrophic hydrate formation occurs and a plug of hydrate was observed in the cell at 191 min. Compared to the system containing no inhibitors, where the haziness of the solution was observed after 3 min, for the system containing PEO-VCap 0.1 wt%, the haziness appears at about 136 min. Also the blocking of the cell for the uninhibited system was observed at 27.3 min, compared to 191.2 min in the presence of PEO-VCap (around 2.8 h slower).

For Gaffix® VC713 and Luvicap® EG, a similar pattern of the temperature–pressure plot as a function of the time was observed (Figures 6.11 to 6.13), although the onset temperature, and time for blocking the cell, differs from one to another (see Table 6.7 for the values of these parameters).

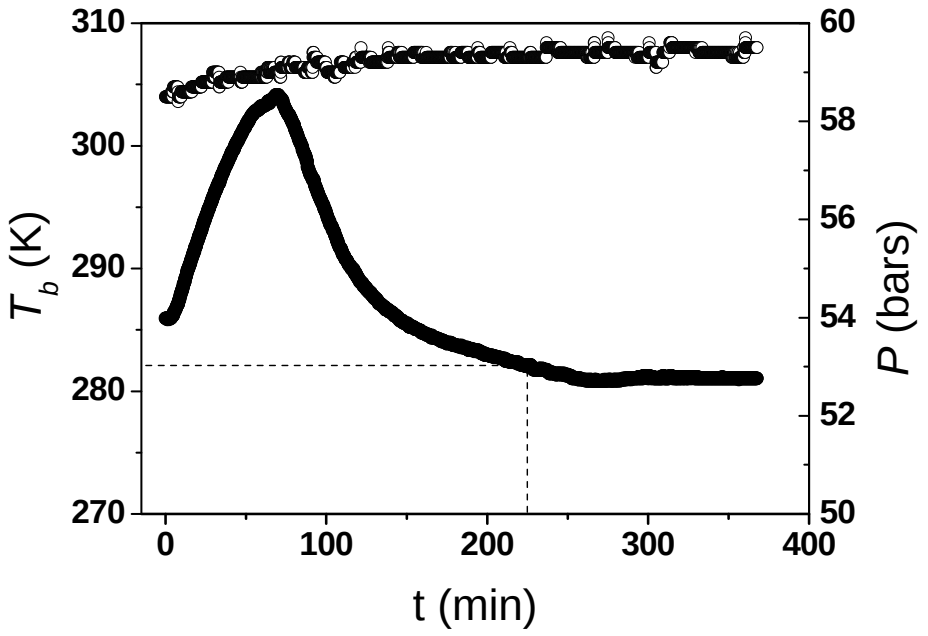

Figure 6.11 Temperature–pressure changes with time for a system containing Gaffix® VC713 0.10 wt%. Initial and final cooling rates 0.34 K/min and 0.04 K/min, respectively. Onset of hydrate formation occurs at 227.3 min (281.95 K).

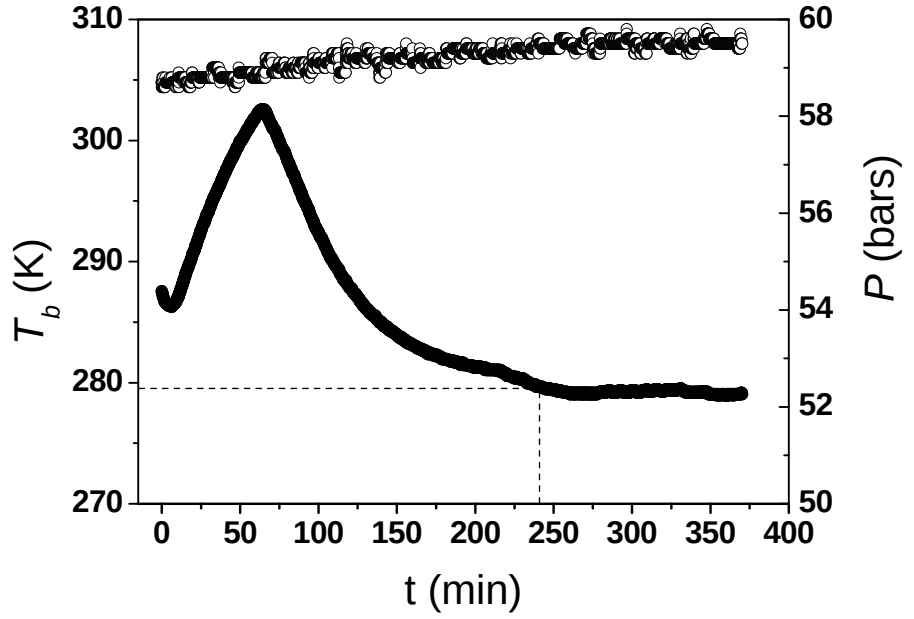

Figure 6.12 Temperature–pressure changes with time for a system containing Gaffix® VC713 0.25 wt%. Initial and final cooling rates 0.27 K/min and 0.04 K/min, respectively. Onset of hydrate formation occurs at 241 min (279.75 K).

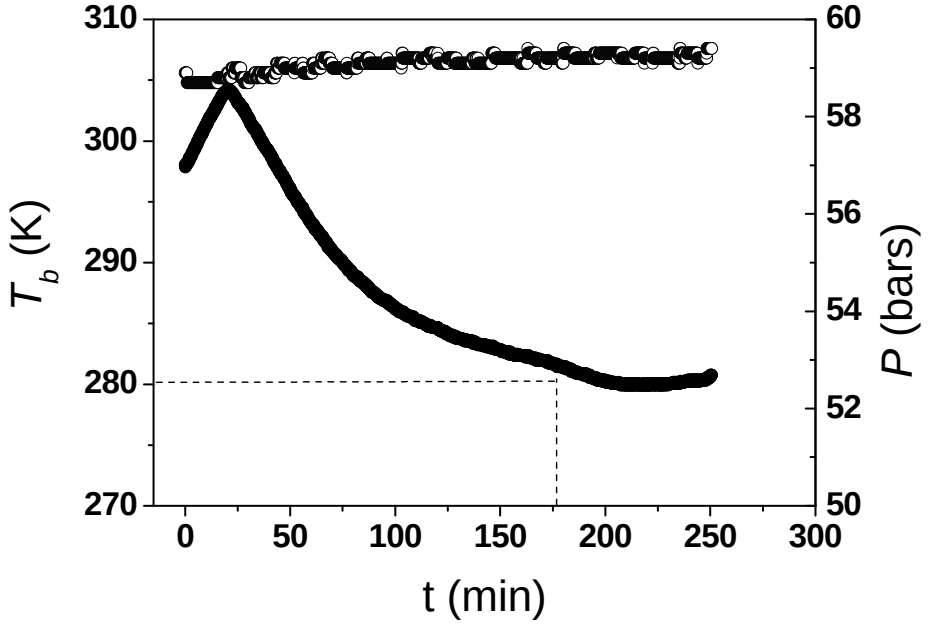

Figure 6.13 Temperature–pressure changes with time for a system containing Luvicap® EG. Initial and final cooling rates 0.28 K/min and 0.05 K/min, respectively. Onset of hydrate formation occurs at 198.1 min (280.35 K).

For PVP40 (Figure 6.14) the temperature was reduced at the beginning at a cooling rate of 0.24 K/min. At around 183 min, the cooling rate was kept constant because the presence of hydrates at this point could not be visually observed clearly (there was condensation in the external walls of the cell). Once the presence of hydrate crystals was discharged, the cooling rate was changed to 0.04 K/min until a clear film of hydrates were formed at around 338 min. Table 6.7 summarises the same parameters reported for the uninhibited system T_i, t_i, T_o, t_o, T_t, T_e, t_e, Δt_1 *and* Δt_2 for the same pressure for the systems containing inhibitors.

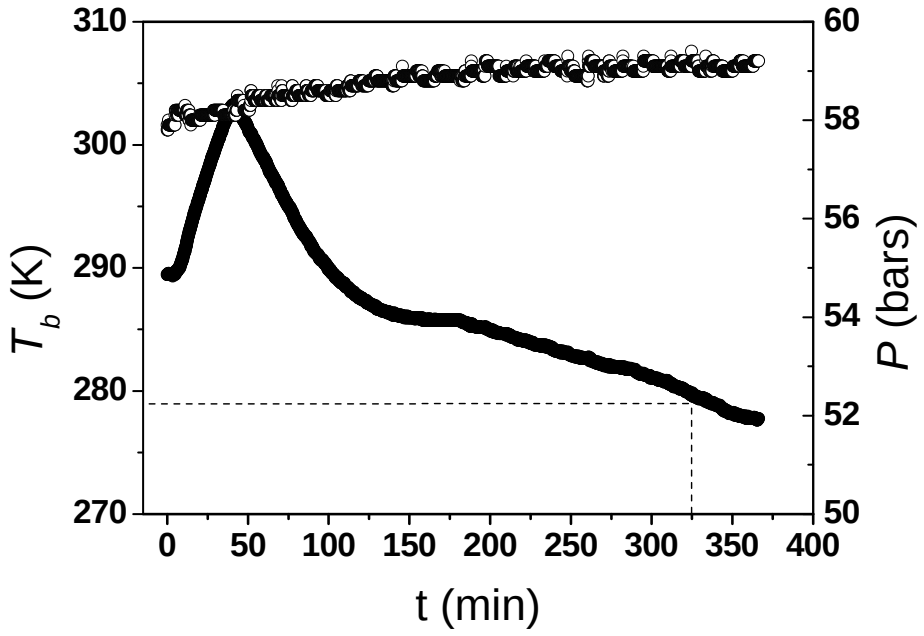

Figure 6.14 Temperature–pressure changes with time for a system containing PVP40 0.10 wt%. Initial and final cooling rates 0.24 K/min and 0.04 K/min, respectively. Onset of hydrate formation occurs at 338.4 min (278.95 K).

Table 6.7 Parameters observed during gas hydrates formation for natural gas in the presence of KHIs.

Inhibitor	P (bars)	T_i (K)	t_i (min)	T_t (K)	T_o (K)	t_o (min)	T_e (K)	t_e (min)	Δt_1 (min)	Δt_2 (min)
No inhibitor	59.3	304.95	19.3	285.80	285.85	155.8	286.05	183.1	136.5	27.3
Gaffix® VC713 0.10 wt%	59.3	304.15	70.3	281.43	281.95	227.3	-	-	196.9	-
Gaffix® VC713 0.25 wt%	59.4	302.55	65.6	279.42	279.75	241.0	-	-	175.4	-
PEO-VCap 0.1 wt%	59.3	303.25	43.9	280.60	280.85	178.8	280.25	370.0	134.8	191.2
Luvicap® EG 0.1 wt%	59.2	304.15	21.7	279.94	280.35	198.1	-	-	176.4	-
PVP40 0.1 wt%	59.1	303.25	42.2	278.52	278.95	338.4	-	-	296.3	-

As reviewed in Table 6.7, at the same pressure, slight decreases in the onset temperature of hydrates formation, in terms of T_t and T_o, was observed in all the cases for the systems containing inhibitors compared to the uninhibited system. T_t and T_o differed little for all the KHIs evaluated, showing maximum differences of about 3 K.

The lowest onset temperature was reached by PVP40 0.1 wt%, showing a difference of 6.9 K lower than the system containing no inhibitor. From the lowest to the highest onset temperature, PVP40 was followed by Luvicap® EG, PEO-VCap and Gaffix® VC713 at 0.1 wt% of polymers concentration. This trend reflects the different interactions of the active groups of the KHIs with the hydrate surface through hydrogen bonds and/or penetration into open cavities.

For Gaffix® VC713, an increase in the concentration of the polymer has resulted in a further reduction in the onset hydrate formation temperature at around 2.2 K. It suggests that the effect of increasing the concentration of the inhibitor can impact significantly on the performance of the KHIs. This has been observed and reported previously (Lederhos et al., 1996; Ding et al., 2010).

It can also be observed in Table 6.7, that the time difference required for the formation of the hydrates from t_i is in the trend of PEO-VCap 0.1 wt% < no inhibitor < Gaffix® VC713 0.1 wt% < Gaffix® VC713 0.25 wt% < Luvicap® EG 0.1 wt% <

PVP40 0.1 wt%. This means that the best inhibitor controlling the nucleation of the gas hydrates is PVP40, and the worse is PEO-VCap. Because of the presence of KHIs in the systems, the time required for total blocking of the cell was not observed for most of the inhibitors during the 8 h experimental process. For the systems containing inhibitors, t_e was determined only for PEO-VCap, which produced a hydrate plugging 191.2 min after the detection of the hydrates.

The crystals growing evolution with the recorded time is presented in Figures 6.15 to 6.18 for Gaffix® VC713 at different concentrations, Luvicap® EG and PVP40 respectively.

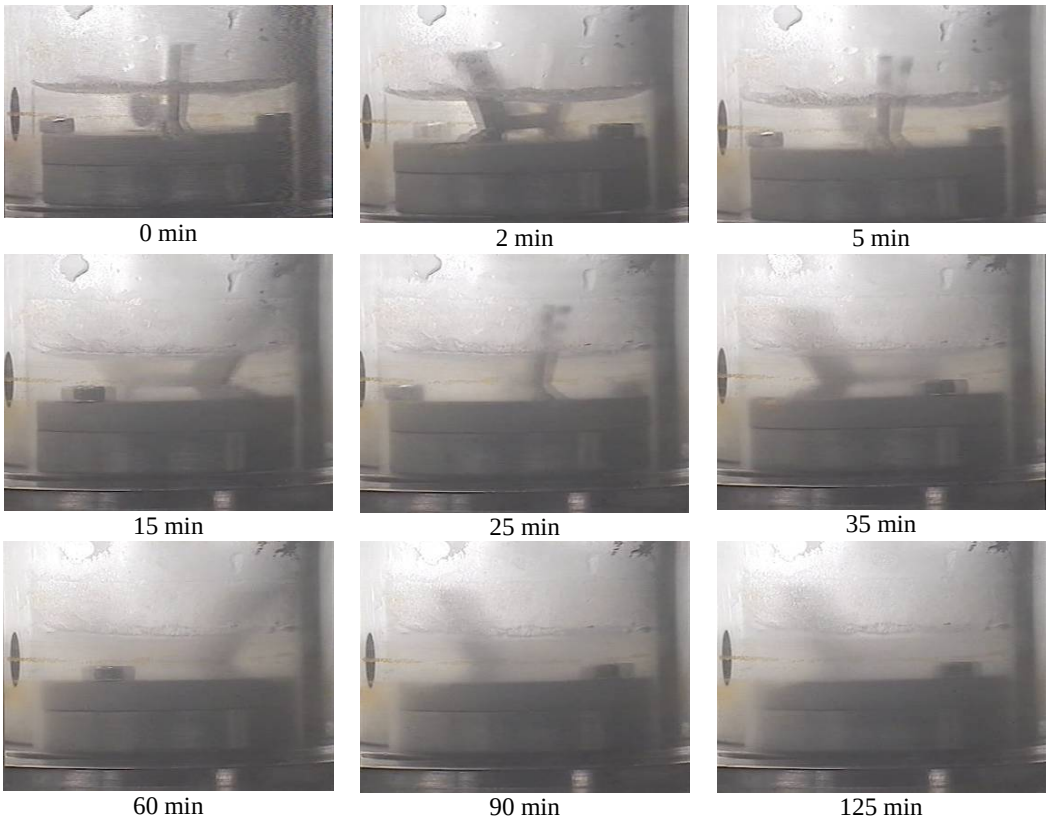

Figure 6.15 Gas hydrates crystals growth observed for Gaffix® VC713 at a concentration of 0.1 wt%.

Figure 6.15 shows the crystals growing evolution with the time for Gaffix® VC713 at 0.1 wt%. Crystals were first observed as a film at the gas–liquid interface at 0 s (it represents 227.3 min in Figure 6.11). After 900s the solution turned hazy, indicating the formation of nuclei of gas hydrates. The haziness increased with time. At 125

min the solution turned milky. However, at that time no hydrate particles were observed in the bulk solution. A similar behaviour was observed for Gaffix® VC713 at 0.25 wt% (Figure 6.16).

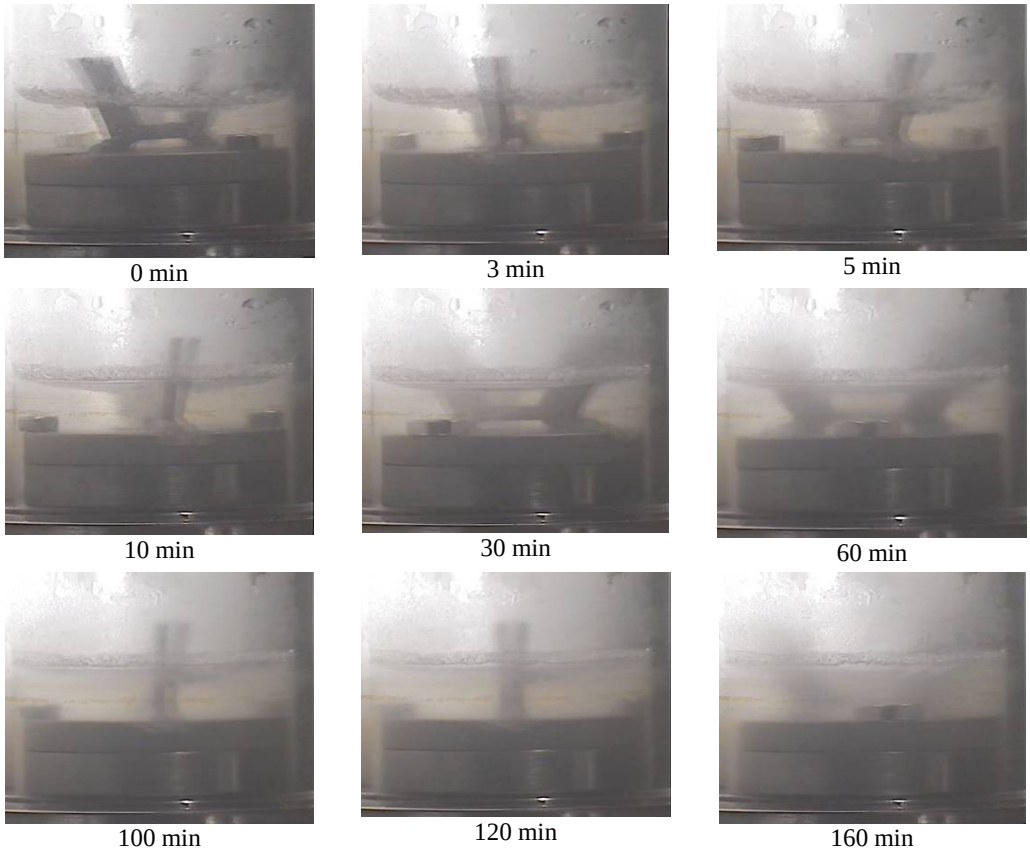

Figure 6.16 Gas hydrates crystals growth observed for Gaffix® VC713 at a concentration of 0.25 wt%.

The evolution of the crystals growing in the presence of Luvicap® EG is observed in Figure 6.17. Crystals formation and haziness of the solution started also at the gas–liquid interface at 0 min. At 10 min the thickness of the hydrate film started to increase with the time. At 41 min the stirrer stopped because of a hydrates plugging at the interface. No crystals were observed at the bulk solution.

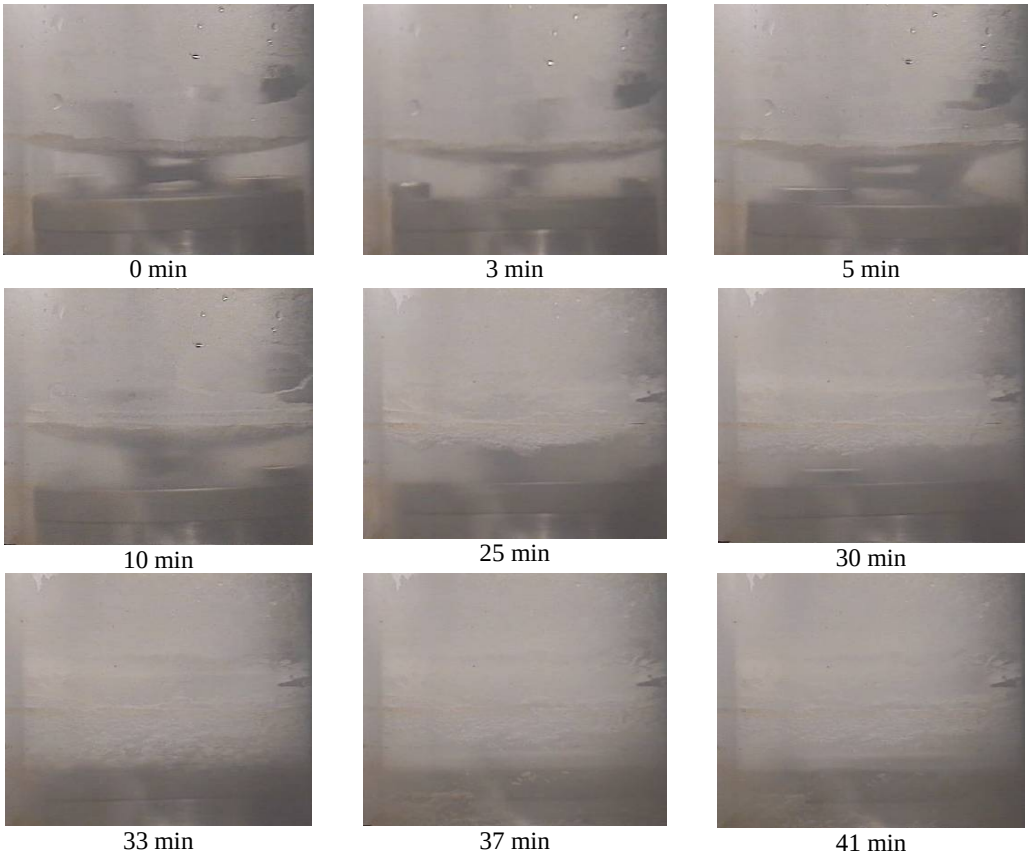

Figure 6.17 Gas hydrates crystals growth observed for Luvicap® EG at a concentration of 0.1 wt%.

The same behaviour observed for the evolution of the crystals growing in the system containing Luvicap® EG was also observed for PVP40 (Figure 6.18). No crystal growth was observed at the bulk solution at 27.8 min. No blocking of the cell was observed at that time.

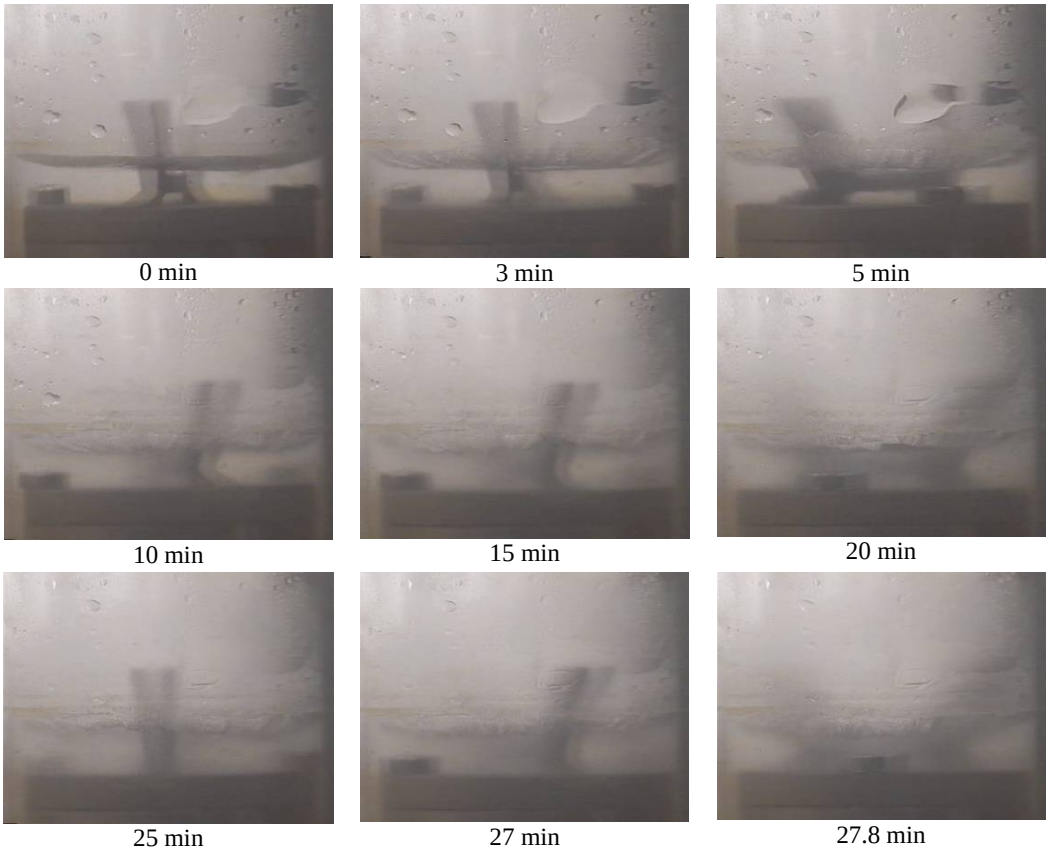

Figure 6.18 Gas hydrates crystals growth observed for PVP40 at a concentration of 0.1 wt%.

When these results are compared with those ones obtained using THF as a hydrate promoter instead of natural gas (Table 3.3 in Chapter 3), it is observed that at the same concentration, KHIs lower the onset temperature of hydrate formation, compared to the uninhibited system for both THF and gas hydrates systems. However, the values of the decreased temperature produced using KHIs are different from the THF hydrate systems for the gas hydrate systems. The highest temperature reductions were 13.9 K (PEO-VCap) for THF hydrates and 6.9 K (PVP40) for gas hydrates.

Table 6.8 Onset temperatures for THF and gas hydrate systems containing 0.1 wt% of KHIs.

Inhibitor	THF hydrates (P =1 bar)		Gas hydrates (P=59.3 bars)	
	T_o (K)	Δt_2 (min)	T_o (K)	Δt_2 (min)
No inhibitor	275.1	38-61	285.85	27.3
Gaffix® VC713	269.4	14-25	281.95	-
PEO-VCap	263.5	19-23	280.85	191.2
Luvicap® EG	271.6	26-116	280.35	-
PVP40	273.3	7	278.95	-

For THF hydrates the trend showed from the best inhibitor to the worse one (in terms of the reduction of the onset temperature) was PEO-VCap, Gaffix® VC713, Luvicap® EG and PVP40. This was different to that one showed in gas hydrate systems which showed PVP40, Luvicap® EG, PEO-VCap and Gaffix® VC713. This means that polymers that show the best inhibition performance in THF crystals do not show the same inhibition performance in gas hydrate crystals. In particular for PVP40, it gave the best results in the gas system and the worse results in the THF system. This indicates that a different mechanism of surface adsorption could be operating, or that polymer adsorption onto hydrate crystals is possibly not the primary mechanism for gas hydrate inhibition by this polymer class. Similar results were reported for KHIs by Kelland (2009), Del Villano and Kelland (2009) and Del Villano et al., (2009). In THF hydrate formation systems, THF is present in high concentration in the water phase throughout the hydrate formation process, whereas constant gas diffusion into the water phase is necessary for gas hydrate formation. It is possible that PVP40 has weak interactions with the THF hydrate crystal surface than that observed with the rest of the polymers, resulting in a poor inhibition performance. Similar to PVP40, PEO-VCap also showed contrary performance inhibiting both THF and gas systems.

It appears that THF tests can provide information on the performance of some KHIs (and crystal growth-modifying AAs), but can be misleading for other KHIs because THF is very water-soluble, and the inhibition mechanism may be different from real gas hydrate systems (Talley et al., 2000; Kelland, 2009) in which gases are hydrophobic. Polymers that show a good inhibition of THF crystals might also show a good inhibition of gas hydrate crystals if the same mechanism of surface adsorption is operating (Kelland, 2006). Some KHI polymers including homopolymers and

copolymers of *N*-vinylpyrrolidone or *N*-vinylcaprolactam, and anti-freeze proteins (Anselme et al., 1993; Long et al., 1994; Larsen et al., 1998; Zeng et al., 2006), have been evaluated using THF hydrate as a model system; one laboratory study clearly demonstrated that these polymers do adsorb onto certain surfaces of THF hydrate crystals as the mechanism by which growth is inhibited (Makogon et al., 1997). However, this is not always so for some polymer classes (Kelland, 2006). For example, THF hydrate ball-stop test results in some ring-close disopropenyloxazolines show that these polymers perform no better than non additive, yet they are fairly effective KHIs, preventing sII hydrate nucleation in mini-loop tests with natural gas mixtures (Colle and Oelfke, 1996). Conversely, tetra alkyl ammonium salts, where the alkyl group iso-butyl or pentyl, are good inhibitors of THF hydrate crystal growth, but poor gas hydrate nucleation inhibitors when used alone (Klomp et al., 1995).

Additionally, it is observed in Table 6.8, that the difference in time required for the hydrates to grow and block the cell, Δt_2, is higher for the uninhibited system in THF hydrates compared to gas hydrates. This could be due to the effect of the high pressure used in the gas system. However, for inhibited systems, the time taken for the crystals to grow are shorter for THF than for gas. For most of the inhibitors studied in gas systems this time could not be determined, because the cell was not fully blocked within observation time (approximately 8 hours). It also suggests that in gas systems different adsorption mechanisms can be operating in the presence of KHIs.

6.4 Conclusions

The kinetic experiments of natural gas hydrates formation in pure water at different pressures has shown a good correlation (theoretically and experimentally) with the current data reported by the hydrate research community. The dependence of both onset temperatures and quantity of hydrate formed in a determine period of time with the increasing pressure has been verified.

For all of the experiments performed in this chapter, the liquid–solid phase transition always started at the gas–liquid interface. In the presence of inhibitors, it took longer time for the hydrates to form. The growth of the gas hydrates was also slower in the presence of inhibitors.

In all cases the presence of KHIs decreases the temperature of the onset hydrate formation. For the same inhibitor concentration of 0.1 wt%, the results show that PVP40 exhibits the lowest temperature to onset of hydrate formation, followed by Luvicap® EG, PEO-VCap and Gaffix® VC713. An increase in the inhibitor concentration of Gaffix® VC713 lowered the onset temperature of hydrates formation.

Polymers such as PVP40 and PEO-VCap, that show the worse and the best inhibition performance respectively in THF crystals, exhibit the opposite inhibition performance in gas hydrate crystals. This suggests that a different mechanism of surface adsorption could be operating when THF and gas hydrates are used.

Chapter 7 GENERAL CONCLUSIONS AND SUGGESTIONS FOR FUTURE WORK

From the studies reported in the previous chapters, we make the following conclusions.

The formation kinetics of the THF hydrate is strongly influenced by the physical chemical environment, which includes the concentration and types of additives used in the hydrate's formation systems. As we mentioned in chapter 3, subcooling is usually considered the driving force for hydrate formation and is a criterion for simulating field conditions (Yousif et al., 1994). An increase in subcooling and a reduced onset temperature of hydrates formation, were observed when various inhibitors were used, compared to the system containing no inhibitor. At the investigated concentration range, 0.1-2.0 wt%, THIs such as MeOH and MEG, were more effective than the KHIs in preventing the formation of THF hydrates, even at such low concentrations. However, the growth of the already formed hydrate crystals was much faster in the presence of THIs. The presence of 0.1 wt% SDS also decreased the temperature required to form the hydrate, but enhanced the rate of THF hydrate formation. So far, THIs and AAs have been more widely used by the industry than KHIs, because of their ability to handle high subcoolings. However, KHIs provide a cost-saving alternative to THIs, and improves operational safety and its environmental impact. NaCl alone was not very effective in preventing the formation of hydrates in a concentration of 3.5wt%. However, the inhibition efficiency of most KHIs used in this study was enhanced with the presence of NaCl 3.5 wt%, showing a strong synergy effect.

Adsorption studies at the air–liquid and THF hydrate–liquid interfaces have shown different adsorption behaviour for all KHI molecules. The fundamental properties of the polymer molecules, such as the monomer moiety, molecular weight and flexibility of the polymer chains have revealed a strong impact on adsorption behaviour. For the same polymer concentrations, a lower surface tension value is associated with a better inhibition performance. The enhanced inhibition efficiency

in the presence of NaCl 3.5 wt% appeared to be associated to a maximum packing of polymer molecules in the monolayer and low surface tension values. The zeta potential results measured at the THF hydrate–liquid interface, have shown some correspondence with the surface tension results at the air liquid–interface. The compound with a higher adsorption on the surface also revealed a higher adsorption at the THF hydrate. Furthermore, it was observed that the inhibitor showing the higher adsorption of zeta potential measurements, was the most effective for reducing the onset temperature of hydrates formation. It was demonstrated that the adsorption of KHIs is directly related to its effectiveness inhibiting hydrates.

Kinetic experiments on natural gas hydrates have indicated that the hydrate formation rate is always slower when KHIs are present in the liquid phase. In all cases, the presence of KHI decreases the temperature at the onset of hydrate formation; this was also observed in the THF hydrates systems. The hypothesis, that the inhibition of natural gas hydrates, involves the adsorption of the KHI polymer on the surfaces of growing particles or crystal of hydrate (sub-critical or super-critical size), and perturbs their nucleation and/or further growth, was verified for all inhibitors. However, polymers that show the best inhibition performance in THF crystals do not show the same inhibition performance in gas hydrate crystals. In particular for PVP40, it gave the best results in the gas system and the worse results in the THF system. PEO-VCap also showed contrary performance in THF and gas systems. This indicates two different adsorption behaviors of polymers in different hydrates systems. We know that in THF hydrate formation systems, THF is present in high concentration in the water phase throughout the hydrate formation process. However, in a gas hydrate system, the gas concentration in liquid is limited due to its poor solubility. Constant gas diffusion into the water phase is necessary for gas hydrate formation. It is possible that PVP40 has weak interactions with the THF hydrate crystal surface than that observed with the rest of the polymers, resulting in a poor inhibition performance. For PEO-VCap, the presence of highly flexible and hydrophilic PEO moieties might have enhanced the THF interaction with the inhibitor, therefore displaying better inhibition efficiency than others. Similar observations were previously reported by Kelland (2009), Del Villano and Kelland (2009) and Del Villano et al., (2009). Regardless, the inhibition mechanism of KHIs

in the THF hydrates systems may vary significantly with that in the gas hydrate systems. Therefore, the traditional concept of investigating THF hydrates formation, and fast screening of KHIs using THF hydrates systems, for the purpose of understanding of the natural gas formation and inhibition, need to be carefully reassessed.

Our findings about the mechanisms of gas hydrates inhibition by KHIs are in agreement with previous authors, who suggested that KHIs adsorb on the surfaces of growing particles or crystal of hydrate (sub-critical or super-critical size) perturbing their nucleation and/or further growth (Carver et al., 1995; Lederhos et al., 1996; Larsen et al., 1998; Hutter et al., 2000; Makogon and Sloan, 2002; Moon et al., 2007).

Based on the results of this study, the following research activities are recommended, in order to further confirm or consolidate our findings,

- Improving the quality of the images taken from the microscope (during THF experiments) and from the video camera (during gas hydrates experiments) will allow the use of special software for imaging processing; therefore, more knowledge about the hydrate crystal morphology and agglomerating behaviour can be extracted from the experiments.

- Monitoring the kinetics of natural gas hydrates formation without continuous injection of the gas during the experiments, will provide the possibility to observe a significant pressure drop in the *T-P* diagram; this will allow for a more precise detection of the onset of hydrates formation.

- In this study, the mechanisms involved in sII THF and natural gas hydrates formation and inhibition were investigated using onset temperature of hydrates formation. It is important to investigate mechanisms involved in hydrate formation and inhibition at a constant temperature, as well as, to evaluate other different liquid and gas hydrate formers.

- How KHIs affect the stable hydrate system with two interfaces, hydrate–liquid water and liquid water–gas requires further study.

REFERENCES

Al-Adel, S., J. A. G. Dick, R. El-Ghafari, and P. Servio. 2008. The effect of biological and polymeric inhibitors on methane gas hydrate growth kinetics. *Fluid Phase Equilibria* 267: 92-98.

Alapati, R., and A. Davis. 2007. Oil-soluble LDHI represents new breed of hydrate inhibitor. *JPT Online: Tech Up* (6).

Anderson, B. J., J. W. Tester, G. P. Borghi, and B. L. Trout. 2005. Properties of inhibitors of methane hydrate formation via molecular dynamics simulations. *Journal of the American Chemical Society* 127 (50): 17852-17862.

Andersson, O., and H. Suga. 1996. Thermal conductivity of normal and deuterated tetrahydrofuran clathrate hydrates *Journal of Physics and Chemistry of Solids* 57 (1): 125-132.

Anklam, M. R., and A. Firoozabadi. 2005. An interfacial energy mechanism for the complete inhibition of crystal growth by inhibitor adsorption. *Journal of Chemical Physics* 123 (144708): 1-12.

Anklam, M. R., J. D. York, L. Helmerich, and A. Firoozabadi. 2008. Effects of antiagglomerants on the interactions between hydrate particles. *American Institute of Chemical Engineers* 54 (2): 565-574.

Arjmandi, M., B. Tohidi, A. Danesh, and A. C. Todd. 2005. Is subcooling the right driving force for testing low-dosage hydrate inhibitors? *Chemical Engineering Science* 60: 1313-1321.

Ashworth, T., L. R. Johnson, and L.-P. Lai. 1985. Thermal conductivity of pure ice and tetrahydrofuran clathrate hydrates. *High Temperatures-High Pressures* 17: 413-419.

Bains, S., R. M. Corfield, and R. D. Norris. 1999. Mechanisms of climate warming at the end of the Paleocene. *Science* 285 (5428): 724-727.

Barker, J. W., and R. K. Gomez. 1989. Formation of hydrates during deepwater drilling operations. *Journal of Petroleum Technology* 41: 297-301.

Bishnoi, P. R., and P. D. Dholabhai. 1999. Equilibrium conditions for hydrate formation for a ternary mixture of methane, propane and carbon dioxide, and a natural gas mixture in the presence of electrolytes and methanol. *Fluid Phase Equilibria* 158-160: 821-827.

Bishnoi, P. R., and V. Natarajan. 1996. Formation and decomposition of gas hydrates. *Fluid Phase Equilibria* 117: 168-177.

Bishnoi, P. R., V. Natarajan, and N. Kalogerakis. 1994. A unified description of the kinetics of hydrate nucleation, growth, and decomposition. *Annals of the New York Academy of Sciences* 715: 311-322.

Bobev, S., and K. T. Tait. 2004. Methanol—inhibitor or promoter of the formation of gas hydrates from deuterated ice? *American Mineralogist* 89: 1208-1214.

Bollavaram, P., S. Devarakonda, M. S. Selim, and E. D. Sloan Jr. 2000. Growth kinetics of single crystal sII hydrates elimination of mass and heat transfer effects. *Annals New York Academy of Sciences* 12 (1): 533-543.

Carstensen, A., J. L. Creek, and C. A. Koh. 2004. Investigating the performance of clathrate hydrate inhibitors using in situ Raman spectroscopy and differential scanning calorimetry. *American Mineralogist* 89: 1215-1220.

Carver, T. J., M. G. B. Drew, and P. M. Rodger. 1995. Inhibition of crystal growth in methane hydrate. *Journal of the Chemical Society, Faraday Transactions* 91 (19): 3449-3460.

Cha, S. B., H. Ouar, T. R. Wildeman, and E. D. Sloan. 1988. A third-surface effect on hydrate formation. *Journal of Physical Chemistry* 92: 6492-6494.

Chang, C.-H., and E. I. Franses. 1995. Adsorption dynamics of surfactants at the air/water interface: a critical review of mathematical models, data, and mechanisms. *Colloids and Surfaces A* 100 (1): 1-45.

Chatti, I., A. Delahaye, L. Fournaison, and J.-P. Petitet. 2005. Benefits and drawbacks of clathrate hydrates: a review of their areas of interest. *Energy Conversion and Management* 46: 1333-1343.

Christiansen, R. L., and J. Sloan, D. 1994. Mechanisms and kinetics of hydrate formation. *Annals New York Academy of Sciences* 715 (Natural Gas Hydrates): 283-305.

Cingotti, B., A. Sinquin, J. P. Durand, and T. Palermo. 2000. Study of methane hydrate inhibition mechanisms using copolymers. *Annals New York Academy of Sciences* 912 (1): 766-766.

Clarke, M. A., and P. R. Bishnoi. 2005. Determination of the intrinsic kinetics of CO2 gas hydrate formation using in situ particle size analysis. *Chemical Engineering Science* 60 (3): 695-709.

Colle, K. S., R. H. Oelfke, and M. A. Kelland. 1999. US Patent 5874660, filed February 23, and issued

Daimaru, T., A. Yamasaki, and Y. Yanagisawa. 2007. Effect of surfactant carbon chain length on hydrate formation kinetics. *Journal of Petroleum Science and Engineering* 56: 89-96.

Dawe, R. A., and S. Thomas. 2007. A large potential methane source—natural gas hydrates. *Energy Sources, Part A* 29: 217-229.

Del Villano, L., and M. A. Kelland. 2009. Tetrahydrofuran hydrate crystal growth inhibition by hyperbranched poly(ester amide)s. *Chemical Engineering Science* 64: 3197-3200.

Del Villano, L., R. Kommedal, M. W. M. Fijten, U. S. Schubert, R. Hoogenboom, and M. A. Kelland. 2009. A study of the kinetic hydrate inhibitor performance and seawater biodegradability of a series of poly(2-alkyl-2-oxazoline)s. *Energy & Fuels* 23: 3665-3673.

Del Villano, L., R. Kommedal, and M. A. Kelland. 2008. Class of kinetic hydrate inhibitors with good biodegradability. *Energy & Fuels* 22: 3143-3149.

Delgado, A. V., F. Gonzalez-Caballero, R. J. Hunter, L. K. Koopal, and J. Lyklema. 2005. Measurement and interpretation of electrokinetic phenomena. *Pure Applied Chemistry* 77 (10): 1753–1805.

Devarakonda, S., A. Groysman, and A. S. Myerson. 1999. THF–water hydrate crystallization: an experimental investigation *Journal of Crystal Growth* 204: 525-538.

Dickens, G. R. 2003. Rethinking the global carbon cycle with a large, dynamic and microbially mediated gas hydrate capacitor *Earth and Planetary Science Letters* 213 (3-4): 169-183.

Díez-Pascual, A. M., A. Compostizo, A. Crespo-Colín, R. G. Rubio, and R. Miller. 2007. Adsorption of water-soluble polymers with surfactant character. Adsorption kinetics and equilibrium properties. *Journal of Colloid and Interface Science* 307: 398-404.

Ding, A., S. Wang, T. Pelemis, C. Crisafio, and X. Lou. 2010. Specific critical concentrations of low dosage hydrate inhibitors in a THF–NaCl hydrate formation solution. *Asian Pacific Journal of Chemical Engineering*:

Drzymala, J., Z. Sadowski, L. Holysz, and E. Chibowski. 1999. Ice/water interface: zeta potential, point of zero charge, and hydrophobicity *Journal of Colloid and Interface Science* 220 (2): 229-234

Duncum, S. N., A. R. Edwards, and C. G. Osborne. 1993. European patent 0536950 Al

Duro, R., C. Souto, J. L. Gomez-Amoza, R. Martinez-Pacheco, and A. Concheiro. 1999. Interfacial adsorption of polymers and surfactants: implications for the properties of disperse systems of pharmaceutical interest. *Drug Development and Industrial Pharmacy* 25 (7): 817-829.

Eastoe, J., and J. S. Dalton. 2000. Dynamic surface tension and adsorption mechanisms of surfactants at the air-water interface. *Advances in Colloid and Interface Science* 85: 103-144.

Englezos, P. 1993. Clathrate hydrates. *Industrial & Engineering Chemistry Research* 32: 1251-1274.

Englezos, P., N. Kalogerakis, P. D. Dholabhai, and P. R. Bishnoi. 1987a. Kinetics of formation of methane and ethane gas hydrates. *Chemical Engineering Science* 42 (2): 2647-2658.

Englezos, P., N. Kalogerakis, P. D. Dholabhai, and P. R. Bishnoi. 1987b. Kinetics of gas hydrate formation from mixtures of methane and ethane. *Chemical Engineering Science* 42 (2): 2659-2666.

Englezos, P., and L. D. Lee. 2005. Gas hydrates: a cleaner source of energy and opportunity for innovative technologies. *Korean Journal of Chemical Engineering* 22 (5): 671-681.

Fainerman, V. B., A. V. Makievski, and R. Miller. 1994. The analysis of dynamic surface tension of sodium alkyl sulphate solutions, based on asymptotic equations of adsorption kinetic theory. *Colloids and Surfaces A* 87: 61-75.

Fleer, G. J., M. A. Cohen Stuart, J. M. H. M. Scheutjens, T. Cosgrove, and B. Vincent. 1993. *Polymers at interfaces*. First ed. London: Chapman & Hall.

Florusse, L. J., C. J. Peters, J. Schoonman, K. C. Hester, C. A. Koh, S. F. Dec, K. N. Marsh, and E. D. Sloan. 2004. Stable low-pressure hydrogen clusters stored in a binary clathrate hydrate. *Science* 306 (5695): 469-471.

Fournaison, L., A. Delahaye, I. Chatti, and J.-P. Petitet. 2004. CO2 hydrates in refrigeration processes. *Industrial Engineering Chemical Research* 43 (20): 6521-6526.

Freer, E. M., and E. D. Sloan Jr. 2000. An engineering approach to kinetic inhibitor design using molecular dynamics simulations. *Annals New York Academy of Sciences* 912 (1): 651-657.

Gargalló, L., A. Leiva, L. Alegría, B. Miranda, A. González, and D. Radic. 2005. Interfacial properties of poly(N-vinyl-2-pyrrolidone) at the air/water interface *Journal of Macromolecular Science, Part B* 43 (5): 913-924.

Gayet, P., C. Dicherry, G. Marion, A. Graciaa, J. Lachaise, and A. Nesteroy. 2005. Experimental determination of methane hydrate dissociation curve up to 55MPa by using a small amount of surfactant as hydrate promoter. *Chemical Engineering Science* 60 (21): 5751-5758.

General discussion. 2007. *Faraday Discussions* 136: 395-407.

Giavarini, C., F. Maccioni, and M. L. Santarelli. 2006. Modulated DSC for gas hydrates analysis *Journal of Thermal Analysis and Calorimetry* 84 (2): 419-424.

Gilányi, T., I. Varga, M. Gilányi, and R. Mészarós. 2006. Adsorption of poly(ethylene oxide) at the air/water interface: A dynamic and static surface tension study. *Journal of Colloid and Interface Science* 301: 428-435.

Gilcreest, V., and V. P. Gilcreest. 2006. Adsorption kinetics of NIPAM-based polymers at the air-water interface as studied by pendant drop and bubble tensiometry. *Journal of Physical Chemistry B* 110 (43): 21903-21910.

Gnanendran, N., and R. Amin. 2004. Equilibrium hydrate formation conditions for hydrotrope–water–natural gas systems. *Fluid Phase Equilibria* 221: 175-187.

Goel, N. 2006. In situ methane hydrate dissociation with carbon dioxide sequestration: current knowledge and issues. *Journal of Petroleum Science and Engineering* 51 ((3-4)): 169-184.

Gough, S. R., and D. W. Davidson. 1971. Composition of tetrahydrofuran hydrate and the effect of pressure on the decomposition. *Canadian Journal of Chemistry* 49 (16): 2691-2699.

Guan, H. 2010. The inhibition of gas hydrates and synergy of the inhibiting molecules. In *CPS/SPE international Oil & Gas Conference and Exhibition*. Beijing, China.

Gudmundsson, J. S., V. Andersson, O. I. Levik, and M. Parlaktuna. 1998. Hydrate concept for capturing associated gas In *European Petroleum Conference* The Hague, Netherlands.

Hammerschmidt, E. G. 1934. Formation of gas hydrates in natural gas transmission lines. *Industrial and Engineering Chemistry* 8: 851-855.

Handa, Y. P., R. E. Hawkins, and J. J. Murray. 1984. Calibration and testing of a Tian-Calvet heat-flow calorimeter enthalpies of fusion and heat capacities for ice and tetrahydrofuran hydrate in the range 85 to 270 K. *The Journal of Chemical Thermodynamics* 16 (7): 623-632.

Hatzikiriakos, S. G., and P. Englezos. 1993. The relationship between global warming and methane gas hydrates in the Earth. *Chemical Engineering Science* 48 (23): 3963-3969.

Hawtin, R. W., D. Quigley, and P. M. Rodger. 2008. Gas hydrate nucleation and cage formation at a water/methane interface. *Physical Chemistry Chemical Physics* 10: 4853-4864.

Hawtin, R. W., and P. K. Rodger. 2006. Polydispersity in oligomeric low dosage gas hydrate inhibitors. *Journal of Materials Chemistry* 16: 1934-1942.

Herri, J. M., F. Gruy, M. Cournil, D. Di Benedetto, and P. Breuil. 1996. *2nd International Conference on Natural Gas Hydrates, June 2-6: A new experimental set-up for the characterization in situ of methane hydrate*. Toulouse, France:

Herri, J. M., F. Gruy, J. S. Pic, M. Cournil, B. Cingotti, and A. Sinquin. 1999. Interest of in situ turbidimetry for the characterization of methane hydrate crystallization: Application to the study of kinetic inhibitors. *Chemical Engineering Science* 54: 1849-1858.

Holder, G. D., V. A. Kamath, and S. P. Godbole. 1984. The potential of natural gas hydrates as an energy resource. *Annual Review of Energy* 9: 427-445.

Huang, Q. R., and C. H. Wanga. 1996. Surface laser light scattering studies of the air/poly(N-vinyl-2-pyrrolidone)-water solution interface. *Journal of Chemical Physics* 105 (15): 6546-6552.

Hutter, J. L., H. E. J. King, and M. Y. Lin. 2000. Polymeric hydrate-inhibitor adsorption measured by neutron scattering. *Macromolecules* 33: 2670-2679.

Iida, T., H. Mori, T. Mochizuki, and Y. H. Mori. 2001. Formation and dissociation of clathrate hydrate in stoichiometric tetrahydrofuran–water mixture subjected to one-dimensional cooling or heating. *Chemical Engineering Science* 56: 4747-4758.

Jager, M. D., C. J. Peters, and E. D. Sloan Jr. 2002. Experimental determination of methane hydrate stability in methanol and electrolyte solutions *Fluid Phase Equilibria* 193 (1-2): 17–28.

Jones, K. W., P. B. Kerkar, D. Mahajan, and R. Kleinberg. 2008. Structure of tetrahydrofuran (THF) hydrates in porous media. In *Advanced Energy Conference "Solutions to a Global Crisis"*. Hauppauge, NY.

Karaaslan, U., and M. Parlaktuna. 2000. Surfactants as hydrate promoters? *Energy & Fuels* 14 (5): 1103-1107.

Karaaslan, U., and M. Parlaktuna. 2002. PEO a new hydrate inhibitor polymer. *Energy & Fuels* 16: 1387-1391.

Kashchiev, D., and A. Firoozabadi. 2002. Nucleation of gas hydrates. *Journal of Crystal Growth* 243: 476-489.

Kashchiev, D., and A. Firoozabadi. 2003. Induction time in crystallization of gas hydrates. *Journal of Crystal Growth* 250: 499-515.

Kelkar, S. K., M. S. Selim, and E. D. Sloan. 1998. Hydrate dissociation rates in pipelines. *Fluid Phase Equilibria* 150-151: 371-382.

Kelland, M. A. 2006. History of the development of low dosage hydrate inhibitors. *Energy & Fuels* 20 (3): 825-847.

Kelland, M. A. 2009. *Production chemicals for the Oil and Gas Industry*. Boca Raton, FL: CRC Press Taylor & Francis Group.

Kelland, M. A., K. Mønig, J. E. Iversen, and K. Lekvam. 2008. *6th International Conference on Gas Hydrates (ICGH 2008), July 6-10: A feasibility study for the use of kinetic hydrate inhibitors in deep water drilling fluids* Vancouver, British Columbia, Canada:

Kelland, M. A., T. M. Svaftaas, and L. Dybvik. 1995. A new generation of gas hydrate inhibitors. *Society of Petroleum Engineers* (30695): 529-537.

Kelland, M. A., T. M. Svartaas, and L. A. Dybvik. 1994. *SPE Annual Technical Conference and Exhibition, 25-28 September: Control of hydrate formation by surfactants and polymers* New Orleans, Louisiana, USA:

Kelland, M. A., Svartaas, T.M., Øvsthus, J., Namba, T.,. 2000. A new class of kinetic hydrate inhibitor. *Annals New York Academy of Sciences* 912 (1): 281-293.

Kerr, R. A. 2004. Gas hydrate resource: Smaller but sooner. *Science* 303 (5660): 946-947.

King Jr, H. E., J. L. Hutter, M. Y. Lin, and T. Sund. 2000. Polymer conformations of gas-hydrate kinetic inhibitors: A small-angle neutron scattering study. *Journal of Chemical Physics* 112 (5): 2523-2532.

Koh, C. A. 2002. Towards a fundamental understanding of natural gas hydrates. *Chemical Society Reviews* 31: 157-167.

Koh, C. A., R. E. Westacott, W. Zhang, K. Hirachand, J. L. Creek, and A. K. Soper. 2002. Mechanisms of gas hydrate formation and inhibition. *Fluid Phase Equilibria* 194-197: 143-151.

Kommaredi, N. S., G. L. McPherson, and V. T. John. 1994. The use of EPR spectroscopy under non-ambient conditions to characterize the consequences of clathrate hydrate formation in water-in-oil microemulsions *Colloids and Surfaces A* 92 (3): 293-300.

KSV minitrough operation manual. Revision 1.1. Helsinki: KSV Instruments Ltd.

Kuzmenka, D. J., and S. Granick. 1988. The collapse of poly(ethylene oxide) monolayers. *Macromolecules* 21: 779-782.

Kvamme, B. 1996. *Second International Conference on Natural Gas Hydrates, June 2-6 A new theory for the kinetics of hydrate formation*. Toulouse, France:

Kvamme, B., and R. Asnes. 2006. Kinetic hydrate inhibitors and mass transport limitations. *WSEAS Transactions on Heat and Mass Transfer* 1 (5): 580-585.

Kvamme, B., T. Kuznetsova, and K. Aasoldsen. 2005. Molecular dynamics simulations for selection of kinetic hydrate inhibitors *Journal of Molecular Graphics & Modelling* 23 (6): 524-536.

Kvenvolden, K. A. 1988. Methane hydrate - a major reservoir of carbon in the shallow geosphere? . *Chemical Geology* 71 (1-3): 41-51.

Kvenvolden, K. A. 2000. Gas hydrate and humans. *Annals of the New York Academy of Sciences* 912: 17-22.

Lachet, V., and E. Béhar. 2000. Industrial perspective on natural gas hydrates. *Oil & Gas Science and Technology – Rev. IFP* 55 (6): 611-616.

Langmuir, I., and V. J. Schaefer. 1939. Properties and structure of protein monolayers. *Chemical Reviews* 24 (2): 181-202.

Lankveld, J. M. G., and J. Lyklema. 1972. Adsorption of polyvinyl alcohol on the praffin-water interface. Interfacial tension as a function of time and concentration. *Journal of Colloid and Interface Science* 41 (3): 454-465.

Larsen, R., C. A. Knight, and E. D. J. Sloan. 1998. Clathrate hydrate growth and inhibition. *Fluid Phase Equilibria* 150-151: 353-360.

Leaist, D. G., J. J. Murray, M. L. Post, and D. W. Davidson. 1982. Enthalpies of decomposition and heat capacities of ethylene oxide and tetrahydrofuran hydrates. *Journal of Physical Chemistry* 86 (21): 4175-4178.

Lederhos, J. P., J. P. Long, A. Sum, R. L. Christiansen, and E. D. J. Sloan. 1996. Effective kinetic inhibitors for natural gas hydrates. *Chemical Engineering Science* 51 (8): 1221-1229.

Lee, H., J.-W. Lee, D. Y. Kim, J. Park, Y.-T. Seo, H. Zeng, I. L. Moudrakovski, C. I. Ratcliffe, and J. A. Ripmeester. 2005. Tuning clathrate hydrates for hydrogen storage. *Nature* 434: 743-746.

Lee, J. W., M. K. Chun, K. M. Lee, Y. J. Kim, and H. Lee. 2002. Phase equilibria and kinetic behaviour of CO2 hydrate in electrolyte and porous media solutions: application to ocean sequestration of CO2. *Korean Journal of Chemical Engineering & Technology* 19: 673-678.

Lee, J. Y., T. S. Yun, J. C. Santamarina, and C. Ruppel. 2007. Observations related to tetrahydrofuran and methane hydrates for laboratory studies of hydrate-bearing sediments. *Geochemistry Geophysics Geosystems* 8 (6): 1-10.

Lee, S., L. Liang, D. Riestenberg, O. R. West, C. Tsouris, and E. Adams. 2003. CO2 hydrate composite for ocean carbon sequestration. *Environmental Science Technology* 37 (16): 3701-3708.

Lingelem, M. N., A. I. Majeed, and E. Stance. 1994. Industrial experience in evaluation of hydrate formation, inhibition, and dissociation in pipeline design and operation. *Annals New York Academy of Sciences* 715 (Natural Gas Hydrates): 75-93.

Lo, C., J. Zhang, A. Couzis, J. W. Lee, and P. Somasundaran. 2008. *Proceedings of the 6th International Conference on Gas Hydrates (ICGH 2008), July 6-10: Zeta potential of THF hydrates in SDS aqueous solutions*. Vancouver, British Columbia, Canada:

Lo, C., J. S. Zhang, A. Couzis, P. Somasundaran, and J. W. Lee. 2010. Adsorption of cationic and anionic surfactants on cyclopentane hydrates. *Journal of Physical Chemistry C* 114: 13385-13389.

Lo, C., J. S. Zhang, P. Somasundaran, S. Lu, A. Couzis, and J. W. Lee. 2008. Adsorption of surfactants on two different hydrates. *Langmuir* 24 (22): 12723-12726.

Long, J., J. Lederhos, A. Sum, R. Christiansen, and E. D. Sloan. 1994. *GPA Annual Convention, Kinetic inhibitors of natural gas hydrates*.

Long, J. P. 1994. Gas hydrate formation mechanism and kinetic inhibition. PhD thesis, Dept. of Chemical Engineering and Petroleum Refining, Colorado School of Mines, Golden, Colorado

Lou, A., B. A. Pethica, and P. Somasundaran. 2000. Interfacial and monolayer properties of poly(vinylcaprolactam). *Langmuir* 16: 7691-7693.

Loveday, J. S., R. J. Nelmes, M. Guthrie, S. A. Belmonte, D. R. Allan, D. D. Klug, J. S. Tse, and Y. P. Handa. 2001. Stable methane hydrate above 2 GPa and the source of Titan's atmospheric methane. *Nature* 410 (6829): 661-663.

Luo, H., C.-Y. Sun, Q. Huang, B.-Z. Peng, and G.-J. Chen. 2006. Interfacial tension of ethylene and aqueous solution of sodium dodecyl sulfate (SDS) in or near hydrate formation region. *Journal of Colloid and Interface Science* 297: 266-270.

MacRitchie, F. 1991. Air/water interface studies of proteins. *Analytica Chimica Acta* 249: 241-245.

Mahajan, D., C. E. Taylor, and G. A. Mansoori. 2007. An introduction to natural gas hydrate/clathrate: the major organic carbon reserve of the Earth. *Journal of Petroleum Science and Engineering* 56: 1-8.

Makogon, T. Y., R. Larsen, C. A. Knight, and E. D. J. Sloan. 1997. Melt growth of tetrahydrofuran clathrate hydrate and its inhibition: method and first results. *Journal of Crystal Growth* 179: 258-262.

Makogon, T. Y., and E. D. J. Sloan. 2002. *Fourth International Conference on Gas Hydrates, Mechanism of kinetic hydrate inhibitors*. Yokohama, Japan:

Makogon, Y. F. 1997. *Hydrates of natural gas*. Tulsa, OK: Penn Well Publishing Company.

Makogon, Y. F., and S. A. Holditch. 2001. Experiments illustrate hydrate morphology, kinetics. *Oil & Gas Journal*: 45-50.

Makogon, Y. F., S. A. Holditch, and T. Y. Makogon. 2007. Natural gas-hydrates — a potential energy source for the 21st Century *Journal of Petroleum Science and Engineering* 56 (1-3): 14-31.

Makogon, Y. F., T. Y. Makogon, and S. A. Holditch. 1999. Gas hydrate formation and dissociation with thermodynamic and kinetic inhibitors. In *SPE Annual Technical Conference and Exhibition*. Houston, USA.

Makogon, Y. F., T. Y. Makogon, and S. A. Holditch. 2000. Kinetics and mechanisms of gas hydrate formation and dissociation with inhibitors. *Annals New York Academy of Sciences* 12 (1): 777-796.

Malone, R. D. 1994. Hydrate characterization research overview. *Annals New York Academy of Sciences* 715 (Natural Gas Hydrates): 358-363.

Mao, W. L., and H. K. Mao. 2004. Hydrogen storage in molecular compounds. *Proceedings of the National Academy of Sciences of the United States of America* 101 (3): 708-710.

Matsumoto, M., S. Saito, and I. Ohmine. 2002. Molecular dynamics simulation of the ice nucleation and growth process leading to water freezing. *Nature* 416: 409-413.

Max, M. D., S. R. Tatro, J. P. Osegovic, L. A. Brazel, and K. M. Sheps. 2006. New method for extraction of water from natural gas. In *Offshore Technology Conference*. Houston, Texas, U.S.A.

Mehta, A. P., P. B. Hebert, E. R. Cadena, and J. P. Weatherman. 2002. Fulfilling the promise of low dosage hydrate inhibitors: journey from academic curiosity to successful field implementation. *Offshore Technology Conference* (14057): 1-7.

Miller, R., V. B. Fainerman, R. Wtistneck, J. Krfigel, and D. V. Trukhin. 1998. Characterization of the initial period of protein adsorption by dynamic surface tension measurements using different drop techniques. *Colloids and Surfaces A* 131 (1-3): 225-230.

Miller, R., V. B. Fainerman, R. Wustneck, J. Kragel, and D. V. Trukhin. 1998. Characterization of the initial period of protein adsorption by dynamic surface tension measurements using different drop techniques. *Colloids and Surfaces, A: Physicochemical and Engineering Aspects* 131 (1-3): 225-230. :Caplus

Mokhatab, S., R. J. Wilkens, and K. J. Leontaritis. 2007. A review of strategies for solving gas-hydrate problems in subsea pipelines. *Energy Sources, Part A*: 39-45.

Monfort, J. P., L. Jussaume, T. El Hafaia, and J. P. Canselier. 2000. Kinetics of gas hydrates formation and tests of efficiency of kinetic inhibitors. *Annals New York Academy of Sciences* 912 (1): 753-765.

Monfort, J. P., and A. Nzihou. 1993. Light scattering kinetics study of cyclopropane hydrate growth. *Journal of Crystal Growth* 128 (1-4): 1182-1186.

Moon, C., R. W. Hawtin, and P. M. Rodger. 2007. Nucleation and control of clathrate hydrates: insights from simulation. *Faraday Discussions* 136: 367-382.

Moon, C., P. C. Taylor, and P. M. Rodger. 2003. Clathrate nucleation and inhibition from a molecular perspective. *Canadian Journal of Physics* 81: 451-457.

Murthy, S. S. N. 1999. Detailed study of ice clathrate relaxation: evidence for the existence of clathrate structures in some water−alcohol mixtures. *Journal of Physical Chemistry A* 103 (40): 7927-7937.

Nahringbauer, I. 1995. Dynamic surface tension of aqueous polymer solutions, I: Ethyl(hydroxyethyl)cellulose (BERMOCOLL cst-103). *Journal of Colloid and Interface Science* 176 (2): 318-328.

Natarajan, V., P. R. Bishnoi, and N. Kalogerakis. 1994. Induction phenomena in gas hydrate nucleation. *Chemical Engineering Science* 49 (13): 2075-2087.

Nerheim, A. R., T. M. Svartaas, and E. K. Samuelsen. 1992. Investigation of hydrate kinetics in the nucleation and early growth phase by laser light scattering. In *2nd International Offshore and Polar Engineering Conference*. San Francisco, USA.

Netz, R. R., and D. Andelman. 2003. Neutral and charged polymers at interfaces. *Physics Reports* 380: 1-95.

Ng, H. J., and D. B. Robinson. 1985. Hydrate formation in systems containing methane, ethane, propane, carbon dioxide or hydrogen sulfide in the presence of methanol. *Fluid Phase Equilibria* 21 (1-2): 145-55.

Nicholas, J. W., L. E. Dieker, E. D. Sloan, and C. A. Koh. 2009. Assessing the feasibility of hydrate deposition on pipeline walls—Adhesion force measurements of clathrate hydrate particles on carbon steel. *Journal of Colloid and Interface Science* 331: 322-328.

Nogami, T., N. Oya, H. Ishida, and H. Matsumoto. 2008. *6th International Conference on Gas Hydrates (ICGH 2008), July 6-10: Development of natural gas ocean transportation chain by means of natural gas hydrate (NGH)*. Vancouver, British Columbia, Canada:

Ogawa, T., T. Ito, K. Watanabe, K.-i. Tahara, R. Hiraoka, J.-i. Ochiaib, R. Ohmura, and Y. H. Mori. 2006. Development of a novel hydrate-based refrigeration system: a preliminary overview *Applied Thermal Engineering* 26 (17-18): 2157-2167

Ohmura, R., M. Ogawa, K. Yasuoka, and Y. H. Mori. 2003. Statistical study of clathrate-hydrate nucleation in a water/hydrochlorofluorocarbon system: search for the nature of the "memory effect". *Journal of Physical Chemistry B* 107 (22): 5289-5293.

Ohmura, R., S. Takeya, T. Uchida, and T. Ebinuma. 2004. Clathrate hydrate formed with methane and 2-Propanol: confirmation of structure II hydrate formation. *Industrial & Engineering Chemical Research* 43 (16): 4964-4966.

Ohmura, R., S. Takeya, T. Uchida, I. Y. Ikeda, T. Ebinuma, and H. Narita. 2004. Clathrate hydrate formation in the system methane plus 3-methyl-1-butanol plus water: equilibrium data and crystallographic structures of hydrates. *Fluid Phase Equilibria* 221 (1-2): 151-156.

Ohtake, M., Y. Yamamoto, T. Kawamura, A. Wakisaka, W. F. de Souza, and A. M. V. de Freitas. 2005. Clustering structure of aqueous solution of kinetic inhibitor of gas hydrates. *Journal of Physical Chemistry B* 109: 16879-16885.

Okuchi, T., I. L. Moudrakovski, and J. A. Ripmeester. 2007. Efficient storage of hydrogen fuel into leaky cages of clathrate hydrate. *Applied Physics Letters* 91:

Okutani, K., Y. Kuwabara, and Y. H. Mori. 2008. Surfactant effects on hydrate formation in an unstirred gas/liquid system: An experimental study using methane and sodium alkyl sulfates. *Chemical Engineering Science* 63: 183-194.

Østergard, K. K., B. Tohidi, R. Anderson, A. C. Todd, and A. Danesh. 2002. Can 2-propanol form clathrate hydrates? *Industrial & Engineering Chemical Research* 41 (8): 2064-2068.

Peng, B.-Z., C.-Y. Sun, P. Liu, Y.-T. Liu, J. Chen, and G.-J. Chen. 2009. Interfacial properties of methane/aqueous VC-713 solution under hydrate formation conditions. *Journal of Colloid and Interface Science* 336: 738-742.

Peng, B., C. Sun, P. Liu, and G. Chen. 2009. Adsorption of methane on water under hydrate formation conditions. *Chinese Journal of Chemistry* 27: 703-706.

Phan, C. M., A. V. Nguyen, and G. M. Evans. 2006. Dynamic adsorption of beta-casein at the gas-liquid interface. *Food Hydrocolloids* 20 (2-3): 299-304.

Pic, J.-S., J.-M. Herri, and M. Cournil. 2000. Mechanisms of methane hydrate crystallization in a semibatch reactor. Influence of a kinetic inhibitor: polyvinylpyrrolidone. *Annals New York Academy of Sciences* 912 (1): 564-575.

Pickering, P. F., B. Edmonds, R. A. S. Moorwood, R. Szczepanski, and M. J. Watson. 2001. Evaluating new chemicals and alternatives for mitigating hydrates in Oil and Gas production. In *IIR Conference*. Aberdeen, Scotland.

Pinder, K. L. 1965. A kinetic study of the formation of the tetrahydrofuran gas hydrate. *The Canadian Journal of Chemical Engineering* 43 (5): 271-274.

Profile analysis tensiometer PAT1 operation manual. 2005. Vol. Version 5. Berlin: SINTERFACE Technologies.

Purwanto, Y. A., S. Oshita, Y. Seo, and Y. Kawagoe. 2001. Concentration of liquid foods by the use of gas hydrate. *Journal of Food Engineering* 47: 133-138.

Radhakrishnan, R., and B. L. Trout. 2002. A new approach for studying nucleation phenomena using molecular simulations: Application to CO2 hydrate clathrates. *Journal of Chemical Physics* 117 (4): 1786-1796.

Ribeiro Jr, C. P., and P. L. C. Lage. 2008. Modelling of hydrate formation kinetics: state-of-the-art and future directions. *Chemical Engineering Science* 63: 2007-2034.

Ripmeester, J. A., J. S. Tse, C. I. Ratcliffe, and B. M. Powell. 1987. A new clathrate hydrate structure. *Nature* 325: 135-136.

Rojas, Y., and X. Lou. 2009. Surface behaviour of polyvinylcaprolactam at the air-liquid interface. In *Chemeca*. Perth, Western Australia, Australia.

Rojas, Y., and X. Lou. 2010. Instrumental analysis of gas hydrates. *Asian Pacific Journal of Chemical Engineering* 5 (2): 310-323.

Rosen, M. J. 1989. *Surfactants and interfacial phenomena*. Second ed. New York: John Wiley & Sons.

Ross, R. G., and P. Andersson. 1982. Clathrate and other solid phases in the tetrahydrofuran-water system: thermal conductivity and heat capacity under pressure. *Canadian Journal of Chemistry* 60: 881-892.

Ross, R. G., P. Andersson, and G. Bäckström. 1981. Unusual PT dependence of thermal conductivity for a clathrate hydrate. *Nature* 290: 322-323.

Rovetto, L. J., T. A. Strobel, C. A. Koh, and E. D. Sloan Jr. 2006. Is gas hydrate formation thermodynamically promoted by hydrotrope molecules? . *Fluid Phase Equilibria* 247 (1-2): 84-89.

Rueff, R. M., and E. D. Sloan. 1985. Effect of granular sediment on some thermal properties of tetrahydrofuran hydrate. *Industrial & Engineering Chemistry Process Design and Development* 24 (3): 882-885.

Saji, A., H. Yoshida, M. Sakai, T. Tanii, T. Kamata, and H. Kitamura. 1992. Fixation of carbon dioxide by clathrate hydrate. *Energy Conversion and Management* 33: 643-649.

Sakaguchi, H., R. Ohmura, and Y. H. Mori. 2003. Effects of kinetic inhibitors on the formation and growth of hydrate crystals at a liquid-liquid interface. *Journal of Crystal Growth* 247 (3-4): 631-641.

Scanlon, W. J., and O. Fennema. 1971. Gas hydrates in aqueous-organic systems *1: VII. Linear crystallization velocities of the hydrates of ethylene oxide and tetrahydrofuran *Cryobiology* 8 (3): 249-254.

Serdyuk, I. N., N. R. Zaccai, and J. Zaccai. 2007. *Methods in molecular biophysics: structure, dynamics, function*. New York: Cambridge University Press.

Sivaraman, R. 2003. Understanding the mechanisms of hydrate nucleation and inhibition. *Gas TIPS*, 28-33.

Skovborg, P., H. J. Ng, P. Rasmussen, and U. Mohn. 1993. Measurement of induction times for the formation of methane and ethane gas hydrates. *Chemical Engineering Science* 48 (3): 445-453

Sloan, E. D. 1997. *Clathrate hydrates of natural gases*. 2nd ed. New York: Marcel Dekker Inc.

Sloan, E. D. 2000. Clathrate hydrates: the other common solid water phase. *Industrial & Engineering Chemistry Research* 39 (9): 3123-3129.

Sloan, E. D. 2003a. Clathrate hydrate measurements: microscopic, mesoscopic, and macroscopic. *Journal of Chemical Thermodynamics* 35: 41-53.

Sloan, E. D. 2005. A changing hydrate paradigm—from apprehension to avoidance to risk management. *Fluid Phase Equilibria* 228-229: 67-74.

Sloan, E. D., and C. A. Koh. 2008. *Clathrate hydrates of natural gases*. Third ed. Boca Raton, Florida: Taylor & Francis Group.

Sloan, E. D., S. Subramanian, P. N. Matthews, J. P. Lederhos, and A. A. Khokhar. 1998. Quantifying hydrate formation and kinetic inhibition. *Industrial & Engineering Chemistry Research* 37 (8): 3124-3132.

Sloan, E. D. J. 1998. Gas hydrates: review of physical/chemical properties. *Energy & Fuels* 12: 191-196.

Sloan, E. D. J. 2003b. Fundamental principles and applications of natural gas hydrates. *Nature* 426: 353-359.

Sloan, J. 1995. Method for controlling clathrate hydrates in fluid systems. USA 5432292, filed June 24, 1993, and issued

Sloan Jr, E. D. 1994. Conference overview. *Annals New York Academy of Sciences* 715 (Natural Gas Hydrates): 1-23.

Spelt, J. K., D. R. Absolom, and A. W. Neumann. 1986. Solid surface tension: the interpretation of contact angles by the equation of state approach and the theory of surface tension components. *Langmuir* 2: 620-625.

Storr, M. T., and P. M. Rodger. 2000. A molecular dynamics study of the mechanism of kinetic inhibition. *Annals New York Academy of Sciences* 912: 669-677.

Storr, M. T., P. C. Taylor, J.-P. Monfort, and P. M. Rodger. 2004. Kinetic inhibitor of hydrate crystallization. *Journal of the American Chemical Society* 126: 1569-1576.

Strobel, T. A., C. J. Taylor, K. C. Hester, S. F. Dec, C. A. Koh, K. T. Miller, and E. D. Sloan Jr. 2006. Molecular hydrogen storage in binary THF-H2 clathrate hydrates. *Journal of Physical Chemistry B* 110: 17121-17125.

Suga, H., T. Matsuo, and O. Yamamuro. 1992. Thermodynamic study of ice and clathrate hydrates. *Pure & Appl. Chem* 64 (1): 17-26.

Sum, A. K., C. A. Koh, and E. D. Sloan. 2009. Clathrate hydrates: from laboratory science to engineering practice. *Industrial & Engineering Chemical Research* 48 (16): 7457–7465.

Sun, C.-Y., G.-J. Chen, and L.-Y. Yang. 2004. Interfacial tension of methane + water with surfactant near the hydrate formation conditions. *Journal of Chemical Engineering Data* 49: 1023-1025.

Susilo, R., J. A. Ripmeester, and P. Englezos. 2007. Characterization of gas hydrates with PXRD, DSC, NMR, and Raman spectroscopy. *Chemical Engineering Science 62* 62: 3930-3939.

Sze, A., D. Erickson, L. Ren, and D. Li. 2003. Zeta-potential measurement using the Smoluchowski equation and the slope of the current–time relationship in electroosmotic flow. *Journal of Colloid and Interface Science* 261: 402–410.

Takahashi, M., H. Moriya, Y. Katoh, and T. Iwasaki. 2008. *6th International Conference on Gas Hydrates (ICGH 2008), July 6-10: Development of natural gas hydrate (NGH) pellet production system by bench scale unit for transportation and storage of NGH pellet*. Vancouver, British Columbia, Canada:

Takeya, S., K. Honda, T. Kawamura, Y. Yamamoto, A. Yoneyama, Y. Hirai, K. Hyodo, and T. Takeda. 2007. Imaging and density mapping of tetrahydrofuran clathrate hydrates by phase-contrast x-ray computed tomography. *Applied Physics Letters* 90 (081920): 1-3.

Talley, L. D., and M. Edwards. 1999. First low dosage hydrate inhibitor is field proven in deepwater. *Pipeline & Gas Journal* 226 (3): 44-46.

Talley, L. D., G. F. Mitchell, and R. H. Oelfke. 2000. Comparison of laboratory results on hydrate induction rates in a THF rig, high-pressure rocking cell, miniloop, and large flowloop. *Annals New York Academy of Sciences* 12 (1): 314-321.

Tartakovsky, A., D. M. Drutis, and J. O. Carnali. 2003. The adsorption of cationic and amphoteric copolymers on glass surfaces: zeta potential measurements, adsorption isotherm determination, and FT Raman characterization. *Journal of Colloid and Interface Science* 263: 408-419.

Taylor, C. J., L. E. Dieker, K. T. Miller, C. A. Koh, and E. D. J. Sloan. 2007. Micromechanical adhesion force measurements between tetrahydrofuran hydrate particles. *Journal of Colloid and Interface Science* 306: 255-261.

Thomas, S., and R. A. Dawe. 2003. Review of ways to transport natural gas energy from countries which do not need the gas for domestic use *Energy* 28 (14): 1461-1477

Trurnit, H. J. 1960. A theory and method for the spreading of protein monolayers. *Journal of Colloid Science* 15: 1-13.

Tse, J. S., and M. A. White. 1988. Origin of glassy crystalline behavior in the thermal properties of clathrate hydrates: a thermal conductivity study of tetrahydrofuran hydrate. *Journal of Physical Chemistry* 92 (17): 5006-5011.

Tulk, C. A., J. A. Ripmeester, and D. D. Klug. 2000. The application of Raman spectroscopy to the study of gas hydrates. *Annals New York Academy of Sciences* 912 (1): 859-872.

Udachin, K. A., C. I. Ratcliffe, and J. A. Ripmeester. 2001. A dense and efficient clathrate hydrate structure with unusual cages. *Angew Chem Int Ed Engl* 40 (7): 1303-1305.

Udachin, K. A., C. I. Ratcliffe, and J. A. Ripmeester. 2002. Single crystal diffraction studies of structure I, II and H hydrates: structure, cage occupancy and composition. *Journal of Supramolecular Chemistry* 2 (4-5): 405-408.

Von Stackelberg, M. 1949. Feste gashydrate. *Naturwissenschaften* 36: 327-333.

Vysniauskas, A., and P. R. Bishnoi. 1983. A kinetic study of methane hydrate formation. *Chemical Engineering Science* 38: 1061-1072.

Ward, A. F. H., and L. Tordai. 1946. Time-dependence of boundary tensions of solutions. The role of diffusion in time-effects. *Journal of Chemical Physics* 14 (7): 453-61.

Weiner, B. B., W. W. Tscharnuter, and D. Fairhurst. 1993. Zeta potential: a new approach. In *Canadian Mineral Analysts Meeting*. Winnipeg, Manitoba, Canada.

White, M. A., and M. T. MacLean. 1985. Rotational freedom of guest molecules in tetrahydrofuran clathrate hydrate, as determined by heat capacity measurements. *Journal of Physical Chemistry* 89 (8): 1380-1383.

Wilson, P. W., D. Lester, and A. D. J. Haymet. 2005. Heterogeneous nucleation of clathrates from supercooled tetrahydrofuran (THF)/water mixtures, and the effect of an added catalyst. *Chemical Engineering Science* 60: 2937-2941.

Xie, Y., K. Guo, D. Liang, S. Fan, and J. Gu. 2005. Steady gas hydrate growth along vertical heat transfer tube without stirring *Chemical Engineering Science* 60: 777-786.

Yamamoto, Y., K. Nagashima, T. Kornai, and A. Wakisaka. 2000. Effect of inhibitor methanol on the microscopic structure of aqueous solution. *Annals New York Academy of Sciences* 12 (1): 797-806.

Yamasaki, A., M. Wakatsuki, H. Teng, Y. Yanagisawa, and K. Yamada. 2000. A new ocean disposal scenario for anthropogenic CO2: CO2 hydrate formation in a submerged crystallizer and its disposal. *Energy* 25: 85-96.

Young, W. D. 1994. How to characterize the effectiveness of kinetic hydrate inhibitors. *Annals New York Academy of Sciences* 715 (Natural Gas Hydrates): 341-343.

Yousif, M. H. 1997. A preliminar study of the morphology of gas hydrates. In *SPE International Symposium on OIlfield Chemistry*. Houston, Texas, USA.

Yousif, M. H., R. B. Dorshow, and D. B. Young. 1994. Testing of hydrate kinetic inhibitors using laserlight scattering technique. *Annals New York Academy of Sciences* 715 (Natural Gas Hydrates): 330-340.

Zang, X.-Y., S.-S. Fan, D.-Q. Liang, D.-L. Li, and G.-J. Chen. 2008. Influence of 3A molecular sieve on tetrahydrofuran (THF) hydrate formation. *Science in China Series B: Chemistry* 51 (9): 893-900.

Zatz, J. L., and B. Knowles. 1971. Monolayers of polyvinylpyrrolidone copolymers. *Journal of Pharmaceutical Sciences* 60 (11): 1731-1733.

Zeng, H., H. Lu, E. Huva, V. K. Walker, and J. A. Ripmeester. 2008. Differences in nucleator adsorption may explain distinct inhibition activities of two gas hydrate kinetic inhibitors. *Chemical Engineering Science* 63: 4026-4029.

Zeng, H., I. L. Moudrakovski, J. A. Ripmeester, and V. K. Walker. 2006. Effect of antifreeze protein on nucleation, growth and memory of gas hydrates. *American Institute of Chemical Engineers* 52 (9): 3304-3309.

Zeng, H., Walker, V.K., Ripmeester, J.A.,. 2007. Approaches to the design of better low-dosage gas hydrate inhibitors. *Angew. Chem. Int. Ed.* 46: 5402-5404.

Zeng, H., L. D. Wilson, V. K. Walker, and J. A. Ripmeester. 2003. The inhibition of tetrahydrofuran clathrate-hydrate formation with antifreeze protein. *Canadian Journal of Physics* 81 (1/2): 17-24.

Zeng, H., L. D. Wilson, V. K. Walker, and J. A. Ripmeester. 2006. Effect of antifreeze proteins on the nucleation, growth and the memory during tetrahydrofuran clathrate hydrate formation. *Journal of the American Chemical Society* 128: 2844-2850.

Zetasizer nano series user manual. MAN 0317 issue 2.1 2004. England: Malvern Instruments Ltd.

Zhang, J. S., S. Lee, and J. W. Lee. 2007. Kinetics of methane hydrate formation from SDS solution. *Industrial & Engineering Chemistry Research* 46: 6353-6359.

Zhang, J. S., C. Lo, A. Couzis, P. Somasundaran, J. Wu, and J. W. Lee. 2009. Adsorption of kinetic inhibitors on clathrate hydrates. *Journal of Physical Chemistry C* 113: 17418-17420.

Zhang, J. S., C. Lo, P. Somasundaran, S. Lu, A. Couzis, and J. W. Lee. 2008. Adsorption of sodium dodecyl sulfate at THF hydrate/liquid interface. *Journal of Physical Chemistry C* 112 (32): 12381-12385.

Zhang, W., J. L. Creek, and C. A. Koh. 2001. A novel multiple cell photo-sensor instrument: principles and application to the study of THF hydrate formation *Measurement Science and Technology* 12 (10): 1620–1630.

Zhong, Y., and R. E. Rogers. 2000. Surfactant effects on gas hydrate formation. *Chemical Engineering Science* 55: 4175-4187.